An exploration into the link between brain rhythms and synaptic plasticity in health and infectious disease

Iain James Hartnell

PhD

University of York

Biology

September 2018

Abstract

During wakefulness, synapses are strengthened to enable memory formation. Whereas, during sleep, weaker connections are 'pruned' to help consolidate memories. These synaptic alterations are related to cortical oscillations, which are generally faster during wakefulness (30-80Hz, gamma), and slower during deep sleep (1-4Hz, delta). Synaptic strength is thought to decrease during delta rhythms (compared to gamma rhythms). Neuroinflammation can disturb these brain rhythms and lead to a decline in cognitive function, which may result from aberrations in synaptic plasticity.

To test the laminar and cellular changes in synaptic plasticity during sleep- and wake-related oscillations, *in vitro* electrophysiology and immunofluorescence were employed using acute rat neocortical slices. To examine the effect of neuroinflammation on these brain states, systemic infection was induced using synthetic analogues of pathogenic bacterial and viral material, and a biological parasitic disease model.

The expression of an immediate early gene (IEG) marker of neuronal plasticity (Arc) was higher during delta oscillations compared to gamma oscillations and was concentrated to mid-apical dendrite bundles from layer V intrinsically bursting cells. These bundles represented cortical microcolumns which are known to exhibit synchronous activity, allowing parallel processing of information. Increased Arc expression in these columns during delta oscillations may promote synaptic rescaling and highlights the role of cortical microcolumns in memory consolidation.

A balance of pro- and anti-inflammatory cytokines was found after short term systemic infection which gave way to a predominately pro-inflammatory state when the infection was longer term. The oscillatory activity also changed, with a continued decline in gamma power. However, delta power increased short term but decreased with a longer infection. The systemic infection had no effect on cortical plasticity. These results were corroborated in a mouse model of Leishmaniasis and show that systemic infection alters neuronal communication by changes to oscillatory activity, but does not change synaptic plasticity levels.

Declaration

3

I declare that this thesis is a presentation of original work and I am the sole author except where otherwise indicated in the text. This work has not previously been presented for an award at this, or any other, University. All sources are acknowledged as References.

Contents

Acknowledgements.

Wow, it's all over! What a mammoth task that was! But I cannot take full credit for it as so many people were involved in turning out this thesis.

Firstly, my thanks go to my supervisors, Miles and Sangeeta. You have both helped me immensely, both technically and academically. You have encouraged me when we found something cool and kept my spirits up when things weren't working. Thanks also for the many pints and Indian meals (thanks Sanjoy!) that sustained me throughout my PhD!

Fiona, massive thanks to you for looking after me whilst I was in America and putting up with people thinking you were my mum! Also, many thanks to my TAP members, Darren and Chris for overseeing my progress and giving me invaluable help and ideas.

My four years in York and Boston would have sucked if it weren't for the lovely people I worked with every day. Steve, a massive amount of credit goes to you, for your dirty jokes, horrendous farts, oh and for teaching me ephys (it kinda helped). Annie, I'm gutted we only had a year of working together. I'll really miss chatting about random crap with you! Grace, I would thank you too… but I could only find the dog. Nat, for the Game of Thrones dinners and taking me snowboard and teaching me the wonderful *ahem* world of MATLAB.

Dee-duh-dee-deeeeee…. That's for you, Anna! Kaz, thanks for all the great nights out, I'll never forget our California road trip. Best holiday ever! Faheem, urban dictionary was pretty accurate. Bottoms up to the world's greatest pub quiz team: Nick, Jack (…Jaaaaack), Laura, Alex – and all the others! Also, to Lauren, Jo, Mark, Matt, Ming, BSF people, TF people and Jenny. Sarah, Abby, Ash, Roman, Clare, Jess, Craig and Fatima… thanks for helping to make my time in America so amazing. Chuck, for the guitar loan and the jam sessions! Hans thanks for all the beer!

To all those people who have nothing to do with science, who have generally kept me sane during this whole thing, thank you. That's you Alex, Bella, Poopshoe & Kara. This last year has been fab, cus I've had the best housemates, Sarah, Dan and Phil (also special thanks to Phil for help with my thesis, best of luck with yours!). Also, to my family: Mum, Dad, Emma, Tim and Joshua, I love you all and thanks for helping me escape PhD things when I've needed to get away. Lastly to all those people I will kick myself for not mentioning here, you can tell me off later! And to you the reader, good luck…

Abbreviations

1ry	Primary	**KA**	Kainate
2ry	Secondary	**LFP**	Local Field Potential
ACSF	Artificial Cerebrospinal Fluid	**LPS**	Lipopolysaccharide
AHP	After Hyperpolarisation Potential	**LTD**	Long Term depression
AMPA	α-amino-3-hydroxy-5-methyl-4-isoxazolepropionic acid	**LTP**	Long Term Potentiation
ANOVA	Analysis of Variance	**LTS**	Low Threshold Spike
APV	(2R)-amino-5-phosphonovaleric acid	**MEG**	Magnetoencephalography
Arc/ Arg 3.1	Activity-regulated cytoskeleton-associated protein	**mGluR**	Metabotropic Glutamate Receptor
Au1	Primary Auditory Cortex	**NMDA**	N-Methyl-D-aspartic acid
A1R	Adenosine type 1 receptor	**NREM**	Non-Rapid Eye Movement
BDNF	Brain-derived neurotrophic factor	**PING**	Pyramidal-interneuron network gamma
CA 1/3	Cornu Ammonis Area 1/3	**Poly I:C**	Poly Inosinic: Cytidylic Acid
CCH	Carbachol	**RAS**	Reticular Activating System
c-Fos	Finkel-Biskis-Jinkins Osteogenic Sarcoma homolog	**REM**	Rapid Eye Movement
D1R	Dopamine 1 Receptor	**RS**	Regular Spiking (Neuron)
ECoG	Electrocorticography	**SCH**	SCH-23390 (D1R Antagonist)
EEG	Electroencephalogram	**SD**	Sleep Deprivation
EPSP	Excitatory Post-Synaptic Potential	**SEM**	Standard Error of the Mean
FRB	Fast Rhythmic Bursting neuron	**SHY**	Synaptic Homeostasis Hypothesis
FS	Fast-Spiking neuron	**SS**	Spontaneous Sleep
GABA	Gamma-aminobutyric acid	**SW**	Spontaneous Waking
GluR	Glutamate Receptor	**SWA**	Slow Wave Activity
IB	Intrinsically Bursting (Neuron)	**SWS**	Slow Wave Sleep
IEG	Immediate early gene	**S1**	Primary Somatosensory Cortex
ING	Interneuron network gamma	**S2**	Secondary somatosensory cortex
IPSP	Inhibitory Post Synaptic Potential	**TC**	Thalamocortical

List of Figures

Aims and Objectives

In general, this thesis uses *in vitro* oscillations generated in neocortical slice preparations of rat brain. Using this model system the overarching objectives are to assess the changes in synaptic plasticity that occur between different classifications of pharmacologically induced brain rhythms and to investigate the effect of neuroinflammation on that interaction. With this in mind this thesis outlines experiments that were carried out:

- To generate sleep and wake-related oscillations in neocortical slice preparations and assess the effects of those oscillations on neuronal activity and plasticity through changes to immediate early gene expression.

- To localise oscillation related immediate early gene changes across neocortical laminae and different cell types.

- To monitor sleep and wake related oscillations in brain slice preparations after bath application of inflammatory agents that mimic bacterial and viral sequences (lipopolysaccharide and polyinosinic:cytidylic acid respectively).

- To raise a systemic immune response using those inflammatory agents that mimic bacterial and viral sequences recognised by the peripheral immune system and analyse the resulting inflammation in the brain.

- To compare the effect of the time scale of a mimicked systemic infection on sleep and wake-related oscillations generated in brain slice preparations.

- To evaluate the effect of a real-life systemic infection on sleep and wake related oscillations generated in brain slice preparations, and investigate changes to plasticity across these oscillations.

Chapter One – General Introduction

1.1 The Neocortex

This thesis focusses on markers of plasticity associated with different patterns of electrical activity in the neocortex. The neocortex in humans is the largest part of the cerebral cortex and is the most developed in terms of its organisation. It is arranged into six layers (designated by Roman numerals I-VI) each with a unique neuronal subtype composition *(see Figure 1.1)*. Twenty percent of the neurons of the neocortex are inhibitory interneurons and use γ-aminobutyric acid (GABA) as their main neurotransmitter. They synapse with proximal pyramidal cells and other interneurons to provide the inhibitory balance essential for neuronal oscillations within their local neuronal networks (see section 1.2 below) (Dupret et al., 2008; Middleton et al., 2008). The majority of the neurons (80%) within the neocortex are excitatory and as such exert a depolarising influence on other neurons conferred by the excitatory neurotransmitter glutamate (Han and Sestan 2013). Pyramidal cells make up most of the neocortical excitatory cells and can span several layers and project between regions allowing long-range connectivity. Thus, they are ideally designed to transfer information both within laminae and also between different brain areas. Spiny stellate cells are also excitatory but are less widespread, with cell bodies primarily restricted to layer IV of primary sensory areas (Costa and Muller, 2014).
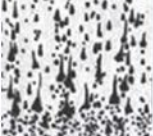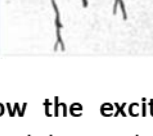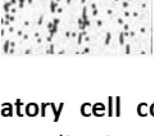
Layers	Golgi Stain	Nissl Stain	Composition
I – Molecular Layer			Axons and dendrites
II – External Granular Layer			Dense stellate and small pyramidal cells
III – External Pyramidal Layer			Sparse stellate cells and medium pyramidal cells
IV – Internal Granule Layer			Dense stellate cells
V – Internal Pyramidal Layer			Large pyramidal cells
VI – Multiform Layer			Varied pyramidal cells and stellate cells

Figure 1.1. A table to show the excitatory cell composition of the 6 layers of the neocortex. Each layer is named due to the qualitative nature of the cell bodies in that layer. Golgi staining images show up pyramidal cells and Nissl stain highlights nuclei of all cells. Images taken are from Ramon y Cajal (1911).

Whilst communication across the cortex is important, the arrangement of neurons throughout the layers suggests that the predominant flow of information is vertically between layers within a columnar arrangement. This has been confirmed functionally in the somatosensory cortex (Mountcastle et al., 1957), and primary visual cortex (Hubel and Wiesel, 1962). Although not necessarily representative of these 'functional' columns, a columnar organisation is conserved throughout the neocortex and across many species with surprising uniformity in cell number and density (Rockel et al., 1980; Carlo and Stevens, 2013).

1.1.1 Intracortical transfer of information through the neocortex

Sensory inputs, relayed mostly by specific thalamic nuclei, enter cortical columns first at layer IV (Bode-Greuel et al., 1987). They are conveyed mainly by parvalbumin immune reactive neurones (PIR neurones), however, calbindin immune reactive neurones (CIR) also exist which have dispersed projections to superficial layers of the cortex I-III (Jones, 2002). The targets for these dispersed projections are presumed to be the apical dendrite of layer V pyramidal cells (Rubio-Garrido et al., 2009; Bonjean et al., 2012)

The first stage of information processing in the cortex involves the initial receipt of an input from the thalamus and its subsequent intracortical projection for the next phase of processing. The cells of layer IV (also called 'first order cells') receive the majority of the thalamic inputs and are known to deal with information from small receptive fields (Hubel and Wiesel, 1962) (Chapin, 1986). These cells have been shown to predominantly project terminals into layer II/III (also known as the supra-granular layer) (Gilbert and Wiesel, 1979) although the axons also descend into the white matter with arborisation into layer V/VI.

These projections to layer II/III mostly synapse onto the basal dendrites of layer III pyramidal cells (Watts and Thomson, 2005) which are responsible for the second level of neocortical processing. It is at the transfer between the first and second levels that sensory information is strongly gated so that weaker stimuli cause less firing in layer II/III neurons than the presynaptic layer IV cells (Brumberg et al., 1999), whereas firing levels in response to stronger stimuli are preserved (Zhu and Connors, 1999). These cells also only respond to more complex stimuli such as those including motion or to expanded receptive fields (possibly from the integration of several smaller receptive fields from converging layer IV neurons) (Simons, 1978). The layer III pyramidal cells' axons descend all the way through the cortex to layer VI, but only connect to

pyramidal cells in layers II/III and V. These cells rarely target layer V regular spiking cells but connect much more abundantly with layer V bursting cells (Thomson et al., 2002).

The involvement of layer V bursting cells in the third level of processing, along with their ability to receive higher order feedback from their layer I projecting apical dendrites (Rockland and Drash, 1996), highlight their importance as a major processing unit in the neocortex. They also provide a major output pathway from the cortex, with corticothalamic projections as well as projections to other subcortical structures such as the pons (Gao and Zheng, 2004).

The aforementioned studies on the interlaminar network of neurones within the cortical column looked at the anatomical projections and arborisation of cells but did not consider the strength of the connections between layers *(Figure 1.1A).* Interlaminar connections can be measured *in vitro* by stimulating a particular layer of the cortex and recording the amplitude of EPSPs in the target layer. The prominence of certain interlaminar connections can be estimated finding the product of the EPSP amplitude and the probability of locating a synaptic connection between cells of the stimulated and target layers. This gives a measure that takes into account the strength and the relative number of synaptic connections between layers. Using this method it has been shown that intra-laminar connections are particularly strong in layers II, III and IV (Lefort et al., 2009). This study also corroborated the evidence (highlighted by anatomical investigations) that suggested that the main routes of information flow are between layer IV and layer II/III and between layer II/III and layer V cells *(Figure 1.1B).* This further highlights the importance of layer V neurons as an information processing unit in the cortex.

1.1.2 Oscillatory activity in neocortical columns

The cells of the neocortex are arranged into ca. 0.5mm diameter vertically oriented columns with adjacent cells having very similar receptive fields – these are called macro columns. As mentioned above, this was originally described by Mountcastle (1957) in the cat somatosensory cortex and was found to be conserved in ocular dominance columns of the striate (primary visual) cortex (Hubel and Wiesel, 1962). Responses to particular elements of a visual stimulus are also dealt with in columns of the inferotemporal cortex, known as 'feature columns' (Tsunoda et al., 2001).
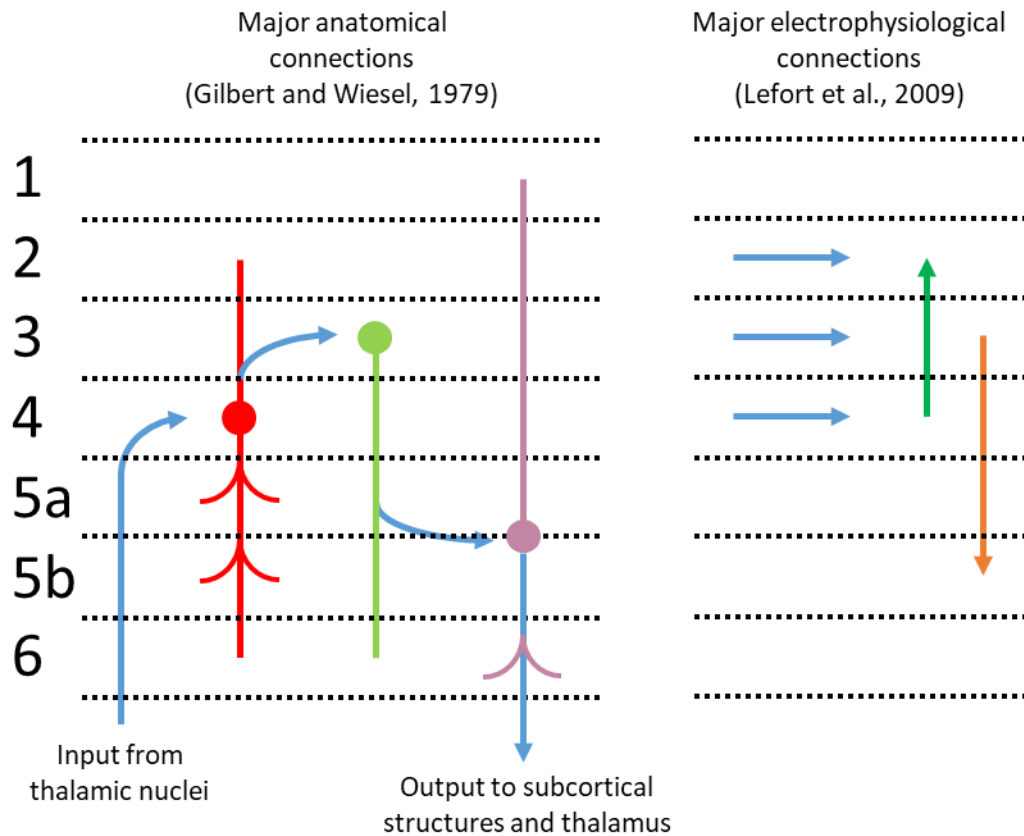
Figure 1.2. A diagrammatic comparison of anatomical and electrical observations of the process of information transfer in the cortex. A. Diagram shows cells that contribute to the main pathway of cortical processing and their connections with other cells. Circles denotes cell bodies. Red = first order cells, Green = second order cells, Purple = third order cells. Blue = route of signal. Illustrated from Gilbert and Wiesel (1979). B. The main electrophysiological connections in the neocortex calculated by the product of the amplitude of EPSPs and the probability of finding connections between/within layers. Threshold for connection was product = 0.1mV. Adapted from Lefort et al. (2009).

Oscillatory activity occurs in these columns after stimulation with sensory input via the thalamus. Experiments on cat visual cortex have shown that oscillatory activity occurs at 40Hz after the presentation of a stimulus and the amplitude of the oscillation correlates with the closeness in orientation selection of that column (Gray and Singer, 1989). Single cells of the target network are also more likely to fire in the negative phase of the oscillation. The synchronisation of the activity of cells in dispersed areas of the cortex may allow for the coherence of the different features of a stimulus into a single sensory object (Gray et al., 1989).

Neurons within certain columns can synchronise their activity with disparate columns, in the same and other cortical areas. Long range pyramidal cell projections may be the functional unit that allows this to occur. These horizontal axonal arbours were first discovered when tracing degeneration of fibres and are important for the visual cortex to code for the relationship between spatially distinct, but connected patterns within the visual field (Gray and Singer, 1989).

Evoked potentials in these columns have also been used to understand more about their function. It is known that the amplitude of auditory evoked potentials are brain state-specific, with the highest amplitudes recorded during deep sleep (Weitzman and Kremen, 1965). Differences of this kind are not consistent across the brain and are even altered between cortical columns. This means that cortical columns may fluctuate between wake and sleep-like states in a manner that is partly independent of the mean, whole brain state - although more columns exist in a sleep-like state during whole-brain sleep and vice versa (Rector et al., 2005). This is a use-dependent process, with the duration of the sleep-like state (defined by higher amplitude evoked potentials) correlating with the duration of the preceding wake-like state within the column (Rector et al., 2005).

1.1.3 Intercolumnar communication in the neocortex

Much of what is known about horizontal connections in the neocortex, has been uncovered by lesion studies. These have shown that pyramidal cells in middle layers can extend axons horizontally or obliquely between 0.5 – 3mm in distance, up into layer I and II or down into layers V and VI (Creutzfeldt et al., 1977). These pyramidal cell axons spread in 'clumps' and mostly synapse with other pyramidal cells (Kisvarday et al 1986) in the same and other layers (Gilbert and Wiesel, 1983). However, the pattern of these horizontal connections varies considerably depending on neocortical region and whether the connection is to a higher hierarchical area (e.g. primary sensory to association cortex) or a lower one (e.g. frontal cortex to association cortex). Regional details are briefly considered below, that focus on the brain regions explored in this thesis. These regions were chosen due to their importance in processing sensory information which affords high levels of plasticity as well as the existence of optimised protocols to model oscillations within these regions *in vitro.*
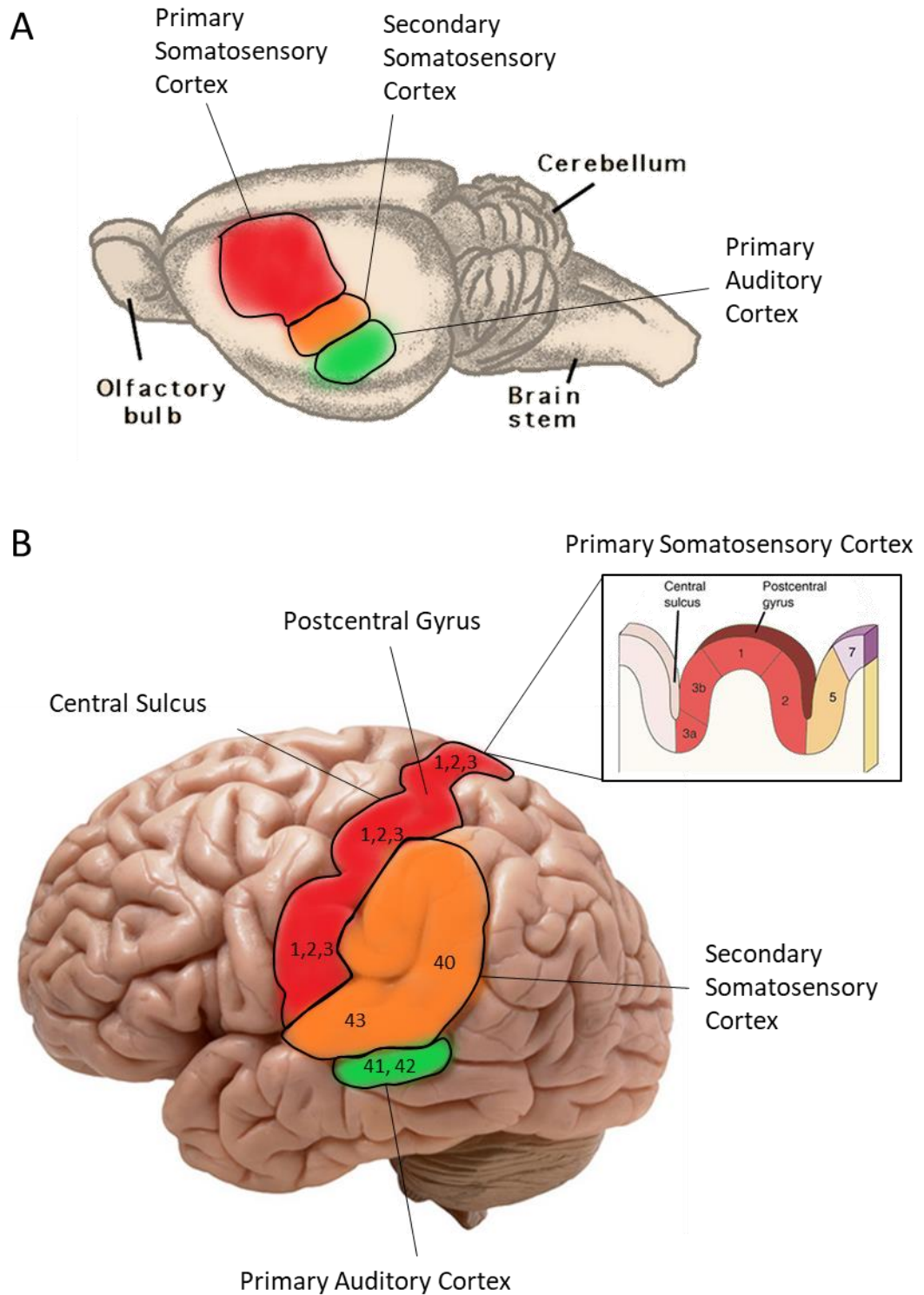
Figure 1.3. A graphical representation of the regions of the rat brain studied in this thesis and their counterparts in the human brain. A. A diagram of the rat brain with the locations of the primary (red) and secondary (orange) somatosensory cortices and primary auditory cortex (green). **B.** A diagram of the human brain with the locations of the primary (red) and secondary (orange) somatosensory cortices and primary auditory cortex (green). Numbers on the diagram refer to Brodmann areas. Pop out shows delineation of Brodmann areas 1-3b in the post central gyrus

1.1.4 Primary somatosensory cortex

The primary somatosensory cortex (S1) is in the post-central gyrus of the human brain. It was once considered a single area, but current understanding has it segregated into four functional maps related to Brodmann areas 1, 2, 3a and 3b. Excitatory inputs relayed by thalamic nuclei (located predominantly in ventrobasal areas) enter S1 mostly at layer VI and trigger the activity of cells of this layer, though there are also modulatory inputs to layer II/III (Viaene et al., 2011). Inputs are arranged in a topographic map within cortical regions, but the four regions deal with different sorts of somatosensory inputs. Area 3b is the primary recipient of touch information and projects to Areas 1 and 2 (Kaas et al., 1983) which process with texture and size/shape information respectively (Purves et al., 2008). Area 1 and 3b are also known to primarily deal with cutaneous information whereas Areas 2 and 3a processing muscle receptor inputs. All of these areas further project to other regions of the cortex such as the motor cortex for sensory guidance of motor actions and the secondary somatosensory cortex for further sensorimotor and polymodal processing (Kaas, 1993). They also project to non-neocortical areas like the amygdala and hippocampus to facilitate tactile memory formation (Mishkin, 1979)

1.1.5 Secondary somatosensory cortex

The secondary somatosensory cortex (S2) includes parts of Brodmann areas 40 and 43. It receives input from S1 (above) and less specifically from matrix thalamic nuclei. In response to nociceptive stimuli, parallel activity in both S1 and S2 occurs, however the secondary somatosensory cortex unlike its primary counterpart, responds to stimuli bilaterally (Ploner et al., 1999). It is thought that S2 has a role in higher order processing of tactile information, particularly with relevance for working memory and attention. Higher fMRI activation of S2 than S1 was seen when human subjects focussed attention on a stimulated area (Hämäläinen et al., 2002). This finding is corroborated by increasing cell firing (Hsiao et al., 1993) and the amount of synchronous activity (Steinmetz et al., 2000) in S2 also related to attention.

Despite its importance in somatosensory processing, different sub-regions of S2 have been shown to respond to multisensory inputs (Brett-Green et al., 2004). This has been suggested to involve polymodal transition zones between S2 and adjacent regions responsible for the processing of other modalities of uni-sensory information (Wallace et al., 2004), (Menzel and Barth, 2005). This further suggests that S2 may have as much a role in sensory integration as it does in the processing of somatosensory information from S1.

1.1.6 Primary auditory cortex

The primary auditory cortex (Brodmann areas 41 and 42) exists in Heschl's gyrus of the temporal lobe. It deals with the conscious perception of sound. This is evident when lesions of this area result in people stating they are deaf while still retaining reflexive responses to sound. These reflexive responses originate in brainstem and midbrain areas (Cavinato et al., 2012). Auditory information from the cochlea is transferred to the primary auditory cortex, first through the inferior colliculus and then through the medial geniculate nucleus in the thalamus. The primary auditory cortex is organised into a tonotopic map based on the cochlear response. The cochlea separates an auditory stimulus by frequency in its own tonotopic map, that organisation of frequency information is conserved in the primary auditory cortex (Lauter et al., 1985; Humphries et al., 2010). As well as processing tonal information, it binds elements of complex sounds together, so they are perceived as a single entity. The auditory cortex also processes more abstract elements of the auditory landscape such as echoes and background noise (Chechik and Nelken, 2012).

1.2 Neural Oscillations

1.2.1 Recording the electrical activity of the human brain

The electrical activity of large populations of millions of neurons often organises into oscillations, particularly in receipt of sensory information (1.1.2 above). These oscillations can occur in local sites in the brain or involve long distant synchronisation in the timing of electrical activity across dispersed brain areas. The oscillatory activity results from the recruitment of networks of neurons of different types whose firing temporally summates to form rhythmic fluctuations in the potential difference between different locations in the extracellular environment. This electrical activity was first recorded using a technique called electroencephalography (EEG), developed initially by William Caton (1875) and first used in human subjects by Hans Berger (1929). EEG uses electrodes placed on the scalp to remotely monitor neuronal population-generated voltage fluctuations through the scalp and skull. This technique readily demonstrates oscillations, or rhythms, as perhaps the most obvious feature of brain electrical activity.

The first rhythm observed in humans by Berger is now known as the alpha oscillation. It defines electrical oscillations of a frequency between 8-12 Hz, and Berger noticed how it dominated the visual cortex EEG recordings when the patient's eyes were closed. This was replaced by the beta rhythm (12 – 30Hz) when the patient opened their eyes – a process he called 'alpha blockade' (Berger, 1929).

Since then, further connections between EEG oscillations and the subjects' sensory, cognitive, and behavioural state have been widely studied. In general, the electrical oscillations are slowest during sleep and increase in frequency with the state of arousal *(see Figure 1.2)*. The slowest, 'delta' waves (1-4Hz) are apparent during deep sleep. This stage is also called non-rapid eye movement sleep (NREM sleep) or slow wave sleep (SWS). Theta frequency oscillations (4-8Hz) are prevalent during the stage known as rapid eye movement (REM) or paradoxical sleep. Two types of electrophysiological events also occur during sleep. Large very slow events called k-complexes occur during NREM sleep in response to external stimuli and are thought to aid in suppressing cortical arousal (Cash et al., 2009), and are also thought to play a role in memory consolidation and synaptic plasticity (Tononi and Cirelli, 2006). Similar arousal suppression (particularly auditory) has been shown to be a function of fast transient bursting events called sleep spindles (Dang-Vu et al., 2010). They have also been correlated with memory performance (Holz et al., 2012).

The theta and delta oscillations that occur during sleep have low metabolic demand (Madsen and Vorstrup, 1991; Maquet, 1997) compared to the faster oscillations associated with wakefulness (such as gamma, 30-80Hz) (Nishida et al., 2008), and are even suggested to be restorative to neurons and their connections (Eugene and Masiak, 2015). This highlights the payoff between the ability to transfer information and process sensory input quickly (as occurs during wakefulness using higher frequency oscillations), with the ability for the brain to keep its metabolic demand satisfied (Tononi and Cirelli, 2006).

Although the initial discovery of neuronal oscillations involved the EEG technique, there are many other techniques by which these phenomena can be studied. Electrocorticography (ECoG) is an invasive version of EEG, which involves recording from the pial surface of the brain itself and is therefore only usually carried out during neurosurgical operations (Khodagholy et al., 2016). Magnetoencephalography (MEG) is similar to EEG in that recordings are made non-invasively, but it measures changes in the magnetic field caused by the activity of neurons rather than the voltage changes constituting the electric field (Baillet, 2017). Both ECoG and MEG offer recordings with better spatial localisation than EEG, but at the cost of their invasiveness and expense respectively. These techniques, in conjunction with the subject's performance during specific cognitive tasks, have allowed the discovery of the processes and brain structures involved in many areas of cognition and sensory processing. This thesis concerns itself only with

the gamma/beta and delta EEG oscillations as markers of wakefulness and NREM sleep respectively, but many far more detailed correlations between oscillations and brain function have arisen in the last 20-30 years, including sensory perception and binding, attention and sleep (Singer, 1993; Kahana, 2006; Wang, 2010; Jutras and Buffalo, 2014).
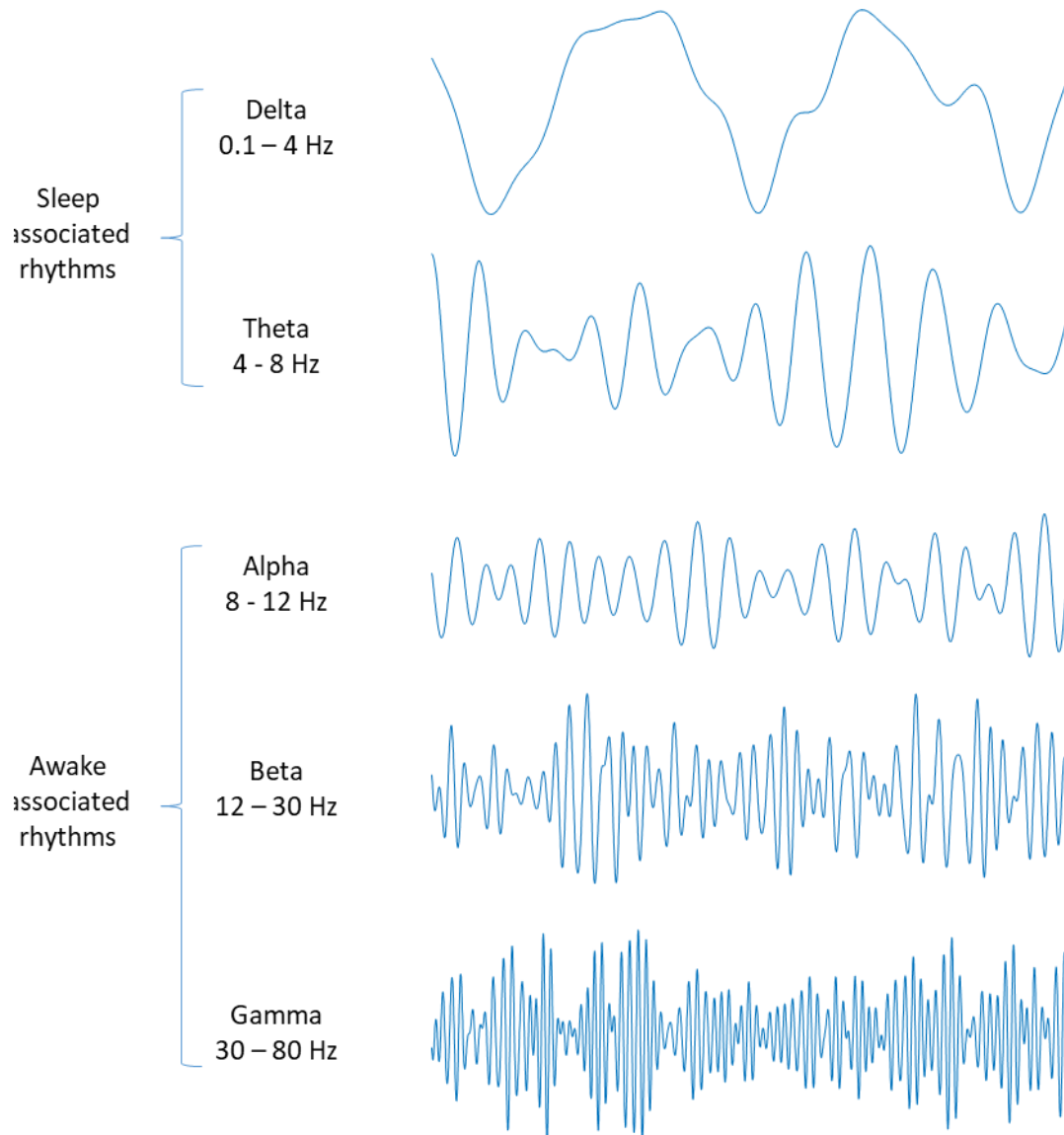
Figure 1.4. A graphical representation of the different classifications of brain rhtyhms. All waves are 2 seconds taken from the same 1 minute recording of *in vitro* delta rhythms in rat somatosensory cortex. The trace was band pass filtered according to the limits shown.

1.2.2 Recording oscillatory activity *in vivo*

To understand the mechanisms involved in generating and maintaining cortical oscillations, animals have often been used. *In vivo* recordings from mammalian brains (mostly rats, mice monkeys and cats) have been useful in this respect. In general, electrodes are placed within specific brain structures by stereotaxic surgery on living animals and can record the local population, single cellular and even subcellular (e.g. dendritic) activity. Through this method, activity can be measured during different brain states and can be related to the functional behaviours seen in the animal. This can also be applied to observe changes in disease models to increase the understanding of the mechanisms behind the pathology and the effect of pharmacological manipulations to recover normal function. Whilst *in vivo* studies have been very useful, they also have their disadvantages. Accurate electrode placement is challenging and once placed the electrode can shift due to the general movement of the animal, blood flow, or breathing - however, the technology in this regard is improving rapidly. There is also limited scope in the ability to manipulate the activity of the networks of cells involved. For these reasons, the electrophysiological studies in this thesis employed recordings from brain tissue *in vitro*.

1.2.3 Recording oscillations *in vitro*

In vitro electrophysiology eliminates many of the above shortfalls of *in vivo* studies by allowing the isolation of neuronal networks, whilst maintaining them in a viable electrically active state in slices of neural tissue. This is achieved at the expense of being able to interrogate relationships between electrical brain activity and behaviour. However, specific regions of the brain can be isolated, and sections can be made from them that can be maintained for many hours. This isolation allows absolute certainty regarding the regional origin of any activity seen and facilitates a controlled manipulation of electrical excitability and overall neuromodulatory state without complexity from unknown variables such as spontaneous activity from multiple afferent connections e.g. from sensory stimuli, brainstem and even 'top-down' influences from other brain areas.

It also allows for more precise electrode placement and makes intracellular recording experiments much more technically manageable. However, without afferents and efferent connections, there is no sensory input or communication with brain regions that are absent from the slice and therefore little to drive spontaneous electrical activity. Therefore, electrical stimulation or pharmacological manipulation of the isolated networks, maintained within the

slice, must be carried out to mimic the input those networks would normally receive. Furthermore, the ionic composition of the artificial cerebrospinal fluid (ACSF) used to maintain the slice can be changed to further investigate a role for cellular and synaptic mechanisms underlying certain electrical activities. This then provides a basis by which to probe the mechanisms behind the oscillatory activity of the brain and study its changes in health and disease. What is already known about these mechanisms, and how they may relate to brain plasticity is introduced below.

1.2.4 Gamma Oscillations

The work in this thesis uses a model of gamma oscillations as an experimental model representation of cortical dynamics associated with sensory perception during wakefulness. Gamma oscillations were one of the first oscillatory conditions to be modelled *in vitro.* They are fairly ubiquitous in most behavioural states, from wakefulness to deep sleep, but are particularly prevalent during primary sensory processing during wakefulness (Gray and Singer, 1989)**.** The synchronous activity of presynaptic neurons at gamma frequency increases post-synaptic responses (especially on convergent targets) and allows for more efficient propagation of sensory information. This process also aids in attentional processing (Magazzini and Singh, 2018), working memory (Lundqvist et al., 2016) and contributes to de novo memory formation in the hippocampus (Axmacher et al., 2006; Sederberg et al., 2007; van Vugt et al., 2010).

The importance of gamma oscillations has been highlighted by studies which have shown that there is a correlation between the firing rate of cortical neurons and the amplitude of gamma band activity in the local field (Ray et al., 2008). In fact, the timing of cell firing during gamma oscillations is critical as it allows the segregation of cells that carry information of the salient stimuli (and thus fire in time with the gamma oscillation) from cells that carry other information (Engel and Singer, 2001). From this, it is apparent that the relationship between gamma-band synchrony between regions and the timing of neuronal firing contributes to the processing of sensory information and also forms the basis of short-term memory (Engel et al., 2001; Kaiser and Lutzenberger, 2005)**.**

It is not surprising then that gamma oscillations have also been shown to be important in visual processing (Henrie and Shapley, 2005), auditory processing (Haenschel et al., 2000), olfaction (Adrian, 1942), somatosensory perception (Rossiter et al., 2013) and nociception (Gross, 2007). Gamma oscillations are not just critical for processing sensory information from a single source

but also for perceptual binding (Tallon-Baudry and Bertrand, 1999). To make sense of the world we need to be able to combine individual sensory items into a unified neural representation of the sensory object as a whole. Perceptual binding (particularly visual perception) allows us to take different features - such as the lines, faces, angles, and depth required to perceive a table – and combine them into a single sensory object. This is also important across senses (particularly between seeing and hearing) for example in the combination of the visual movement of a speakers face with the auditory processing of their speech (Stevenson et al., 2014; Lin et al., 2015).

1.2.4.1 Mechanisms of gamma – ING

There are several mechanisms describing how gamma oscillations are generated *(see Figure 1.3)*. The most basic (in terms of network simplicity) of these mechanisms is interneuron network gamma (ING).

ING describes a mechanism of gamma band network activity in which interconnected interneurons alone are capable of generating the population rhythm. This was originally shown by eliciting 40Hz oscillations in the cornu ammonis area 1 (CA1) region of the hippocampus with trains of electrical stimulation that activate metabotropic glutamate receptors (mGluR) or through direct mGluR activation by an agonist (Whittington et al., 1995). This mGluR activation increases interneuron depolarisation by reducing K+ currents through secondary messenger signal activity on K+ channels (Miles and Poncer, 1993). This was shown to be independent of pyramidal excitation as the 40Hz rhythms were conserved the after the blockage of glutamate receptors (NMDAr, AMPAr and kainate receptors) (Whittington et al., 1995).

Depolarisation of one interneuron generates a train of action potentials whose frequency is dictated by the amount of depolarisation and the duration of the after-hyperpolarisation potential (or refractory period). However, with interconnected interneurons, the action potentials from the first interneuron generate IPSPs in the second, which silences that interneurons activity until the IPSP is over. This means that the second interneuron is most likely to fire in tandem with the first. It also means that the oscillation is possible due to the interneurons' ability to recover from inhibition with enough tonic depolarisation (by mGluR activation) to fire again. Through this mechanism, each interneuron entrains others nearby and interneuron network gamma oscillations are generated (Whittington et al., 2000).

ING is only possible due to the short range of projections from the interneurons involved (like those in CA1). However, it unlikely to be a conserved mechanism in the cortex due to the long-distance synchronisation of gamma oscillations readily observed in many conditions. Furthermore, the physiological relevance of ING is dubious due to the need to isolate networks of interneurons from excitatory cell influence and is only possible experimentally through the blockage of NMDA and AMPA activity (Whittington et al., 1995). It is unlikely that excitatory cells play no part in gamma oscillations due to their dense connectivity with interneurons and the fact that hippocampal and neocortical afferents activate both excitatory and inhibitory cells during *in vivo* gamma oscillations (Burchell et al., 1998).

1.2.4.2 Mechanism of gamma – PING

To be more relevant to the conditions of the brain *in vivo*, the reciprocal influence of excitatory neurons need to be included in with the interneuron network activity. Pyramidal-interneuron network gamma (PING) describes this interplay (Traub et al., 1997). Metabotropic receptor activation (mGluR and mAChR) recruits pyramidal cells (as well as other interneurons) to the network (Whittington et al., 1997) and because pyramidal cells recover from inhibition before interneurons, they provide phasic excitation and cause the interneurons to fire again (Whittington et al., 2000).

Therefore, as the pyramidal cells fire, their EPSPs cause the activation of fast spiking (FS) interneurons (primarily by glutamatergic neurotransmission and action via AMPA receptors). The interneuron output then causes the inhibition of other interneurons (the ING mechanism above) as well as the reciprocal inhibition of the locally connected pyramidal neurons. This process has a decay, which then allows the pyramidal neurons to fire again and thus generates rhythmic oscillations at gamma frequency (Whittington et al., 2011). Each interneuron may have reciprocal innervation with nearly 1000 different pyramidal cells (Halasy et al., 1996), convergence and divergence that highlights the importance of interneurons in the generation of the gamma rhythm and the synchronisation of pyramidal cells in the network (Whittington et al., 2000).

<u>*1.2.4.3 Mechanisms of gamma oscillations - Persistent gamma oscillations*</u>

Although the PING model provides the basis for how a gamma rhythm may work in the cortex, experimentally it only exists for brief periods of time following glutamate pressure injection (Whittington et al., 1998), tetanic stimulation (Whittington et al., 1997) and potassium concentration increases (LeBeau et al., 2002). Though PING may be related to certain *in vivo* states, the persistent gamma oscillations seen *in vivo* and *in vitro* require an adaptation of the model to explain their mechanism. The fundamental conceptual problem with the PING model is that it involves the somatic spiking of pyramidal cells, which has only been seen to occur at 1-4Hz during persistent gamma (Fisahn et al., 1998; Chapman and Lacaille, 1999; Gillies et al., 2002). Spiking at this frequency range is, at least experimentally, insufficient alone to provide the excitatory drive for a persistent rhythm (Whittington and Traub, 2003), even with the huge convergence of pyramidal cells onto single interneurons (Gulyas et al., 1999). It would seem, that for persistent gamma oscillations to occur another form of input is needed. This comes from fast rhythmic bursting (FRB) neurons which spike multiple times per wave of the gamma oscillation and require the gap junctions that exist between these and other pyramidal neurons to broadcast this additional spiking throughout an electrically connected network of axons (Cunningham et al., 2004).

Stable persistent gamma oscillations can be generated in acute slices of rat brain by the bath application of carbachol (CCH), an agonist of both muscarinic and nicotinic acetylcholine receptors (Fisahn et al., 1998). Whilst carbachol has been shown to generate robust hippocampal gamma oscillations, it's the induction of cortical gamma oscillations is less successful (Dickson and Alonso, 1997; Gloveli et al., 1999). Kainic acid (kainic acid, KA), an exogenous ligand for the glutamate-sensitive excitatory kainate receptors is even more reliable as a manipulation to induce persistent gamma oscillations. This has led to well characterised *in vitro* oscillation models - believed to reliably represent the *in vivo* oscillation - in the hippocampus (Traub et al., 1996), entorhinal cortex (Cunningham et al., 2003), primary auditory cortex (Ainsworth et al., 2011) and secondary somatosensory cortex, S2 (Roopun et al., 2008). This thesis, therefore, used kainate application to brain slices containing auditory and secondary somatosensory cortex to generate gamma oscillations as an *in vitro* model of an active, awake cortex.

A. Interneuron Network Gamma (ING)

Oscillations exist in networks of interconnected interneurons that rely on the decay of suppression of inhibition to set the timing for the gamma oscillations. They can influence pyramidal cells but excitatory neurotransmission is blocked.
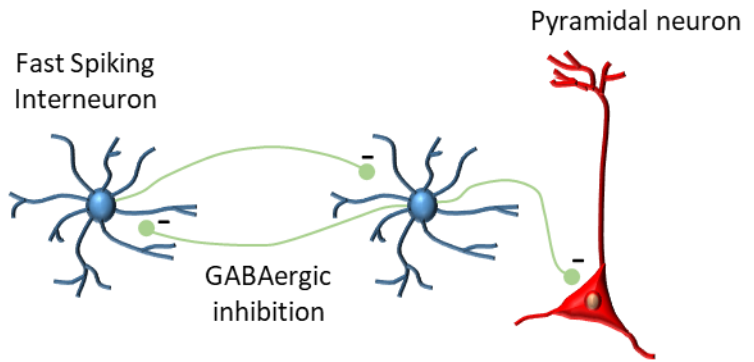
B. Pyramidal - Interneuron Network Gamma (ING)

Pyramidal cells provide the excitatory drive for the gamma oscillation as they recover from inhibition faster than interneurons so fire first. This causes interneurons to fire and inhibit pyramidal cells and other interneurons.
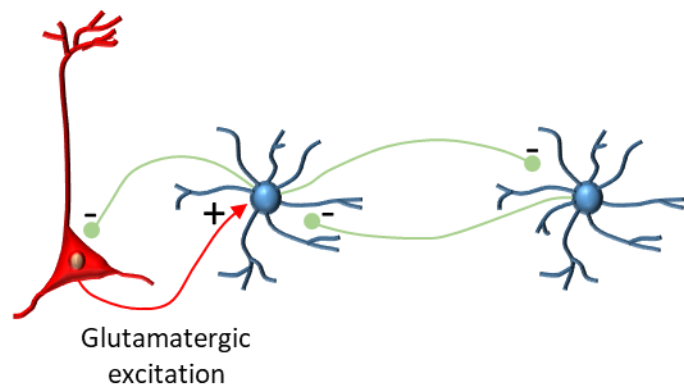
C. Persistent Gamma

Fast rhythmic bursting fire fast bursts of action potentials (that are transmitted to other pyramidal cells through gap junctions) which provide the excitatory drive required to maintain a persistent gamma rhythm. Pyramidal cells do not fire fast enough on there own to do this.
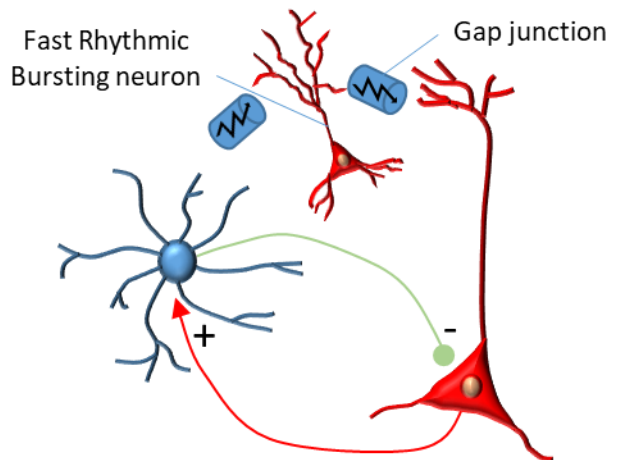
Figure 1.5 A diagrammatic representation of the contribution of different cell types to various mechanisms of gamma oscillations. Adapted from Shin et al (2011) and Whittington et al (2000).

1.2.4.4 Features of auditory gamma in vitro*.*

In the primary auditory cortex (Au1) the gamma rhythm can be generated by bath application of 400nM kainate, where the power of the oscillation is highest in layer III (Cunningham et al., 2004). There is also a kainate concentration-dependent frequency split in the auditory gamma oscillation with bath concentrations over 600nM. The faster gamma oscillation (known as γ2) at 50-80Hz originates from layer IV whereas the slower gamma (γ1) is generated from layers II/III (Ainsworth et al., 2011). Layer V synchronises with layer II/III in low gamma and with layer IV at the kainate concentration at which the layers frequencies split. This suggests that differences by subject and task of the *in vivo* rhythm in this area may be related to the strength of the auditory input to the cortex, which is mimicked *in vitro* by the kainate concentration. As we wished to model background gamma rhythms we used lower concentrations of kainite, where only the slower rhythm was seen.

1.2.4.5 Features of S2 gamma oscillations in vitro

In the secondary somatosensory cortex (S2) a different frequency split is seen similar to that of the auditory cortex. In superficial layers II/III a gamma rhythm exists at around 40Hz whereas in layer V the oscillation is in the β2 range (20-30 Hz). These oscillations are maintained after a cut is made in layer IV to separate superficial and deeper layers (Roopun et al., 2006). Additionally, the power of both oscillations increases after the cut and could be due to destructive interference between the two rhythms in the intact slice. The beta rhythm may recruit cells in the gamma generators' layer (and vice versa) and thus the number of cells contributing to each rhythm in their respective layers is decreased, which has a detrimental effect on oscillation power.

The dual rhythms seen in these cortices (Au1 and S2) are consistent with the idea that the sensory information entering the cortex at layer IV can be transferred to both superficial and deep layers (Thomson and Bannister, 2003). As superficial layers are known to have strong intralaminar connections with other regions (Gilbert and Wiesel, 1979; Lefort et al., 2009), this pathway may allow for perceptual binding (discussed above) to create a neural representation of the somatosensory perception of an object (combining size, shape and texture). Deeper layers project to subcortical regions, such as the thalamus, which controls the response to the stimulus, which is especially important in the feedback to control motor actions (Kaas, 1993).

1.2.4.6 Multimodal nature of auditory cortex and secondary somatosensory cortex.

The auditory cortex and somatosensory cortex were both thought to be involved with the processing of unimodal sensory information, however studies have since suggested not only synchronous activity between these two areas of the neocortex but also that they may encode multimodal sensations rather than just dealing with discretely different modes of sensory input (some of this with respect to S2 is introduced above).

This has been shown in human fMRI with certain areas of the auditory cortex responding to somatosensory input as well as auditory input and subsequently integrating these two inputs (Foxe et al., 2002). Also, the responses to joint inputs have been seen to sum to more than oscillations resulting from single sensory cues (Ro et al., 2013).

Structurally the auditory cortex has also been found to have connections to the secondary somatosensory cortex in humans. These ipsilateral white matter tracts allow the interaction between somatosensory and auditory sensory inputs in which sounds can elicit or increase tactile perception (Ro et al., 2009). Abnormalities in these connections are known to be present in auditory-tactile synaesthesia (Beauchamp and Ro, 2008).

1.2.4.7 Gamma oscillations and plasticity.

Several lines of evidence link the generation of gamma rhythms to neuronal network plasticity. The synchrony of activity between areas of the cortex, mediated by gamma-band frequencies, have been linked to memory, with rhinal-hippocampal gamma synchrony underlying successful (but not failed) memory formation tasks in humans (Fell et al., 2001). Synchrony has also been shown in the rat brain to be generated via fast gamma oscillations between the entorhinal cortex and CA1 which underlies the mnemonic encoding of position in space, and in slow gamma between CA1 and CA3 for information storage (Colgin et al., 2009b). A reason for the prominence of gamma oscillations in the communication between regions, encoding of information and memory, could be because the timing of excitatory postsynaptic spikes required for synaptic plasticity lies within the gamma range (Bi and Poo, 1998). Plasticity afforded by synchronous gamma rhythms has been shown to potentiate excitatory synaptic connections between principal cells, leading to changes in the neuronal activity of the hippocampus (Whittington et al., 1997) and neocortex (Roopun et al., 2008).

The above studies on synchrony between regions in the cortex and the transfer of information strongly suggest that synaptic plasticity may be a consequence of the generation of gamma rhythms. But what relation do gamma rhythms have to such synaptic plasticity?

Gamma oscillations in neuronal membrane potentials have been suggested to be the mechanism by which plasticity can be modulated. One finding that supports this mechanism is that layer II/III pyramidal cells undergo LTP or LTD (in the form of changes in EPSP amplitude) depending on the phase of the EPSP in relation to the membrane potential oscillation (Wespatat et al., 2004). If these cells are part of the network that creates gamma oscillations in the local field, they may link gamma rhythms and plasticity via control of neuronal output timings. Moreover, repeated stimulation of layer 4 (causing ascending cortical activation to more superficial layers) with the specific application of glutamate 1 hour apart can cause plasticity which alters gamma oscillation dynamics. After repeated stimulation, there was an increase in the power of the oscillation, as well as superficial enhancement and deeper layer suppression of spike firing frequencies and their timing to the field oscillation (Ainsworth et al., 2016). These processes are thought to be important for attentional modulation and short-term memory. Another way of answering the question is to look at gamma rhythms related to memory - an outcome of plasticity. This approach has shown that the spectral power of gamma-band oscillations in the auditory cortex appears to be predictive of the formation of an associative (auditory fear conditioning) long-term memory (Headley and Weinberger, 2011).

From the above evidence, it appears that gamma rhythms play a role in the formation of new memories. However, this alone is usually not enough to generate life-long memories. The formation of new memories needs to be 'consolidated' somehow. Current theories suggest this is done during sleep, so we next consider sleep-related cortical dynamics.

<u>1.2.5 Delta Oscillations</u>

This thesis uses an *in vitro* model of delta rhythms to represent the cortical dynamic state during sleep. During deep sleep (NREM stages 3 and 4) the brain exhibits slow wave activity (SWA), which is dominated by delta oscillations (1-4Hz) in the EEG. Oscillations in this band are believed to play a role in synaptic homeostasis and memory consolidation vital for long-term learning in humans (Huber et al., 2004; Walker, 2009) and have been shown to be amplified during sleep in rats in specific brain regions related to a learning task during prior wakefulness (Hanlon et al., 2009).

Delta waves were once believed to be only physiologically relevant to sleep, and their presence during wakefulness was considered a response to brain injury or pathology (see section 1.4 below). However, there has also been emerging evidence for the impact of wake state delta rhythms on normal attentional processing, and the inhibition of sensory input that would interfere with the concentration required to carry out a task (Harmony et al., 1996). It is possible this is a similar mechanism involved in the functional separation of the whole brain from sensory input during sleep (Alper et al., 2006). Contrasting this idea, experiments have shown that whilst there is a positive correlation between delta rhythms and metabolism during wakefulness, the relationship is negative during sleep (Maquet, 1997). This disparity may suggest a functional difference between physiological waking delta oscillations and those seen during sleep that is beyond the scope of this thesis.

1.2.5.1 Mechanisms of delta oscillations

Delta oscillations are believed to have at least two components to their generation – one neocortical, one thalamic. In the thalamus, delta rhythms are generated after neuromodulatory afferent changes from brain stem nuclei (McCormick, 1992; Varela and Sherman, 2009). These brainstem nuclei are responsible for cholinergic and aminergic signalling (dopamine, histamine, noradrenaline and serotonin) in the brain and make up the reticular activating system (RAS) which controls arousal and sleep. Cholinergic neurons within the RAS promote cortical activation via the thalamus, whereas as the activity of brainstem aminergic nuclei is relayed through the hypothalamus. During sleep, neurons in the reticular activating system have a lower firing rate (due to inhibition by GABAergic neurons of the preoptic area). This leads to a reduction in neuronal activity propagated to thalamocortical neurons.
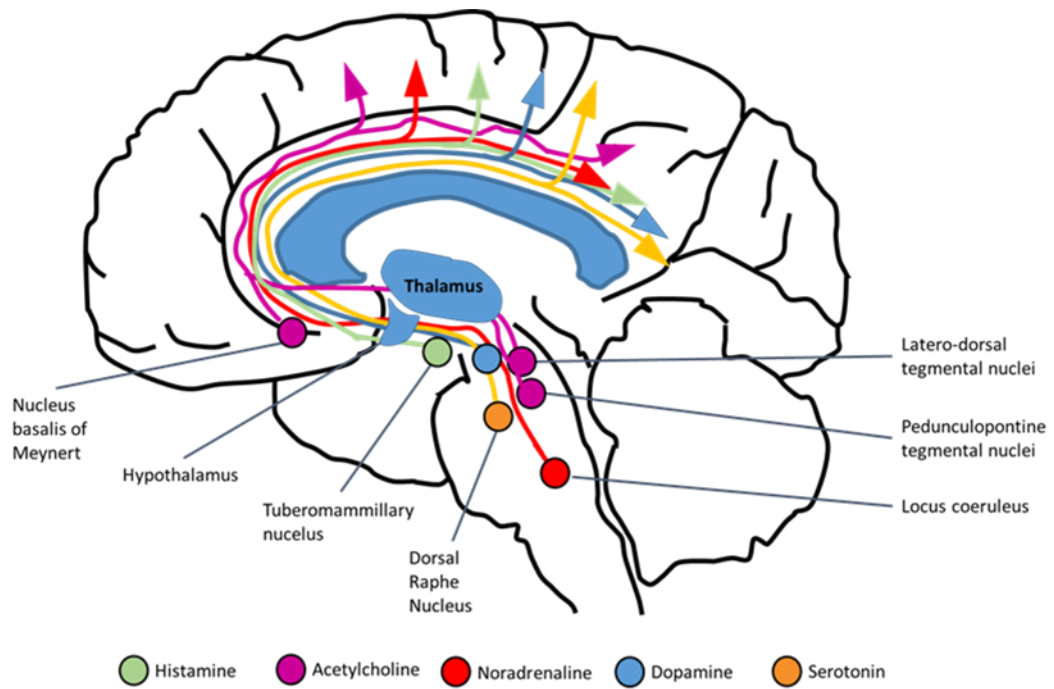
Figure 1.6 A diagram of the reticular activating system in the brain. Activity in the brainstem nuclei controlling cholinergic and aminergic systems is relayed to the cortex via the thalamus and hypothalamus respectively. The activation of these systems increases activity in the cortex and promotes arousal and wakefulness Adapted from Iwanczuck and Guzniczak (2015).

Hyperpolarisation of thalamocortical cells by the reticular activating system generates low threshold spiking (LTS) at 1-2Hz. The delay between periods of this activity occurs due to the time courses of intrinsic conductances expressed by thalamocortical (TC) neurons. This includes the activation and inactivation of the hyperpolarisation-activated (I_h) current and its interaction with the low threshold calcium (I_T) current which occurs after LTS (Soltesz et al., 1991; Brown et al., 2012) as well as the delayed rectifier current (I_K) (Emri et al., 2000). In fact, the ablation of the I_h current (by ZD7288 application abolished TC delta activity) and an increase in I_h also increases this oscillatory activity (Hughes et al., 1998). Furthermore, this thalamic activity can be synchronised by the inhibitory activity of reticular (RE) cells that hyperpolarises TC cells at a membrane potential at which delta frequency LTS occur (Steriade et al., 1991).

However, the importance of the thalamus for conferring and organising oscillations within the cortex is debated. The sheer extent of the thalamocortical projections could allow for the cortical delta rhythm to merely be the propagation of the thalamic oscillation. However, *in vivo* experiments using surgical procedures to isolate the cortex have still shown the presence of 0.1-

4 Hz oscillations, even without thalamic inputs (Kellaway et al., 1966; Timofeev et al., 2000). Indeed, some cortical forms of delta rhythm have been shown to be reliant intrinsic properties of cortical neurons and are reflected in thalamocortical neurons, rather than the other way around (Amzica and Steriade, 1998; Fell et al., 2002). It has also been suggested that during sleep different cortical areas locally generate delta rhythms in a use-dependent manner (Vassalli and Dijk, 2009), a feature that has also been in awake animals. (Vyazovskiy et al., 2011). The association areas of frontal cortex and parietal cortex are the predominant proposed delta rhythm generators in human cortex during sleep (Ioannides et al., 2009), and each cortical region may have its own local delta rhythm generator (Mormann et al., 2008) interacting with the thalamic generators (described above). This occurs through excitatory glutamatergic corticothalamic projections to thalamocortical neurons or reticular neurons. The inhibitory relay through GABAergic reticular neurons to thalamocortical neurons overcomes the direct excitatory feedback (Steriade, 2003).

1.2.5.2 In vitro Delta Oscillations

In vitro preparations have also shown the ability of the isolated neocortex to generate delta oscillations. This requires using a combination of very low levels of the cholinergic agonist Carbachol (10% that used for *in vitro* gamma oscillations) and a dopaminergic (D1R) antagonist SCH23990 to mimic the low dopaminergic tone seen during sleep (Watson et al., 2010) to generate a burst firing pattern from intrinsically bursting (IB) cells in an NMDAR dependent manner (Traub et al., 2017). The periodicity of the delta rhythms is determined by the duration of the after-hyperpolarisation potentials (AHP) of IB cells. The AHPs reflect the inhibitory GABA$_B$ currents which occur in IB cells and are caused by GABA signalling from neurogliaform cells. They cause a refractory period in which the IB cells are hyperpolarised, preventing their firing until the AHP event is over. Layer V regular spiking (RS) neurons are also involved; spiking only a few times per delta period causing (Carracedo et al., 2013). This sparse spiking correlates with EPSPs (~2 per delta period) in layer 2/3 which are thought to converge to facilitate the excitation of burst firing of layer V IBs (Kampa et al., 2006).

Much of what is known about the mechanism of the delta rhythms was studied in the secondary somatosensory cortex as it is known to generate strong delta rhythms in rodents – where it forms part of the parietal cortex - (Carracedo et al., 2013) and in humans (Ioannides et al., 2009).

1.2.5.3 Delta activity and memory consolidation

One of the putative functions of delta oscillations is the consolidation of memories. Consolidation is the process whereby a memory trace, which is the neuronal representation of a recently encoded memory, is stabilised and reinforced. It is a two-part process, with both roles requiring different cortical dynamics. Synaptic consolidation, which occurs during REM sleep (Diekelmann and Born, 2010) (and is thus associated with the theta rhythms) is the process whereby the circuit in which the memory trace exists is strengthened, through molecular mechanisms to increase synaptic efficacy. To transfer the memory held in short term circuits to long-term memory, the process of 'systems consolidation' occurs (Dudai and Eisenberg, 2004). Systems consolidation is thought to consist of many waves of synaptic consolidation that reorganise the representation of a long term memory to dispersed neuronal networks and can occur over a period of months (Dudai et al., 2015). This process happens during SWS when acetylcholine levels are at their lowest (Gais and Born, 2004).

During wakefulness, high levels of acetylcholine have been shown to decrease EPSPs in the feedback pathway from CA3 to CA1 and entorhinal cortex (Rovira et al., 1983; Herreras et al., 1988). This process is known as excitatory feedback suppression and is mediated by high levels of acetylcholine. This limits the spread of information to hippocampal circuits and prevents their interference with memory traces in the cortex. Oppositely, reduced levels of acetylcholine during sleep prevents feedback suppression to allow the transfer of information through the hippocampus to the entorhinal cortex and association cortex to allows the consolidation of memory (Hasselmo, 1999). Although delta oscillations are prevalent during SWS and are known to be associated with low cholinergic tone, little is known about their contribution to this mechanism of memory consolidation.

1.2.5.4 Delta activity and plasticity

Delta band activity is known to increase during sleep with the amount of time spent awake; particularly in areas related to the sensory modality of experience during prior wakefulness (Kattler et al., 1994; Huber et al., 2004; Miyamoto and Murayama, 2016). Some theorise that this is a restorative response to the neuronal fatigue built up by greater firing rates during wakefulness, (Rechtschaffen, 1998; Vyazovskiy and Harris, 2013). To test this theory optogenetics have been used. This uses the delivery of a viral vector to allow local populations of neurons to be stimulated to fire after the delivery of a light pulse. Rodriguez et al. (2016) compared mice that displayed wake-like tonic firing in the frontal cortex when optogenetically

stimulated (during each NREM cycle occurring in the previous 6 hours), with mice that had been sleep deprived for 6 hours by the placement of a novel object in their cage whenever they appeared to be inactive. After treatment conditions, mice were allowed to sleep and their SWA was monitored. It was shown that an increase in the amplitude of SWA only occurs during sleep deprivation and the frequency of 'off' periods of the oscillation increased in correlation with neuronal activity during prior wakefulness. No such changes were seen in the optogenetic stimulated mice. This suggests that the response in SWA is to increases in synaptic strength during wakefulness rather than just a blanket increase in neuronal activity. It may, therefore, follow that SWA is required for the renormalisation of synaptic strength accrued during wakefulness to relieve the metabolic demand.

This is the proposed process at the core of the synaptic homeostasis hypothesis (SHY). This theory suggests that during the wake state there is a net strengthening of synapses in the brain, as a result of the sensory processing and learning that occurs. This leads to a cellular need for space in which to build additional synaptic connections and more energy to strengthen them and maintain them, however, both of these demands are limited. It is suggested that sleep is required to generally normalise these synaptic connections, by globally decreasing synaptic strength so that the process of synaptic strengthening can continue again the following day (Tononi and Cirelli, 2014).

The idea that there is a general decrease in synaptic strength during sleep is corroborated by structural, molecular and electrophysiological evidence. There has been shown to a net loss in number and size of synaptic spines during sleep in Drosophila (Bushey et al., 2011) and mice (Maret et al., 2011). The number of excitatory AMPA receptors is known to be increased during wakefulness and decreased in sleep (molecular markers of synaptic strength) (Vyazovskiy et al., 2008; Lante et al., 2011). Furthermore, sleep also leads to decreased cortical firing rates (Vyazovskiy et al., 2009).

An expansion on the theory also exists suggesting that the decrease in synaptic strength does not affect all synapses, but those which are stronger (with larger spines) are unaffected which improves the increase signal to noise ratio of those synaptic connections. Looking at the physical connections between dendritic spines and axon terminals - called the axon spine interface (ASI) - by electron microscopy has shown that there is a shrinkage of 18% in the area of contact at the ASI during sleep (de Vivo et al., 2017). This also correlated to the size of the dendritic spines,

with the largest 20% of spines being spared. There has also been shown to be a net loss of synaptic spines during sleep (Maret et al., 2011), although it is not clear as to whether it is the smaller spines that are lost.

Further to these structural changes, electrical changes at the synapse and at the neuronal level occur during sleep. In general, the firing rates of neurones are decreased during sleep in the cortex (Vyazovskiy et al., 2009; Watson et al., 2016) and hippocampus (Miyawaki and Diba, 2016). Additionally, the general efficacy of cortico-cortical synapses has been shown to be decreased after sleep (Vyazovskiy et al., 2008). However looking at individual neurons, it was found that their firing rates during sleep are equalised from initially higher or lower rates (Watson et al., 2016). These changes - along with the divergent changes in synaptic size and contact highlighted by de Vivo et al. (2017) suggest that homeostatic rescaling during sleep is more complex than the global downscaling of synapses. It appears that different processes occur at synapses depending on their strength, to increase the 'signal-to-noise' ratio (rather than maintain it as suggested in the general downscaling hypothesis).

Molecular changes at the synapse have been implicated in this synaptic scaling during sleep. Along with the decrease in spines size, the internalisation and dephosphorylation of glutamatergic AMPA receptors in specific synapses occurs during sleep (Diering et al., 2017). The decrease in postsynaptic AMPA receptor number reduces the number of cations entering through the associated ion channels after glutamate binding, and thus decreases the size of EPSPs propagated across the synapse as the postsynaptic membrane (Luscher et al., 1999). The ability of spines to regulate their synaptic homeostasis in response to local activity (through this AMPA receptor endocytosis) requires the activity of the immediate early gene Arc (Béïque et al., 2011), which is discussed further below and is a focus of this thesis.

A further link between AMPA receptor internalisation and sleep is through adenosine signalling. Adenosine receptor activation is known to cause the internalisation of AMPA receptors (Chen et al., 2016). Furthermore, the accumulation of adenosine during wakefulness is known to lead to the inhibition of the aminergic systems of the reticular activating system *(see Chapter 1.2.4.1 and Figure 1.4)* otherwise promote wakefulness and activate the cortex after conscious disconnection during sleep. Adenosine accumulation causes the disinhibition of GABAergic neurones of the ventrolateral preoptic area which in turn causes the inhibition of aminergic and cholinergic nuclei of the reticular activating system to promote sleep (Pace-Schott and Hobson,

2002). Adenosine also directly facilitates SWA in thalamocortical neurons (Pape, 1992). It is likely that synaptic plasticity through NMDAR activation would lead to an increase in adenosine concentrations in thalamocortical circuits and thus subsequently increases SWA (Bjorness and Greene, 2009), as NMDAR activation is known to increase adenosine concentrations in brainstem cholinergic nuclei (Brambilla et al., 2005).

The cholinergic system plays an important role in the presence of SWA. Increased cholinergic tone to levels associated with wakefulness inhibits SWA in cortical neurons (Marrosu et al., 1995), and is managed by adenosine-1 receptor (A1Rs) activation which inhibits acetylcholine release from tegmental nuclei and the nucleus basalis of Meynert to decrease arousal (Porkka-Heiskanen et al., 1997).

Dopamine is also crucial in controlling the sleep-wake cycle, with dopaminergic cells in the ventral tegmental areas responsible for controlling arousal (Monti and Jantos, 2008). Stimulants that increase dopamine signalling either through the KO of the dopamine transporter (Wisor et al., 2001) or through the exogenous activation of dopamine receptors (Isaac and Berridge, 2003) all serve to promote wakefulness. Whereas the antagonism of the receptors has the opposite effect (Monti et al., 1990). Antagonism of hippocampal D1 receptors has also been shown to have a negative effect on the persistence of fear memory (Rossato et al., 2009), which may point at a role of low dopamine in the processed of depotentiation needed for synaptic rescaling.

1.3 Immediate early genes (IEGs)

To quantify activity and plasticity levels associated with wake and sleep rhythms this thesis uses immediate early genes as markers. Immediate early genes (IEGs) are the first genetic response to cellular signals and their transcription is rapidly induced (in as little as 15 minutes) in response to a wide variety of stimuli (Hu et al., 1994). Many IEGs are transcription factors and as such are involved in triggering a cascade of activation that leads to the downstream expression of further genes and cellular effects. These effects relate to the classes to which the IEG belongs, with some (regulatory transcription factors) exerting a wide cellular effect through the genes they activate, whereas others have a more focussed role in specific cellular processes (Guzowski et al., 2001). The experiments performed here used 2 IEGs as activity/plasticity markers: *c-fos* and *Arc*.

1.3.1 *C-fos* - Finkel–Biskis–Jinkins osteogenic sarcoma homologue

C-fos is a member of the Fos family of transcription factors. It was originally discovered as a proto-oncogene and is the mammalian homolog of the Finkel-Biskis-Jinkins osteogenic sarcoma virus gene that was found in mouse tumours (Finkel et al., 1966). It is now known to be an immediate early gene due to its rapid transcriptional induction and has been used as a marker for recent neuronal activation (Morgan and Curran, 1989; Hoffman et al., 1993).

The c-fos protein contains a region common to many transcription factors, known as the leucine zipper. It is so called as every seventh amino acid in its sequence is a leucine residue. This zipper allows the heterodimerisation of c-Fos protein with Jun family proteins such as c-Jun – a product of another immediate early gene (Gentz et al., 1989; Turner and Tjian, 1989). This heterodimer forms the protein complex known as AP-1 (Activator Protein 1) that acts as a transcription factor involved in many cellular processes. The c-Jun protein can also homodimerize in the absence of c-Fos, but in this form, its binding affinity for DNA is 25 times less that of the AP-1 complex (Halazonetis et al., 1988).

1.3.1.1 C-fos as a marker of neuronal activation

The low expression of *c-fos* in basal conditions allows its transcription and translation to be accurately monitored. As *c-fos* is an immediate early gene, the time-scale of its upregulation is relatively fast, with *c-fos* mRNA levels peaking after 30 minutes and protein expression being elevated from 60 minutes after the induction stimulus (Morgan et al., 1987).

Early studies that examined the activity-dependent expression of *c-fos* did not look at single neurons but at changes in expression in neuronal populations in response to a wide variety of stimuli. These studies showed *c-fos* expression could be induced in certain brain areas in response to: noxious sensory stimulation (Hunt et al., 1987; Coggeshall, 2005) sciatic nerve stimulation (Bojovic et al., 2015), dehydration (Carter and Murphy, 1990) myocardial infarction (Ahn et al., 2015)**,** seizure (Morgan et al., 1987), (Smeyne et al., 1992), instrumental learning (Svarnik et al., 2005), novel environment exposure (VanElzakker et al., 2008) and various stressors (Chowdhury et al., 2000; Ubeda-Contreras et al., 2018).

To understand the mechanism behind *c-fos* induction, it is important to see how *c-fos* upregulation occurs in single cells. It is now known that *c-fos* expression can be induced in neurons by membrane depolarisation, as well as brain-derived neurotrophic factor (BDNF)

signalling and Forskolin application (i.e. increased cAMP levels) (Joo et al., 2016). These stimuli induce *c-fos* gene expression through the activation of the transcription factors CREB and SRF by protein kinases, such as Ca^{2+}/calmodulin-dependent protein kinases, MAP kinases and protein kinase A (West and Greenberg, 2011). Furthermore, from experiments using Channelrhodopsin-2 transfected pyramidal hippocampal cells, trains of action potentials were stimulated, firing spikes in response to light pulses. Stimulation in this way increased in the expression of c-Fos protein in single neurons in an NMDA and AMPA receptor-independent manner; though it required the activity of the sodium channels (Schoenenberger et al., 2009). This suggests that neuronal output (action potentials) alone are sufficient to upregulate *c-fos* expression.

The situation becomes a little more complex when it is considered that generation of antidromic action potentials causes an insignificant increase in *c-fos* mRNA levels in magnocellular neurons of the hypothalamus, compared to muscarinic acetylcholine activation by carbachol (Luckman et al., 1994). Whether this discrepancy is due to the cell types involved, or different stimulation regimes, is uncertain. It does suggest however that *c-fos* expression may be specific to orthodromic action potentials alone, a factor that may influence its use as a marker for activity during persistent gamma rhythms (see above).

Further evidence also suggests that the mechanism of neuronal *c-fos* induction is more complicated than a straightforward orthodromic action potential leading to *c-fos* transcription relationship. At least in terms of the amount of expression, it has been shown that under seizure stimulation the number of action potentials is not correlated with the magnitude of *c-fos* induction (Labiner et al., 1993). There is also no direct correlation between the percentage of c-Fos-positive neurons and percentage of active neurons (Svarnik et al., 2005). This is emphasised by Kovacs (2008) who points out that if depolarisation alone were sufficient to induce the expression of *c-fos*, then under basal conditions there would be robust staining in millions of cells throughout the brain, which is not the case.

In addition, c-fos expression has been shown to exhibit a high degree of region-specificity. For example, in an appetitive reaching task, the motor cortex showed no induction of c-Fos protein, whereas the retro-splenial cortex (involved in 'learning' the task) showed a significant increase (Svarnik et al., 2005). During different stress conditions, different patterns of up and downregulation of c-Fos expression are seen within different regions of the brain related to the

intensity of the stress and also qualitative aspects of the stressor (Chowdhury et al., 2000; Ubeda-Contreras et al., 2018).

Therefore, it seems that *c-fos* is induced not by the simple firing of action potentials in existing patterns, but to *changed* patterns of neuronal activity (Svarnik et al., 2013). This may explain why stimulation of unusual brain activity (e.g. evoked seizures) and behavioural tasks that involve the activation of new circuits induce *c-fos* expression.

This is particularly true for a novel experience (VanElzakker et al., 2008), visual stimulation (Rosen et al., 1992) and learning (Anokhin et al., 1991; Kleim et al., 1996) where the induction of *c-fos* expression was seen to be specifically increased in cortical areas related to the task. This increase was not seen in control animals or those repeating already learned behaviour.

1.3.1.2 C-fos and memory

The above evidence suggests that *c-fos* expression may be related to the formation of memory and its persistence. This has also been more directly tested, with evidence showing that delayed expression of *c-fos* mRNA is necessary for the persistence of a long-term memory trace that would have otherwise have decayed (Katche et al., 2010).

Looking more in depth at the mechanism to link learning and memory to *c-fos* expression, it has been shown that using chemical and electrical methods that induce synaptic plasticity - through long-term potentiation (LTP) - cause increases in c-Fos protein (Abraham et al., 1991). However, the amount of LTP evoked by this method does not correlate with the extent of *c-fos* induction (Dragunow et al., 1989)**.** This suggests that either there is a non-linear relationship between LTP induction and *c-fos* expression, or it may be neuronal activation and not the potentiation of the synapse that causes the *c-fos* upregulation. Brain-specific *c-fos* knockout mice have been used to directly interrogate the role of *c-fos* in plasticity and memory. Using the Cre/LoxP system to ablate *c-fos* expression in nestin-expressing cells, Fleischmann et al. (2003) showed that knockout of *c-fos* from the CNS led to impaired spatial memory and a concurrent decrease in LTP between CA1 and CA3 regions of the hippocampus.

Although these studies all link changes in the levels of c-Fos directly and indirectly to synaptic plasticity, they do not suggest the mechanism of molecular involvement of c-Fos in this process. C-Fos likely acts through AP-1 in the process of synaptic plasticity. AP-1 regulates the expression

of plasticity-associated genes (Eagle et al., 2016) including BDNF (Tuvikene et al., 2016) and cyclic AMP response-element-binding protein (Sanyal et al., 2002). AS induced BDNF and CREB can further activate transcription to regulate synaptic strength and number, AP-1 mediated gene expression appears to act via positive feedback loops to influence synaptic plasticity.

1.3.2 *Arc* - Activity-related cytoskeleton-associated protein

Another immediate early gene, with a more direct link to synaptic plasticity, is the activity-regulated cytoskeleton-associated protein, *Arc* (also known as Arg3.1). Most immediate early gene products are translated in the cell body where they remain to mediate their cellular actions (Wallace et al., 1998). *Arc* is a neuron-specific IEG and its expression is regulated at the level of transcription, mRNA trafficking and protein translation. Synaptic activity not only induces *Arc* mRNA but also triggers the trafficking of *Arc* mRNA to dendrites where it is subsequently locally translated (Steward et al., 1998)*.* Its increased expression has been related directly to learning and memory and has been shown to participate in several different forms of synaptic plasticity.

1.3.2.1 Arc and long-term potentiation

Early studies on *Arc* induction showed that *Arc* mRNA and Arc protein were seen to be increased for up to 4hrs by high-frequency stimulation (400Hz); known to induce LTP (Lyford et al., 1995). This increase was blocked by pre-treatment with the NMDA receptor antagonist MK801, which suggested that NMDA receptor-dependent signalling cascades are, at least in part, responsible for the increase in *Arc* mRNA (Link et al., 1995). The role of Arc in LTP was found to be related to its involvement in the stabilisation and growth of filamentous actin in the synaptic cytoskeleton (Guzowski et al., 2000; Messaoudi et al., 2007).

Arc expression can also be induced chemically (with BDNF, bicuculline or glutamate) rather than with electrical stimulation, in an NMDAR dependent manner. Whilst NMDA receptor activation induces Arc expression the activation of AMPA receptors have been shown to inhibit Arc expression. Rao et al. (2006) showed that the inhibition of AMPA receptors with NBQX and GYKI 52466 had the opposite effect, increasing both basal and BDNF-induced Arc expression. This suggests that *Arc* expression is balanced by NMDAR and AMPAR activation.

The knockout of *Arc* impairs spatial learning (Managò et al., 2016), fear conditioning (Gouty-Colomer et al., 2016) and taste aversion (Plath et al., 2006), due to impaired long-term memory related to late-phase LTP. This occurs despite intact short-term memory and increased early

phase LTP (Plath et al., 2006). Using antisense oligonucleotides to inhibit Arc protein expression leads to impaired maintenance of LTP but does not affect its induction (Guzowski et al., 2000; Messaoudi et al., 2007). It also appears that inhibition of such maintenance of LTP impairs memory consolidation (Guzowski et al., 2000; Bramham et al., 2010).

1.3.2.2 Arc and Long-Term Depression

Although the process of memory consolidation requires the strengthening of more important memories, forgetting things that are trivial or unimportant is also crucial. This would require the weakening of synaptic strength which occurs in by a process called long-term depression (LTD) (Tononi and Cirelli, 2014). In this process, metabotropic glutamate receptors (mGluR) can reduce synaptic strength between neurons through mGluR dependent-LTD (Lüscher and Huber, 2010). One of the key mechanisms that underpin this, which Arc plays a role in, is the rapid endocytosis of AMPA receptors from the post-synaptic membrane (Wall and Correa, 2018). This, in turn, reduces the post-synaptic response to glutamate release. This is likely to be an important factor in the process of memory consolidation during sleep, since AMPA receptors in synapto-neurosomes (isolated synaptic vesicles and terminals from brain homogenate) have been shown to be decreased in rat brains at the end of the rest phase (when 75% of the previous dark phase was spent awake) compared to the active phase (when 75% of the light phase was spent asleep) (Vyazovskiy et al., 2008).

Arc enables AMPAR endocytosis through its interaction with two endocytic proteins endophilin and dynamin that bring AMPA receptors into endosomes where they are recycled, lysed or trafficked to the nucleus (Chowdhury et al., 2006; Rial Verde et al., 2006; Shepherd et al., 2006). This process is crucial in the rescaling of synapses during sleep (Diering et al., 2017) and is crucial for the maintenance of synaptic homeostasis and memory consolidation. This mGluR-LTD can be induced electrically with low-frequency stimulation (LFS) or pharmacologically using dihydroxyphenyl-glycine (DHPG) as an exogenous agonist for the mGluR-1 and 5 (Waung et al., 2008). Blocking Arc gene expression inhibits the induction of LTD by either method (Park et al., 2008).

1.3.3 General IEG changes during different brain states

The expression of IEGs in the brain been compared between sleep and wakefulness by cDNA microarray. *C-fos* (Cirelli and Tononi, 1999) and *Arc* (Cirelli and Tononi, 2000b) mRNA levels were increased in all layers of the cortex after 3 hours of spontaneous wakefulness (SW – where the

animals spent >75% of the last 3 hours awake) compared to spontaneous sleep (SS – animals spent >75% of the last 3 hours asleep). There was no significant difference between 3 hours SW and 3 hours sleep deprivation (SD – by stroking with a paintbrush once animals appeared drowsy), and after 24 hours SD the IEG expression was lower still (Cirelli et al., 1995). These comparison studies were carried out on wide regions of the brain rather than specific areas, so the increases are general during the awake state compared to sleep, which would point to a general decrease in synaptic strength during sleep. This contrasts with other studies looking at regional changes to immediate early gene levels during post-learning sleep.

1.3.4 Regional IEG changes across brains states

Regional differences in IEG expression have been related to synaptic plasticity and IEG expression is increased in certain areas of the brain as a result of learning tasks in rats and mice. During REM sleep, animals recently exposed to a visually enriched environment showed a significant increase in the expression of the plasticity-related gene IEG *zif268* in the cortex and hippocampus during subsequent REM sleep (Ribeiro et al., 1999). Further to this, there is a positive correlation between the amplitude of spindle firing events (which exist in the transition between REM and SWS) and the level of IEGs such as Arc (Ribeiro et al., 2007)*.* Other studies have shown a link between zif268 and consolidation of fear conditioning memories in the hippocampus (Lee et al., 2004), which seems to point at a role of sleep and the long-term preservation of memories. These studies suggest a relationship between certain brain states and synaptic plasticity. Since neural oscillations vary during different brain states too, it is thought that they may have a part to play in this memory formation and plasticity.

This is reinforced by findings that link the expression of c-Fos (an IEG marker for 'new' patterns of cellular activation, see above) and Arc (an IEG core to mechanisms of neural plasticity) with task-related sleep slow wave activity (SWA). In mice performing a unilateral reaching task, there was an increase in SWA in the learned hemisphere. This was seen in conjunction with an increase in Arc and c-Fos protein levels (Hanlon et al., 2009). The relationship between REM sleep and memory consolidation has also been investigated as REM is the sleep stage that is classically associated with theta frequency oscillations. These theta oscillations are thought to induce synaptic memory in the form of late LTP in the hippocampal CA1 region (Huang and Kandel, 2005).

1.4 Neuroinflammation

Neuroinflammation is the normal response of the immune system of the CNS to the presence of foreign material and damaged endogenous cells that may prove harmful to the surrounding nervous tissue. Associations have been discovered between neuroinflammation and altered sleep patterns (Mullington et al., 2010). The cause and effect of these associations appear to go both ways, with sleep loss in humans inducing increases in proinflammatory markers in the blood inflammatory (Vgontzas et al., 2004; Irwin et al., 2008) and infusion of proinflammatory cytokines promoting sleep in animals (Krueger et al., 1984). Furthermore, the immune challenge in humans prior to sleep reduces the duration of REM sleep, but increase the time spent in NREM sleep with no effect of oscillatory amplitude (Pollmacher et al., 1993). However if the inflammatory challenge occurs during sleep there is no alteration in the duration of any sleep stage but increases in delta and theta power during NREM sleep are seen (Haack et al., 2001).

There have also been many studies to look at the relationship between inflammation and cognitive function**.** Neuroinflammation had been associated with deficits in attention (Holden et al., 2008), working memory (Buchanan et al., 2008), contextual fear memory (Barrientos et al., 2009a) episodic and spatial memory (d'Avila et al., 2018) and object recognition memory (Hirshler et al., 2010) in animals. Similar associations have been seen in humans with increases in inflammatory markers associated with mild cognitive impairment (Magaki et al., 2007), decline in verbal and non-verbal memory (Reichenberg et al., 2001) as well as specific cognitive tests after stroke (Rothenburg et al., 2010) and normal ageing (Dik et al., 2005; Simen et al., 2011). Therefore neuroinflammation is considered in this thesis as a potential means to perturb the pattern of cortical dynamics and subsequently change IEG markers. These are quantified in the early sections of this thesis.

The inflammatory environment can be triggered in the brain after a physical, pathogenic, toxic, or autoimmune insult. Whilst most disease-relevant cases relate to chronic neuroinflammation, it can also occur acutely, most commonly related to a physical brain injury sustained during contact sports. Neuroinflammation may also manifest aberrantly, where the response to the above insults is excessive. In these cases, the normal, healthy aspects of neuroinflammation can become part of primary pathology. Whilst the peripheral immune system is responsible for initiating an inflammatory response to fight infection and remove foreign agents, under normal conditions peripheral immune cells are restricted from entering CNS tissues by the blood-brain barrier (BBB). However, in the case of brain trauma or disease conditions infiltration may occur.

Thus, any study of neuroinflammation secondary to systemic infection (or model thereof) needs to consider the BBB.

1.4.1 The blood-brain barrier

The blood-brain barrier (BBB) is a unique feature of the microvasculature of the CNS. It prevents the passage of larger objects and molecules (such as bacteria) from the circulation into the CSF whilst allowing the movement of smaller homeostatic molecules necessary for the maintenance of the CNS tissue. The BBB is mainly formed by specialised endothelial cells (ECs) that are 39% thinner than ECs in other tissues. This allows faster diffusion of water, gases and lipid-soluble molecules to provide nutrients more easily for the highly metabolically active CNS tissue (Coomber and Stewart, 1985)**.** The ECs of the CNS are uniquely held together by tight junctions that limit the paracellular flow of solutes between the blood and the extracellular environment of the CNS (Brightman and Reese, 1969).

Transcellular movement across the BBB ECs occurs through several systems. Gases (O_2 and CO_2) and smaller polar molecules can diffuse across easily across the BBB. The passive movement of ions and smaller molecules occurs through channels, whilst active transport of molecules also occurs across the BBB, which expresses high levels of the glucose transporter (GLUT1) (Boado et al., 1994) and amino acid transporter (LAT1) (Boado et al., 1999)**.** Larger molecules are carried across the blood-brain barrier in vesicles and it is this transcytosis that is also of high importance for the delivery route of drugs across the BBB (Andreone et al., 2017)**.**

Other cells and structures support the BBB. Astrocytes ensheath blood vessels and neurons and provide communication between neurons and contractile pericytes (PCs) to allow changes in blood flow (through alterations in vascular diameter). This allows the provision of a nutrient supply to be tailored to the tissue's requirement, often in accordance with neuronal activity (Gordon et al., 2011). A basement membrane is also provided by PCs and ECs to provide structural integrity to the neurovascular system.

Although the blood-brain barrier is designed to isolate the brain from the inflammatory environment of the body, a systemic infection can still affect the CNS. This can occur through several means: using the BBBs para- or transcellular mechanisms for the transport of inflammatory signalling molecules or through immune cells; entry by the disruption of the blood-

brain barrier or through the circumventricular organs; or through the peripheral activation of the autonomic nervous system sending signals to the brains (Varatharaj and Galea, 2017).

1.4.2 Microglia

The blood-brain barrier keeps the CNS isolated from pathogens that may be present in the peripheral circulatory system, however, this also means that it is separated from the peripheral immune system. Therefore, the CNS has specialised resident immune cells called microglia, which are responsible for the coordination of the brain's immune response. Infections in the CNS occur infrequently however and recently studies have found microglia have a wide range of other roles in neuroprotection (Vinet et al., 2012) and in the pruning of neuronal processes and synapses (Paolicelli et al., 2011).

Microglia are derived from myeloid progenitor cells in the embryonic yolk sac during development (Ginhoux et al., 2010). The maintenance of the microglia population post-development primarily involves self-replication in the CNS rather than replenishment from the circulation (Ajami et al., 2007) as is the case with other tissue-resident macrophages such as Kupffer cells in the liver (Hashimoto et al., 2013).

Microglia exhibit two main functional morphological states in the brain. In the healthy brain, they are found in a 'resting state' - these microglia have a ramified morphology with small cell bodies and many-branched processes. Despite being 'at rest', ramified microglia are in fact very active as their projections survey their microenvironment for damage or pathogenic signals (Nimmerjahn et al., 2005).

Microglia can be activated by TLRs (Toll-like receptors), which are pattern recognition receptors that detect certain sequences in pathogens, known as pathogen-associated molecular patterns (PAMPs) types. There are 9 subtypes of TLRs found in the human brain (Bsibsi et al., 2002) which recognise and initiate immune responses to different pathogens. They also respond to the presence of pro-inflammatory cytokines (Hanisch, 2002), apoptotic and necrosis signals (Burguillos et al., 2011), lipopolysaccharides (Chen et al., 2012) and viral RNA (Zhu et al., 2016). Microglia are also very sensitive to increases in extracellular potassium (Gehrmann et al., 1995) which occurs after the rupture of neurons.

Upon activation, microglia begin proliferation (Gómez-Nicola et al., 2013) and begin to change morphology. This involves the retraction of the branches used to detect the pathogenic signals and an increase in motility, migrating to the site of injury where they can phagocytose the foreign material. They also begin feedforward signalling mechanisms whereby they release proinflammatory cytokines to activate more microglia, perpetuating the innate immune response.

1.4.3 Cytokines and chemokines

Cytokines are very important signalling molecules between cells and differ from hormones in that their circulating concentrations are more variable and are released and used by a large range of cell types. These include macrophages, microglia, B cells, T cells, mast cells, neutrophils, basophils and eosinophils. Different cytokines can be released by different cell types and can also act on cell types, often with multiple cytokine subtypes have similar functions (Zhang and An, 2007). Neuroinflammation is induced and propagated by a subset of these cytokines known to be pro-inflammatory. They play roles in recruiting microglia to limit the damaging effect of pathogens and necrotic/apoptotic cellular material (Kim et al., 2016). As well as cytokines that perpetuate the inflammatory response, there are also anti-inflammatory cytokines that modulate the response. This anti-inflammatory, negative feedback helps reinstate the homeostasis of the brain (Opal and DePalo, 2000). Chemokines are also at work during inflammation to act as chemo-attractants for immune cells like microglia (Ransohoff et al., 2007). They are a critical component of the neuroinflammatory response so are considered separately below.

1.4.3.1 Tumor Necrosis Factor Alpha (TNFα)

TNFα has emerged as one of the most important proinflammatory cytokines in mediating a suitable and sufficient inflammatory response to pathogen or damage. TNFα has been shown to be produced by many cells including neurones and other immune cells such as neutrophils, eosinophils, CD4+ T cells and natural killer cells (Gahring et al., 1996). In the CNS, microglia are the predominant producers of TNFα (Gregersen et al., 2000) and therefore are likely to work in an autocrine (self-stimulating) positive feedback loop (Kuno et al., 2005). They are also driven by its release to begin phagocytosing material, particularly neurons (Neniskyte et al., 2014). TNFα is in part responsible for the chronic pathological activation of microglia that is common in neurodegenerative disorders such as Alzheimer's (Combs et al., 2001) and Parkinson's disease (Barcia et al., 2011)

Cultured TNFα null microglia that are activated by lipopolysaccharide treatment have been shown to secrete lower levels of several other cytokines (IL- 1β, IL-6, IL-10 and IL-12) suggesting that TNFα is also important in propagating the inflammatory cascade (Harms et al., 2012). It is also known that a deficiency in TNFα causes a decrease in the activation of microglia (Sriram et al., 2006).

One of the signalling pathways through which TNFα is released is through metabotropic glutamate receptors present on microglia. mGluR2 activation induces neurotoxicity through the enhanced release of TNFα and downstream activation of the apoptotic pathway protein caspase 3 (Taylor et al., 2005). Interestingly activation of microglia is decreased after activation of mGluR3, which thus has an opposite, neuroprotective effect compared to mGluR2 (Taylor et al., 2003).

1.4.3.2 Interleukins

Interleukins are also important signalling cytokines in the inflammatory response, and there are pro- and anti-inflammatory subtypes meaning they are involved in the initiation and regulation of the immune response. The main proinflammatory interleukins are IL-6, IL-1α and IL-1β. The latter two are the two most studied of the 11 cytokines in the IL-1 subfamily and they possess the strongest proinflammatory effect (Dinarello, 2011). They bind to IL-1R1 (the IL-1 Receptor type 1) which causes the activation of the myeloid differentiation primary response 88 (MYD88) pathway (Weber et al., 2010). This can also activate other key proinflammatory cytokines TNFα and IL-6 (Oppenheim et al., 1989).

It is assumed that IL-1α and β have redundant effects as they can both bind to the same receptor however it has been shown they more often act in important independent roles. IL-1α can signal to the innate immune system through its action as a damage-associated molecular pattern signalling molecule. This highlights its importance in the stimulation of an inflammatory response in conditions devoid of infection such as brain injury or stroke (Luheshi et al., 2011). IL-1β release can then be stimulated by IL-1a. This then allows the perpetuation of the immune response through the activation of microglia (Monif et al., 2016).

IL-6 is another proinflammatory interleukin, which has been shown to be expressed by microglia and astrocytes (Frei et al., 1989). It can also be expressed by neurons, an induction that is stimulated by IL-1β and TNFα (Ringheim et al., 1995), or even the depolarisation of neurons

(Sallmann et al., 2000). These cytokine signalling molecules may transfer systemic inflammation to the CNS due to their ability to cross the BBB (Banks et al., 1995).

Of the anti-inflammatory interleukins, IL-13 and IL-4 are particularly important as they work together to exert their neuroprotective effects. The genes encoding for IL-13 and IL-4 are at similar loci on chromosome 5 and their receptors exist in a complex through which they exert their anti-inflammatory effects (Rael and Lockey, 2011). Once the receptor complex is activated it causes the activation (through phosphorylation of the transcription factor STAT6) of anti-apoptotic genes (Ohmori and Hamilton, 1998). IL-4 and 13 signalling also cause the inhibition of inflammatory cytokine production (Minty et al., 1993). This is through a change to the microglial expression of other cytokines: decreasing TNF and increasing insulin-like growth factor 1 (IGF-1) (Butovsky et al., 2005). IL-4 also acts on astrocytes inhibiting their activation and reactive oxygen species production and inducing NGF to release all of which are immunosuppressive effects (Brodie et al., 1998).

1.4.3.3 Chemokines

Chemokines are a family of chemotactic peptides involved in the inflammatory response. They are divided into four main classes (CXC, CC, CX3C and XC), which are linked to the nomenclature describing the chemical structure of their receptors (CC chemokines bind to CC receptors). The chemokines themselves are named I recognition of the amino acid chain of the N-terminus of their structure, be it with two adjacent cysteine residues (CC) or with up to three amino acids between these cysteine residues (CX3C) (Lata and Raghava, 2009). There are 48 chemokines across these groups but only 19 receptors (Zlotnik and Yoshie, 2012), suggesting a complex ligand-receptor relationship. Indeed some chemokine-receptor relationships are exclusive, whereas other receptors have up to 10 ligands (Ransohoff, 2009).

Chemokines exert their effects through these G-protein coupled receptors (Murphy, 1994) whose binding leads to the release of calcium from intracellular stores which activates MAP kinases. One of the major effects this mechanism plays a role in is the mediation of chemotactic effects (Murdoch and Finn, 2000). This chemotaxis is caused by the chemoattractant nature of chemokines which cause cells to follow increased concentrations of the chemokine to its source. It has been shown that in response to even a small chemoattractant gradient, neutrophil cells can amplify the asymmetry by upregulating the polymerisation of actin preferentially at the leading edge of the cell (Weiner et al., 1999). This occurs through the increased signalling of

receptors and downstream protein kinase upregulation (Servant et al., 2000) as receptors have been shown to be evenly distributed throughout the membrane of neutrophils (Servant et al., 1999).

Functionally chemokines are split into two groups. Homeostatic chemokines are constitutively expressed in certain tissues or cells to exert roles in cell migration (particularly leukocytes) for the development and maintenance of cells and tissues. Inflammatory chemokines are only seen in meaningful concentrations during infection or injury to attract leukocytes and other immune cells to the site of damage. There appears to be much more cross-talk between inflammatory chemokines and as such some of their receptors and ligands have been labelled as redundant, however, this is controversial (Schall and Proudfoot, 2011).

Some chemokines are also involved in the chemotaxis of microglia to the site of inflammation. Such chemokines like Fractalkine (CX3CL1) are mainly expressed by neurones and act as chemo-attractants for microglia (Harrison et al., 1998), which exclusively house the receptor CX3CR1). In fact, this is an example of the importance of chemokine signalling in neuronal-microglia interactions (Paolicelli et al., 2014; Eyo et al., 2016).

This also points towards a neuroinflammatory role of chemokines, as dysregulation has been shown to play a role in pathologic, chronic inflammation in the brain, just as with cytokines (Ransohoff et al., 2007; Ramesh et al., 2013; Thuc et al., 2015).

1.4.4 Neuroinflammation in disease

Although inflammation is a by-product of the clearance and/or repair of damaging material, sometimes the inflammatory condition becomes protracted and the protective mechanism it serves becomes damaging. This is a known feature of many neurodegenerative disorders and may be the function of an exaggerated reactive state of microglia in the healthy brain, causing an augmented pro-inflammatory response (Godbout et al., 2005). Chronic neuroinflammation of this kind is a common pathology in many neurodegenerative disorders such as Alzheimer's and Parkinson's diseases.

Alzheimer's disease is a typical disease in which neurodegeneration is becoming increasingly related to an uncontrolled or exacerbated neuroinflammatory response (Heneka et al., 2015). The presence of plaques of aggregated insoluble β-amyloid, created from the improper cleavage

of amyloid precursor protein (APP), is a hallmark of the disease. Other features include tangles of the hyperphosphorylated tau protein, neuroinflammation and neurodegeneration (Duyckaerts et al., 2009). Amyloid plaques are associated with a pro-inflammatory response through activated microglia and astrocytes. TLR 2 and 4 are the pattern recognition receptors for β-amyloid, and their blockage (Udan et al., 2008) or knockout (Reed-Geaghan et al., 2009) causes a reduced inflammatory response in microglia to β-amyloid.

1.4.4.1 Peripheral infiltration of immune cells

Despite the existence of the blood-brain barrier, it is still possible for microglia to be activated without any physical changes to the BBB. This is triggered through direct TLR ligand or cytokine signalling from a peripheral immune response at regions of the brain that lack the protection of the tight vasculature. These areas are known as circumventricular organs and are areas where pro-inflammatory agents can pass more easily from the bloodstream to the parenchyma

Furthermore, although microglia are the resident macrophages in the CNS, peripheral immune cells can be often seen in the CNS during severe peripheral infections. This infiltration is due to the pathological breakdown of the blood-brain barrier and is usually associated with the breakdown of the tight paracellular junctions than an increase in transcellular permeability (Stamatovic et al., 2008). Microglia are even known to increase the permeability of the BBB to peripheral immune cells through the release of cytokines (Prat et al., 2001). It is also possible that peripheral immune cells such as macrophages and T cells can interact with the healthy BBB themselves to enter the CNS (Daneman and Prat, 2015).

1.4.4.2 Peripheral infections and neurodegeneration

The idea that peripheral infections have some association with neurodegenerative diseases is well known and many studies support some sort of link, however, the cause and effect of these is unclear. In fact, there have been many examples linking specific pathogens with neurodegenerative disorders (McManus and Heneka, 2017).

In patients with dementia, there are many studies reporting correlations between underlying illnesses and the progression of dementia. In a study of patients living with various dementias, patients with underlying conditions had significantly decreased cognition and general function scores (Hodgson et al., 2011).

Illnesses, and in particular viral infections have been shown to contribute to cognitive decline in dementia patients (Strandberg et al., 2004). Severe infections leading to sepsis are also known to cause a permanent cognitive disturbance in the elderly (Widmann and Heneka, 2014). These infections can lead to delirium, and it has been shown that whilst patients may improve upon treatment of the infection, long-term the incidence and progression of dementia progression is far worse than in control subjects (Davis et al., 2012)

This is particularly prominent when the infection causes delirium in Alzheimer's disease patients. In this case, the rate of cognitive decline nearly doubles (Fong et al., 2009). To make matters worse, infectious diseases are more common in patients with dementia than in healthy aged-matched controls (Natalwala et al., 2008). The related potentiation of neurodegeneration has been seen in to be mediated by a long-term upregulation of pro-inflammatory cytokines such as IL-1β and TNFα, even after the systemic infection is over (Holmes et al., 2003; Holmes et al., 2009).

Other non-dementia type neurodegenerative disorders have shown links between peripheral infections and their progression. The bacteria Clostridium *perfringens* was first seen in humans in the gut biota of a patient with multiple sclerosis. This bacterium releases a toxin (epsilon toxin) which has a 10-fold incidence in multiple sclerosis CSF samples, compared to those from healthy subjects (Rumah et al., 2013). Also, in mouse models of Parkinson's disease, α-synuclein deposition increases in transgenic mice that are administered samples of PD patients' gut bacteria. This has been shown to increase their motor deficits (Sampson et al., 2016). This highlights the importance of peripheral viral and bacterial infections on the brain, particularly in patients with genetic risk factors for neurodegenerative disorders.

1.4.4.3 Investigating peripheral infection effects on brain oscillations and plasticity
Studies investigating the effects of peripheral inflammation often use synthetic analogues of ligands for TLR receptors to induce an inflammatory response. This allows immune challenges (such as bacterial or viral infections) to be mimicked, which elicits a particular response that is mediated through the TLR that is targeted. It also allows the control of the strength of the infection through the dose of the infectious agent, and the time scale to compare acute to chronic or repeated infections. In this thesis, 2 models of peripheral infection are used: lipopolysaccharide and Poly Inosinic: Cytidylic acid administration.

Lipopolysaccharide (LPS) is a large molecule on the extracellular membrane of gram-negative bacteria that is recognised by the immune system causing the mobilisation of a response to the pathogenic bacteria. Isolated preparations of LPS can be used to mimic a bacterial infection. The recognition of LPS is through its structure as a ligand that specifically activates TLR4 receptors, and it is widely used to study the effects of systemic infection on the brain. It is thought that LPS in the blood activates TLR4 receptors in the circumventricular organs, which leads to the production of tumour necrosis factor (TNF). TNF then induces the expression of NF-kB that is a pro-inflammatory gene transcription signaller thus perpetuating the spread of the pro-inflammatory response throughout the brain (Nadeau and Rivest, 2000).

Poly Inosinic: Cytidylic Acid (Poly IC) is another agent that is used to activate an immune response. It is a synthetic copy of double-stranded RNA, found in some virus structures, and as such can mimic the action of viral infection through the binding to TLR3 receptors.

It has been shown that peripheral immune challenge with LPS causes an exaggerated pro-inflammatory response in prion disease models compared to controls (Combrinck et al., 2002) as well as mouse models of Alzheimer's disease (Sly et al., 2001; Lee et al., 2002). Also, LPS and β-amyloid induce a pro-inflammatory response through class-II major histocompatibility proteins (MHC-II) which causes cytotoxicity (Butovsky et al., 2005). For this reason, the injection of LPS and Poly IC are widely used to study systemic infections, as well as their knock-on effect on the brain.

1.5 Leishmaniasis

The peripheral models described above are quite simple versions of infectious agents. To validate the findings from these models this thesis also uses a 'natural' infectious agent related to the disease Leishmaniasis. Leishmaniasis is caused by a group of protozoan parasites of the genus Leishmania. There are 20 different species of Leishmania parasites that cause the various forms of the disease. Parasites are transmitted through the bite of an infected female phlebotomine sandfly (females blood feed only when they are producing eggs). This means that the global spread of Leishmaniasis centres on areas where sand-flies are common – mostly tropical and subtropical areas.

During the initial infection stage, parasites are in their promastigote phase. The parasites in this phase possess long flagella which means they are highly motile. They exist as promastigotes in

sandfly proboscis and when injected during blood feeding they travel around the new host's blood stream. The parasites are phagocytosed by host macrophages where they transform to their amastigote phase**.** In this phase, the flagellum contracts and the parasites focus on multiplication. Parasites build up in the macrophage before it ruptures, spreading the parasite in the bloodstream to be taken up by other macrophages.

The disease takes three main forms: cutaneous (CL), mucocutaneous (MCL), and visceral (VL/kala-azar). A fourth form also exists, known as post kala-azar dermal leishmaniasis (PKDL), which occurs as a cutaneous presentation of VL years after treatment. Cutaneous leishmaniasis is the most common form, but also least severe as it only affects the skin – usually around the bite sites. However, CL still produces open sores and skin lesions that resemble those in leprosy. Visceral leishmaniasis (VL) is less common but is more dangerous than CL as it is typically fatal if left untreated.

1.5.1 Visceral Leishmaniasis

Although there are accounts, throughout history, of diseases that resemble what is now known to be CL (Steverding, 2017), the visceral form of Leishmaniasis didn't appear until 1824 in Bengal, India (Gibson, 1983). At the time it was referred to as Kala-azar (or 'black disease') due to the skin discolouration it caused. Patients showed symptoms of fever, enlarged spleens and livers, and anaemia (Steverding, 2017). It wasn't until the early 20th century that the unnamed bodies (then thought to be trypanosomes) were discovered in patients with kala-azar (Donovan, 1994; Leishman, 2006). These parasites were recognised as a novel protozoan organism and found to cause the kala-azar disease (Ross, 1903b) and named Leishmania *donovani* after their initial discoverers (Ross, 1903a). There are now two species of Leishmania known to cause VL, and their infections are geographically localised with L. *infantum (*aka. L. *chagasi)* prevalent in North Africa, Europe and Latin America, and L. *donovani* infections occurring in the remainder of Africa, and India and surrounding countries (Chappuis et al., 2007). It is the visceral leishmaniasis caused by L. *donovani* that is studied in this thesis.

VL is the second most deadly parasitic disease in the world (after malaria) and is considered to be nearly always fatal in left untreated (Desjeux, 2001). Over 90% of the occurrence of new cases of VL are restricted to 6 countries: Bangladesh, Brazil, Ethiopia, India, South Sudan and Sudan (Alvar et al., 2012). This is due to the climatological conditions in which the sand-flies

thrive, although there are also socioeconomic factors that are correlated to infection such as malnutrition, poor living conditions and lack of medical resources (Georgiadou et al., 2015).

1.5.2 Leishmaniasis and peripheral neuropathy

The list of signs and symptoms that are associated with leishmaniasis do not classically include neurological effects, however, emerging evidence is uncovering changes to the nervous system during leishmaniasis infections. It is more common for neurological effects to be present in the peripheral nervous system than the CNS, however, both have been recorded.

Cutaneous leishmaniasis classically is only thought to affect the skin. A study of patients infected with the Leishmaniasis *major* showed that in 5% of cases, patients with cutaneous leishmaniasis presented with increase inflammatory cells around peripheral nerves, neuritis and even neural infiltration of amastigotes (Kubba et al., 1987).

Peripheral neurological disturbances have also been seen in cases studies of 13 visceral leishmaniasis infected patients in Sudan who presented with varying neurological symptoms mostly affecting the lower limbs such as hyperaesthesia, impaired vibration, pain and touch, cranial nerve palsies and foot drop. However, malnutrition could not be ruled out as a factor in these symptoms (Mustafa, 1965). Further characterisation of the neurological effects of VL used nerve conduction studies to highlight evidence of neuronal demyelination and axonal degeneration in 15 patients. The recovery of neuropathy after treating the Leishmaniasis infection, along with tests confirming no vitamin deficiency suggest that these infections caused neurological problems for these patients (Hashim et al., 1995).

There have also been cases of Guillain-Barre syndrome diagnoses secondary to leishmaniasis infection (Prasad and Sen, 1996). Guillain-Barre syndrome occurs when the immune system attacks the peripheral nerves leading to muscle weakness and changes in sensation such as tingling and pain (Fasanaro et al., 1991; Attarian et al., 2003). It may be that a Leishmania infection recruits the host's immune system to attack the peripheral nerves, especially considering there is evidence of immune cell invasion of nerves (Kubba et al., 1987).

1.5.3 Leishmaniasis in the CNS

Although visceral leishmaniasis classically infects the spleen, liver and bone marrow, Leishmaniasis *donovani* parasites (responsible for VL) have been shown to infiltrate the brain as

little as 3 days after infection by intraperitoneal injection in mice (Melo et al., 2017). This is in tandem with increased leukocyte and macrophage presence in the brain tissue. These cell types could provide the route by which the intracellular parasite infiltrates the CNS. Amastigote stage Leishmania *donovani* parasites have also been found in the CSF of a human patient. The patient presented with pyrexia and headaches leading to a diagnosis of "leishmanial meningitis". This was unresponsive to older anti-leishmaniasis drugs pentamidine isethionate and sodium antimony gluconate, which fail to cross the blood-brain barrier, therefore amphotericin B was finally able to cure the patient. It is possible infiltration to the CNS was a response to a previous removal of the spleen the year before (Prasad and Sen, 1996).

Further case studies have found likely CNS problems in patients with visceral leishmanias. One patient in Kenya presented with a tremor of the torso and limbs (Chunge et al., 1985). Often symptoms of this nature are related to malnutrition however this was unlikely as the malnutrition was reversed before any improvement in symptoms. Only after treatment with the anti-leishmaniasis drug, sodium stibogluconate, was there any improvement and eventual reversal of the tremor in correlation with the parasite load being neutralised. Despite this, it is not clear as to the neurological cause of the tremor (Chunge et al., 1985). Another patient in Brazil presented with similar tremor further to VL which was alleviated with sodium stibogluconate treatment. Again, vitamin deficiency was possible, yet other characteristics of this were not seen and the patient's symptoms were reversed without any treatment with vitamin supplements (Diniz et al., 2010). Although by no means definitive proof of CNS effects of VL, several patients have also presented with mental changes or depression-like symptoms (Carswell, 1953; Maru, 1979).

1.5.4 Leishmaniasis and neuroinflammation

Further to showing neurological complications with both cutaneous and visceral leishmaniasis and the presence of Leishmania parasites in the brains, infection has also been shown to induce neuroinflammation. Increased levels of three cytokines associated with the initiation and maintenance of inflammation IL-1β, IFN-γ and TNF-α were found to be upregulated in the brains of VL infected dogs. The levels of these cytokines did not correlate with parasite load (Melo et al., 2013).

Initially (3 -14 days post-infection) there is an early inflammation response with upregulation of certain chemokines (CCL-5, 7 & 12 and CXCL-10), chemokine receptors (CCR-1 & 2 and CXCR-3)

and pro-inflammatory cytokines (IL-1β, IL-6, IFN-γ and TNFα). This initial wave of inflammation is curtailed by anti-inflammatory cytokines (IL-10, TGF-β). However, 90 days post-infection, there is a re-upregulation of the proinflammatory cytokines and chemokines, with no change in the anti-inflammatory cytokines (Melo et al., 2017)

It is clear therefore that whilst CNS system effects of leishmaniasis may be uncommon, Leishmaniasis may not only affect the CNS, but parasites can also overcome the blood-brain barrier. Whether increased neuroinflammation in these brains occurs as a spreading of peripheral inflammation, or infection within the brain is also unclear.

1.6 Aims and Objectives

The state of the field as outlined in the chapter above shows that changes occur to synaptic plasticity which are related to certain brain states and electrical rhythms, and changes to immediate early gene expression across the sleep/wake cycle may also be related.

The initial aims of this thesis are then:

- To generate sleep and wake-related oscillations *in vitro* using previously optimised pharmacological models in slice preparations of rat neocortex.
- To assess the effects of oscillations, generated *in vitro,* on neuronal activity and plasticity using immunohistochemistry to monitor immediate early gene expression changes.
- To localise oscillation related immediate early gene changes across neocortical laminae and identify specific cell types involved.

Since inflammation in the brain is a common feature in many disorders that affect normal brain function, and peripheral infections are known to induce neuroinflammation even in healthy individuals, the further aims of this thesis are:

- To monitor the direct activity of pathogenic signals on sleep- and wake-related oscillations in preparations of rat neocortex by bath application of agents that mimic pathogenic bacterial or viral sequences (LPS or Poly I:C respectively).
- To test the effects of the longevity of a peripheral immune response in a cohort of rats through a regime of dosing rats with repeated peripheral injections of LPS and Poly I:C for up to 28 days. Then:
  - To compare the effect of the longevity of a mimicked systemic infection on sleep and wake-related rhythms by generating oscillations in slice preparations of neocortex take from dosed animals.
  - To monitor the resulting inflammation in the brain of dosed rats through a multiplex cytokine panel assay to analyse pro- and anti-inflammatory cytokine and chemokine expression.
- Finally, to evaluate the effect of a real-life systemic infection (visceral leishmaniasis) on sleep and wake related oscillations generated in slice preparations of mouse neocortex. Then, investigate the general effects of those oscillations on plasticity through the use of immunohistochemistry and seek to corroborate changes previously seen in immediate early gene expression in the initial investigation.

Chapter Two – Materials and Methods

2.1 Materials

2.1.1 List of drugs and chemicals used

The following drugs were used in experiments discussed in this thesis:

ACSF salts	Various
Biocytin hydrochloride	Sigma-Aldrich, UK
Carbachol	Tocris Biosciences, UK
Ethanol	BDH-Merck
Fluoromount	Sigma-Aldrich, UK
Normal Goat Serum	Sigma-Aldrich, UK
Isoflurane (Vetflurane)	Virbac, UK
Kainic Acid	Tocris Biosciences, UK
LPS	Sigma-Aldrich, US
Ketamine (hydrochloride, Ketavet)	Zoetis UK Ltd
Methanol	Fisher Scientific, UK
Optimum Cutting Temperature	Fisher Scientific, UK
Paraformaldehyde	Affymetrics USB, UK
Phosphate Buffered Saline	Gibco, UK
Poly Inosinic: Cytidylic Acid	Sigma-Aldrich, US
Potassium Acetate	Sigma-Aldrich, UK
SCH 33920	Tocris Biosciences, UK
Sucrose	Fischer Scientific, UK
Triton X-100	Sigma-Aldrich, UK
Xylazine (hydrochloride, Rompun)	Bayer, UK

2.1.2 ACSF Formulations

Normal artificial cerebrospinal fluid (ACSF) was used in the recording chamber and holding chamber and consisted of (in mM): 126 NaCl, 3 KCl, 1.25 NaH_2PO_4, 1 $MgSO_4$, 1.2 $CaCl_2$, 10 glucose, 24 $NaHCO_3$.

Sucrose artificial cerebrospinal fluid (sACSF) – for perfusion and cutting - was made by substituting the sodium chloride in the above composition above with sucrose. This reduced the passive influx of sodium ions which leads to cell swelling by osmosis of water into the cell which limits cell survival (Ting et al., 2014). Divalent cations were also present in a higher concentration in sACSF as they stabilise excitable cell membranes, and raise the threshold for action potentials.

This is thought to be because divalent cations adsorb to the negatively charged outer side of the membrane and create an electrical field that repels cations away from the membrane surface (Frankenhaeuser, 1957; Frankenhaeuser and Hodgkin, 1957). Divalent cations also bind to ion channels and limit the passage of ions through them, again minimising excitotoxicity (Brown and Ransom, 2002). Interneurons are more susceptible to damage as they are more constitutively active than principal cells. As interneurons are critical for oscillation generation the replacement of the sodium in the solutions was particularly important. Considering these points, the sACSF was made up (in mM) of: 3 KCl, 1.25 NaH_2PO_4, 2 $MgSO_4$, 2 $CaCl_2$, 10 glucose, 24 $NaHCO_3$ and 252 Sucrose.

2.1.3 Antibodies used

Primary Antibodies	Manufacturer
Arc (Rabbit, 156003)	Synaptic Systems Gmbh
C-Fos (Rabbit, SC52)	Santa Cruz Biotechnology
Iba-1 (Rabbit, 019-19741)	Wako
GAD67 (Mouse, MAB5406)	Millipore
NeuN (Guinea Pig, ABN90)	Millipore

Secondary Antibodies	Manufacturer
Alexa Fluor 488 Goat Anti-Rabbit IgG (H+L) – A11008	Invitrogen
Alex Fluor 488 Goat Anti-Rabbit IgG (H+L) Highly Cross-Adsorbed, A11034	Invitrogen
Alexa Fluor 546 Goat Anti-Mouse IgG (H+L) Highly Cross-Adsorbed, A11030	Invitrogen
Alexa Fluor 633 Goat Anti-Guinea Pig IgG (H+L) Highly Cross-Adsorbed, A21105	Invitrogen
Alexa Fluor 568 Streptavidin conjugated, S112265	Invitrogen

2.2 Electrophysiology

2.2.1 Animal provision

The experiments in this these were carried out in two different institutions. Experiments for Chapter 3 and 5 were carried out in the Department of Biology, University of York, UK. Experiments for Chapter 4 were carried out at Eisai Inc. Andover Innovative Medicines (AiM) Institute, USA.

Adult male Wister rats used for experiments in Chapter 3 and 4 were obtained from either the UK or US divisions of Charles River Laboratories Inc. Mice were used for Leishmaniasis experiments in Chapter 5 owing to the lack of appropriate Home Office license and existing expertise at the University of York regarding the pattern of infection and immune responses observed in mouse models (Engwerda and Kaye, 2000; Bunn et al., 2014; Pinto et al., 2017). The mice were of C57/Bl6 background strain and were bred at the Biological Services Facility (BSF) at the University of York.

All animals were housed in either the Biological Services Facility in the University of York or the Life Sciences Facility at the Eisai Inc. AiM Institute. Animals were allowed a constant supply of food and water and were subject to a 12-hour light-dark cycle. All animals were taken for slice preparation 3-4 hours into the light cycle.

All animal procedures in the UK were carried out under the Animals (Scientific Procedures) Act 1986 as approved by the Home Office and Animal Welfare and Ethical Review Body at the University of York.

All animal procedures in the USA were carried out under the Animal Welfare Act (AWA) and PHS Policy on Humane Care and Use of Laboratory Animals USA and were approved by the Institutional Animal Care and Use Committee.

2.2.2 Brain slice preparation

Animal sacrifice was carried out slightly differently between institutions in which work was carried out. In particular, rats used in Chapter 4 were terminally anaesthetised without prior anaesthesia whereas isoflurane inhalant was used for all other experiments.

Rats and mice were terminally anaesthetised with a cocktail of the anaesthetic ketamine (an NMDAR antagonist) (Ketavet, Zoetis, 100 mg/ml) and the anaesthetic and muscle relaxant xylazine (an agonist for α2 adrenoreceptors) (Rompun, Bayer PLC, 20mg/ml) by either intraperitoneal or intramuscular injection. The routes of administration were different due to the difference in pre-terminal anaesthesia and efforts to minimise the suffering of the animals (as intramuscular injections are more painful).

	Institute	Species	Pre-Terminal Anaesthesia	Terminal Anaesthesia	Route of Administration
Chapter 3	University of York, UK	Wistar Rat	Isoflurane	Ketamine (0.4ml) and Xylazine (0.2ml)	Intramuscular
Chapter 4	Eisai Inc. AiM Institute, USA	Wistar Rat	None	Ketamine (0.4ml) and Xylazine (0.2ml)	Intraperitoneal
Chapter 5	University of York, UK	C57/Bl6 mice	Isoflurane	Ketamine (0.4ml) and Xylazine (0.2ml)	Intramuscular

Figure 2.1. A table to show the difference in animal sacrifice procedures across chapters, institutes and species in this thesis.

Once the animal no longer showed eye blink and pedal withdrawal reflexes, the abdomen was opened, and the rib cage and diaphragm cut, to expose the heart. An incision was made in the right atrium and the left ventricle of the heart was punctured with the perfusion needle. Perfusion with 20ml (mice) or 50ml (rats) of an ice-cold (~4°C) artificial cerebrospinal fluid solution containing sucrose (sACSF) was then carried out to exsanguinate the animal and protect the brain during the cutting process. This solution had also been oxygenated with carbogen gas (95% O_2/5% CO_2). Sucrose ACSF is explained in more detail in Chapter 2.1.2 and consists of: 3 KCl, 1.25 NaH_2PO_4, 2 $MgSO_4$, 2 $CaCl_2$, 10 glucose, 24 $NaHCO_3$ and 252 Sucrose.

Once the transcranial perfusion was completed, the skull was exposed and the animal decapitated. The skull was cut down the midline and the bone removed to expose the brain. The brain was then removed and placed into the ice-cold, oxygenated sACSF. The cerebellum was removed and discarded, and the remaining brain was then glued onto a metal vibratome plate using Loctite Precision Superglue. The brain was oriented either dorsal side (for horizontal slices) or caudal side (for coronal slices) down. The brain was supported by a 1x1cm block of agar to aid cutting. The plate was attached to a Leica VT-1000S vibratome and submerged in ice-cold oxygenated sACSF and horizontal or coronal slices were cut to 450µm thickness. The cutting blade oscillated a frequency of 80Hz, with an amplitude of 0.6mm, and advanced through the slices at 0.15mm/s.

For experiments investigating the delta rhythm, coronal sections were cut. Whole slices were sub-sectioned to keep primary somatosensory and secondary somatosensory cortical areas as well as deeper white matter and striatal structures.

For experiments investigating the gamma rhythm, horizontal slices were cut. These were either sub-sectioned to retain the hippocampus and caudal cortical regions (to generate and record hippocampal oscillations) or cut to preserve the primary auditory and secondary somatosensory cortices for cortical gamma oscillations, with some subcortical structures retained for orientation *(Figure 2.1)*.

2.2.3 Slice maintenance

The first slices were placed on a double thickness of Whatman paper in an interface chamber *(see Figure 2.2a)* between artificial cerebrospinal fluid (ACSF) and a humid carbogen environment (95% oxygen, 5% carbon dioxide). Slices were left to acclimatise for 1 hour at room temperature and then maintained at 30-32°C thereafter. The ACSF was circulated through the chamber at 1.5mls/min. ACSF is explained in more detail in Chapter 2.1.2, and consists of: 126 NaCl, 3 KCl, 1.25 NaH_2PO_4, 1 $MgSO_4$, 1.2 $CaCl_2$, 10 glucose, 24 $NaHCO_3$. Subsequent slices were placed on tissue paper in a holding chamber *(see Figure 2.2b)*. These slices were maintained at an interface between oxygenated ACSF and carbogen gas at room temperature and partially sealed with parafilm.
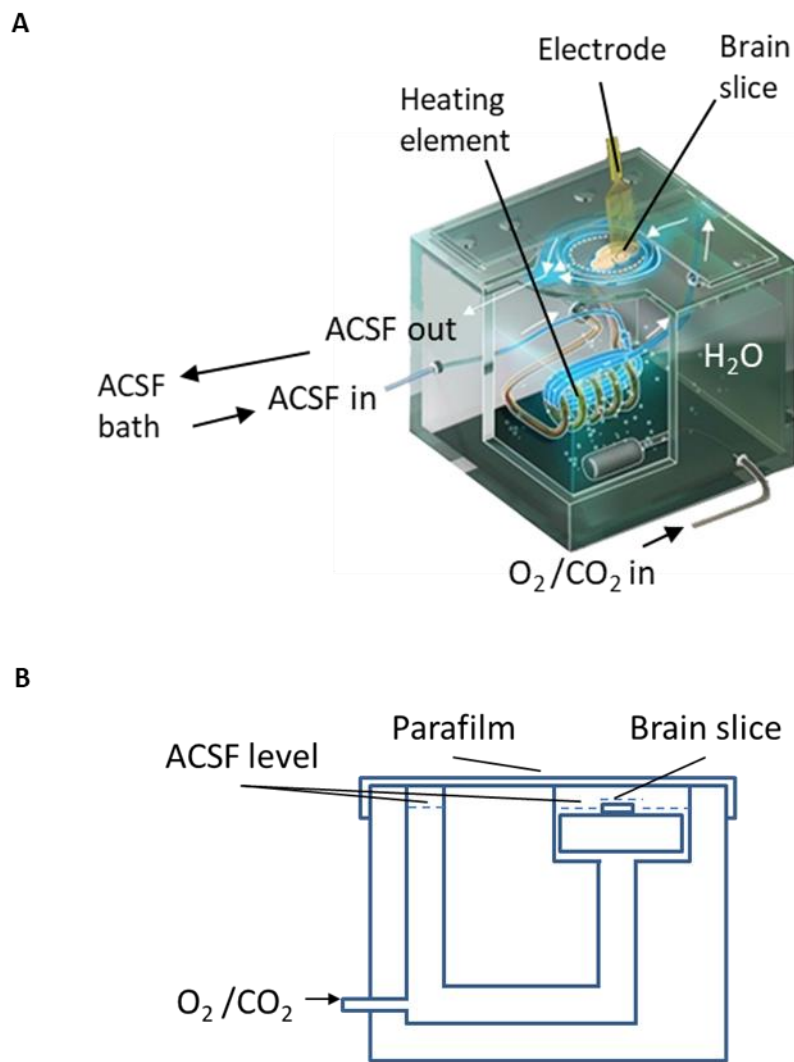
Figure 2.2. Diagrams of the recording and holding chambers used for maintaining slices for electrophysiology. A) A diagram of a recording chamber used for electrophysiology. Heating element warms H_2O in chamber which is also bubbled with 95% O_2 /5%CO_2 mix. ACSF from the bath is also warmed as it its pumped through a submerged tube in the water bath before perfusing over slice back to the bath. Adapted from Tsintsadze et al. (2015) **B)** A diagram of the cross section of a holding chamber. The bath of ACSF remains in the holding chamber and forms a meniscus over the slices. ACSF is bubbled with 95% O_2 /5%CO_2 mix and is kept at room temperature.
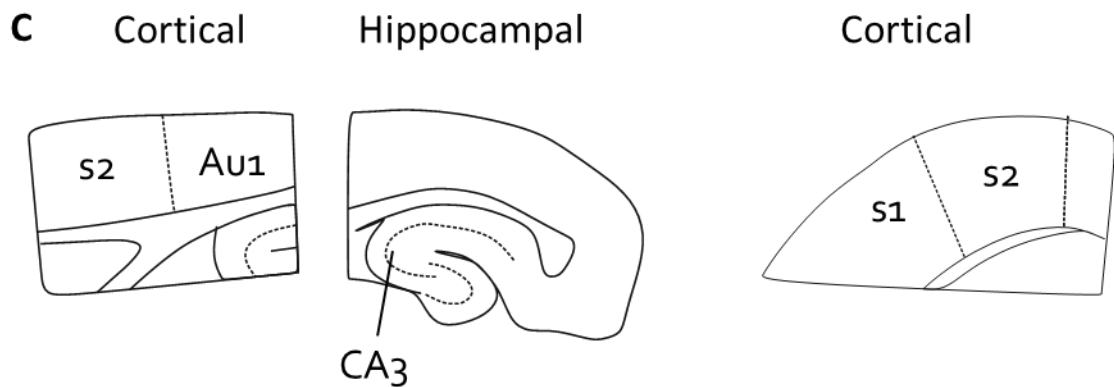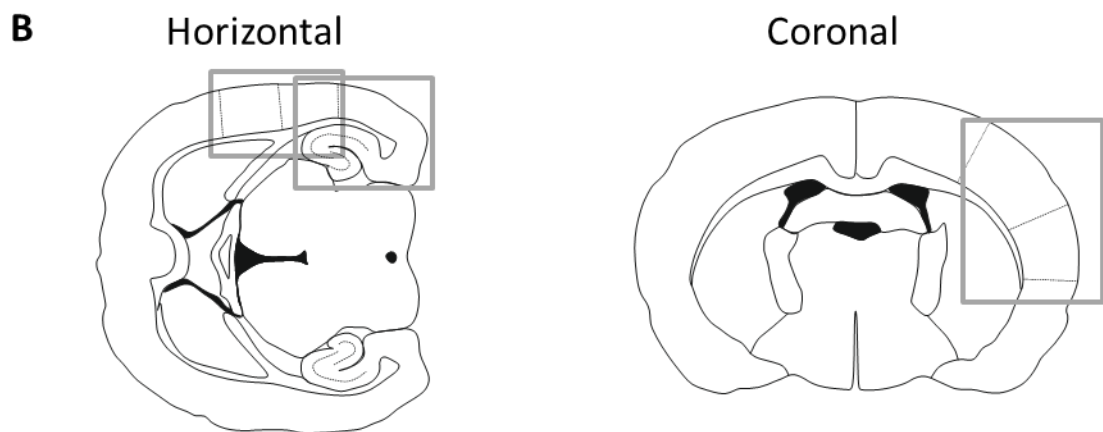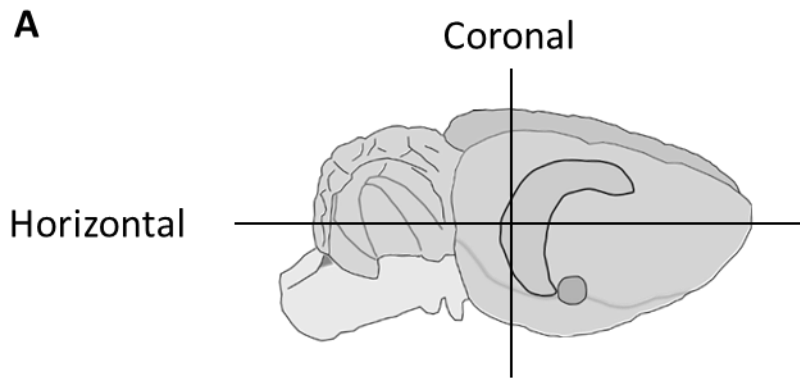
Figure 2.3. Diagrammatic images of the rat brain and sections used in electrophysiology experiments. A) A near-sagittal diagram of the rat brain including cerebellum and brain stem. The planes of dissection for electrophysiology experiments are shown. B) Examples of full horizontal and coronal slices and the areas that are sub-sectioned for electrophysiological experiments. **C)** Annotated diagrams of the sections of brain used for gamma (horizontal cortical and horizontal hippocampal slices) and delta (coronal cortical) experiments. S1 – primary somatosensory cortex, S2 – secondary somatosensory cortex, Au1 - Primary Auditory Cortex, CA3 – Cornu Amonnis 3 region of the hippocampus.

2.2.4 Oscillation induction

Different oscillations were more robustly generated in slices of different orientations, which were cut as outlined below *(and in Figure 2.3)*. To maintain slices in a viable state they were dissected down to reatin only the necessary areas of observation (and subcortical structures for orientation) – this was done as larger slices require more oxygenation. The slices were viewed with a light microscope to ensure correct and consistent placement of the electrodes for local field potential (LFP) recordings.

To generate delta frequency oscillations in the primary and secondary somatosensory cortices of the coronal brain slices, a combination of the acetylcholine agonist, Carbachol (4 µM) and dopaminergic antagonist, SCH23990 (10 µM) were simultaneously added to the circulating ACSF. Cortical LFP recordings were made from layer 5 of the primary and secondary somatosensory cortex in coronal slices as previously described (Carracedo et al., 2013).

To generate gamma frequency oscillations in the primary auditory and secondary somatosensory cortices of the horizontal brain slices, kainic acid was used (400nM). Cortical LFP recordings were made from layer 3 of the primary auditory and secondary somatosensory cortex, in horizontal slices according to the *in vitro* procedure already characterised (Ainsworth et al., 2011).

Kainic acid was also used to generate hippocampal oscillations, though at a lower concentration (50nM). Recordings were made from the stratum radiatum of the cornu ammonis 3 (CA3) region of the hippocampus *(see Figure 2.5 for example oscillations).*

2.2.5 Extracellular (LFP) Recordings

Extracellular electrodes were made from borosilicate glass capillaries and were pulled to form a tip with a Model P-1000 Flaming-Brown micropipette puller. Micropipettes were then filled with normal ACSF and placed in pipette holders with silver wire used to form a conducting bridge between the ACSF and the amplifier electronics. These holders were then attached to head stages that could be finely moved by micromanipulators. The electrical signal from slices was conducted through the micropipette solution and to the silver wire. The signal was digitised at a sampling frequency of 2000 and filtered between 0.1 and 300Hz, before being visualised and saved on a computer. The hardware and software used to relay the electrical signal to the computer were different between institutions (see Figure 2.4).

	Headstages	Amplifier	Digitisation	Line noise removal	Software
University of York, UK (Chapter 3 & 5)	HS-9A (Axon Instruments)	Axoclamp 900A (Axon Instruments)	ITC018 A/D converter (HEKA Instruments)	Humbug (Quest Scientific)	Axograph
Eisai Inc. AiM Institute, USA (Chapter 4)	CV-7B (Axon Instruments)	Multiclamp 700B (Axon Instruments)	Power 1401 (Cambridge electronic design)	Humbug (Quest Scientific)	Spike 2

Figure 2.4. A table to show the different hardware and software used for electrophysiological recording between institutes.

In all experiments after application of drugs, slices were left for 2 hours to allow them to generate oscillations, and recordings were made during this time to assess the build-up of any oscillations seen.

In Chapter 3, because IEG protein levels are thought to be at their highest at 2 hours (Morgan et al., 1987), final recordings were made then, and oscillating slices were then fixed for IEG measurements. Slices were considered to have generated delta oscillations if the peak power (between 0.5 and 4Hz) was above 100μV². For gamma oscillating slices the threshold for inclusion was a peak power of 10μV².

In Chapter 4 and 5, because the oscillatory ability of slices was compared, oscillations were left to stabilise (>2 hours), and once the peak power did not change by more than 10% in 15 minutes. The oscillation was considered stable and a final recording was made. The same frequency bands were used for all but the chronic dosing hippocampal experiments of Chapter 4. Due to the low frequency of the oscillation (discussed in Chapter 4.3.2), a 20 – 50 Hz band was used.
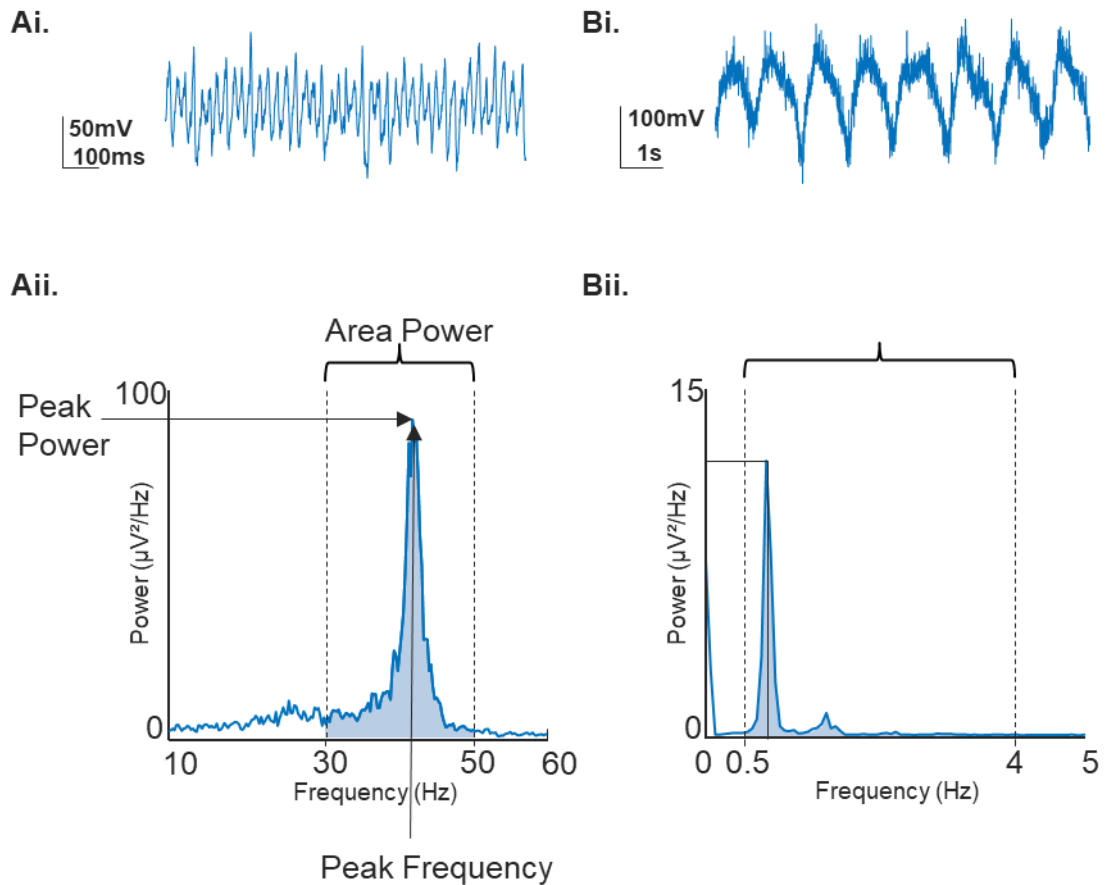
Figure 2.5 Examples of delta and gamma oscillations and power spectra for analyses.
Ai) Example of 1 second recording of gamma oscillations (from a larger 1 minute recording) **ii)** Power spectrum made from the 1 minute recording of gamma oscillations. Grey shading represents the area under the curve used to calculate area power (between 30 and 50Hz). Arrows highlight where peak power and peak frequency measures are taken from. **Bi)** Example of 10 second recording of delta oscillations (from a larger 1 minute recording) **ii)** Power spectrum made from 1 minute recording of delta oscillations. Grey shading represents the area under the curve used to calculate the area power (between 0.5 and 4Hz). Lines highlight where peak power and peak frequency measures are taken from.

2.2.6 Analysis of field potential recordings

Data was collected through either Spike2 (Cambridge Electronic Design Ltd., UK) or Axograph (Axograph, USA). The recordings were filtered between 0.1 and 300Hz and the sampling frequency was 2000. The recorded data was exported to MATLAB (MathWorks Inc., Natick, USA) where bespoke programs were created to analyse certain features of the data.

The LFP recordings were analysed for oscillatory activity and several characteristics of this activity were measured. These measures were made from the computation of an overlapping window Discrete Fourier Transform (DFT) using the MATLAB program '*pwelch'*, computed from 60 seconds of data. This DFT algorithm produces a power spectrum whereby the time domain is converted to frequency. This is done by separating the waveform into its frequency components (as a mixture of sine waves) and calculating the absolute magnitude squared (power) at each of these frequencies.

From the power spectra, measures of the frequency and modal peak power were taken. In addition, power was integrated from the lower to the upper boundaries of the frequency bands of interest to give an 'area power' measurement. Limits of the frequency band were set for calculations of power: for gamma oscillations, these were 30-50Hz, and for delta, these were 0.5-4 Hz *(Figure 2.5)*. These measures could then be averaged within conditions to monitor the changes to these properties over different conditions.

Statistical analysis of the data was performed by Sigmaplot 12.3 (Systat Software Inc, Hounslow, UK). Data were presented graphically using Microsoft Excel (Microsoft Corp., Redmond, USA)

2.2.7 Intracellular Recordings

For intracellular experiments, sharp electrodes were made from borosilicate glass capillaries using the micropipette puller with a resistance of 70-200 MΩ. Electrodes were filled with a solution of potassium acetate (2M) and 2% biocytin hydrochloride. To make intracellular recordings, cells were punctured by sharp electrodes using the micromanipulator to track the electrode tip through the thickness of a 450µM slice. A constant hyperpolarising holding current (-0.2nA) was applied as well as a constant tuning step (-0.2nA at 2Hz) during this process**.** With each increment of the descent through the slice, a slight 'buzz' (by immediate increasing of capacitance neutralisation of the electrode) was applied to the electrode tip which facilitated the piercing of the membrane of the neuron. Once a membrane was penetrated the holding

current was hyperpolarised further to stabilise the cell while the membrane formed a seal around the penetrating tip of the electrode. This was maintained for ~5 minutes until the membrane had formed a seal around the electrode, allowing the cell to stabilise at its resting membrane potential (RMP). Cells with an RMP below -50mV with action potential amplitude above 60mV were considered suitably impaled for recording.

To record excitatory postsynaptic potentials (EPSPs), cells were hyperpolarised to -70 mV. Further to this, depolarisation of the cell to -20mV, by injection of positive current prevented the cell from firing and allowed the IPSPs received by the cell being recorded.

To visually highlight single neurons that had been previously characterised by intracellular recording, the cell was maintained in a slightly hyperpolarised state whilst a small amount of tuning current allowed the biocytin (in the electrode) to fill the cell and its projections. The cell was filled for 30 – 60 minutes and when complete the slice was removed and fixed in 4% paraformaldehyde (PFA).

2.2.8 Biocytin labelling and imaging

The fixed 450µM slices containing the biocytin labelled neurons were washed (3x 15 minutes) in phosphate buffer (PB) 0.1M to remove the fixative. Slices were then embedded in 10% gelatine on ice and then incubated in PFA for 60 minutes to fix the gelatine. A Leica VT1000S Vibratome was then used to slice these to 30µM (a thickness penetrable by a secondary antibody).

All sub-sectioned slices were retained and taken through the staining process as the precise location of the biocytin labelled cell was not known. After two 15-minute washes with PB, each section was incubated in phosphate buffered saline (PBS) containing 0.2% Triton-X 100 (PBS-TX) for 10 minutes.

To co-stain for the biocytin labelled cell Arc, the slices were blocked in normal goat serum (NGS) for 2 hours and incubated in the primary antibody overnight at 4°C (for details see Chapter 2.4.1 below). Further to this, slices were incubated for two hours with Alexa Fluor Goat-α-Rabbit 488 (1:500) and Alexa Fluor 568 Streptavidin conjugate (1:500). The streptavidin binds and fluorescently labels any biocytin that has diffused into the cell. On completion of the secondary incubation, slices were washed twice with TBS for 15 minutes and mounted on slides.

Slides were viewed using a Zeiss LSM 710 motorised confocal microscope to locate any cells or cell segments containing the biocytin label. Since slices were cut to 30μM, there was no guarantee of one section containing the entirety of the cells structures, therefore all sections were collected and images of multiple sections which had segments of the cell were taken. Most segments were imaged using an x20 objective. The cell body was imaged at x10 as well, to view its location within the cortex. Alex Fluor 488 (to show Arc) and Alexa Fluor 568 (to show biocytin) were excited using 488 and 561nm lasers respectively and the light emitted was collected in 495-548nm and 578-735nm ranges respectively for each stain. Images at x20 had a pixel scale of 0.415μm x 0.415μm. Line averaging was used taking 8 passes of each scan line and averaging to increase signal: noise by minimising random and background fluorescence. These images were also taken as z-stacks with the maximum intensity projection calculated for each image presented.

2.3. Infection and inflammation models

2.3.1 Acute inflammation

In Chapter 5 two different compounds were used to observe the effect of inflammatory agents upon *in vitro* models of cortical rhythms.

To see whether there was any direct effect upon sleep and wake-related rhythms in acute *in vitro* brains slices, lipopolysaccharide (LPS, Sigma L4130) was used. LPS is a ligand for TLR 4 receptors which also responds to pathogenic bacterial signals. Gamma and delta rhythms were generated and recorded according to the methods outlined in Chapter 2.2.4-6. Once the oscillations were considered stable 500ng/ml LPS was added to the bath and recordings were made every 15 minutes up to 1hr. The final stable recording was compared with the final recording 1 hour after LPS.

2.3.2 Chronic inflammation

For chronic inflammation experiments, the effect of LPS was compared to that of Polyinosinic: Polycytidylic Acid (Poly I:C, Sigma I3036), which is a ligand for TLR 3 receptors that also respond to viral infections.

A dosing schedule was set up whereby rats were injected intraperitoneally with either 0.9% Saline (a.k.a. vehicle), 250μg/kg LPS (in saline) or 6mg/kg Poly I:C. Some animals were dosed once, 24 hours prior to sacrifice and brain slice preparation. Others were dosed every three days

for 7 or 28 days, with Vehicle, LPS or Poly I:C and all animals survived the dosing regime (Tchessalova and Tronson, 2019). Once again, *in vitro* gamma or delta rhythms were generated (as above) and were recorded to track the build-up of the oscillations. Once the oscillations had stabilised a final recording was taken, and the slices immediately removed from the recording chamber on filter paper (to reduce injury) and put into 4% paraformaldehyde.

2.3.3. Leishmaniasis Infection

Parasites of the Ethiopian strain of Leishmaniasis *donovani (LV9)* were incubated in an immunosuppressed host male *Rag1 -/-* mouse, which had suppressed T cell and B cell maturation. Amastigotes were extracted from the spleen of the host mouse and C57/BL6 mice were then infected by intravenous injection of $3x10^7$ amastigotes through the lateral tail vein. These mice were 5-8 weeks old at the time of injection and were then left for 33-37 days until sacrifice.

Animals were weighed after sacrifice and brain removal and their spleens and livers were also isolated. These tissues were weighed separately and then cut in cross-sections to analyse parasite count by impression smear. Cut sections were pressed against a microscope slide which is then methanol fixed and stained with Giemsa reagent, which shows up nuclei. 1000 host nuclei were then counted along with the number of parasite nuclei in the within the 1000 nuclei. This number was also used to calculate the LDU (Leishmania do notani units), which is the number of parasite nuclei/1000 host nuclei multiplied by the organ weight in grams. These experiments were carried out by Najmeeyah Brown.

2.4. Immunofluorescence

2.4.1 Immediate early gene and cell marker staining

Following the completion of the electrophysiological measurements, the 450µm brain slices were immediately removed from the recording chamber on filter paper (to reduce injury) and put into a fixative solution of 4% paraformaldehyde (PFA) in Phosphate Buffered Saline (PBS). Slices were left in the fixative for 24-48 hours and then cryoprotected with sucrose solutions. This involved a 2hr incubation in 10% Sucrose in PBS, followed by overnight incubation of 30% Sucrose in PBS. After fixation, slices used in experiments from Chapter 5 were stored in PBS with 0.1% Azide and shipped to the UK where they were processed for immunohistochemistry.

Slices were then placed in plastic moulds before being immersed in optimum cutting temperature compound (OCT). The moulds and contents were then frozen in Iso-pentane (2-Methylbutane) in dry ice. They were then re-sectioned to 30µm using a cryostat.

For the immunohistochemistry, the 30µm slices were washed in PBS, and the cells membranes were permeabilised with PBS-TX (with 10% Methanol to permeablise the nuclear membrane for nuclear stains) for 10 mins. This was followed by a blocking step in 3% normal goat serum (NGS) for 2 hours. The serum contains albumin, antibodies and other proteins that bind to non-specific sites in the sample to prevent the non-specific binding of the secondary antibody and thus reduce background staining. The primary antibody was applied at the stated concentration diluted in PBS containing 1% NGS and incubated overnight at 4°C. Primary antibodies used were: Millipore ABN90 Anti NeuN (guinea pig, 1:500), Millipore MAB5406 Anti GAD67 (mouse, 1:500), Santa Cruz Biotechnology SC52 Anti c-Fos (rabbit, 1:200), Synaptic Systems Gmbh 156003 Anti Arc (rabbit, 1:500 rat tissue or 1:100 mouse tissue), and Wako 019-19741 Anti Iba1 (rabbit, 1:1000).

The secondary antibody incubation lasted 2 hours and was carried out at room temperature in PBS with 1% NGS. Secondary antibodies used were: Alexa Fluor Goat-α-Rabbit 488 (1:500), Alexa Fluor Goat- α-Mouse 546 (1:500) and Alexa Fluor Goat-α-Guinea Pig 633 (1:500). Slices were finally mounted on slides with Fluoromount and protected with coverslips. They were then imaged on an AxioScan Z1 machine. Tile scanned images were taken using a 20x lens, with pixel scaling at 0.325µm x 0.325µm per pixel. The immediate early gene was imaged as Alexa Fluor 488 (excitation/emission 493/517), GAD67 was imaged as Alexa Fluor 546 (excitation/emission 557/572), and NeuN was imaged as Alexa Fluor 633 (excitation/emission 631/647).

Example, raw images for each of these labels are shown in *Figure 2.6.* Higher resolution images of the Arc stain were captured using a 63x lens on a Zeiss LSM 710 microscope, running Zeiss Zen software. Images were taken as tile scans from pia to cortical white matter using a 63x objective. Alexa Fluor 488 was excited with a 488nm laser and emitted light was collected was from 487-600nm. Resulting images had a pixel scale of 0.132µm x 0.132µm. Line averaging was used taking 8 passes of each scan line and averaging to collect only real staining. These images were also taken as z-stacks with the maximum intensity projection calculated for each image presented.

2.4.2 Image Analysis for cortical IEG profile measurement

Images of immunofluorescent slices taken at x20 magnification with the Zeiss Axioscan Z1 slide scanner were manipulated in Zen 2 Lite (Blue) software, which uses '.czi' files. Each of the intensity scales and upper/lower set limits of immediate early gene images were conserved across conditions to retain the original brightness of the staining and allow direct comparison between scans. Images were then exported as .tiff files and all subsequent image manipulation and analysis executed in MATLAB. The images were then flipped so that the secondary somatosensory cortex was on the right for the batch processing of the MATLAB programme, and were then converted to grayscale using the '*rgb2gray*' function to allow numeric comparison of pixel intensities and further manipulation of the datasets as described below.

To extract the cortical regions required for analysis, the three images (one per fluorescence signal channel) were rotated to the same orientation so that the pia was at the very top of the image and layer VI of the cortex and cortical white matter were at the bottom. The NeuN image was used as a standard to provide the coordinates for the region to be cropped. The auditory cortex and secondary somatosensory cortex were identified with reference to an anatomical atlas (Paxinos and Watson, 1998) and a rectangular box was manually drawn around them (between the pia and cortical white matter) to provide coordinates by which to crop the image *(Figure 2.7)*. Since, using the above method, the images from each channel of the triple staining all have the same dimensions. This allowed the coordinates of the cropped regions from the NeuN image to be then directly translated to the related GAD67 and Arc/c-Fos stained images *(Figure 2.8)*.

2.4.2.1 General regional IEG intensities

Initially, to provide a general interpretation of changes in IEG expression, the c-Fos and Arc staining in cropped regions of neocortex were compared between delta oscillating slices and gamma oscillating slices. The images were processed to remove nonspecific background staining using a rolling kernel of 30 pixels in area. The measure of the mean intensity of the staining in each region and for each condition was then calculated.

2.4.2.2 Identifying neuronal cells

NeuN is an antigen located in the nucleus and the immediately surrounding cytoplasm of neurons and is present in nearly all neuronal subtypes in the CNS (with the exceptions of Cajal-

Retzius cells, Purkinje cells, inferior olive neurons) (Gusel'nikova and Korzhevskiy, 2015). Antibodies to NeuN have long been used as an immunohistochemical marker of neurons.

To provide a template by which to analyse the presence of Arc or c-Fos in all neurons, the IEG image was compared to a binary image of the corresponding NeuN stain. This was created using the *im2bw* function in MATLAB. This function requires the input of a thresholding value which was calculated by taking one standard deviation above the mean intensity of all pixels in the whole image. The resulting binary image retained all the cells in the foreground of a now 'zero' background. However, speckles were also present from less brightly stained background cells and nonspecific staining. These speckles were removed using the '*bwareaopen'* function in MATLAB, which removed any objects in a binary image by size – in this case, any object smaller than 600 pixels *(Figure 2.9)*. Each pixel of images taken on the Axioscan slide scanner is 0.325μm x 0.325μm, therefore 600 relates to ~65μm² which is much smaller than the average cell body size which ranges from 150-200μm²

2.4.2.3 Identifying Interneurons

To analyse the presence of Arc or c-Fos in all interneuron cell bodies, the IEG signal was compared to a binary image template of the corresponding GAD67 stain. This was created in a similar way to the NeuN template above. However, GAD67 antibody stained a large density of interneuron synaptic terminals as well as cell bodies, therefore additional steps had to be employed to separate cell bodies from the terminal staining for the template.
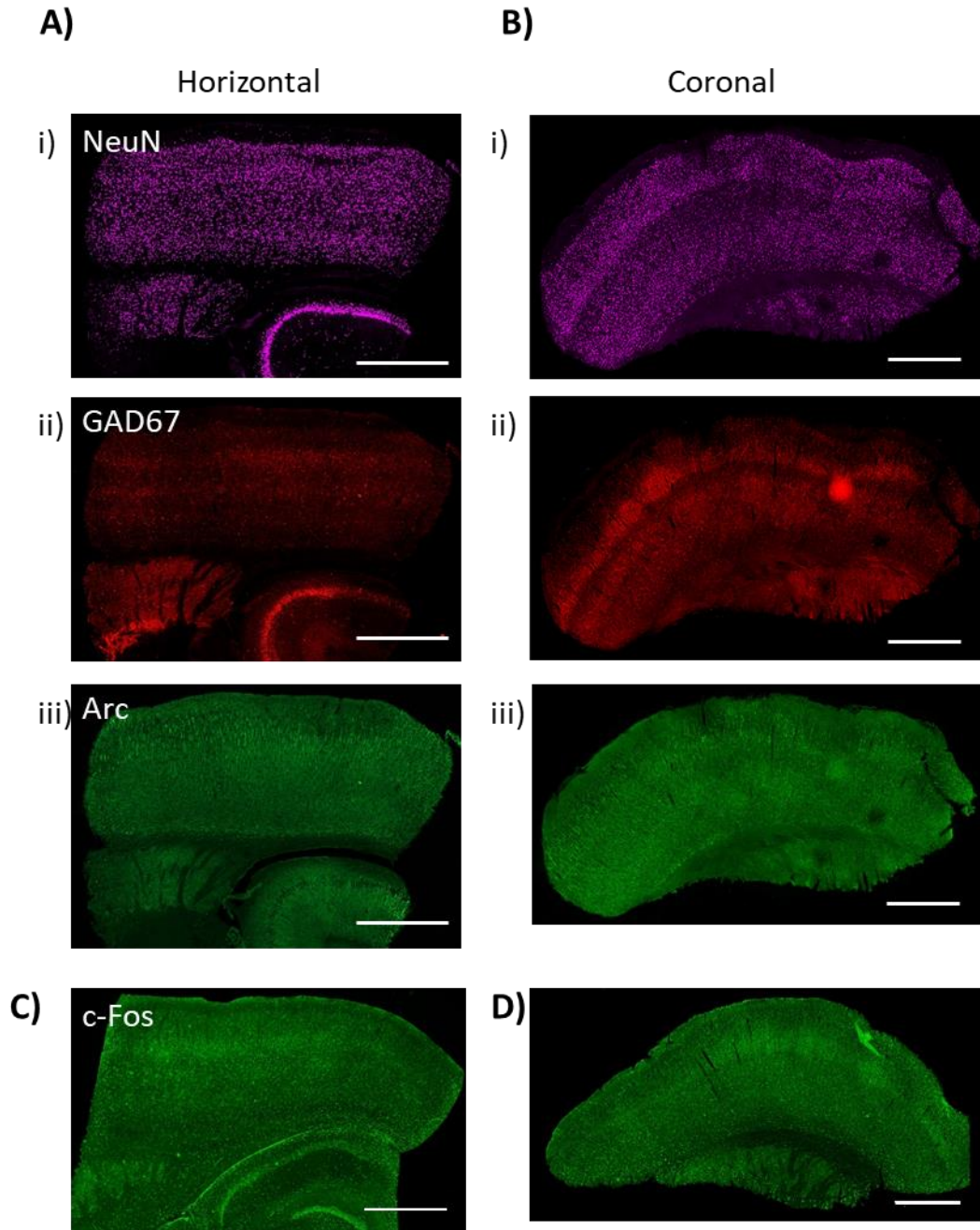
Figure 2.6. Example images of horizontal and coronal slices use for immediate early gene analyses. A) Example images of from a co-stained horizontal slice stained for **i)** NeuN **ii)** GAD67 **iii)** ARC, scale bars are 1000μM. **B)** Example images of from co-stained coronal slice stained for **i)** NeuN **ii)** GAD67 **iii)** ARC, scale bars are 1000μM. **C)** Example image from a c-Fos stained horizontal slice, scale bar = 1000μM. **D)** Example image from a c-Fos stained coronal slice, scale bar = 1000μM.

A)
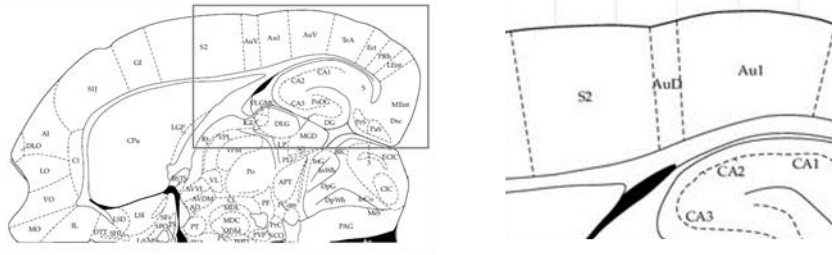
Bi)
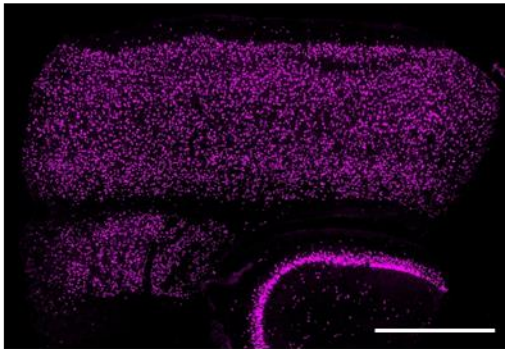
Bii)
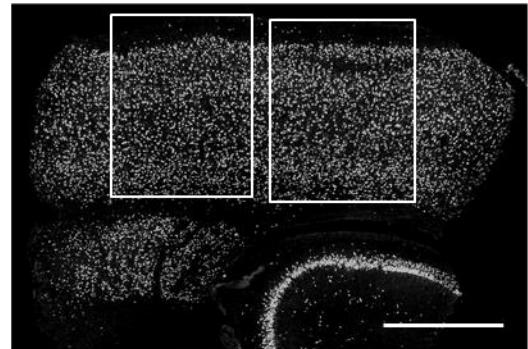
Ci)
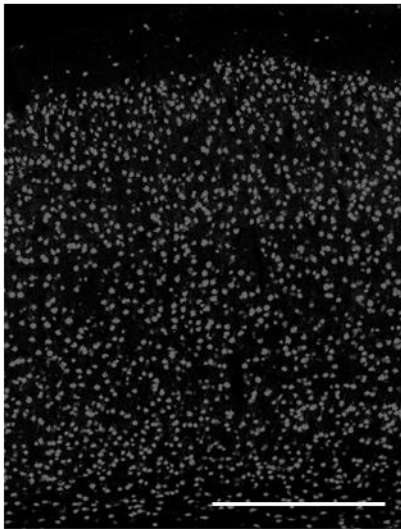
Cii)
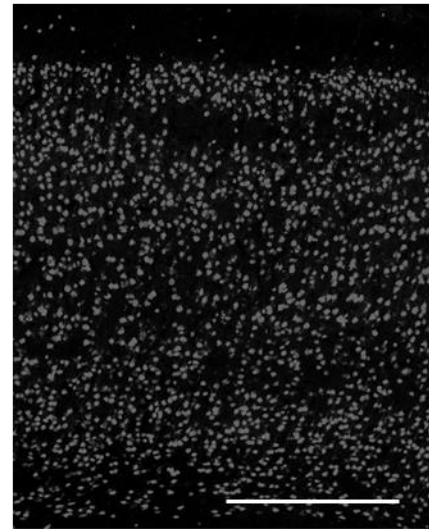
Figure 2.7. Example images of cropping of primary cortical and secondary association areas.
A) Examples of diagrammatic maps of horizontal sections of rat brain used for reference
when locating region. Right image is blown up from left image **Bi)** A full colour image of NeuN
stain in a horizontal section. Scale bar is 1000μM. **ii)** The grayscale converted image from Bi.
White boxes represent areas cropped for analyses, left is S2 right is Au1. **Ci)** Zoomed in image
of the cropped Area S2 from NeuN stain in Cii. Scale bar is 500μM. **ii)** Zoomed in image of the
cropped Area Au1 from NeuN stain in Cii. Scale bar is 500μM.
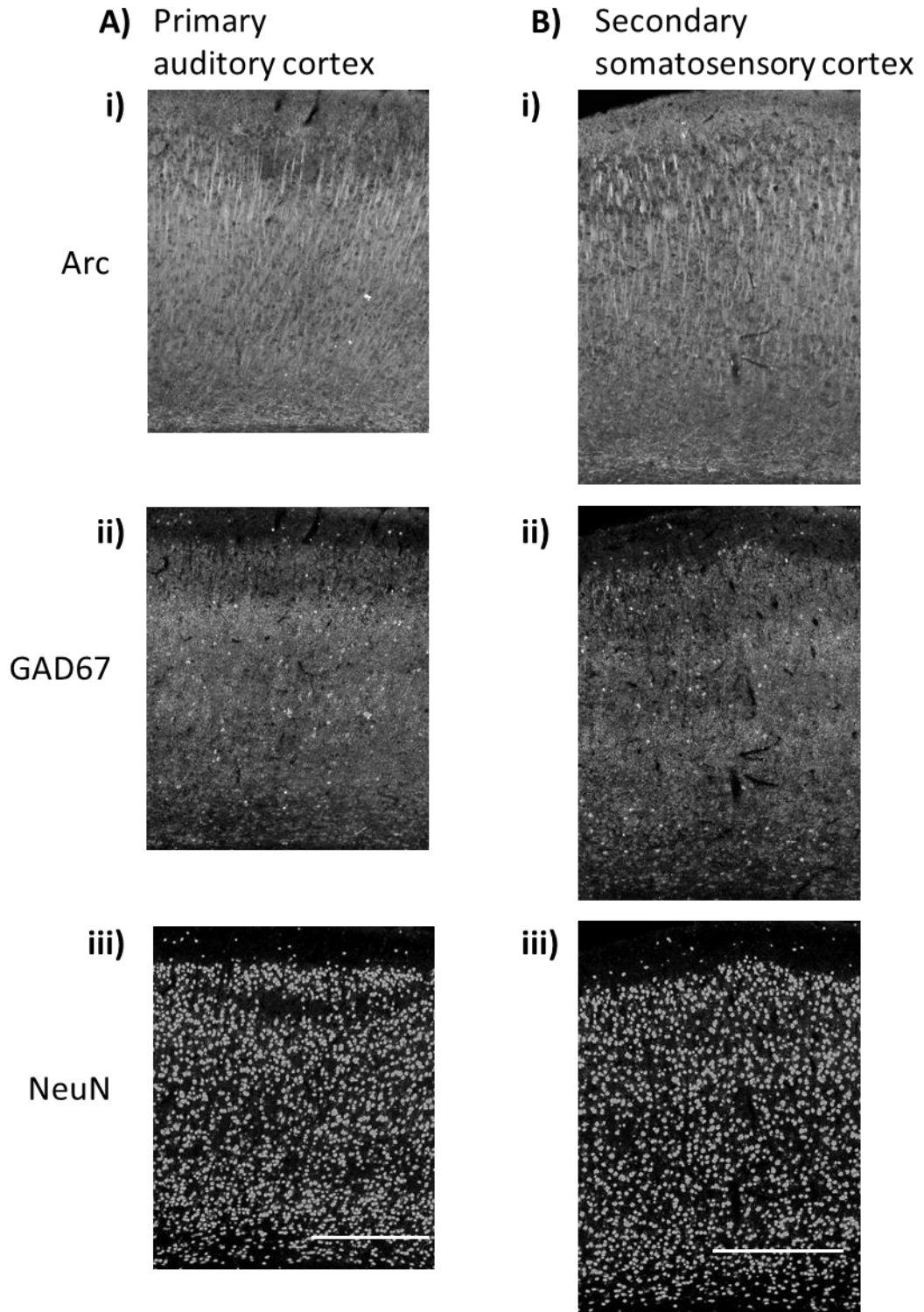
Figure 2.8. Example images of horizontal cortical gamma slices after cropping regions (A) Co-stained cropped auditory cortex images from a horizontal slice stained with **i)** ARC **ii)** GAD67 **iii)** NeuN, scale bar is 500μM **(B)** Co-stained cropped secondary somatosensory cortex images from a horizontal slice stained with **i)** ARC **ii)** GAD67 **iii)** NeuN, scale bar is 500μM.
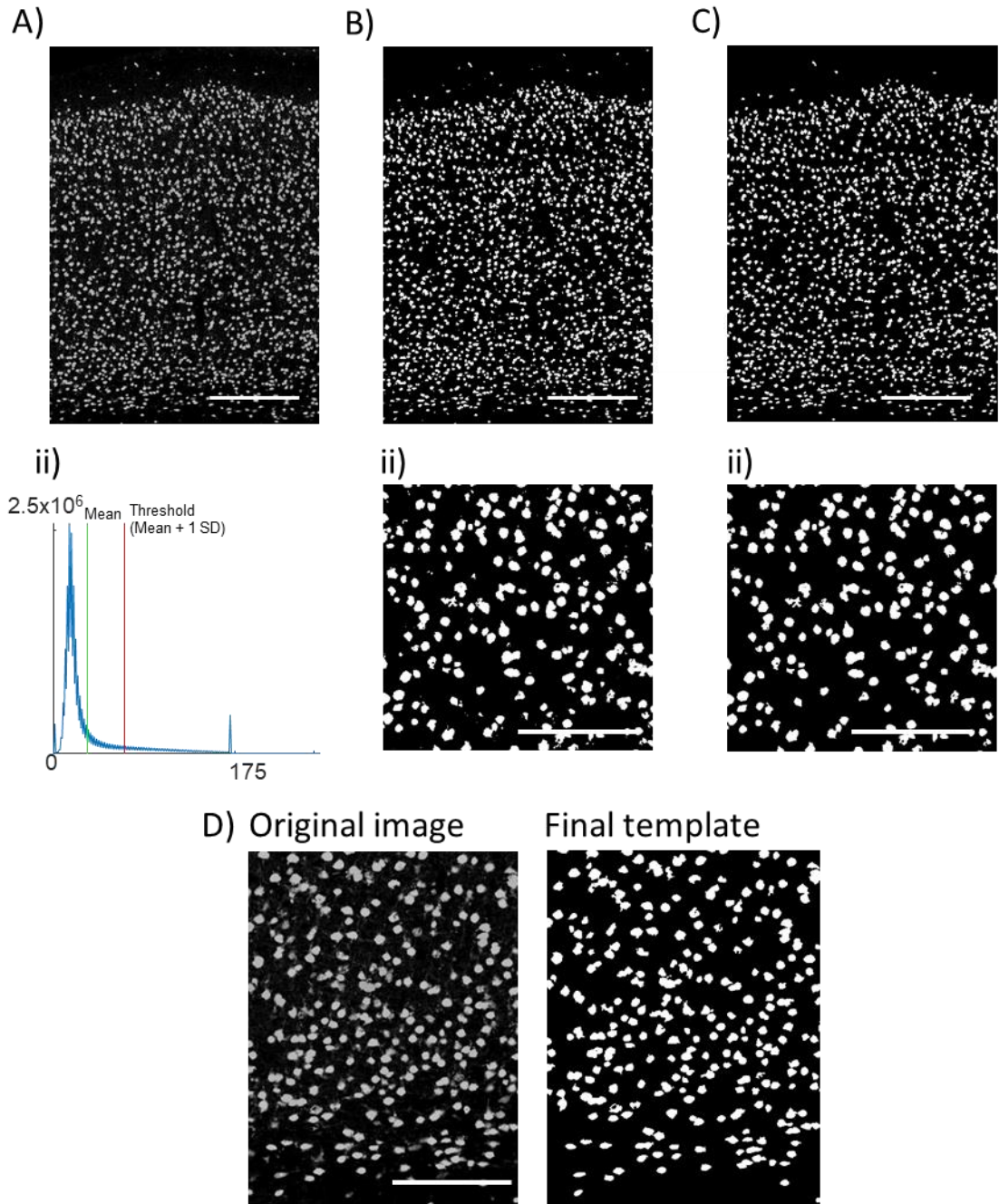
Figure 2.9. Example images of the creation of a NeuN template from S2 in a horizontal brain section. Ai) The grayscale cropped NeuN image. Scale bar is 500μM **ii)** A graphical representation if the frequencies of pixel intensities in the original grayscale NeuN image (green = mean, red = mean+1 standard deviation i.e. Thresholding value) **Bi)** The subsequent binary NeuN image as created using a thresholding value of 'mean +1 standard deviation' from Aii. Scale bar is 500μM **ii)** A zoomed portion of the binary NeuN image, to display the speckles. Scale bar is 250μM **Ci)** The binary NeuN image after the removal of all objects <600 pixels in area. Scale bar is 500μM . **ii)** A zoomed portion of the binary image to display the absence of the speckles. Scale bar is 250μM **D)** Comparison of the original NeuN image compared to final image after processing to create template. Scale bar is 500μM
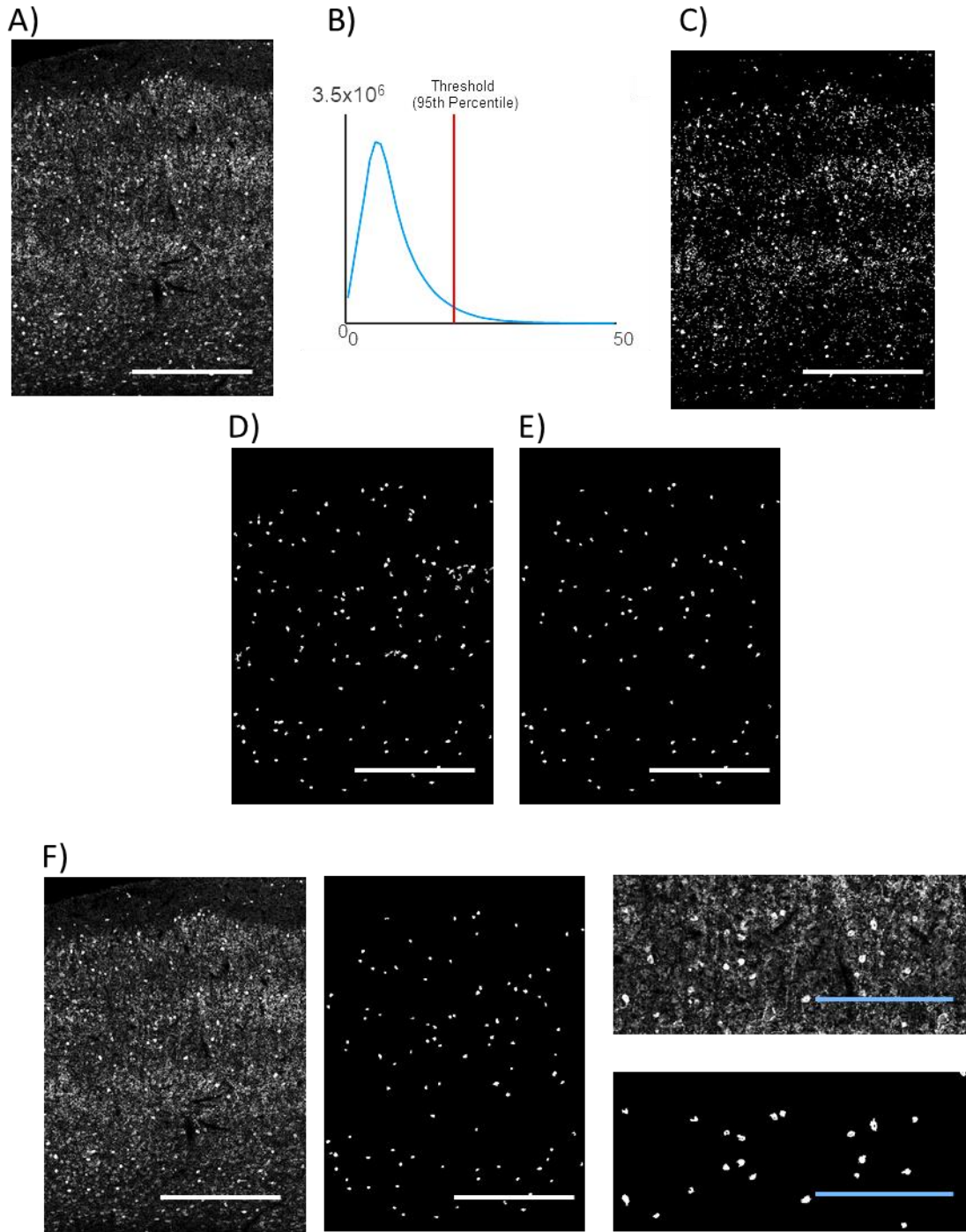
Figure 2.10. Example images of the process of creating the GAD67 template from the secondary somatosensory cortex of a horizontal cortical gamma slice. Ai) The grayscale cropped GAD67. **B)** A graphical representation of the frequencies of pixel intensities in the original grayscale GAD67 image (red = 95th percentile limit). **C)** The binary GAD67 image created using 95th percentile as threshold. **D)** The binary GAD67 after the removal of speckles but with some neuropil staining still present. **E)** The binary GAD67 image after speckle removal and removal of remaining neuropil staining by lack of roundness. **F)** Comparison of original GAD67 image, and GAD67 template after all processing steps. All white scale bars are 500µm, blue scale bars are 250µm

For this reason, the threshold value used with the *'im2bw'* function used the 95th percentile rather than 1 standard deviation above the mean. Speckles smaller than the cells (<600 pixels in area) were again removed using '*bwareaopen'*. A further processing step removed the terminal staining (yet retained cell body staining) by retaining only the roundest objects in the image. This was done by creating a metric from the circumference and the area of each object using the formula (4π*area/perimeter²). Objects with a roundness metric of less than 0.25 were removed (an object with a roundness metric of 1 is approximately round) (*Figure 2.10)*.

2.4.2.4 Analysing IEG signals using NeuN and GAD67 Templates

The NeuN and GAD67 templates were binary images so they were used to separate somatic levels of IEG from general background staining and staining in unidentified structures in the neuropil. Once the templates were created as described in the above two sections, the immediate early gene signal image was transposed onto the template only in areas that are positive for the cell-specific marker (NeuN+ve or GAD67+ve). The resulting image of the immediate early gene signal in the cell-specific marker template was then further processed by intensity. To retain only real cell immediate early gene staining, objects with an average intensity of less than the mean of all objects' intensities, were removed *(Figure 2.11)*.

2.4.2.5 Analysing Arc in Dendrites

Images of the Arc staining using the above template method contained signal arising only from the cell bodies. However, visual inspection of the raw images revealed there was also staining evident in dendrites traversing layers 2/3 of the neocortex. This extra-somal signal was excluded from the analysis which measured somatic staining using NeuN and GAD67 templates. Therefore, to analyse Arc in dendrites the original Arc image only was used, and the dendritic staining isolated. This was carried out by initially subtracting the background signal with a rolling kernel of 30 pixels in area. A binary image was then created of the background subtracted image and the threshold used was 1 standard deviation above the mean. Since the analysis only required information about the location of the dendrites and not the intensity of the signal, the binary image was then used for the final measurement. Speckles were removed to the same parameters used throughout other analyses (<600 pixels in area). To attain the final dendritic images, the cells stained had to be removed, therefore any objects with a roundness measure of more than 0.15 were removed). Roundness was calculated using the same formula (4π*area/perimeter²) as section 2.3.2.2. (*Figure 2.12).*
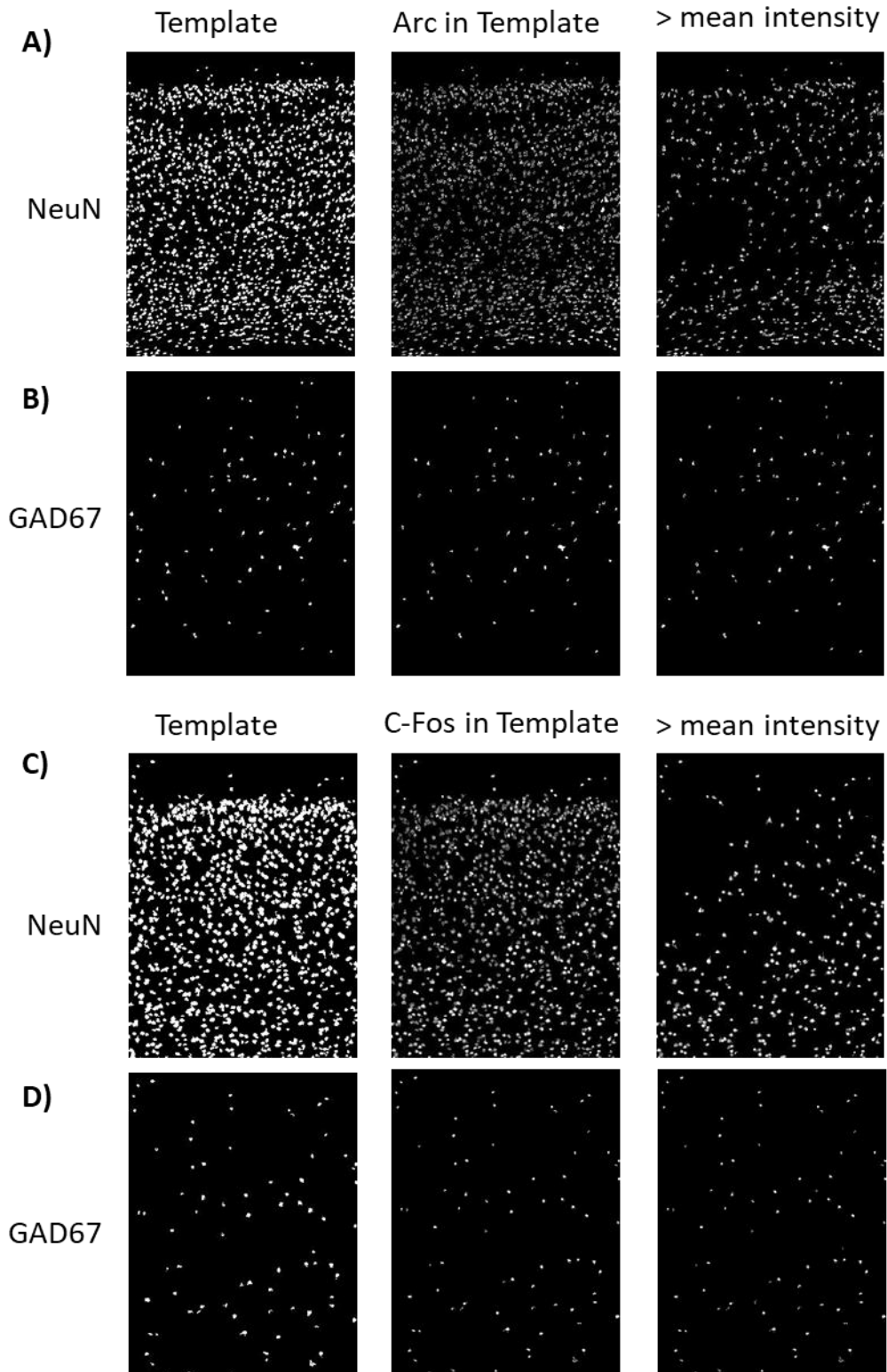
Figure 2.11. Example images of the colocalization of Arc and C-Fos in Neun and GAD67+ve cells. Ai) NeuN template **ii)** The composite of the ARC stain in all NeuN+ve cells **iii)** Thresholded Arc/NeuN composite image to retain objects brighter than the mean. **Bi)** GAD67 template **ii)**, the composite of the ARC stain in all GAD67+ve cells **iii)** Thresholded Arc/GAD67 composite image to retain objects brighter than the mean **Ci)** NeuN template **ii)** The composite of the c-Fos stain in all NeuN+ve cells **iii)** Thresholded c-Fos/NeuN composite image to retain objects brighter than the mean. **Di)** GAD67 template **ii)**, the composite of the c-Fos stain in all GAD67+ve cells **iii)** Thresholded c-Fos/GAD67 composite image to retain objects brighter than the mean.
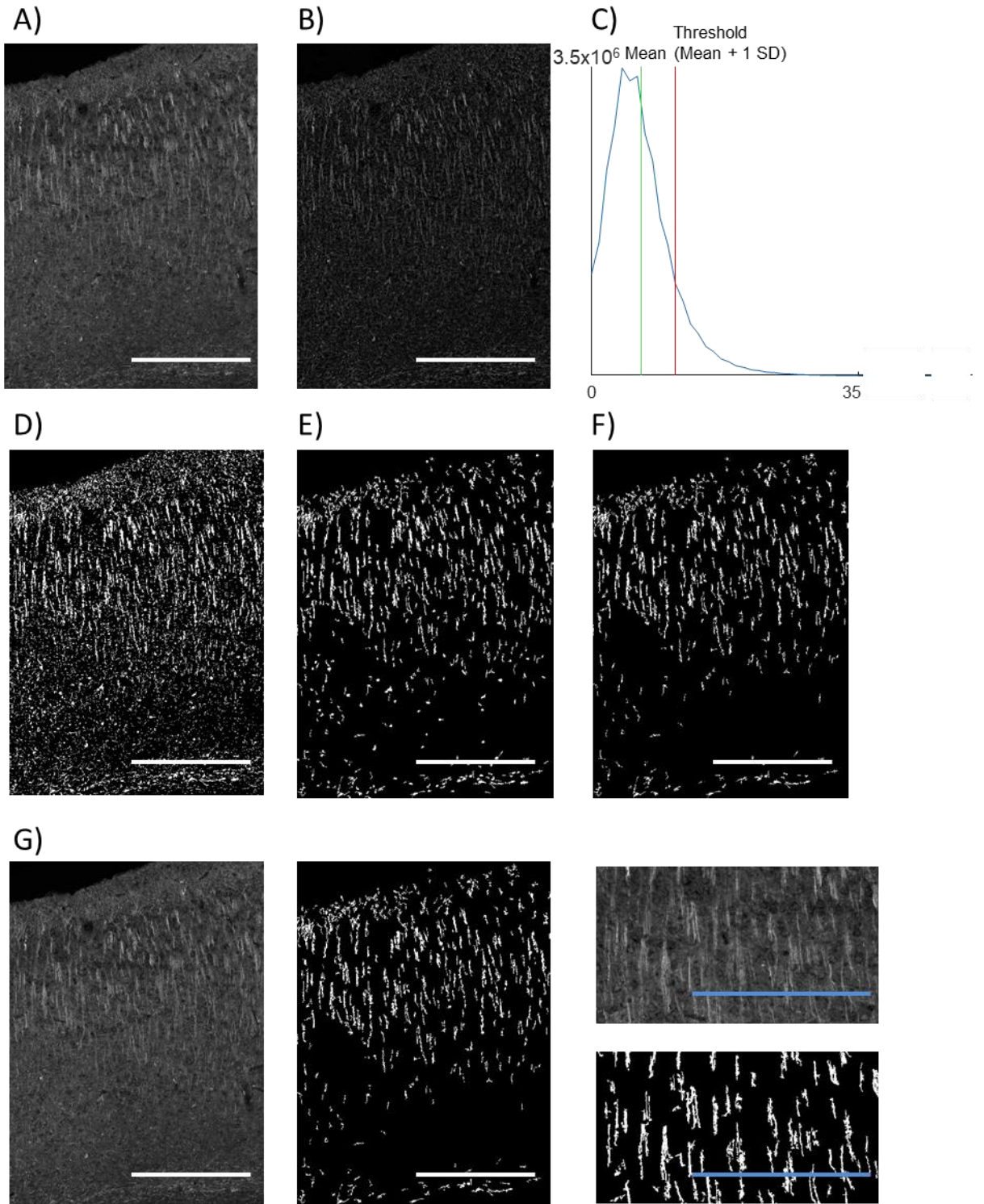
Figure 2.12. Example images of the processing of the ARC image to analyse dendritic expression. A) An example of the original Arc image. **B)** Background subtracted image. **C)** A graphical representation of the frequencies of pixel intensities in the image from B. (green = mean intensity of image, red = 1 standard deviation above the mean) **D)** A binary image after thresholding image C. by 1 standard deviation above the mean of the intensities in the images. **E)** Binary image after subtraction of objects less than 600 pixels in area from D. **F)** Binary image after removal of the roundest objects. **G)** Comparison of the original image and image after post-processing to reveal dendrites. White scale bars are 500µM, blue scale bars are 250µM.

2.3.2.5 The distribution of immediate early genes after image processing

Once the template co-localisations and dendrites were isolated, the number of pixels that survived processing for each measurement were quantified across the width of the cortical regions of interest to create cortical profiles (from pia to subcortical white matter) for every repeat (gamma, delta, and matched controls) which were then normalised for length and width.

To quantify the expression of c-Fos or Arc relative to oscillatory activity, matched slices from the same animal were used as a control. These control slices were processed in the same way as oscillating slices but were not exposed to the rhythm-generating drugs (Chapter 2.2.4). The mean profile of the oscillating condition minus matched controls were then calculated. These resulting profiles were also compared with the mean gamma vs. matched control profile being subtracted from the mean delta vs. matched control.

Because no significant differences were seen between delta and gamma conditions when compared to control, the original raw data was scrutinised more thoroughly, and it was noticed that there was large variability in the data set. This was primarily down to a large variation in the staining in slices deemed 'controls'. Therefore, direct comparisons between delta and gamma slices were also made to exclude the 'control' variability.

To mathematically interrogate the difference between gene expression profiles of each condition without controls, the problem of multiple comparisons was encountered. Each profile contained 6000 data points from (pia to cortical white matter), meaning that there was a high possibility of encountering false detection of significance (Type 1 error). Due to the considerable number of comparisons carried out, a Bonferroni correction was deemed unfit as it was too conservative and would very likely cause the false exclusion of significant (Type 2 error). Therefore, a moderate post hoc test was considered, based on the false detection rate (FDR) (Storey and Tibshirani, 2003). Although the most overt changes appeared to be in the dendritic Arc signal, this method was also used to assess the direct comparison somatic c-fos and Arc in neurons and interneurons.

2.4.3 Oscillation and dendritic Arc expression correlations

Upon creation of the cortical profile for each repeat of the experiment, the related electrophysiological data was used to compare with the distribution of Arc in dendrites. The cortical profiles were bisected tangentially, so that information regarding superficial and deep dendritic Arc signalling could be quantified separately. This was then compared with the area power, peak power, and peak frequency of the oscillation present (see Chapter 2.2.6). This was carried out for gamma and delta oscillating slices and included slices that were treated pharmacologically but did not generate an oscillation (to control, in part, for the presence of the drugs used to generate the oscillations).

2.4.4 Tangential and radial arrangement analysis

2.4.4.1 Radial and section analysis
To look further at the tangential arrangement of Arc in dendrites, a bespoke MATLAB program was written. This took the example image of Arc staining and applied a high pass filter to remove any objects within the image that had a patterned separation larger than that of the visual dendrite clusters. After this an autocorrelation on each row of the image to visualise the average spatial arrangement of the dendrites.

2.4.4.2 Preparation of tangential sections and analysis
Since radial sections of the Arc stained sections spread out in the cortex, which was curved, to obtain tangential sections of these the brain had to be flattened out. This was done with care to obtain tangential sections of S2. The subcortical structures were dissected out and the cortex was carefully flattened and place on filter paper to hold the flattened conformation. This was then fixed in PFA for 24 hours. The flattened brain was then glued to a vibratome plate with the subcortical white matter facing downwards before being cut to 30μM on a vibratome. All sections were retained and sections from layers II/III were then stained with Arc as in Chapter 2.4.1. Images were taken with a Zeiss LSM 710 motorised upright microscope with either x20 or x63 lens for different image resolutions. Images were taken as z-stacks and then the maximum intensity projection image was calculated in Zeiss Zen Software.

The spatial distribution of Arc stained dendrites in the tangential plane were analysed using a program written in MATLAB. This involved the thresholding of the image using the MATLAB program '*imquantize'* and the calculation of a normalised 2-d rotational autocorrelation of the image which is presented as a heat map.

2.5 Milliplex Cytokine Panel

2.5.1 Overview of the cytokine panel kit.

To analyse the presence of a systemic and neuroinflammatory environment after LPS and Poly I:C dosing, we analysed concentrations of cytokines and chemokines in the serum and brain of treated rats using a Milliplex MAP Rat Cytokine/Chemokine Magnetic Bead Panel Kit. This allows simultaneous quantification of 27 cytokine and chemokine analytes in samples of tissue lysate and serum: EGF, Eotaxin (CCL11), Fractalkine (CXC3L), G-CSF, GM-CSF, GRO/KC, IFN-γ, IL-1α, IL-1β, IL-2, IL-4, IL-5, IL-6, IL-10, IL-12 (p70), IL-13, IL-17A, IL-18, IP-10 (CXCL10), Leptin, LIX (CXCL5), MCP-1 (CCL2), MIP-1α (CCL3), MIP-2 (CXCL2), RANTES (CCL5), TNF-α, and VEGF

2.5.2 Milliplex sample preparation

To prepare brain tissue for the assay, remnants of the cerebral cortex that were not used for electrophysiology experiments were kept in the -80°C before protein extraction. Tissue was defrosted to room temperature and then transferred to a 15ml tube, with 1.5ml of homogenisation buffer.

The homogenate was transferred to a milli-tube containing an AFA fibre (Covaris, USA) these tubes were transferred to an E220 Focused-ultrasonicator (Covaris, USA) to lyse the tissue further by ultrasonication. The homogenate was then centrifuged at 4°C and 12000rcf for 5 minutes. The supernatant was then removed and again centrifuged for 2 minutes at 2000rcf.

For blood serum, 0.5 – 1ml of blood was taken from the heart immediately prior to transcardial perfusion. This blood was left to clot at room temperature for 30 minutes, before being centrifuged at 2,000 x g for 10 minutes. The supernatant serum was then collected and kept in the fridge for use in a cytokine panel.

2.5.3 Milliplex plate setup

To begin the assay, quality control samples (provided with the kit) were reconstituted and a serial dilution made of the standard solution (also provided) for comparison to allow eventual calculation of the concentration of cytokines/chemokines in experimental samples. The plate was washed with the assay buffer. Bead solution was added to every well analysed. The standard, quality controls and experimental samples were added to appropriate wells on the plate. Some wells were also left blank as a negative control. Serum matrix was added to the blank, standard, and quality control, and assay buffer (to make up the volume) was added to the samples wells and the blank.

The plate was then shaken for 2 hours at room temperature, after which the plate was washed and detection antibodies (provided with the kit) added into each well. The plate was then shaken for another 2 hours before adding Streptavidin-Phycoerythrin (provided with the kit) to each well and shaking for another 30 minutes. The plate was then washed, and sheath fluid was added to each well and shaken for 5 minutes before plate reading. The plate was then run on a Luminex 200 System.

2.5.4 Analysis of Milliplex assay results

Once the samples had been read and concentrations analysed, the data went through several quality control steps to extract accurate results. Firstly, the assay analysed how many beads were counted per well. Any observed concentrations from wells where <50 beads were counted were discounted from analyses. Further to this, the coefficient of variation (CV) was calculated for each of the triplicated samples any result with a CV percentage >30% was removed from further analyses. The mean was found from the remaining technical replicates, to provide a mean concentration for each sample, which was then averaged across biological replicates.

Chapter Three – Plasticity related gene changes in sleep- and wake-related oscillations

3.1 Introduction

3.1.1 Immediate early genes, plasticity, and brain states

Immediate early genes (IEGs) are rapidly transcribed in response to certain cellular stimuli and can provide information about the nature of the recent cellular activity. The two immediate early genes of particular interest in this chapter are c-fos and ARC/Arg3.1. C-fos upregulation was once believed to be entirely dependent upon general levels of neuronal activity. However more recent evidence suggests that it may be more specifically related to the generation of new patterns of activity (Svarnik et al., 2013). Arc, on the other hand, has a direct, activity-dependent association with synaptic plasticity involving both AMPA receptor internalisation and synaptic stabilisation (Shepherd et al., 2006).

The mRNAs for both these immediate early genes exhibit different expression patterns between sleep and wakefulness (Cirelli and Tononi, 2000b). This is not surprising as different networks of neurons fire in contrasting patterns in these brain states, and different modes of plasticity are dependent upon the timing of spikes that occur subsequent to different network oscillations (Markram et al., 2012). Delta oscillations are classically associated with deep (non-rapid eye movement, NREM) sleep and have been shown to associate with the consolidation of declarative memories, a process that requires synaptic plasticity. Cortical gamma oscillations, on the other hand, are associated with the processing of sensory information during wakefulness. The relationship between different spike timings during these oscillations and the type of synaptic plasticity they induce are not fully understood to date.

What is known is that synaptic interconnections become stronger during novel experiences in the wake state – a substrate for memory (Bliss and Collingridge, 1993). This represents Hebbian plasticity, whereby neuronal connections are selectively modified in a use-dependent manner (Turrigiano and Nelson, 2000). This form of plasticity may account for increases in immediate early gene expression seen after learning-dependent tasks (Guzowski et al., 2001; Kelly and Deadwyler, 2003; Hanlon et al., 2009). For these memories to be made permanent they need to be consolidated during sleep (Dudai et al., 2015). This requires another plastic process which is thought to prune away weaker synaptic connections. This process, known as synaptic rescaling, has been proven on the anatomical (de Vivo et al., 2017) and molecular level (Diering et al., 2017).

The pruning and depotentiation of weaker synapses, as suggested by the synaptic rescaling hypothesis, is not just important in memory consolidation but has also been implicated in a process known as synaptic homeostasis. The scaling of synaptic strengths is needed to balance the formation of new memories with the metabolic nutrient supply and availability of physical space in the neuropil for new connections.

It is likely that processes underlying synaptic scaling occur during sleep as it is a state with less propensity for LTP. This is thought to be due to several factors: Firstly, dopamine levels need to be low in the brain to facilitate deep (slow-wave/delta) sleep (Dzirasa et al., 2006) and lower dopamine levels have a detrimental effect on long term potentiation of synaptic strengths (Li et al., 2003). Secondly, there is a strong diminishment (if not complete absence) of long-term memory acquisition during deep sleep due to the absence of sensory input (Tononi and Cirelli, 2001). Furthermore, the amount of SWA during NREM sleep was found to be related to increased synaptic strength during prior wakefulness and not simply a response to increasing cell firing (Rodriguez et al., 2016). So, whilst NREM sleep may be the target for this synaptic rescaling, exactly which connections are altered, between which neuron subtypes, during NREM sleep is not known.

3.1.2 Aims of this chapter

This chapter aims to use immediate early gene expression changes to map the location and levels of cortical plasticity during rhythms associated with NREM sleep and cortical activation in wakefulness. For this *in vitro* preparations of brain tissue were used, in which pharmacologically induced oscillations (delta oscillations and gamma oscillations respectively) were generated to differentiate regional and laminar cortical changes in network dynamics associated with NREM sleep and cortical activation. Analyses of IEG signals in these conditions was carried out, with respect to specific cell subtypes and sub-compartments that contribute to these rhythms, and their patterned organisation.

3.2 Results

3.2.1 Regional difference in overall IEG expression in different brain states

The presence of IEG protein expression was first analysed in sub-sectioned slices of *in vitro* preparations of rat neocortex in the absence of any templates for co-expressed neuronal markers. This expression was compared between slices that had previously generated wake-state (gamma) or sleep-related (delta) oscillations and those that had been left untreated with oscillation-inducing drugs.

The overall expression of c-Fos and Arc were analysed in isolated primary sensory and secondary association cortical regions; the same regions were used in more detailed, further analyses using neuronal templates. The mean intensity of staining in each region (minus background) was analysed and compared between conditions and matched controls.

There was no significant difference in C-fos intensity when comparing each oscillating condition to the matched control data (S1. Control vs. Delta, 11.64 ± 1.86 vs. 10.52 ± 0.81, T-test, p = 0. 530; S2. Control vs. Delta, 10.95 ± 1.41 vs. 10.10 ± 0.89, T-test, p = 0.604; Au1. Control vs. Gamma, 9.87 ± 1.52 vs. 6.98 ± 0.94, T-test, p = 0.127; S2. Control vs. Gamma, 10.377 ± 4.95 vs. 7.01 ± 0.98, T-test, p = 0.098). However, the mean C-fos intensity was lower in gamma oscillating slices compared to slices exhibiting a delta rhythm *(Figure 3.1A)*. In the primary sensory cortex, the mean intensity of c-Fos staining was more from in gamma oscillating slices than delta oscillating slices (gamma: 7.04 ± 1.07; delta: 10.52 ± 0.81, p = 0.013, n=9/8, T-test). In the secondary association cortex, the mean intensity of c-Fos staining was also more (gamma: 7.11 ± 1.10; delta: 10.10 ± 0.88 in, p = 0.034, n=9/8, T-test).

There was also no significant difference in Arc intensity when comparing each oscillating condition to the matched control data (S1. Control vs. Delta, 8.00 ± 1.64 vs. 5.66 ± 0.56, T-test, p = 0.162; S2. Control vs. Delta, 8.38 ± 2.15 vs. 5.68 ± 0.66, T-test, p = 0.208; Au1. Control vs. Gamma, 10.70 ± 2.43 vs. 7.85 ± 0.61, T-test, p = 0.320; S2. Control vs. Gamma, 11.22 ± 2.46 vs. 7.75 ± 0.67, T-test, p = 0.195). However, there was lower overall expression seen in delta oscillating slices compared to those exhibiting gamma oscillations *(Figure 3.1B)*. In primary sensory cortex, the mean intensity of Arc staining was lower from 7.85 ± 0.61 in gamma oscillating slices to 5.66 ± 0.56 in delta oscillating slices to (p = 0.024, n=7/6, T-test). Secondary association cortex the mean intensity of c-fos staining was less, from 7.75 ± 0.67 in gamma oscillating slices to 5.68 ± 0.66 in delta oscillating slices (p = 0.024, n=7/6, T- test).
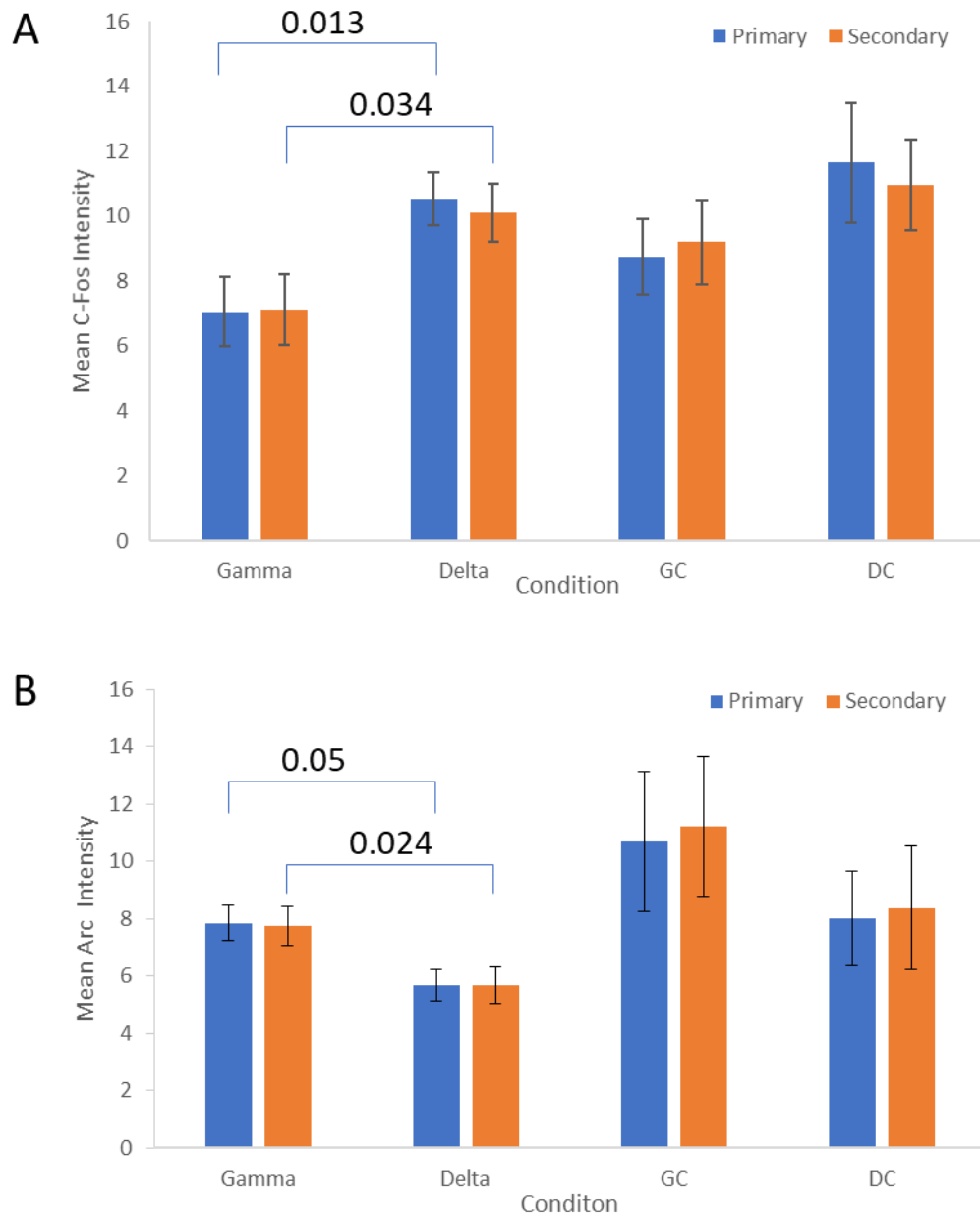
Figure 3.1. Bi-directional gross changes to c-Fos and Arc expression are seen in the neocortex between gamma and delta oscillations slices. A. The mean intensity of total c-Fos staining after background subtraction in primary and secondary cortical regions in in vitro slices exhibiting gamma (n=9) and delta oscillations (n=8) as well as matched controls to gamma slices (GC, n=9) and controls to delta slices (DC, n=4) . Numbers represent p values after t-test. Error bars show standard error of the mean. **B.** The mean intensity of Arc staining after background subtraction in primary and secondary cortical regions in in vitro slices exhibiting gamma (n=6) and delta oscillations (n=6) as well as matched controls to gamma slices (GC, n=9) and controls to delta slices (DC, n=4). Numbers represent p values from t-test. Error bars show standard error of the mean.

3.2.2 Laminar, soma-specific IEG during different brain states compared to control

Looking further into the cytoarchitectural origin of the above differences in immediate early gene expression, dual immunostaining was used to look at the localisation of IEG signals in cell bodies in certain cell types and cortical layers. C-fos expression was analysed in cells also stained with NeuN, a marker for neuronal nuclei and GAD67, a marker for ca. 96% of cortical interneurons (Sahara et al., 2012). Primary sensory and secondary association areas were analysed separately and the laminar distribution of c-fos in NeuN+ve cells was measured in oscillating slices. T-tests were run on every data point from the pia to subcortical white matter.

For any points that were statistically significant a modified q value was calculated using a false detection rate (FDR) correction for multiple comparisons. The difference between the oscillating condition and untreated controls from the same animal were then compared to display the activity change due to the oscillation.

During delta oscillations, the neuronal c-Fos expression did not show any significant differences across the cortex (*Figure 3.2 Ai and Bi)* compared to control in either the primary sensory cortex (biggest difference in S1 at 607.8 μm. Control vs. delta, 0.449 ± 0.276 vs. 0.996 ± 0.262, T-test, p = 0.2, with FDR, q = 0.9589) or in the secondary association cortex (biggest difference in S2 at 437.8μm. Control vs. delta, 0.543 ± 0.484 vs. 1.139 ± 0.492, T-test, p = 0.4211, with FDR, q = 0.890). During gamma oscillations the largest difference was a decrease in the mean c-Fos levels compared to control in superficial layers *(Figure 3.2 Aii and Bii)* but this was not significant in either the primary sensory cortex (Au1 at 710.8μm. Control vs. gamma, 1.056 ± 0.449 vs. 0.227 ± 0.071, T-test, p = 0.093, with FDR, q = 0.312) and secondary association cortices (S2 at 1408.6μm. Control vs. gamma, 0.833 ± 0.236 vs. 0.130 ± 0.038 T-test, p = 0.0123, with FDR, q = 0.344)*.

To compare delta and gamma oscillating conditions, the control-subtracted profiles related to the gene expression gamma oscillating condition were subtracted from the delta condition profile *(Figure 3.2 Aiv and Biv)*. There was an higher mean c-fos levels in NeuN+ve cells during delta conditions but this was not significant in primary cortex (681.5μm. Delta - Control vs. Gamma – Control: -0.043 ± 0.307 vs. -0.826 ± 0.510, T-test, p = 0.262, with FDR, q = 0.554) or secondary association cortex 607.8μm. Delta - Control vs. Gamma – Control: 0.534 ± 452 vs. -0.427 ± 0.171, T-test, p = 0.040, with FDR, q = 0.478)*.

In line with the lack of change in c-Fos expression in NeuN+ve cells when comparing each oscillation, c-Fos expression in GAD67+ve cells also showed no change. Even the largest difference from control levels of c-Fos expression was not significant in either region during gamma *(Figure 3.3 A/B, i&ii)* (Au1 at 436.2µm. Control vs. gamma, 0.401 ± 0.238 vs.0.095 ± 0.055, T test, p = 0.2332, with FDR, q = 0.529; S2 at 113.4µm. Control vs. gamma, 0.348 ± 0.312 vs. 0.032 ± 0.016, T test, p = 0.331, with FDR, q = 0.712) or delta (S1 at 1279.9µm. Control vs. delta, 0.240 ± 0.112 vs. 0.035 ± 0.034, T test, p = 0.130, with FDR, q = 0.997; S2 at 745.2µm. Control vs. delta, 0.108 ± 0.071 vs. 0.260 ± 0.120, T test, p = 0.318, with FDR, q = 0.723). Even when directly comparing the two rhythms there were no significant differences *(Figure 3.3 A/Biv)* (primary cortex, 567.5µm. Delta - Control vs. Gamma – Control: 0.055 ± 0.066 vs. -0.215 ± 0.151, T-test, p = 0.225, with FDR, q = 0.831; or secondary association cortex 113.4µm. Delta - Control vs. Gamma – Control: 0.000 ± 0.000 vs. -0.3162 ± 0.309, T-test, p = 0.468, with FDR, q = 0.853)*.

Somatic Arc expression was also measured for its presence in neurons (NeuN) and interneurons (GAD67). In neurons, during both gamma rhythms (Au1, 1913.0µm. Control vs. Gamma: 0.397 ± 0.217 vs. 0.913 ± 0.309, T-test, p = 0.197, with FDR, q = 0.713; S2, 637.0µm. Control vs. Gamma: 0.414 ± 0.175 vs. 0.082 ± 0.038, T-test, p = 0.088, with FDR, q = 0.902) and delta rhythms (S1 1940.6µm. Control vs. Delta: 0.960 ± 0.626 vs. 0.272 ± 0.122, T-test, p values = 0.302, with FDR q= 0.480; S2, 1925.6µm, Control vs. Delta: 0.505 ± 0.241 vs. 0.042 ± 0.021, p value = 0.080, q value = 0.420) somatic ARC expression did not show any change from the untreated control condition. When comparing delta and gamma oscillation conditions directly, the difference in layer VI staining was more noticeable, and appeared only in primary cortical regions but was not significant *(Figure 3.4 Aiv)* (1ry: 1922.4µm, Delta-Control vs Gamma-Control: -0.669 ± 0.467 vs. 0.279 ± 0.226, T-test, p = 0.092, with FDR q = 0.513*)*. There was also no difference in somatic Arc distribution in secondary association regions (*Figure 3.4 Biv)* (2ry: 1925.3µm, Delta-control vs Gamma-Control: -0.459 ± 0.235 vs. 0.075 ± 0.207, T-test, p = 0.245, with FDR q = 0.999).

Much like the expression of c-Fos, there was very little change in the GAD67+ve cell expression of Arc compared to control in any condition (*Figure 3.5. A/B, i &ii)* (Au1, 1163.9µm. Control vs. Gamma: 0.0312 ± 0.0149 vs. 0.241 ± 0.020, T-test, p = 0.321, with FDR, q = 0.4351; S2, 1269.1µm. Control vs. Gamma: 0.005 ± 0.004 vs. 0.139 ± 0.124, T-test, p = 0.301, with FDR, q = 0.660; S1, 1297.1µm. Control vs. Delta: 0.147 ± 0.072 vs. 0.020 ± 0.020, T-test, p = 0.117, with FDR, q = 0.647; S2 1623.0µm, Control vs. Delta: 0.190 ± 0.1826 vs. 0.003 ± 0.003, T-test, p = 0.326, with

FDR, q = 0.469). However, there was a decrease in the mean ARC expression in the superficial layers of primary cortical regions during delta compared to gamma, however this was not significant *(Figure 3.5. Aiv)* (1ry, 1162.2µm, Delta-Control vs. Gamma-Control: -0.012 ± 0.018 vs. 0.207 ± 0.208, T-test p = 0.314, with FDR q = 0.388). This difference was very slight and not apparent in secondary association regions *(Figure 3.5. Biv)* (2ry, 1269.5µm, Delta-Control vs. Gamma-Control: -0.063 ± 0.082 vs. 0.133 ± 0.126, T-test, p = 0.217, with FDR, q = 0.697).

Primary Sensory Cortex

Secondary Association Cortex

Ai. Delta Aii. Gamma Bi. Delta Bii. Gamma

Aiii. Aiv. Delta - Gamma Biii. Biv. Delta - Gamma
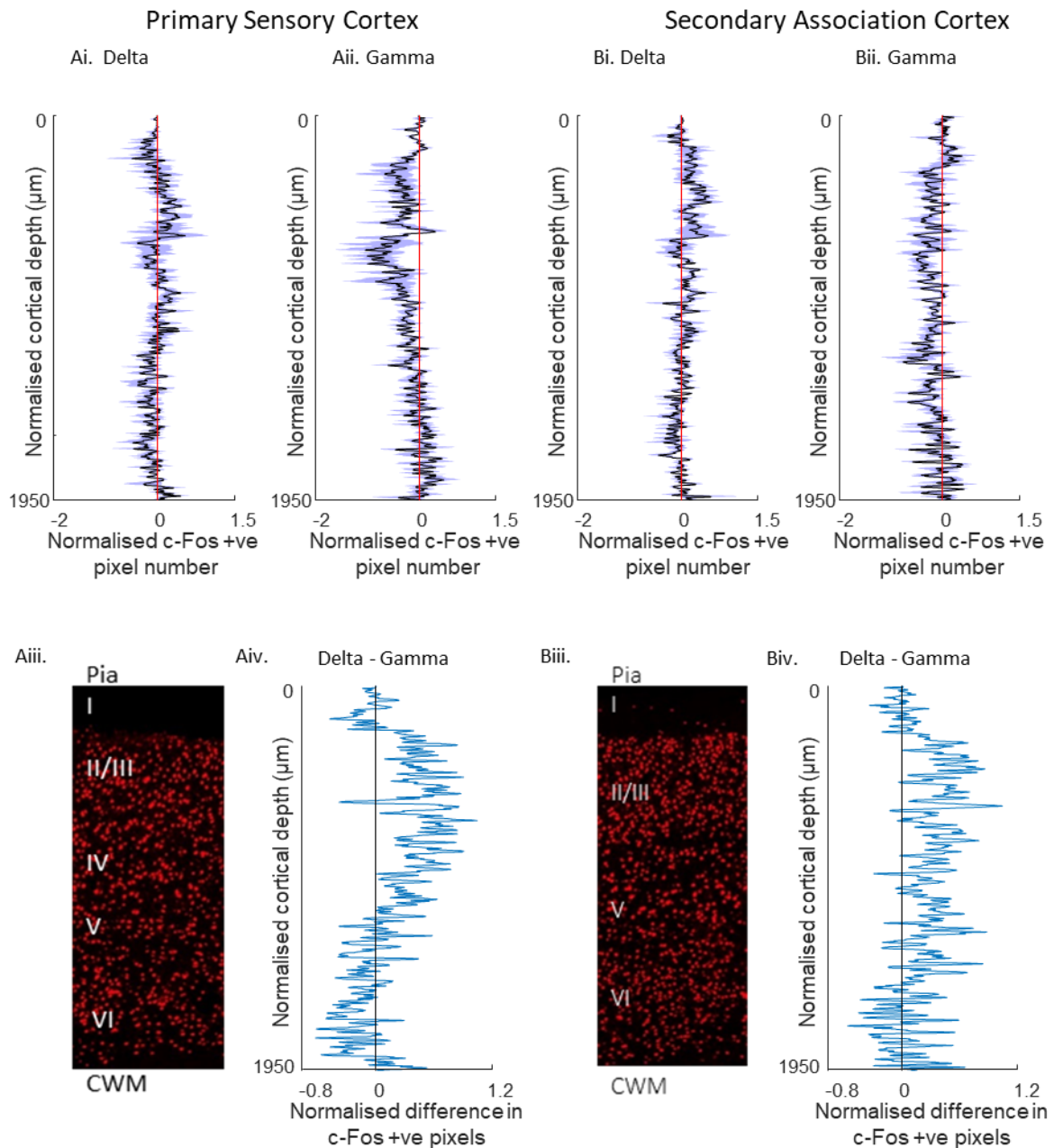
Figure 3.2. The laminar distribution of c-Fos expression in neuronal cell bodies does not change significantly between gamma and delta conditions, in primary and secondary association regions. (A) - The mean distribution of c-Fos in NeuN+ve cells from pia (0µm) to subcortical white matter (1950µm). c-Fos distributions were compared to control in the primary sensory cortex of delta oscillating slices **(Ai)** n=4 and gamma oscillating slices **(Aii),** n=7. Error shown is SEM. **(Aiii)** An example of the distribution of NeuN+ve cells in the primary auditory cortex for comparison. **(Aiv)** The difference, compared to control, of c-Fos expression in NeuN+ve cells across layers between gamma and delta oscillations in primary sensory regions. A positive value describes higher expression during delta than gamma. **(B) -** The mean distribution of c-Fos in NeuN+ve cells from pia (0) to subcortical white matter (1950µm) in the secondary association cortex of delta oscillating slices **(Bii)** n=4 and **(Bii)** gamma oscillating slices, n=7. Both compared to control. Error shown is SEM. **(Biii)** An example of the distribution of NeuN cells in the secondary somatosensory cortex for comparison. **(Biv)** The difference, compared to control, of c-Fos expression in NeuN+ve cells across layers between gamma and delta oscillations in secondary association cortex. A positive value describes higher expression during delta than gamma.

Primary Sensory Cortex

Ai. Delta   Aii. Gamma

Secondary Association Cortex

Bi. Delta   Bii. Gamma

Aiii.   Aiv. Delta - Gamma   Biii.   Biv. Delta - Gamma

Figure 3.3 The laminar distribution of c-Fos expression in GAD67+ve cells shows no change between gamma and delta conditions, in primary and secondary association regions. **(A)** - The mean distribution of c-Fos in GAD67+ve cells from pia (0μm) to subcortical white matter (1950μm). c-Fos distributions were compared to control in the primary sensory cortex of delta oscillating slices **(Ai)** n=4 and gamma oscillating slices **(Aii),** n=7. Error shown is SEM. **(Aiii)** An example of the distribution of GAD67+ve cells in the primary auditory cortex for comparison. **(Aiv)** The difference, compared to control, of c-Fos expression in GAD67+ve cells across layers between gamma and delta oscillations in primary sensory regions. A positive value describes higher expression during delta than gamma. **(B)** - The mean distribution of c-Fos in GAD67+ve cells from pia (0) to subcortical white matter (1950μm) in the secondary association cortex of delta oscillating slices **(Bii)** n=4 and **(Bii)** gamma oscillating slices, n=7. Both compared to control. Error shown is SEM. **(Biii)** An example of the distribution of GAD67+ve cells in the secondary somatosensory cortex for comparison. **(Biv)** The difference, compared to control, of c-Fos expression in GAD67+ve cells across layers between gamma and delta oscillations in secondary association cortex. A positive value describes higher expression during delta than gamma.

Primary Sensory Cortex

Secondary Association Cortex

Figure 3.4. The laminar distribution of Arc expression in neuronal cell bodies does not change between gamma and delta conditions, in primary and secondary association regions. (A) - The mean distribution of Arc in NeuN+ve cells from pia (0µm) to subcortical white matter (1950µm). Arc distributions were compared to control in the primary sensory cortex of delta oscillating slices **(Ai)** n=7 and gamma oscillating slices **(Aii)**, n=7. Error shown is SEM. **(Aiii)** An example of the distribution of NeuN+ve cells in the primary auditory cortex for comparison. (**Aiv)** The difference, compared to control, of Arc expression in NeuN+ve cells across layers between gamma and delta oscillations in primary sensory regions. A positive value describes higher expression during delta than gamma. **(B)** - The mean distribution of Arc in NeuN+ve cells from pia (0) to subcortical white matter (1950µm) in the secondary association cortex of delta oscillating slices **(Bii)** n=7 and **(Bii)** gamma oscillating slices, n=7. Both compared to control. Error shown is SEM. **(Biii)** An example of the distribution of NeuN cells in the secondary somatosensory cortex for comparison. **(Biv)** The difference, compared to control, of Arc expression in NeuN+ve cells across layers between gamma and delta oscillations in secondary association cortex. A positive value describes higher expression during delta than gamma.

Primary Sensory Cortex

Ai. Delta Aii. Gamma

Secondary Association Cortex

Bi. Delta Bii. Gamma

Aiii. Pia / CWM Aiv. Delta - Gamma

Biii. Pia / CWM Biv. Delta - Gamma

Figure 3.5. The laminar distribution of somatic Arc expression in GAD67+ve cells shows no change between gamma and delta conditions, in primary and secondary association regions. (A) The mean distribution of Arc in GAD67+ve cells from pia (0µm) to subcortical white matter (1950µm). Arc distributions were compared to control in the primary sensory cortex of delta oscillating slices **(Ai)** n=7 and gamma oscillating slices **(Aii),** n=7. Error shown is SEM. **(Aiii)** An example of the distribution of GAD67+ve cells in the primary auditory cortex for comparison. **(Aiv)** The difference, compared to control, of Arc expression in GAD67+ve cells across layers between gamma and delta oscillations in primary sensory regions. A positive value describes higher expression during delta than gamma. **(B) -** The mean distribution of Arc in GAD67+ve cells from pia (0) to subcortical white matter (1950µm) in the secondary association cortex of delta oscillating slices **(Bii)** n=7 and **(Bii)** gamma oscillating slices, n=7. Both compared to control. Error shown is SEM. **(Biii)** An example of the distribution of GAD67+ve cells in the secondary somatosensory cortex for comparison. **(Biv)** The difference, compared to control, of Arc expression in GAD67+ve cells across layers between gamma and delta oscillations in secondary association cortex. A positive value describes higher expression during delta than gamma.

ARC is not only expressed in neuronal cell bodies, but also in dendrites. This was clear under visual inspection of oscillating slices in the primary sensory and secondary association cortices. Arc staining was visible in radially arranged dendrites/dendrite clusters that projected across intermediate and superficial layers. Arc staining was also apparent in some layer VI dendrites others of which stretched horizontally *(Figure 3.6 A and B)*.

Whilst this dendritic expression was conserved between delta and gamma, across the regions examined, there were large and contrasting patterns during gamma and delta rhythms. The largest difference in dendritic Arc staining was in superficial layers which was higher in delta conditions compared to gamma *(Figure 3.7Ai/ii)* however this was not significant (S1, 1327.0μm, Control vs. Delta: 27.0 ± 12.4 vs. 7.4 ± 1.5, T-test, p = 0.142, with FDR q = 0.954; S2, 33.1250 μm 22.8 ± 5.1 vs. 47.7 ± 10.8, T-test, p = 0.0587, with FDR q = 0.486). During gamma oscillations dendritic ARC expression there was a mean decrease compared to control in both primary sensory and secondary association cortices, though this was not significant *(Figure 3.7 A&Bii)* (Au1, 659.4 μm, Control vs. Gamma: 30.7 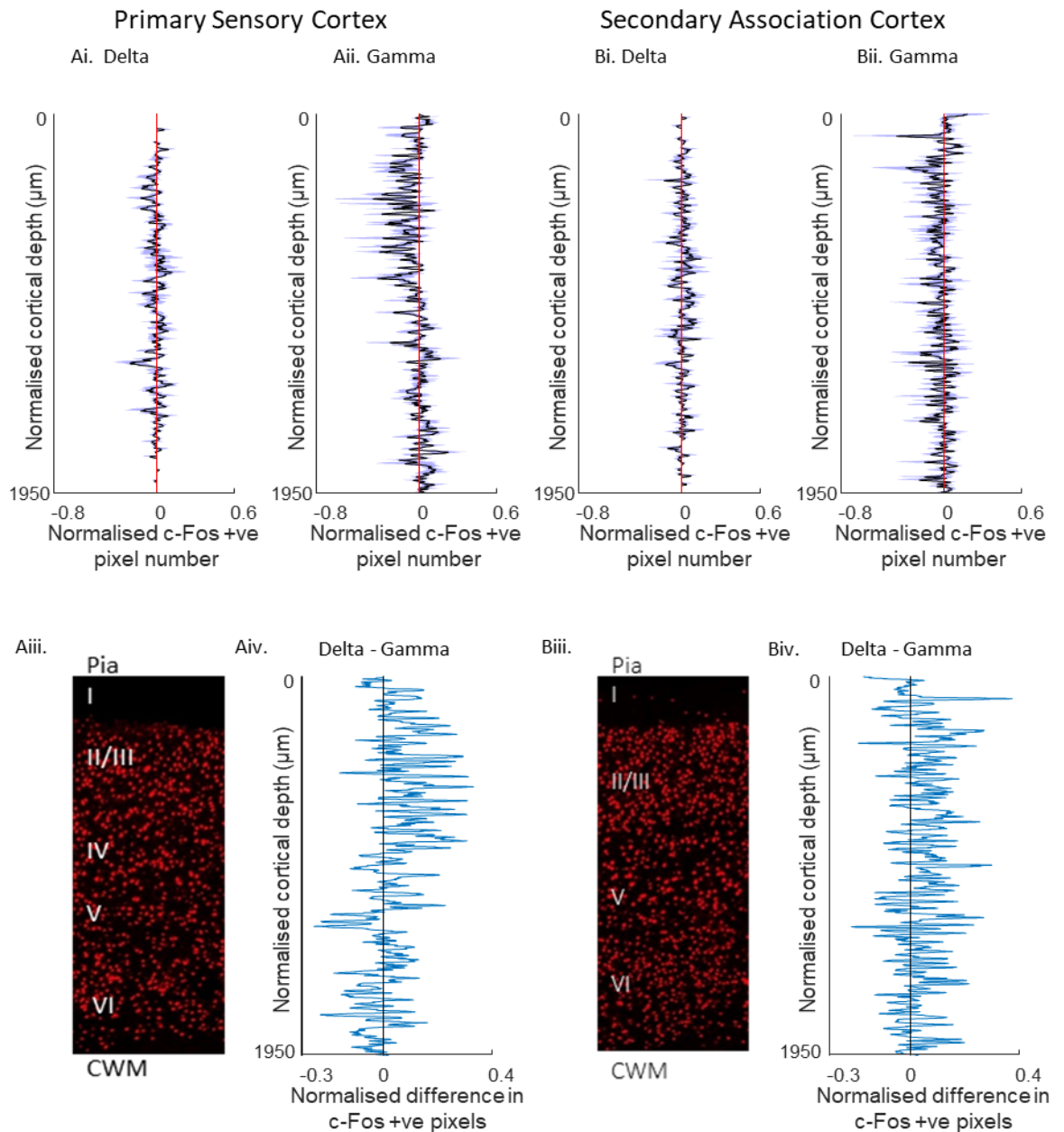± 10.8 vs. 15.2 ± 3.2, T-test, p = 0.1948, with FDR q = 0.972: S2, 225.2 μm Control vs. Gamma: 32.4 ± 12.4 vs. 14.7 ± 5.6, T-test, p = 0.2201, with FDR q = 0.640).

Comparing between oscillation conditions there seemed to be more superficial dendritic Arc signalling in delta oscillations in both regions (*Figure 3.7 Aiv/Biv)*. Only in primary cortical regions did there was a mean decrease in deep layers in delta compared to gamma oscillations. But these differences were not significant (S1, 683.5 μm Delta-Control vs. Gamma-Control: 15.2 ± 8.2 vs. -13.2 ± 10.5, T-test, p = 0.054, with FDR q = 0.981: S2, 233.7 μm, Delta-Control vs. Gamma-Control: 24.6 ± 12.4 vs. -16.9 ± 16.2, T-test, p = 0.0642, with FDR q = 0.129)

Whilst these differences appeared to be noteworthy from visual inspection of the graphs none of the differences seen were significant. On examination of the raw data, the main contributory factor to the variability of the data set was the 'control' values which showed much greater variability (*Figure 3.8 A*) than the oscillatory condition (*Figure 3.8 B).* This added variability once the control data was subtracted from the oscillating profile *(Figure 3.8C)*. This variance was measured with the MATLAB programme *'var'* and the mean variance of the data sets was calculated (matched control vs gamma: 187.72 vs. 120.33). With the high variance in the matched control, this control data was therefore put aside, and the above analyses were repeated with a direct comparison between oscillation states.

A. Delta Oscillating Slice
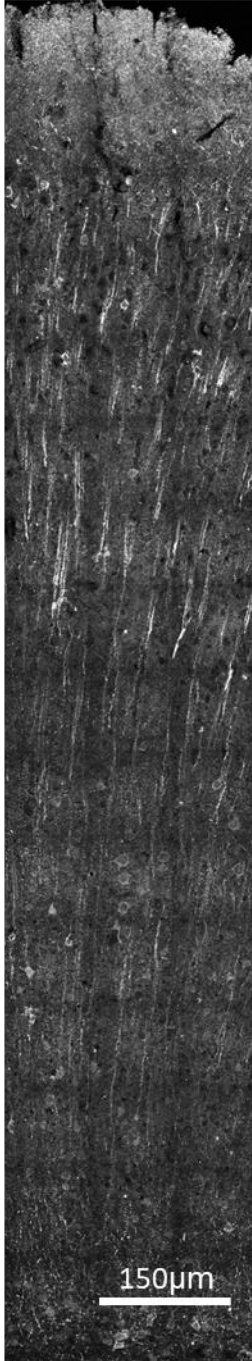
i. Primary Sensory Cortex
ii. Secondary Association Cortex
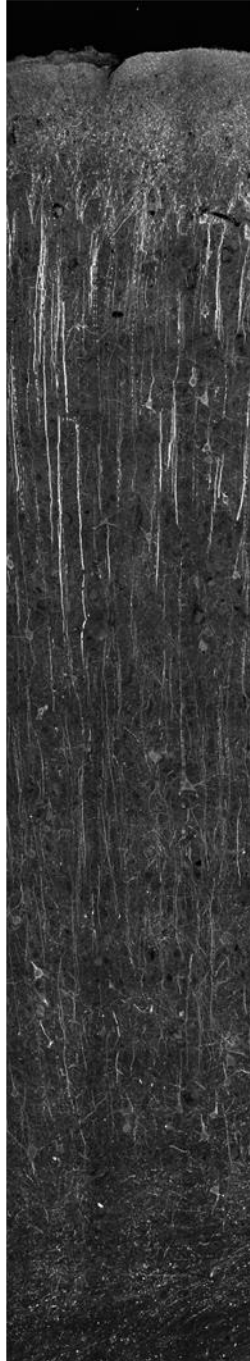
B. Gamma Oscillating Slice
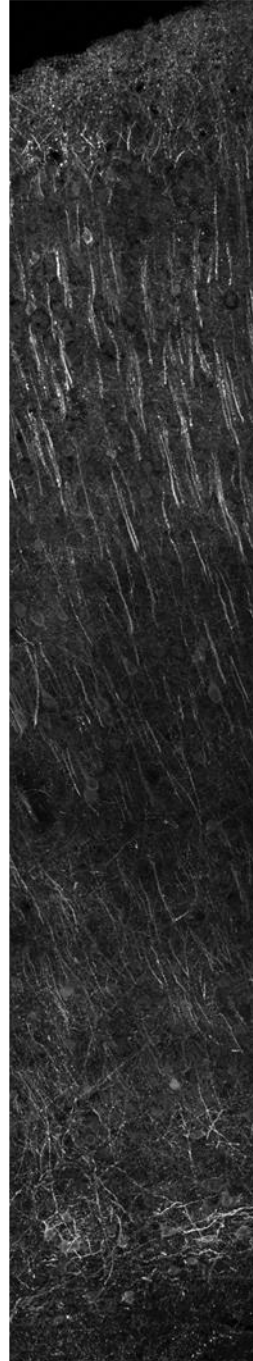
i. Primary Sensory Cortex
ii. Secondary Association Cortex
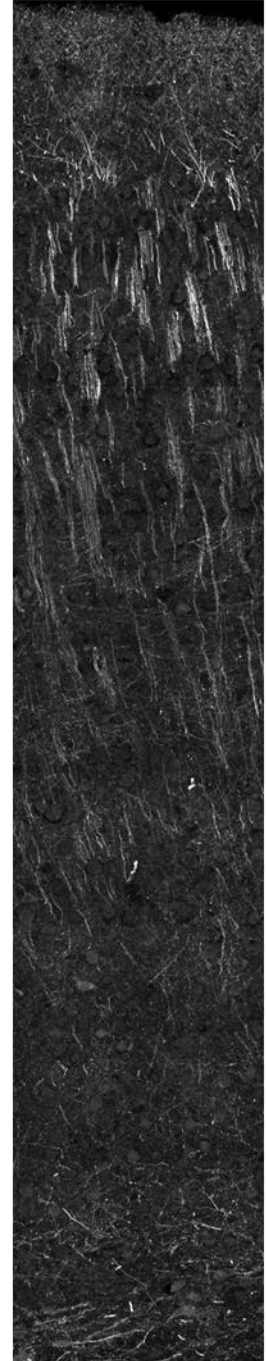
Figure 3.6 Dendritic Arc staining is more prevalent than somatic staining in neocortical regions. A. Confocal tile scan images taken at a magnification of 63x from a slice of neocortex previously exhibiting delta oscillations in the Primary Somatosensory Cortex (i) and the Secondary Somatosensory Cortex (ii). Scale bar is 150μm. **B.** Confocal tile scan images taken at a magnification of 63x from a slice neocortex previously exhibiting gamma oscillations in the Primary Auditory Cortex (i) and the Secondary Somatosensory Cortex (ii). Scale bar is 150μm.

Primary Sensory Cortex

Ai. Delta

Aii. Gamma

Secondary Association Cortex

Bi. Delta

Bii. Gamma

Aiii.

Aiv.

Biii.

Biv.

Figure 3.7. The laminar distribution of dendritic Arc expression does not significantly change between gamma and delta conditions, in primary and secondary association regions. (A) The mean distribution of ARC in dendrites from pia (0µm) to subcortical white matter (1950µm) in the primary sensory cortex of delta oscillating slices **(Ai)** n=7, and gamma oscillating slices **(Aii)** n=7. Both compared to control. Error shown is SEM. **(Aiii)** An example of the distribution of NeuN +ve cells in the primary auditory cortex for comparison. **(Aiv)** The difference, compared to control, of dendritic ARC expression across layers between gamma and delta oscillations in primary sensory regions. A positive value describes higher expression during delta than gamma. **(B)** The mean distribution of ARC in dendrites from pia (0µm) to subcortical white matter (1950µm) in the secondary association cortex of delta oscillating slices **(i)** n=7 and gamma oscillating slices **(Bii)** n=7. Both compared to control. Error shown is SEM. **(Biii)** An example of the distribution of NeuN +ve cells in the secondary somatosensory cortex for comparison. **(Biv)** The difference, compared to control, of dendritic ARC expression across layers between gamma and delta oscillations in secondary association cortex. A positive value describes higher expression during delta than gamma.
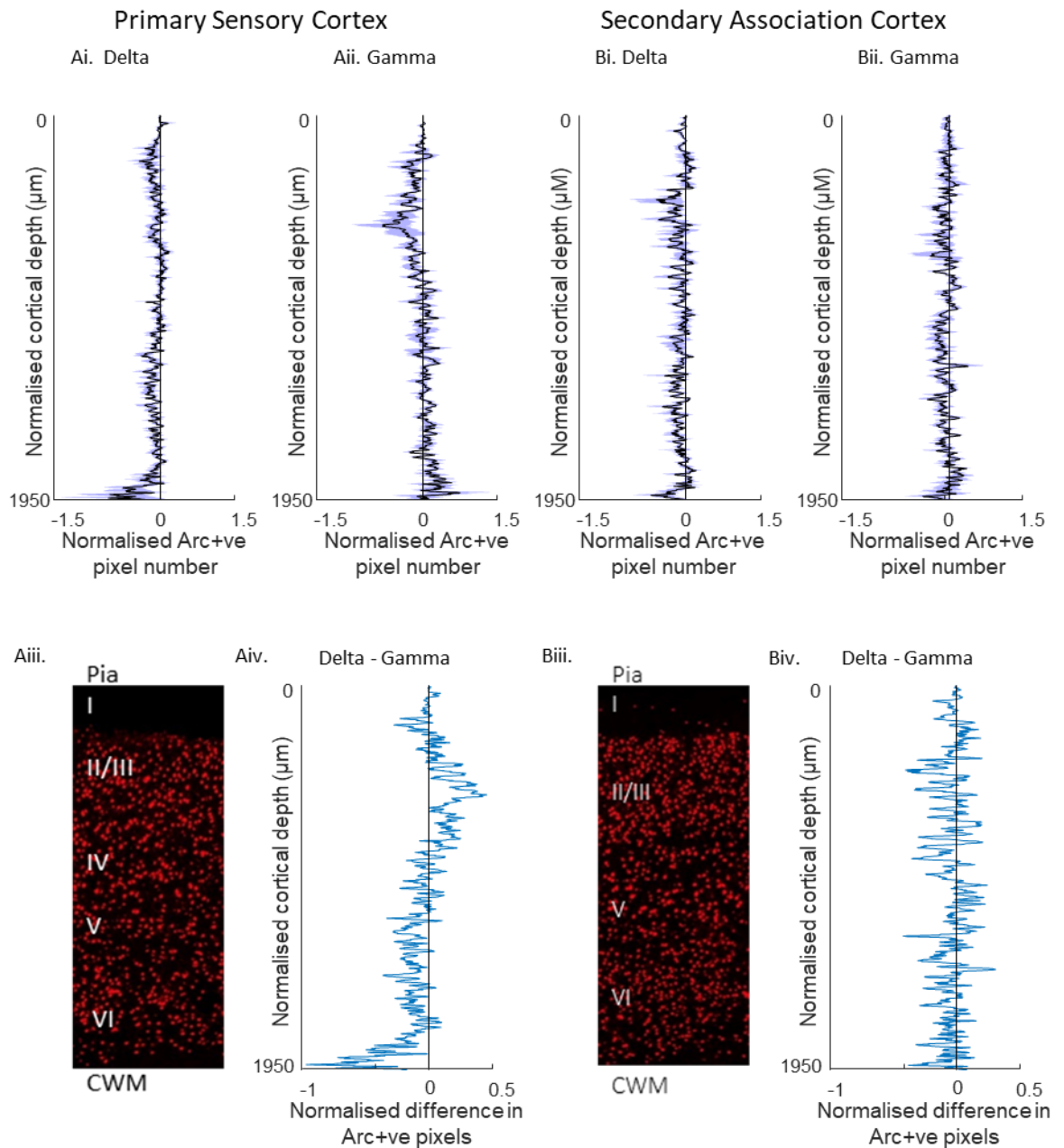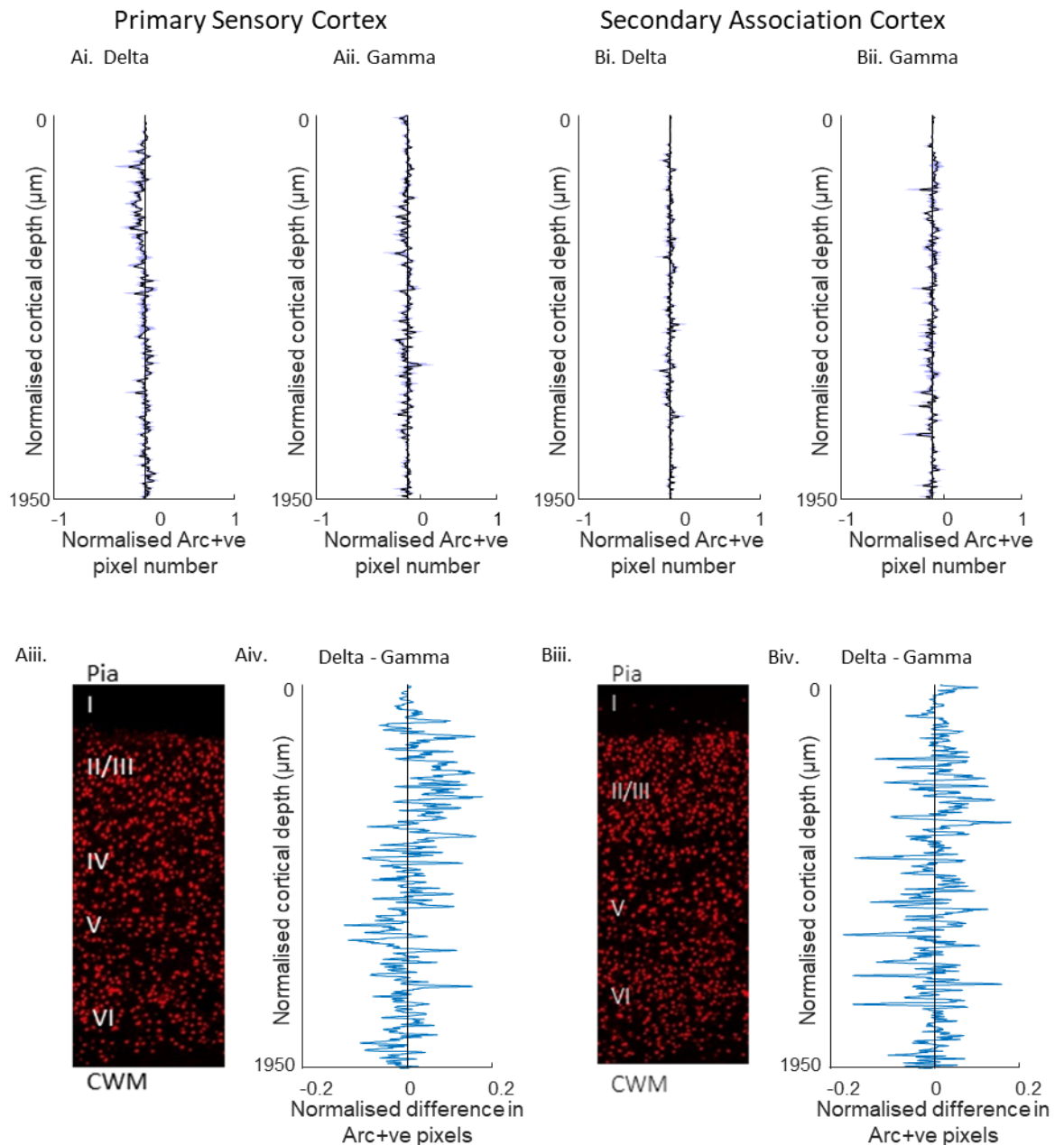
3.2.3 Direct comparison of laminar IEG expression changes in different brain states

The direct comparison of c-fos in NeuN+ve cells did not show any differences in the distribution of c-fos staining between gamma and delta rhythms, however there was a higher mean NeuN+ve cell c-fos expression during delta rhythms (*Figure 3.9A)*, and the mean difference was largest in superficial layers of the primary cortex (*Figure 3.9Ai)*. However, these differences were not significant (S1, 602.6 µm, Delta vs. Gamma: 0.950 ± 0.290, vs. 0.227 ± 0.090, T-test, p = 0.0156, with FDR q = 0.2294: S2, 422.2 µm, Delta vs. Gamma: 1.199 ± 0.661 vs. 0.244 ± 0.148, T-test, p = 0.099, with FDR q = 0.187).

The c-fos expression was unchanged between delta and gamma oscillating slices in GAD67+ve cells *(Figure 3.9B)*. (S1, 1740.1µm, Delta vs. Gamma: 0 ± 0 vs. 0.190 ± 0.122, T-test, p = 0.279, with FDR q = 0.593: S2, 1158.0µm, Delta vs. Gamma: 0.257 ±0.139 vs. 0.071 ± 0.047, T-test, p = 0.152, with FDR q = 0.561).

Directly comparing gamma and delta rhythms for somatic Arc also showed no significant differences between conditions *(Figure 3.10A)*. (S1, 1912.6µm, Delta vs. Gamma: 0.258 ±0.121 vs. 0.906 ± 0.298, T-test, p = 0.067, with FDR, q = 0.318, S2 1898.7µm, Delta vs. Gamma: 0.041 ± 0.027 vs. 0.421 ± 0.120, T-test, p = 0.009, with FDR q = 0.396). There was no significant difference in Arc distribution in GAD67+ve cells between conditions *(Figure 3.10B)*. S1, 1162.9µm, Delta vs. Gamma: 0.009 ± 0.006 vs. 0.241 ± 0.202 T-test, p = 0.274, with FDR q = 0.453; S2 1269.1µm, Delta vs. Gamma: 0.021 ± 0.0179 vs. 0.139 ± 0.124, T-test, p = 0.362, with FDR q = 0.635).
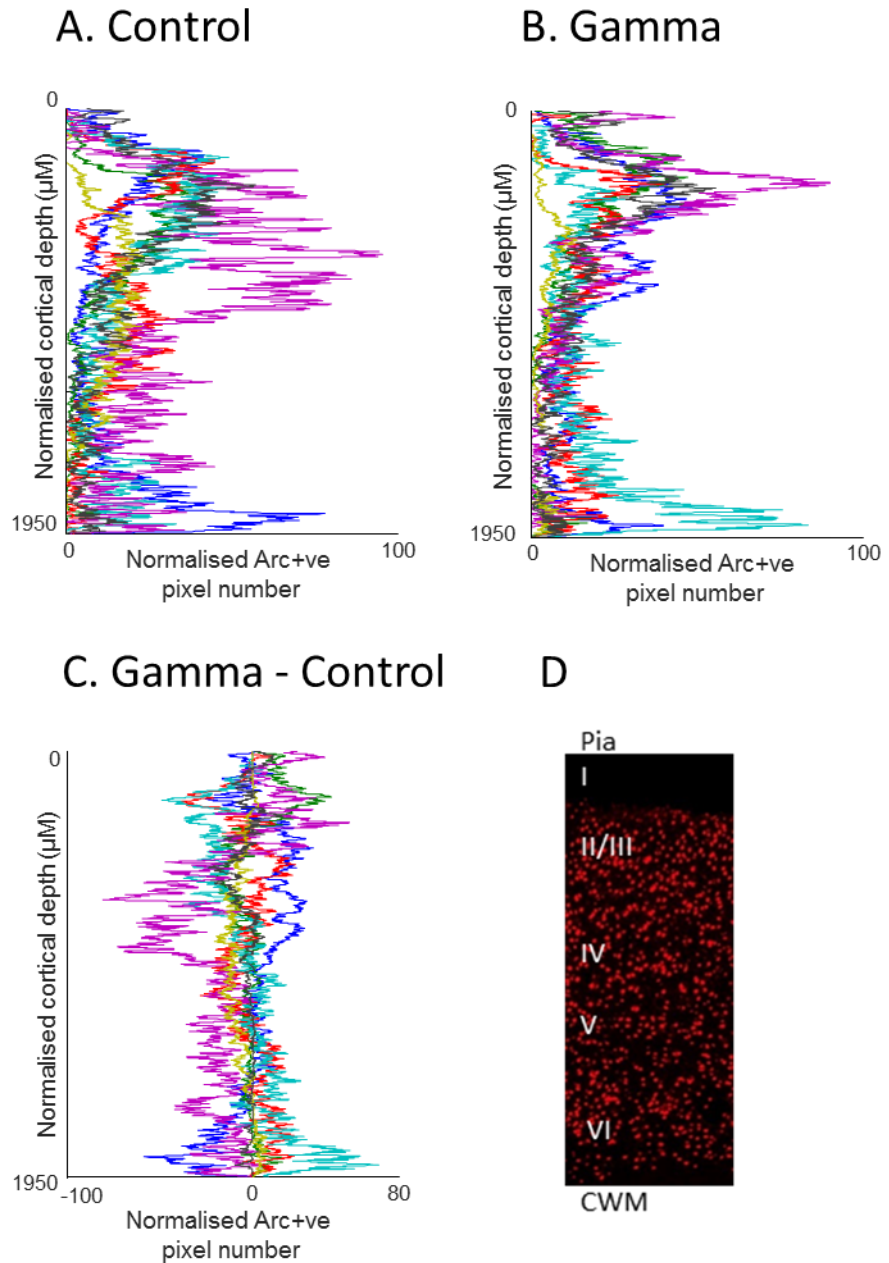
Figure 3.8. The laminar distribution of dendritic ARC expression is more variable in control slices than oscillating slices. (A) Individual profiles of dendritic Arc staining in non-oscillating, control slices. **(B)** Individual profiles of dendritic Arc staining in matched gamma-oscillating slices. **(C)** Individual profiles of dendritic Arc staining after subtraction of matched control profile from gamma oscillating profile. **(D)** An example of the NeuN staining in the primary auditory cortex for reference.
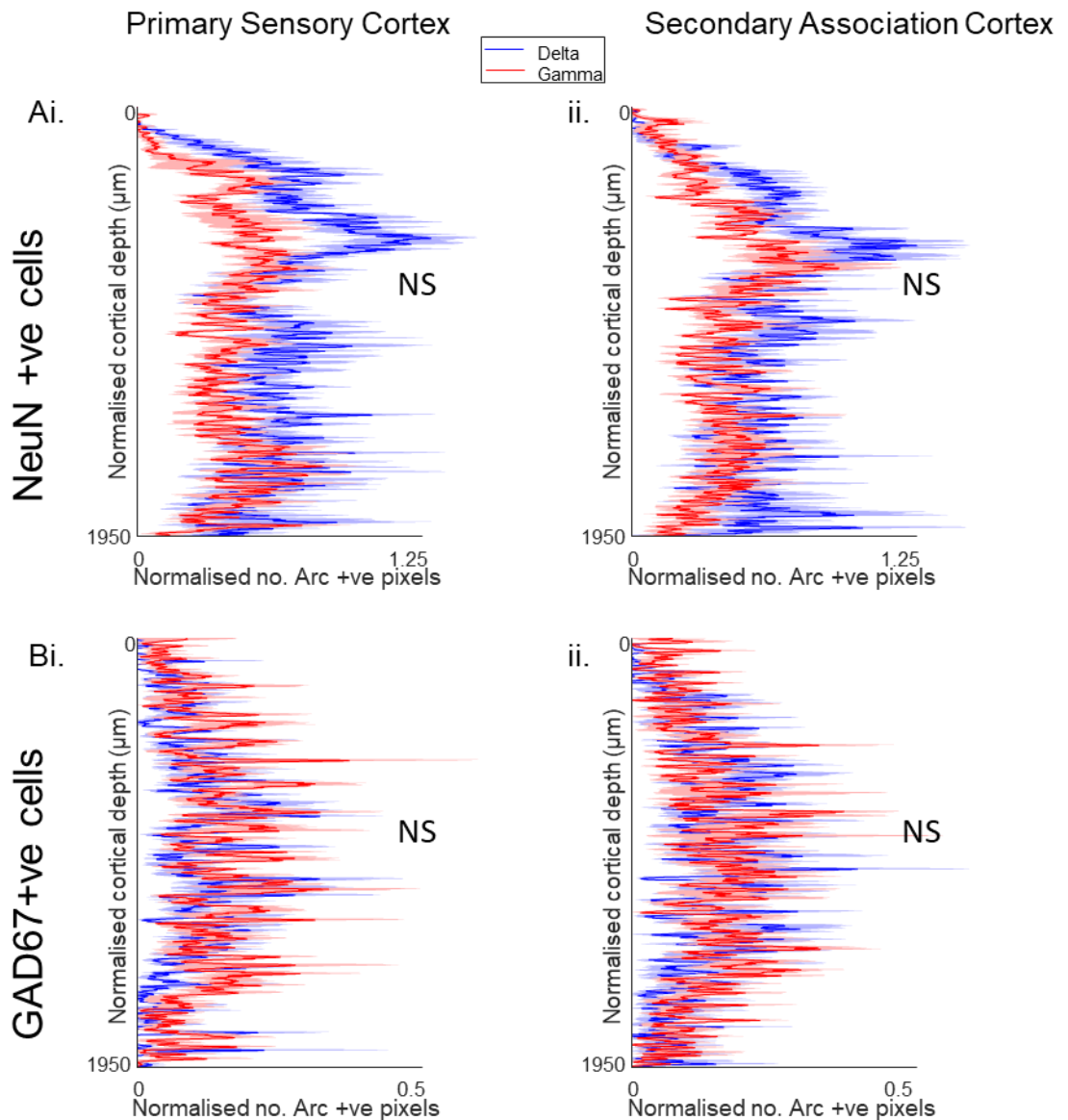
Figure 3.9. The laminar distribution of somatic c-Fos expression does not change significantly between gamma and delta oscillating conditions in primary or secondary association regions when compared directly. (A) The distribution of c-Fos in Neun+ve cells in the primary sensory cortex NOT normalised to non-oscillating slices **(Ai)** and secondary association cortex **(Aii)** from pia (0) to subcortical white matter (1950). c-Fos expression is measured during gamma (Red, n=9) and delta oscillations (Blue, n=8). Shaded error shown is SEM. **(B)** The distribution of c-Fos in GAD67+ve cells in the primary sensory cortex NOT normalised to control slices **(Bi)** and secondary association cortex **(Bii)** from pia (0) to subcortical white matter (1950). c-Fos expression is measured during gamma (Red, n=9) and delta (Blue, n=8).
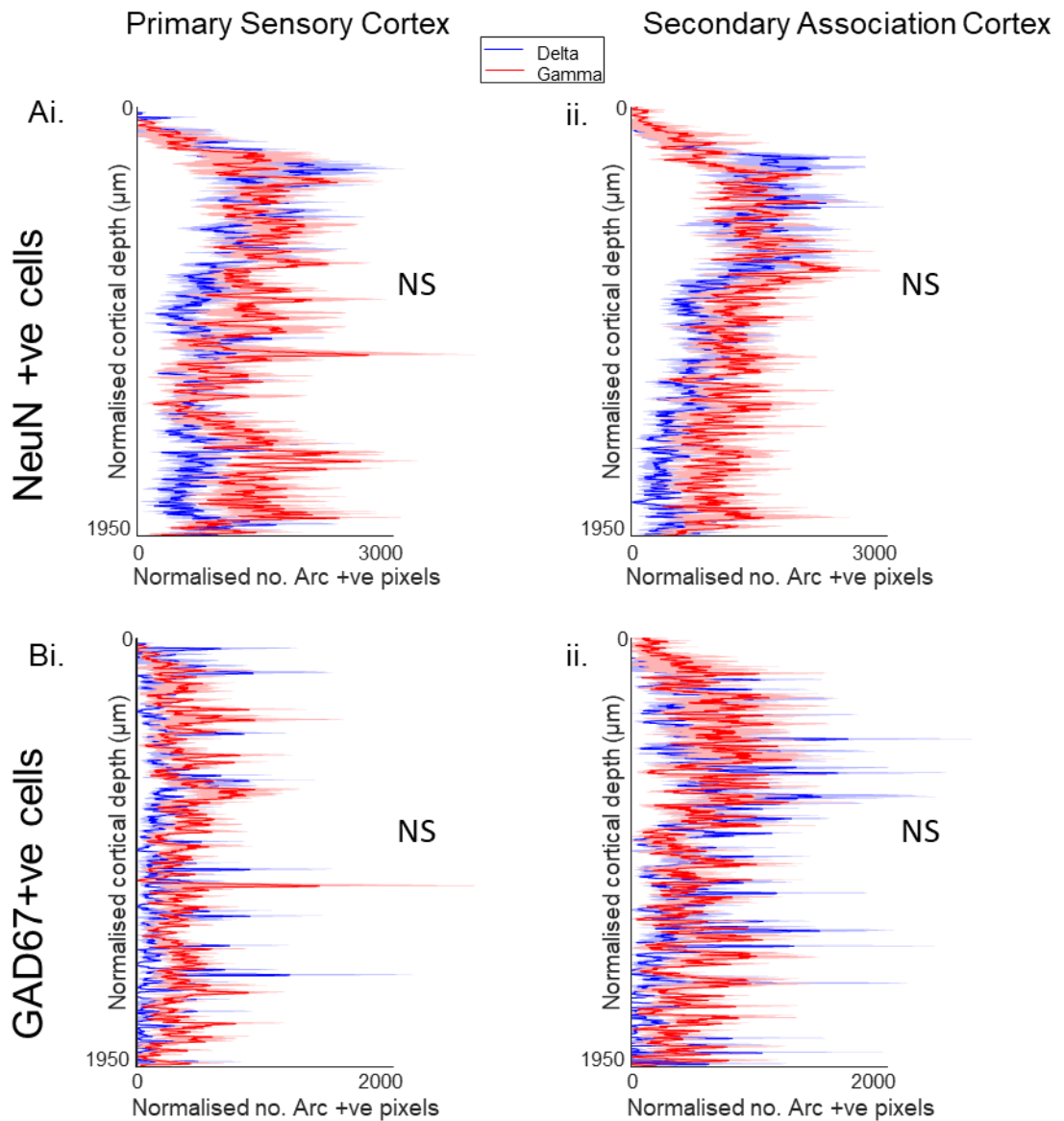
Figure 3.10. The laminar distribution of somatic Arc expression does not change significantly between gamma and delta oscillating conditions in primary or secondary association regions when compared directly. (A) The distribution of Arc in NeuN+ve cells in the primary sensory cortex NOT normalised to non-oscillating slices **(Ai)** and secondary association cortex **(Aii)** from pia (0) to subcortical white matter (1950). Arc expression is measured during gamma (Red, n=7) and delta oscillations (Blue, n=6). Shaded error shown is SEM. **(B)** The distribution of Arc in GAD67+ve cells in the primary sensory cortex NOT normalised to control slices in the primary sensory cortex **(Bi)** and secondary association cortex **(Bii)** from pia (0) to subcortical white matter (1950). Arc expression is measured during gamma (Red, n=7) and delta (Blue, n=6). Shaded error shown is SEM.
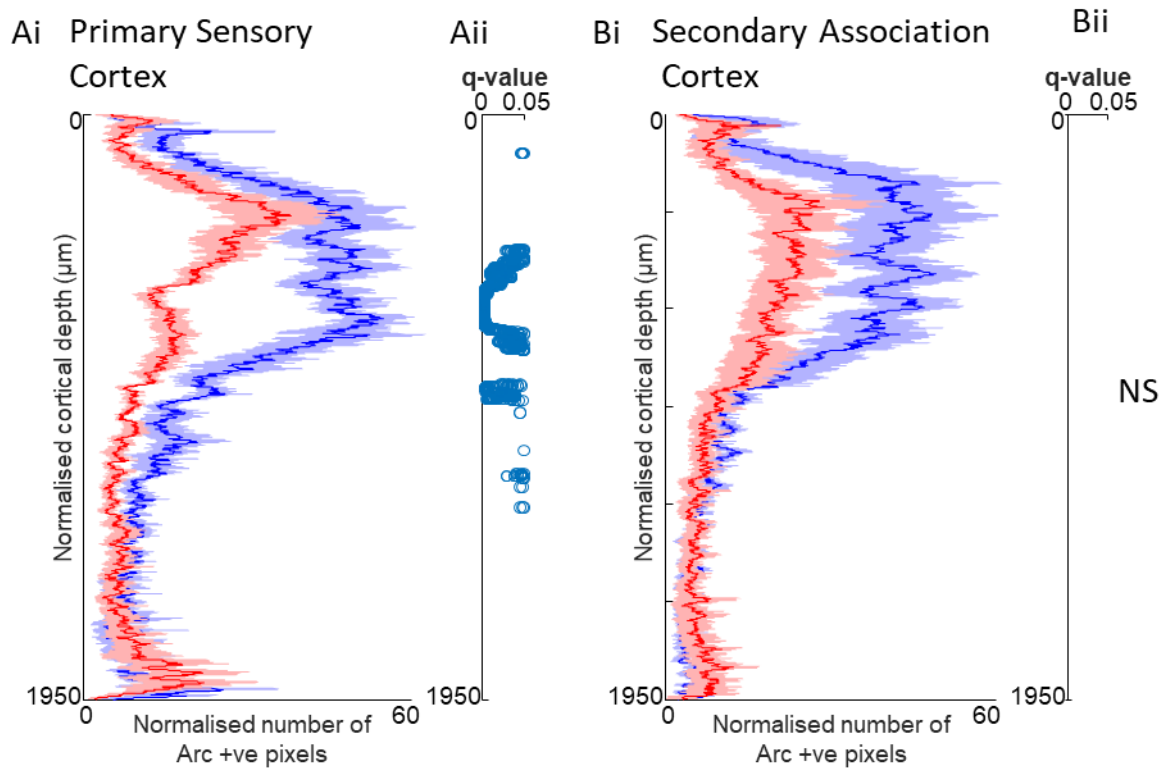
Figure 3.11. The laminar distribution of dendritic Arc expression changes significantly between gamma and delta oscillating conditions in primary but not secondary association regions. Ai – The distribution of Arc in dendrites from pia (0) to subcortical white matter (1950) in primary sensory cortex. Arc expression is measured during gamma in the auditory cortex (Au1) (Red, n=7) and delta in primary somatosensory cortex (S1) (Blue, n=7). Error shown is SEM. **Aii –** The distribution of calculated q-values <0.05 (based on the false detection rate from a t-test) for the significant difference between gamma and delta profiles of ARC in dendrites in the primary sensory cortex. **Bi –** The distribution of Arc in dendrites from pia (0) to subcortical white matter (1950) in secondary association cortex. Arc expression is measured during gamma (Red, n=7) and delta in secondary somatosensory cortex (S2) (Blue, n=7). Error shown is SEM. **Bii –** The distribution of calculated q-values <0.05 for the significant difference between gamma and delta profiles of Arc in dendrites in the secondary association cortex.

A Primary Sensory Cortex
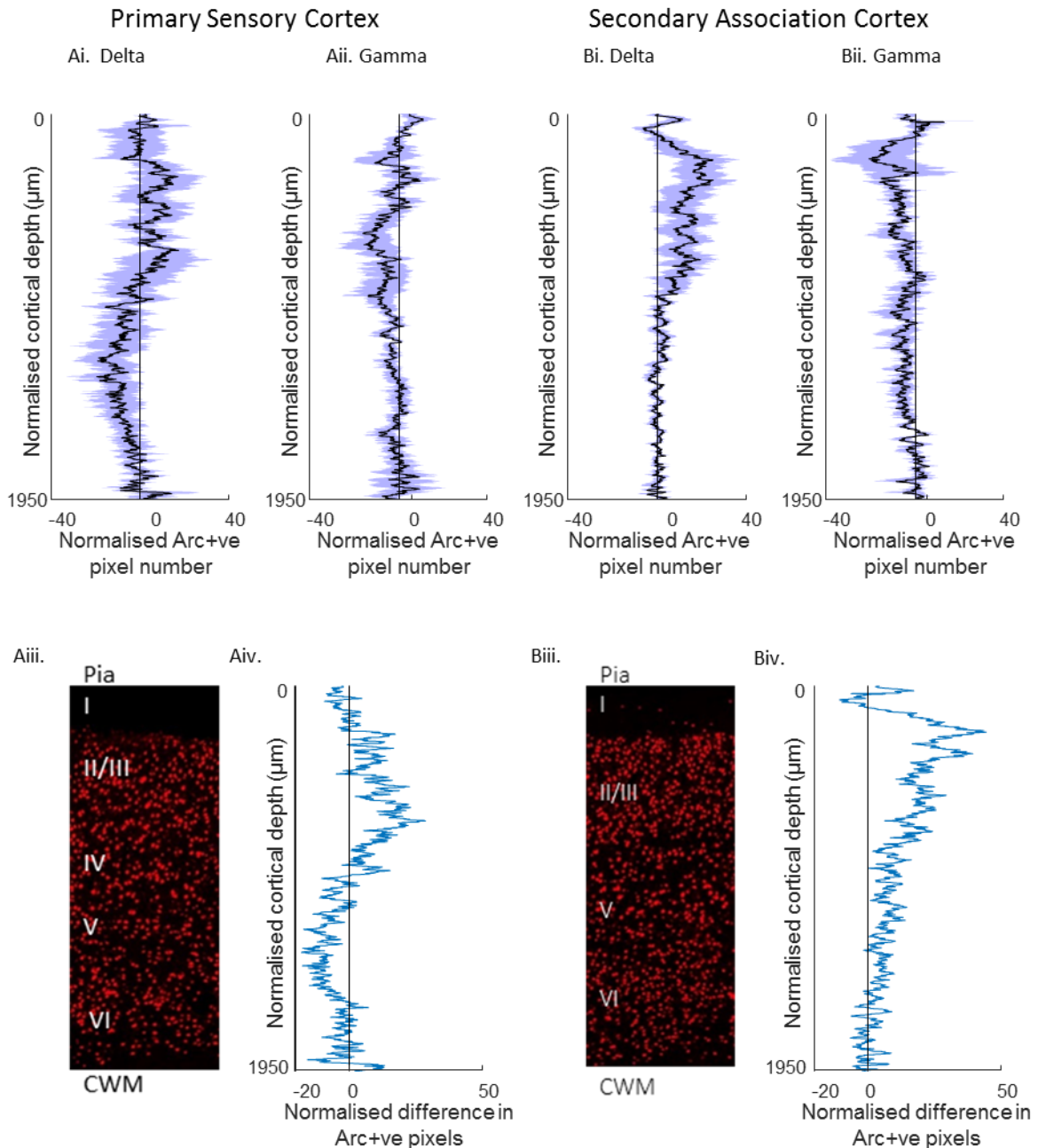

B Secondary Association Cortex
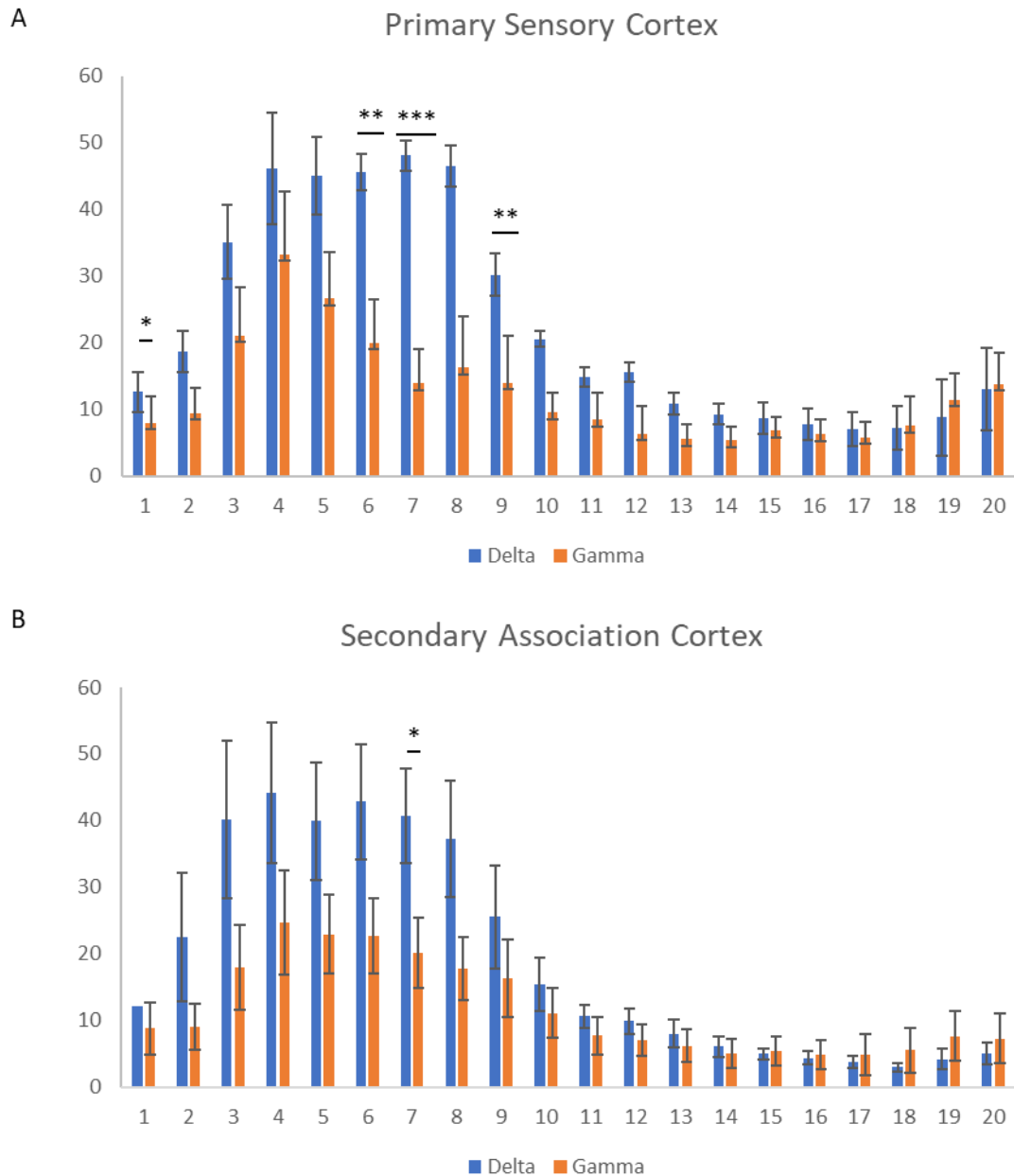
Figure 3.12 The laminar distribution of dendritic Arc expression changes significantly between gamma and delta oscillating conditions in primary and secondary cortices when comparing binned data. A. The distribution of Arc in dendrites split into 20 bins from pia (1) to subcortical white matter (20) Arc expression is measured during gamma (red n = 7) and delta (blue, n = 7) secondary somatosensory cortex. Error shown is SEM. A One Way Anova with Holm-Sidak calculation for multiple comparisons was performed. P values of significance are for bins: 1 = 0.048, 6 = 0.003, 7 < 0.001, 9 = 0.003 **B.** The distribution of Arc in dendrites split into 20 bins from pia (1) to subcortical white matter (20) Arc expression is measured during gamma (red n = 7) and delta (blue, n = 7) secondary somatosensory cortex. Error shown is SEM. A One Way Anova with Holm-Sidak calculation for multiple comparisons was performed. P value of significance for bins was 7 = 0.039 .

The direct comparison of staining showed significantly more dendritic Arc in layer II/II in the primary sensory cortices during delta rhythms compared to gamma rhythms *(Figure 3.11A)* (1ry 616.5µm, Delta vs. Gamma: 50.4 ± 7.0 vs. 11.8 ±   2.2, T-test, p < 0.001, with FDR q = **0.002**). Despite the apparent visible difference in the secondary association cortex (with no overlapping errors), no significance was found in s2 *(Figure 3.11B)* (S2, 233.7µm, Delta vs. Gamma: 46.2 ± 15.4 vs. 15.4 ± 6.5, T-test, p = 0.090, with FDR q = 0.3887).

Whilst significant results were found, the false detection rate analysis assumes each point of comparison is independent of those surrounding it. This, therefore, is not an entirely valid analysis of these data, as it is structural in nature and therefore containing connected objects. To overcome this, data was binned into 20 regions (each bin is 97.5µm wide after interpolation) from pia to cortical white matter to allow for a lower false detection rate due to multiple comparisons. This also meant that a more conventional Holm-Sidak post hoc test could be used (*Figure 3.12*). With this analysis we now found several significant points of higher dendritic Arc in primary cortex (p values for bins are: 1 (97.5µm) = 0.048, 6 (585µm) = 0.003, 7 (682.5 µm) < 0.001, 9 (877.5 µm) = 0.003) and secondary cortex (p-value for bin no. 7 (682.5 µm) was 0.039).

3.2.4 The relationship between dendritic Arc expression and oscillatory properties.

Considering that the 'control' condition slices were abandoned in these analyses owing to the variability of their IEG expression levels, it was important to deduce how much of the expression of dendritic Arc was down to the presence of either delta or gamma oscillations. Therefore, the analysis was carried out to assess the relationship between different features of the oscillatory activity generated (as measured from the power spectrum) and the dendritic Arc signal showing the significant differences above. Primary sensory cortices and secondary association area images were divided in half tangentially to compare the oscillatory characteristics with Arc expression with cortical layers in superficial and deeper portions of the cortex.

In gamma oscillating slices dendritic expression of Arc was lower in deeper layers than in superficial layers. In the deeper half of the cortex, there were no significant correlations between Arc dendritic staining and the area power, the peak power or the peak frequency of the gamma oscillation. Superficial layers did display a negative correlation between dendritic Arc and the area power of the oscillation in Au1 (R^2 = 0.51) *(Figure 3.13Ai)*. This significance was not conserved in S2 *(Figure 3.13Bi).*
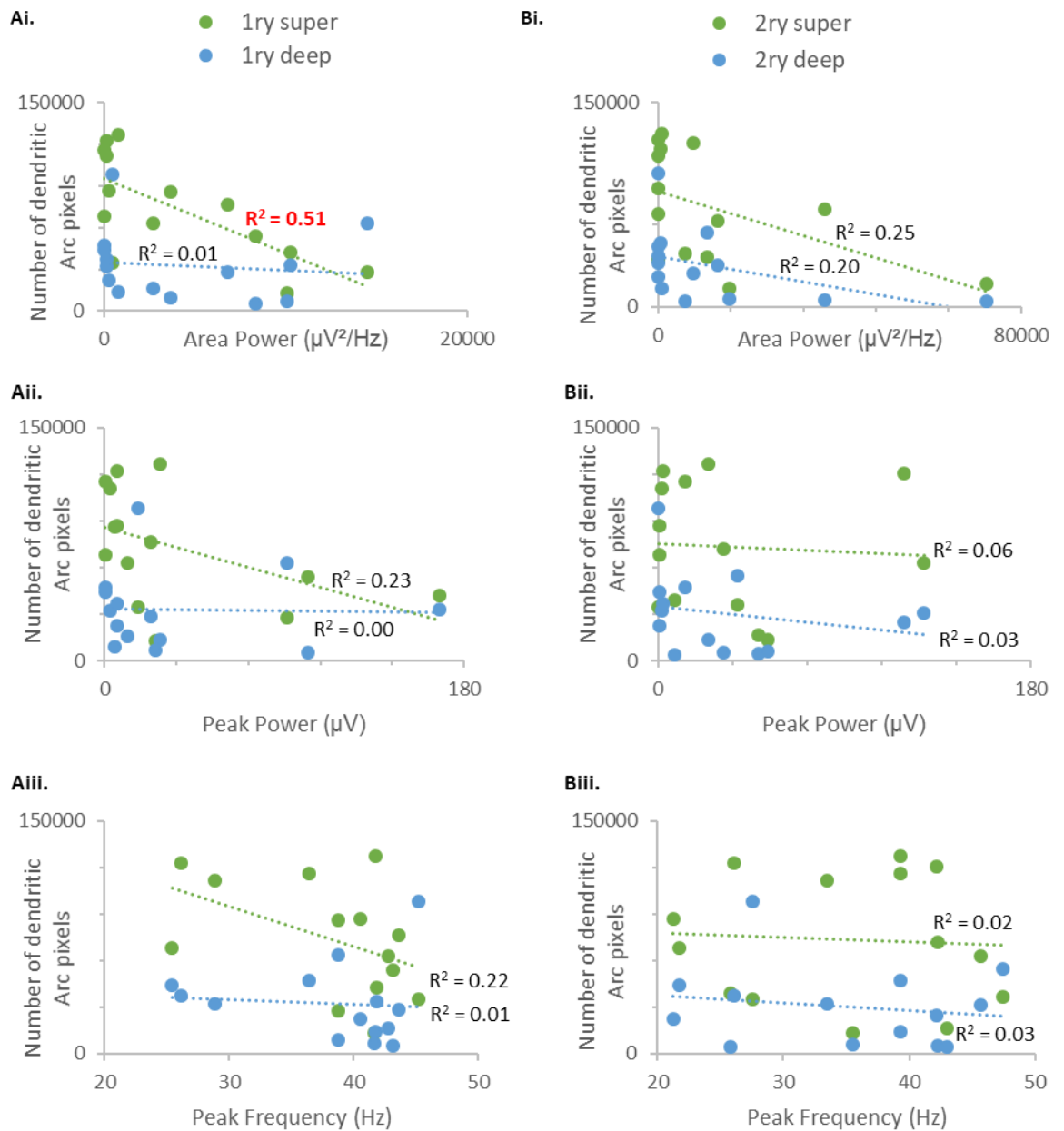
Figure 3.13. There is a relationship between the area power of gamma oscillations and levels of dendritic ARC staining in the neocortex. (A) Linear regression between the distribution of dendritic Arc staining and the area power **(Ai)**, peak power **(Aii)** and peak frequency **(Aiii)** of gamma oscillations in the primary auditory cortex. Dendritic Arc is measured in superficial (green) and deep layers (blue) which were were analysed separately. R squared values were calculated and are shown. Red indicates a correlation deemed to be significant **(B)** Linear regression between the distribution of dendritic Arc staining and the area power **(Bi)**, peak power **(Bii)** and peak frequency **(Biii)** of gamma oscillations in the secondary somatosensory auditory cortex. Dendritic Arc is measured in superficial (green) and deep layers (blue) which were were analysed separately. R squared values were calculated and are shown. Red indicates a correlation deemed to be significant.

Figure 3.14. There is a relationship between the peak power of delta oscillations and the level of dendritic Arc staining in the neocortex. (A) Linear regression between the distribution of dendritic Arc staining and the area power **(Ai)**, peak power **(Aii)** and peak frequency **(Aiii)** of delta oscillations in the primary somatosensory cortex. Dendritic Arc is measured in superficial (green) and deep layers (blue) which were were analysed separately. R squared values were calculated and are shown. Red indicates a correlation deemed to be significant **(B)** Linear regression between the distribution of dendritic Arc staining and the area power **(Bi)**, peak power **(Bii)** and peak frequency **(Biii)** of delta oscillations in the secondary somatosensory auditory cortex. Dendritic Arc is measured in superficial (green) and deep layers (blue) which were analysed separately. R squared values were calculated and are shown. Red indicates a correlation deemed to be significant.

There was also no correlation between the dendritic Arc levels and the power or frequency of the highest peak in the power spectrum *(Figure 3.13 A&B ii/iii).*

In delta oscillating slices the higher expression of Arc during delta *(Figure 3.11 and 3.12)* was conserved under visual comparison with the gamma condition correlation graphs (*Figure 3.13 and 3.14).* Again, no correlation was seen between the dendritic expression of Arc in deeper layers and any measured of features of the delta oscillations. There was also no relationship between area power, peak power, or peak frequency in superficial layers in S1 *(Figure 3.14B)*. However, in S2 a negative relationship was visible between Arc dendritic staining and area power ($R^2 = 0.612$).

3.2.5 Identification of the cells responsible for dendritic Arc expression.

All the data presented thus far has shown that the expression of Arc in dendrites is mostly confined to the superficial layers of the cortex. These dendrites would appear (from visual inspection) to originate in cells whose cell bodies lie in deeper layers and that project their apical dendrites to superficial layers as far as layer I (*Figure 3.6).* To identify the specific subtype of the cell responsible for this Arc expression intracellular electrophysiological recordings were made of single cells, in conjunction with biocytin filling. This allowed for the electrical characterisation of the cells, along with the physical characterisation and co-staining with Arc. This meant that the cell types contributing to the dendritic Arc signal could be revealed.

These experiments ruled out Layer V regular spiking neurones as candidates as they did not show co-expression of Arc in their apical dendrite *(Figure 3.15).* Layer VI regular spiking cells also do not express Arc in their apical dendrite during delta oscillations *(Figure 3.16).* These intracellular experiments did however successfully show co-staining between biocytin labelled layer V intrinsically bursting cells and Arc *(Figure 3.17)*.
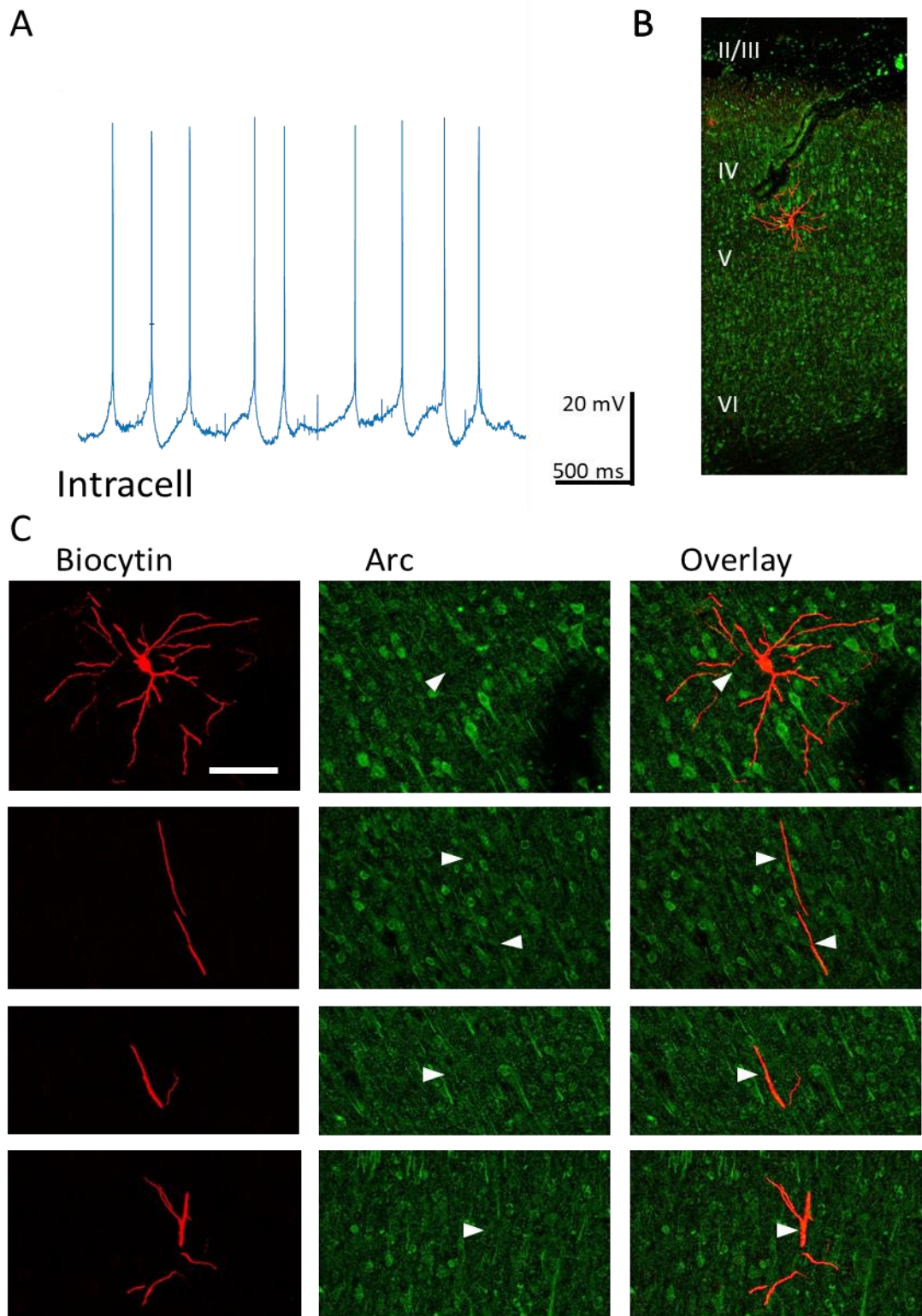
Figure 3.15. Arc is not present in the apical dendrites of layer V regular spiking cells in the secondary somatosensory cortex. (A) 3 second intracellular recording from a layer V regular spiking cell at resting membrane potential. **(B)** Dual stained image of biocytin (red) and Arc (green) from a single sub-slice of the biocytin filled cell, to show the location of the cell body. **(C)** Images of different sections (apical dendrite and cell body) of a layer V regular spiking cell filled with biocytin (red) and co-stained with Arc (green). Scale bar shows 100µm. Arrows highlight the location of cell. Images are scale matched, but cropped for presentation purposes.
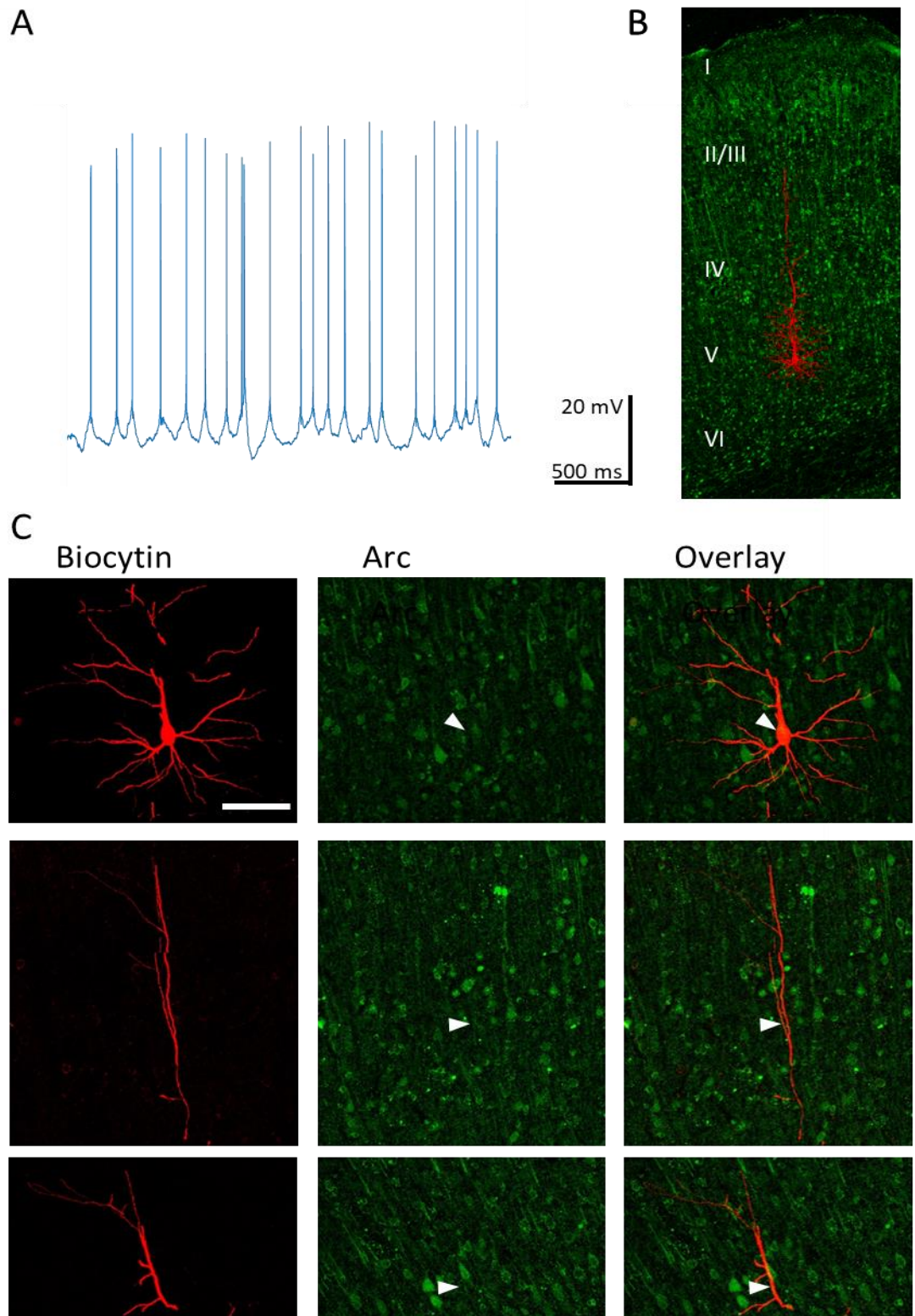
Figure 3.16. Arc is not present in the apical dendrites of layer VI regular spiking cells in the secondary somatosensory cortex. (A) 3 second intracellular recording from a layer VI regular spiking cell at resting membrane potential. **(B)** Dual stained image of biocytin (red) and Arc (green) from a single sub-slice of the biocytin filled cell, to show the location of the cell body. **(C)** Images of different sections (apical dendrite and cell body) of a layer VI regular spiking cell filled with biocytin (red) and co-stained with Arc (green). Scale bar shows 100µm. Arrows highlight the location of cell. Images are scale matched, but cropped for presentation purposes.
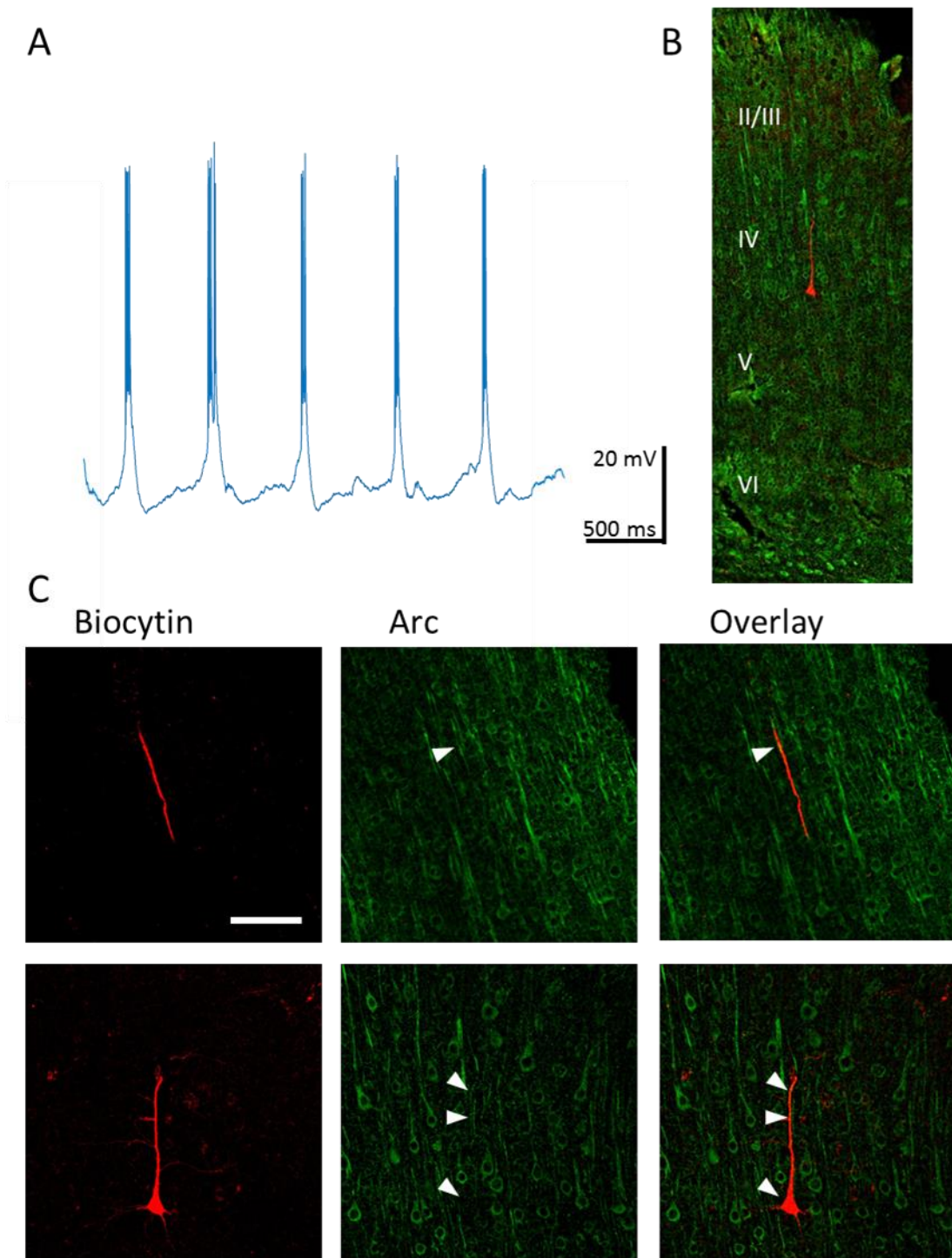
Figure 3.17. Arc is present in the apical dendrites of layer V intrinsically bursting cells in the secondary somatosensory cortex. (A) 3 second intracellular recording from a layer V intrinsically bursting cell at resting membrane potential. **(B)** Dual stained image of biocytin (red) and Arc (green) from a single sub-slice of the biocytin filled cell, to show the location of the cell body. **(C)** Images of different sections (apical dendrite and cell body) of a layer V intrinsically bursting cell filled with biocytin (red) and co-stained with Arc (green). Scale bar shows 100μm. Arrows highlight the location of cell. Images are scale matched, but cropped for presentation purposes.

3.2.6 The arrangement of Arc in dendrites in layer II/III of the cortex.

The Arc staining was localised to the layer II/III portion of the apical dendrites of layer V intrinsically bursting cells. However, it was also apparent that these apical dendrites were not isolated but appeared to be arranged in clusters *(Figure 3.6)*.

To assess this arrangement, first a 1-dimensional autocorrelation was performed on each tangential image scan line from pia to subcortical white matter using the original radial sections (e.g. *Figure 3.18 Ai*). The location of positive pixels of each scan line of the thresholded image was compared with a copy of that line. The copy was then shifted along by one pixel and compared again until there was no overlap. Where there was a strong spatial pattern, a high correlation was revealed. This was done for each line of the image and plotted as a colour map. This showed a strong spatially repeating pattern in layers 2/3 with a spatial frequency of ~50 μm (*Figure 3.18 Aii*).

A 2-dimensional autocorrelation analysis was used on tangential slices from the secondary somatosensory cortex to see if this clustering extended beyond the radial plane captured in the original slices. This used a similar principle to the autocorrelation mentioned above but involved a rotational comparison. This analysis showed that there was a near-hexagonal structural arrangement of Arc-positive dendritic compartments, again with a spatial frequency of ~50μm *(Figures 3.19 Ai, Bi, Ci)*. On closer inspection of the images, the dimensions of this spatial arrangement appeared to capture the interval between dendritic clusters. However, using higher-resolution images the second level of organisation within clusters was apparent *(Figure 3.19 Aii)*. Further analyses of this tangential arrangement, at the higher resolution, were also carried out using 2-D autocorrelations. This allowed the analysis of the relative location of each dendrite and dendrite cluster to its neighbours. This revealed the arrangement of dendrites within clusters. It showed a smaller-spatial scale (ca. 10 μm) version of the hexagonal pattern seen between clusters was also present for individual dendrites within each cluster (*Figure 3.19 Aii/Bii)*. Furthermore, some evidence for the ~50μm hexagonal spatial arrangement between clusters was also still apparent using these higher-resolution images (*Figures 3.19 Ci, Cii*).
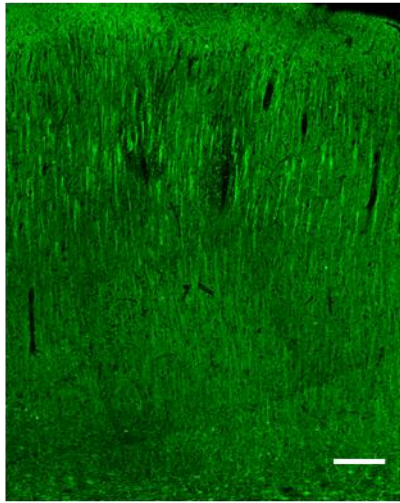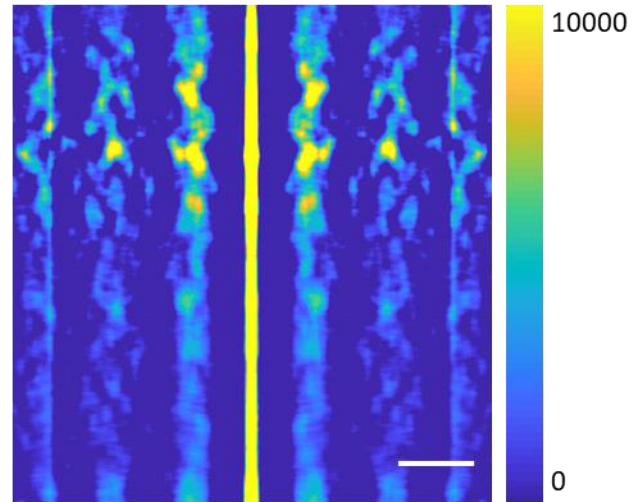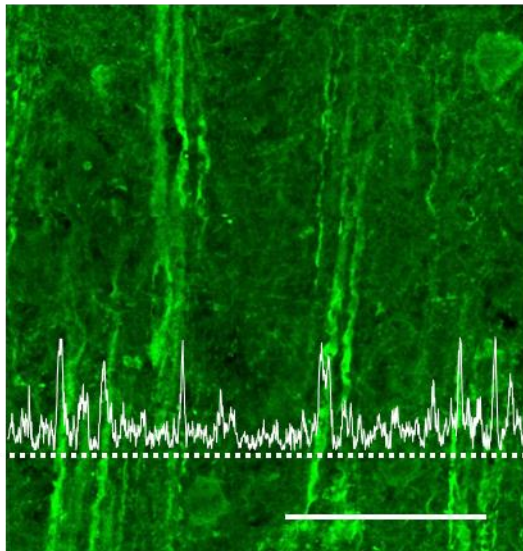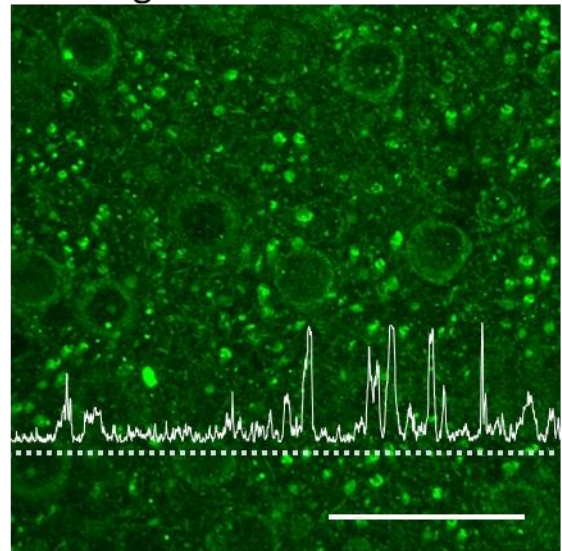
Figure 3.18. There is a spatial organisation in dendritic Arc staining in layer 2/3 of the cortex in radial and tangential sections. Ai. An image of Arc staining in the secondary somatosensory cortex during delta oscillations. Scale bar is 200μm. **Aii.** The autocorrelation of Arc stained image from Ai. Scale bar is 50μm. **B.** An image of layer II/III Arc dendrites during delta oscillations in the secondary somatosensory cortex. Overlay shows intensity measures at the level of the dotted lines. Scale bar is 50μm. **C.** An image of a tangential section of layer II/III Arc dendrites during delta oscillations in the secondary somatosensory cortex. Overlay shows intensity measures at the level of the dotted lines. Scale bar is 50μm.
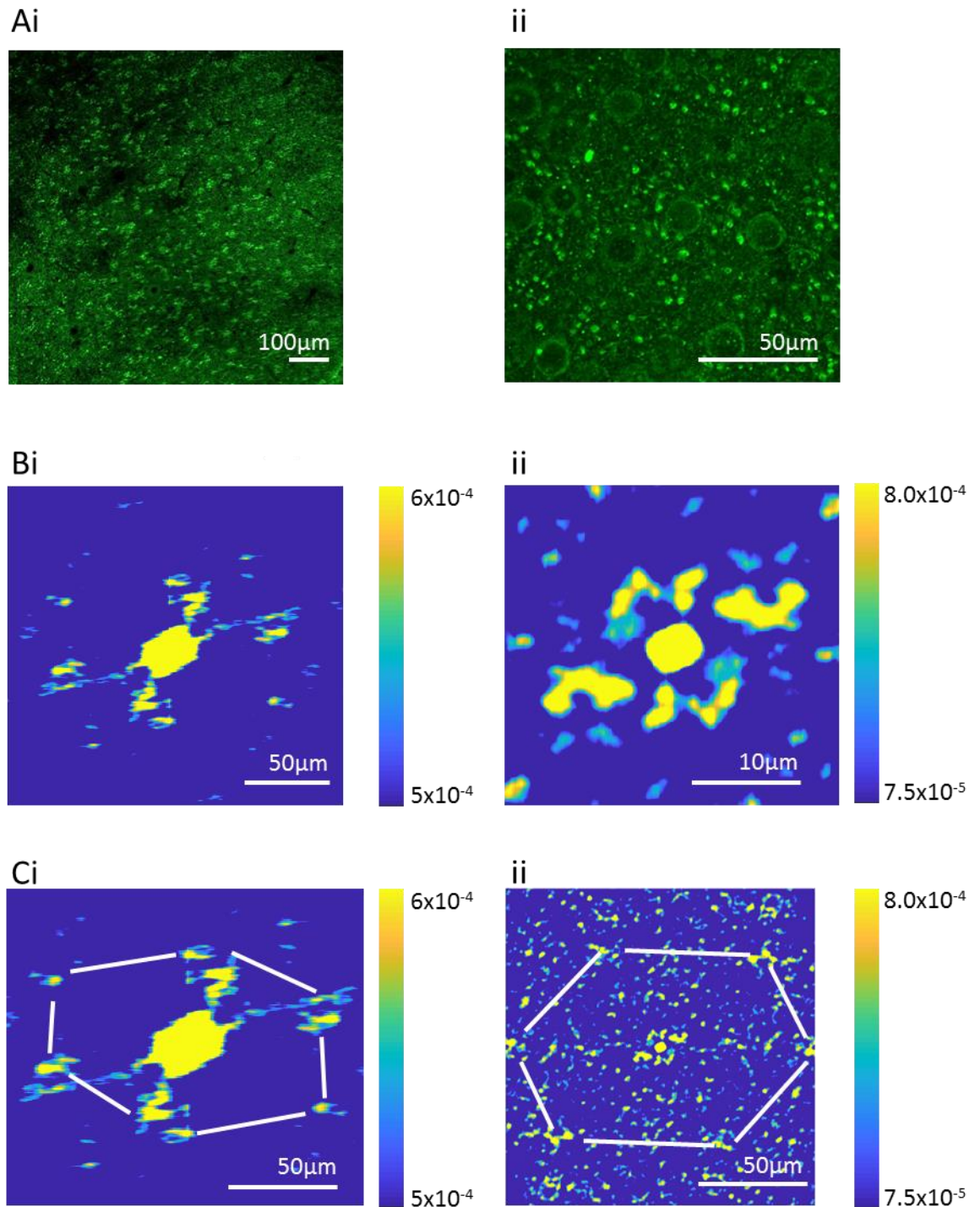
Figure 3.19. There is a hexagonal tangential arrangement in Arc stained dendrites in layer II/III of the secondary somatosensory cortex. Ai. Image of a tangential section of Arc staining in layer II/III of the secondary somatosensory cortex at x10 magnification. Scale bar is 100µm. **Aii.** Image of a tangential section of Arc staining in layer II/III of the secondary somatosensory cortex at x63 magnification. Scale bar is 50µm. **Bi. 2-D** autocorrelation of the image from Ai. **Bii. 2-D** autocorrelation of the image from Aii. **Ci. 2-D** autocorrelation of the image from Bi, image identical to Bi except for scaling for comparison to Cii. – white lines are for diagrammatic purposes only.. **Cii.** Zoomed out diagram from autocorrelation of Aii (central section of Bii) to show second level of organisation – white lines are for diagrammatic purposes only.

3.3. Discussion

3.3.1 Summary

In this chapter, the effect of certain brain rhythms on regional IEG changes was analysed. *In vitro* models of NREM sleep-related delta rhythm (Carracedo et al., 2013), and the wake-related gamma rhythm (Ainsworth et al., 2011) were used to monitor c-fos and Arc changes in response to due to specific network activities unconfounded by other electrical activity that would occur *in vivo*. With this technique, molecular changes were analysed within whole regions, as well as with laminar and cellular specificity.

The summary of key findings from this investigation are:

- The total c-Fos protein expression was elevated in slices oscillating at delta frequency compared to slices oscillating at gamma frequency in primary and association areas equally.
- C-Fos expression in NeuN and GAD67 immunopositive somata was not affected by the nature of brain rhythms in any region/layer studied.
- Total arc protein expression was diminished in slices oscillating at delta frequency compared to slices oscillation at gamma frequency in each area studied.
- Arc expression in NeuN and GAD67 immunopositive somata was not affected by the nature of brain rhythms in any region/layer studied.
- Arc expression in L5 IB neuronal apical dendrites was elevated in delta rhythms.
- Dendritic Arc expression was differentially affected by gamma and delta oscillation power in primary and secondary neocortex respectively.
- The spatial pattern of dendritic Arc expression corresponded to the previously described architecture of neocortical microcolumns.

3.3.2 c-Fos is higher during sleep-related rhythms regionally but not locally

C-Fos, a gene expressed in response to 'new' firing patterns in neurons (Svarnik et al., 2013), showed higher expression in slices oscillating a delta frequency, compared to gamma oscillating slices. These findings are at odds with studies into the expression of c-Fos across the sleep-wake cycle (Pompeiano et al., 1995; Hanlon et al., 2009). However, most of the previous evidence for c-Fos changes are with respect to mRNA data (Cirelli and Tononi, 2000c), and there is known to be a discrepancy with translation across the sleep-wake cycle with an upregulation of protein synthesis during sleep (Ramm and Smith, 1990; Nakanishi et al., 1997)**,** especially with plasticity dependent genes (Seibt et al., 2012).

Many *in vivo* studies also do not monitor the electrical activity of the brain during sleep, only by behaviour**.** Therefore, they do not make a statement about specific stages of the sleep-wake cycle above comparison of 'wake' versus 'sleep'. With the *in vitro* models used in this thesis, specific rhythms related to certain brain function were generated, albeit in a more persistent fashion than is usually seen *in vivo.* It is likely that the changes seen in regional c-Fos levels were specific to the presence of gamma and delta rhythms.

As well as neurons, c-Fos is also expressed glia (Dragunow et al., 1990) (Edling et al., 2007). Therefore, even with a background subtraction process to remove non-specific staining, comparing the gross remaining staining over the whole would also include glial c-Fos staining. To take this into account analyses for neuron-specific staining (NeuN co-localisation) was undertaken. Additionally, to investigate these regional changes further we analysed the change in the distribution of c-Fos throughout the cortical layers and found no difference in neuronal or interneuron c-fos staining in any layer of the cortex in these analyses, although the trend towards general higher c-fos during delta rhythms was still apparent. The specificity in these analyses (both cellular and laminar) is most likely the reason for the lack of significant changes recorded. Especially as observing c-Fos in areas of NeuN immunostaining meant that any extra-somal staining was ignored. This is of particular importance as recently c-fos has been found in synaptic boutons (Nakao et al., 2002)

3.3.3 ARC expression is lower regionally but not locally during delta oscillations

Our initial experiments investigating the changes to Arc (an IEG mediator of plasticity) showed a regional decrease in both primary sensory cortex and secondary association cortex during delta rhythms compared to gamma activity. This is line with findings by Cirelli and Tononi (2000a) that show a global decrease in Arc in the cerebral cortex during sleep compared to wakefulness. This decrease in Arc expression has also been shown to occur more specifically in brain regions associated with task learning – compared to untrained regions - during wakefulness. These changes were abolished after 1 hour of sleep (Hanlon et al., 2009) and were related to increased slow wave activity, which suggests that looking at levels during sleep compared to SWS, the results are comparable.

Trying to localise these sleep-related decreases, we found that the expression of Arc in neuronal cell bodies is similar during delta and gamma rhythms oscillations. This analyses only included

the cell bodies and therefore did not include any synaptic or dendritic signal. It is not surprising that there is little difference in Arc protein in the cell body as *Arc* is transcribed in the nucleus but is mostly shuttled to dendrites for translation (Steward et al., 1998), so it would be expected that the majority of Arc signal would arise from the dendrites, which is indeed the case with these experiments. This would also account for the similarity in the pattern of activity ARC in GAD67+ve interneurons as the analyses only observed changes within the locale of the soma rather than dendrites of interneurons.

3.3.4 Arc expression was elevated in L5 IB neuronal dendrites during delta rhythms

Contrasting the regional decreases, we found that Arc was highest in dendrites in layer II/III *in vitro* delta oscillations compared to gamma oscillations. This finding was also at odds with general changes seen in Arc expression over the sleep-wake cycle, in which *Arc* mRNA is built up during wakefulness and decreased during sleep in the cortex (Cirelli and Tononi, 1999; Cirelli et al., 2004) and hippocampus (Thompson et al., 2010). It also contrasted the gross regional changes which also saw a decrease in Arc signal. The gross analysis not only included the dendritic staining but somatic and extracellular signal. To lead to a net reduction over the whole area, the higher level of dendritic Arc must have a contrasting decrease in the rest of the signal.

Since delta rhythms are associated with SWS, our data would suggest that processes occur during SWS that generally decrease the expression of Arc, but locally has a higher expression in distal dendrites. The mechanism by which this specific increase occurs is unclear, in that whilst its transcription occurs in the nucleus, its mRNA is trafficked to the dendrites where it translated (Steward et al., 1998). Synaptic activity is known to increase both of these processes (Steward and Worley, 2001), so it uncertain whether the increased level of Arc is as a result of *de novo* transcription, or the translation of already synthesised mRNA. Observing the dendritic appearance of Arc In the presence of a transcriptional repressor (actinomycin D) or a protein synthesis inhibitor (cycloheximide) would help elucidate this mechanism.

Whilst the mechanism by which Arc is increased may be uncertain, the processes in which it is involved during delta are clearer. It is known that the landscape of synaptic plasticity during wakefulness is weighted towards potentiation (Bramham and Srebro, 1989), whereas synaptic depression (LTD) dominates sleep (Tononi and Cirelli, 2003; Shepherd, 2012). The process of rescaling synapses during sleep in this way is important for the maintenance of synaptic homeostasis (Tononi and Cirelli, 2014).

These results show that Arc is implicated in this process, through its role in LTD by the internalisation of AMPA receptors from the postsynaptic membrane (Chowdhury et al., 2006; Rial Verde et al., 2006; Shepherd et al., 2006). The role of Arc in synaptic scaling is supported by evidence that shows that the KO of Arc prevents this process in the primary visual cortex (Gao et al., 2010). This endocytosis (and thus LTD) is known to increase during sleep (Vyazovskiy et al., 2008; Lante et al., 2011; Diering et al., 2017) and is also supported by studies that highlight the electrophysiological presence of LTD in sleep too (Vyazovskiy et al., 2008; Liu et al., 2010).

There is also evidence that relates the delta rhythms with LTD, as activity of the delta band reduces with sleep time along with the overall strength of synapses (Riedner et al., 2007). The influence of certain neurotransmitters during delta rhythms also points toward synaptic depression as dopamine (D1) receptors are blocked to enhance delta oscillations *in vitro* (Carracedo et al., 2013) and the activation of these receptors has been shown to impair LTD (Xu and Yao, 2010). Thus, it seems that Arc may play a critical role in this synaptic rescaling during SWS-related delta rhythms through the de-potentiation of synapses in layer II/III.

Intracellular experiments allowed us to pinpoint the layer II/III Arc increase to the apical dendrites of layer V IBs. Structurally, this laminar and cellular localisation corresponds spatially with calcium spike initiation zones (Perez-Garci et al., 2013) which are portions of the apical dendrite of layer V cells that are highly innervated by inhibitory neurones and as such possess a high density of $GABA_B$ receptors. The activation of these receptors has been shown to decrease excitability by the blockage of voltage-dependent calcium channels (VDCCs) which abolishes calcium spikes in these dendrites (Perez-Garci et al., 2006; Breton and Stuart, 2012). Additionally, the $GABA_B$ mediated inhibition of layer V intrinsically bursting cells is implicated in synaptic depression during delta oscillations and is responsible for the separation of each active phase of the rhythm (Carracedo et al., 2013). The burst firing between periods of inhibition seen during delta rhythms is suggested to be associated with huge calcium influx, which is ideal for the induction of immediate early gene expression (Buzsaki, 1998; Das et al., 2018).

Increased calcium influx (following cellular activation) has been shown to be important in synaptic scaling, as it binds to the N-teminus of the postsynaptic density protein-95 (PSD 95) preventing it from anchoring AMPA receptors to the postsynaptic membrane and allowing their internalisation (Chowdhury et al., 2018). The actual removal of AMPA receptors requires Arc,

which binds interacts with endophilin and dynamin to bring AMPA receptors into endosomes and thus cause their endocytosis (Chowdhury et al., 2006). It may be that the calcium spike initiation zones afford a high degree of synaptic plasticity to apical dendrites in layer II/III and help 'allocate' synapses in a calcium-dependent manner, and Arc completes the process. Additionally, some AMPA receptors are permeable to calcium, and it has been shown that the internalisation of all these calcium-permeable AMPA receptors from the membrane of L5 pyramidal cells occurs during sleep (Lante et al., 2011). This may serve as a negative feedback mechanism for synaptic rescaling.

3.3.5 The arrangement of Arc stained of intrinsically bursting cell dendrites

Not only is the nature and cellular localisation of this synaptic scaling of importance, but also the arrangement of cell clusters in which it occurs. We found that there was a tangential spatial organisation of clusters of the Arc immunopositive layer V IB apical dendrites, at a spatial frequency of ~50uM. This was conserved when looking at these dendrites clusters radially and these structures were also found to have quasi-hexagonal arrangement. Additionally, a within-cluster analysis found this hexagonal-like arrangement to be present between the dendrites of each cluster.

Previously, Maruoka et al. (2017) have shown a similar feature in the neocortex of mice, with a hexagonal arrangement (with a spatial frequency of about 30μM) in the pattern of sub-cortical projection neuron (SCPN) dendrites. The cells that make up these clusters were labelled by the injection of a tracer into the pons and were suggested to represent cortical microcolumns. The similar pattern of expression seen in this chapter existed in the apical dendrites of LV IB cells, which are known to project to the pons (Gao and Zheng, 2004) and thus correspond to the SCPNs of cortical microcolumns discovered the aforementioned study. The spatial frequency disparity of the two findings may be a species related difference between rats and mice. Not only are layer V pyramidal cells known to be anatomically clustered, but they are also shown show correlated c-fos expression (Maruoka et al., 2011), and in many areas of the sensory cortex, they fire synchronously with the presentation of stimuli (Maruoka et al., 2017). If the activity of these dendrites is so strongly connected, the high synaptic plasticity between them is unsurprising. The increased change in synaptic plasticity during delta rhythms, most likely related to depression of synapses, occurs in dendrites that form these structures. This suggests that these microcolumns may be the main functional units in the neocortex in which synaptic scaling occurs, and thus highlights the importance of these functional units in the memory process.

It is suggested that whilst in less complex nervous systems single neurons act more independently, the neocortical microcolumn shows that neurons act much synergistically as a single entity in higher animals (Perin et al., 2011). Furthermore, there is a high degree of synaptic plasticity between pyramidal neurons in these circuits. Initially dendrites have indiscriminate contact with axons of other pyramidal cells, only defined by their proximity (with 50µm) (Kalisman et al., 2005) This allows for the modification of synaptic weights in these contacts to occur due to the timing of action potentials and EPSPS (Markram et al., 1997) a preference for the elimination of existing weaker synaptic connections (whilst new 'weak' connections were retained at a similar rate to the remaining stronger connections) has also been shown (Le Bé and Markram, 2006). On a more microscopic level, this has also been shown to occur in dendritic spines during sleep, in a discriminatory fashion based on the smaller size of the spines (de Vivo et al., 2017).

These data in combination with our work point at a system whereby synaptic connection are preferentially made and strengthened, as a result of wakeful experiences, in layer V pyramidal cells within cortical microcolumns. During SWS, Arc is upregulated, possibly by increase Ca2+ entry caused by burst firing of the IB cells (Williams and Stuart, 1999; Yi et al., 2017). This triggers the internalisation of AMPA receptors necessary for synaptic scaling required for the consolidation of memories the maintenance of synaptic homeostasis.

3.3.6. Experimental Limitations

One complication to the experiments in this chapter was the 'control' slices. These were quiescent slices kept in the same conditions as the experimental slices, yet in the absence of an oscillation generating drug and were used to represent random background activity. However, even when discounting slices that were obviously not truly quiescent – for instance those with spontaneous oscillations or epileptiform activity – slice immediate early gene expression was variable. This is most likely because their electrical activity was not 'controlled' or kept consistent in any way. The lower variance in the oscillatory data shows that the generation of the oscillation 'clamps' the network into a specific response mode that is consistent across slices and related to consistent gene expression. Furthermore, the control condition is not representative of an *in vivo* brain state and therefore may not be a reliable comparator.

For the analysis of the cellular signal of immediate early genes, the somatic signal of the IEG was overlaid to the template of NeuN/GAD67 cells. The mean of each NeuN/GAD67 cells' average IEG intensity was used as a threshold by which to count pixels. This meant that the profiles represent counts of positively stained pixels, rather than numbers of cells. This may not be a problem, but it does assume ubiquity in neuronal soma size and staining across each soma.

However, the thresholding method used also did not account for differences in staining intensity across slices or conditions. This means that the general change in IEG levels across conditions was not accounted for and therefore lost from the analysis. For example, even if the mean intensity of all the cells in one image was brighter another, the analyses would just include those brighter than the mean for each image independently. This means any intensity differences between conditions or repeats within the same condition, are lost. Furthermore, thresholding in this way meant that although negatively stained cells were rightly removed, also dimly stained cells, which may have still been classed as immuno-positive for IEG markers, would have also been discounted. However, this means that the analyses using this method did show the distribution of the brightly stained cells in each image.

Setting a threshold to be used for all images across conditions, would allow for a fair comparison between conditions of the numbers and intensities of immunopositive cells. Furthermore, measuring the distribution of cell counts by a lower standard threshold along with separate comparisons for intensity may provide a clearer way by which to present the results and even highlight differences that were lost using the other method.

Chapter Four – The effect of neuroinflammation on sleep- and wake-related oscillations

4.1 Introduction

Neuroinflammation is the response in the CNS to a physical, pathogenic, or toxic insult. The presence of infectious or pathological material (including dead and dying neurons) leads to the production of proinflammatory cytokines and chemokines, which mobilise microglia (amongst other immune cells) to the site of damage to neutralise the threat. Neuroinflammation is usually transient and is curtailed by anti-inflammatory cytokines which reduce the inflammation to baseline levels. Unfortunately as well as offering a defence to the brain from damage, neuroinflammation can occur aberrantly. This is often the case with neurodegeneration, where there is an unnecessary or augmented pro-inflammatory response in the brain (Godbout et al., 2005). Neuroinflammation is involved in the pathophysiology of many neurodegenerative disorders such as Alzheimer's disease (Bronzuoli et al., 2016), Parkinson's disease (Wang et al., 2015b), motor neuron disease (Komine, 2015) and multiple sclerosis (Bjelobaba et al., 2017).

As well as triggers within the CNS, neuroinflammation can occur in cases of systemic infection that either spread to the brain or induce inflammation that is propagated within the CNS. Cytokines can spread from the periphery into the CNS via areas where the blood-brain barrier is compromised and even through molecular transport systems in a healthy blood-brain barrier.

There are many examples where peripheral infections can affect the function of the brain and one particularly severe condition that highlights this is delirium. It is often seen after traumatic brain injury or in serious infection or sepsis (Lemstra et al., 2007; Siami et al., 2008). It is particularly prevalent among the elderly (Luz et al., 2003). Many studies have found inflammatory changes in the brain related to delirium such as increased microglia and astrocytic activity (van Munster et al., 2011) as well as increased pro-inflammatory cytokine signalling (van Munster et al., 2008). In conjunction with dementia, even less serious peripheral infections such as urinary tract infections have been shown to have serious cognitive effects (O'Keeffe and Ni Chonchubhair, 1994; Davis et al., 2012). Some studies also implicate systemic pathogens in the aetiology of neurodegenerative disorders (Rumah et al., 2013)

Studies into the effect of systemic inflammation in the CNS often use synthetic analogues of ligands for TLR receptors (Lipopolysaccharide (LPS) and Poly I:C) to mimic immune challenges (such as bacterial or viral infections) in animal models. Intraperitoneal injections of LPS have been shown to change the inflammatory state of the brain in otherwise healthy animals by inducing the activation of astrocytes (Gautron et al., 2002), and the proliferation of astrocytes

and microglia (Semmler et al., 2005; Nishioku et al., 2009). LPS is also known to increase levels of pro-inflammatory cytokines IL1β, TNFα and the chemokine CCL2 (MCP-1) (Thompson et al., 2008).

In animal models, the peripheral administration of LPS has been shown to cause alterations in sleep-related brain rhythms. LPS increases delta frequency oscillation amplitude and duration, whilst also decreasing REM sleep (Krueger et al., 1986). The same effects have been shown with the administration of viable and heat killed *E. coli* (Toth and Krueger, 1989). Other changes in the brains activity after systemic LPS challenge show spike-wave discharges in the hippocampus, (Mamad et al., 2018). These changes may play a role in the cortical dysfunction seen during delirium.

Associations between neuroinflammation, altered sleep patterns (Mullington et al., 2010) and cognitive function during wakefulness have also been highlighted in humans (Simen et al., 2011; Cortese and Burger, 2017; d'Avila et al., 2018). However changes to sleep-related oscillatory dynamics have also been suggested and are thought to arise from the activity of the autonomic nervous system detecting peripheral infection as opposed to pathological changes due to neuroinflammation, especially as excision of the vagal nerved attenuates the SWS increases (Opp and Toth, 1998).

Whether neuroinflammation causes more direct changes to network stability in the brain, and subsequent modulation of synaptic plasticity markers (Chapter 3) is not known. We therefore examined a series of acute and chronic inflammatory challenges in brain slice models of wake and sleep rhythms to investigate this.

4.1.2 Aims of this chapter

This chapter aims to monitor the effect of the application of inflammatory agents (Lipopolysaccharide and Polyinosinic:Polycytidylic Acid) on *in vitro* models of oscillations associated with certain states (delta oscillations and gamma oscillations respectively) in acute preparations of brain slices. Also to investigate the effect of raising a systemic immune response (in rats by the intraperitoneal injection of LPS and Poly I:C) on the ability to generate cortical oscillations *in vitro*. Finally, to assess the inflammatory environment of the brain after systemic LPS and Poly I:C injection, by monitoring levels of cytokines and chemokines in the brain.

4.2. Results

4.2.1 Acute application of LPS onto oscillating slices

To analyse the direct effect of inflammatory agents on cortical oscillation dynamics, 500ng/ml LPS was added to the circulating ACSF around stably oscillating *in vitro* slices of rat brain. Oscillations were assessed 1 hour after LPS treatment. KA-induced hippocampal oscillations did not change in any characteristics (*Figure 4.1)* (KA vs KA+LPS, area power 19005 ± 14435 vs. 26977 ± 19925 µV², Paired T-test, p = 0.210; peak power 1846 ± 1496 vs. 2178 ± 1631 µV²/Hz, Paired T-test, p = 0.190; peak frequency 26.6 ± 1.7 vs. 26.2 ± 1.4 Hz, Paired T-test, p = 0.244). KA-induced cortical gamma oscillations also showed no change in oscillatory characteristics after application of LPS (*Figure 4.2)* (KA vs KA+LPS, area power 422 ± 188 vs. 455 ± 184 µV², Paired T-test, p = 0.574; peak power 15.25 ± 8.78 µV², vs. 15.82 ± 8.22 µV²/Hz, Paired T-test, p = 0.822; peak frequency 31.1 ± 1.5 vs. 30.5 ± 1.8 Hz, Paired T-test, p = 0.838). The delta oscillation, induced by SCH23390 and Carbachol *(Figure 4.3)* did not show changes to area power (SCH+CCH vs. SCH+CCH+LPS, 1414.4 ± 522.3 vs. 1363.0 ± 610.6 µV², Paired T-test, p = 0.952) or peak frequency (SCH+CCH vs. SCH+CCH+LPS, 1.07 ± 0.08 vs. 1.00 ± 0.04 Hz, One-Way ANOVA, p = 0.413). There was a decrease in mean peak power, although this was not significant (SCH+CCH vs. SCH+CCH+LPS, 335.9 ± 197.1 vs. 121.3 ± 43.3 µV²/Hz, T-test, p = 0.330).
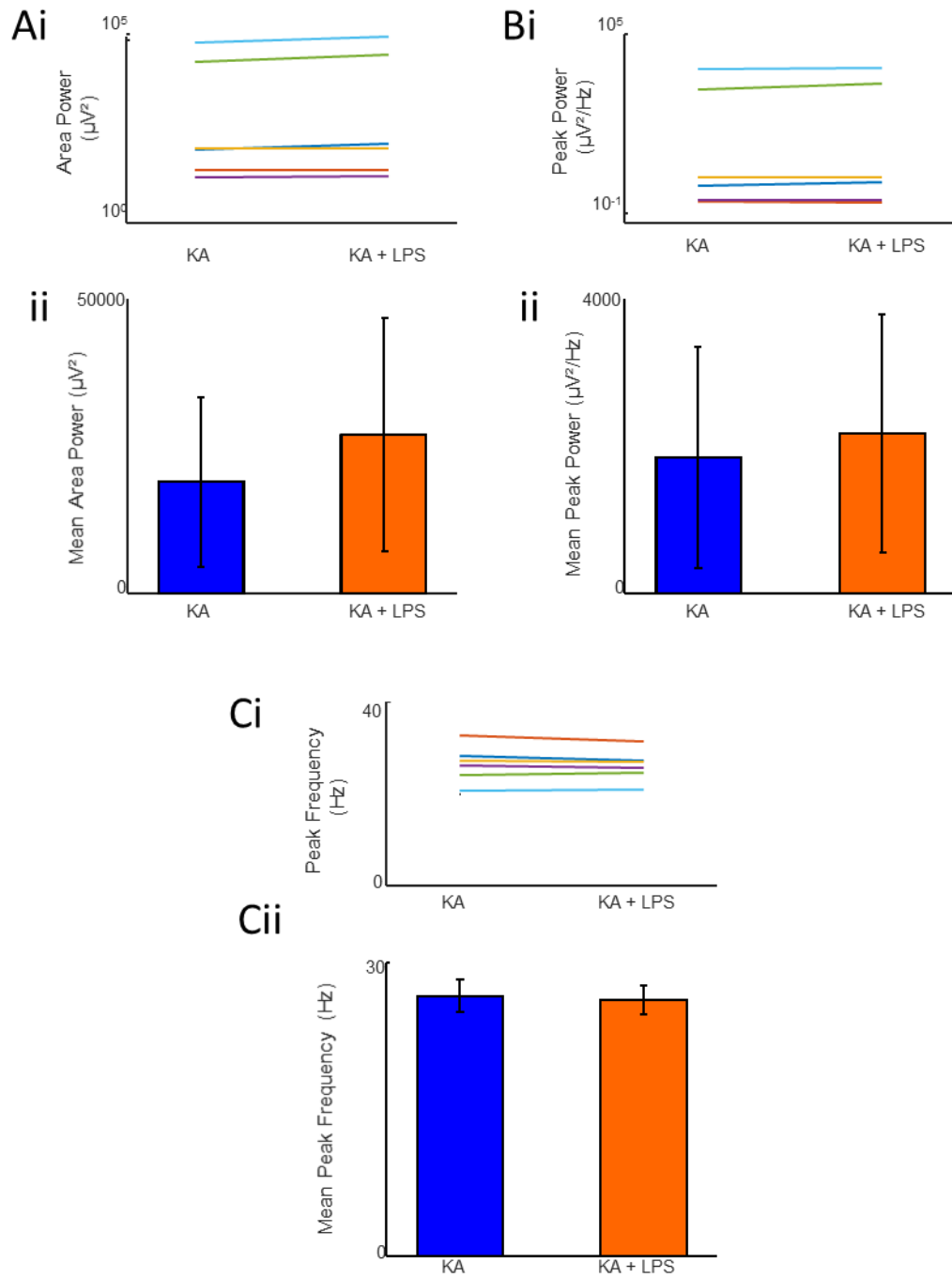
Figure 4.1. Hippocampal gamma oscillations do not change after acute application of LPS.
Ai. The area power of the oscillation in each slice (n = 6) before and after addition of LPS. N.B. y axis is logarithmic. **Aii.** The mean area power of the gamma oscillation before and after addition of LPS (n = 6) . Error bars show SEM. **Bi.** The peak power of each slice's oscillation before and after addition of LPS. N.B. y axis is logarithmic. **Bii.** The peak power of the oscillation in each slice (n = 6) before and after addition of LPS. Error bars show SEM. **Ci.** The modal peak frequency of the oscillation in each slice (n = 6) before and after addition of LPS. **Cii.** The mean modal peak frequency of the oscillation in each slice (n = 6) before and after addition of LPS. Error bars show SEM.
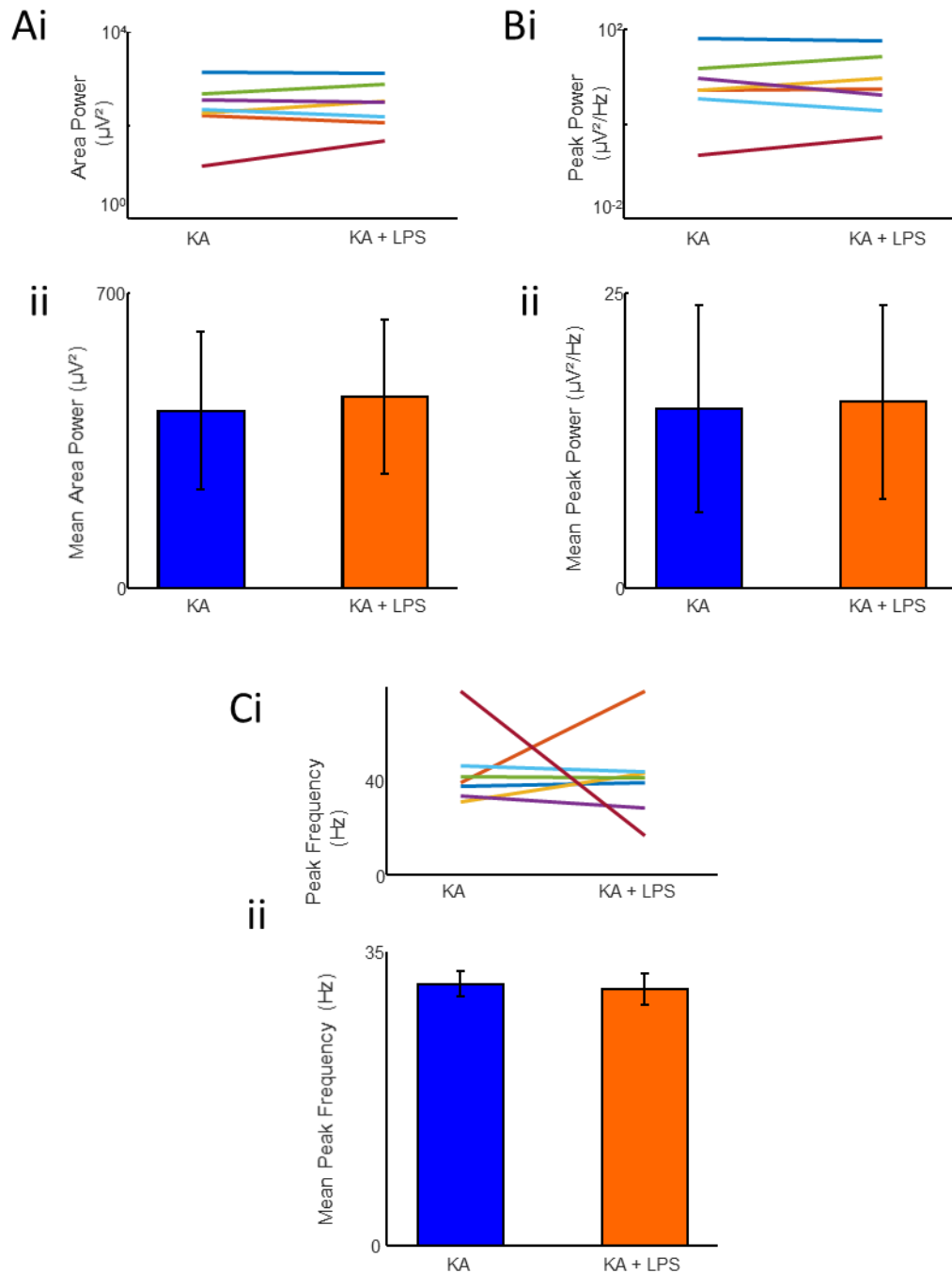
Figure 4.2. Cortical gamma oscillations do not change after acute application of LPS. Ai. The area power of the cortical gamma oscillation in each slice (n = 6) before and after addition of LPS. N.B. y axis is logarithmic. **Aii.** The mean area power of the cortical gamma oscillations before and after addition of LPS (n = 6) . Error bars show SEM. **Bi.** The peak power of the cortical gamma oscillation in each slice (n = 6) before and after addition of LPS. N.B. y axis is logarithmic. **Bii.** The mean peak power of the cortical gamma oscillations before and after addition of LPS (n = 6) . Error bars show SEM. **Ci.** The modal peak frequency of the cortical gamma oscillation in each slice (n = 6) before and after addition of LPS. **Cii.** The mean modal peak frequency of cortical gamma oscillations (n = 6) before and after addition of LPS. Error bars show SEM.
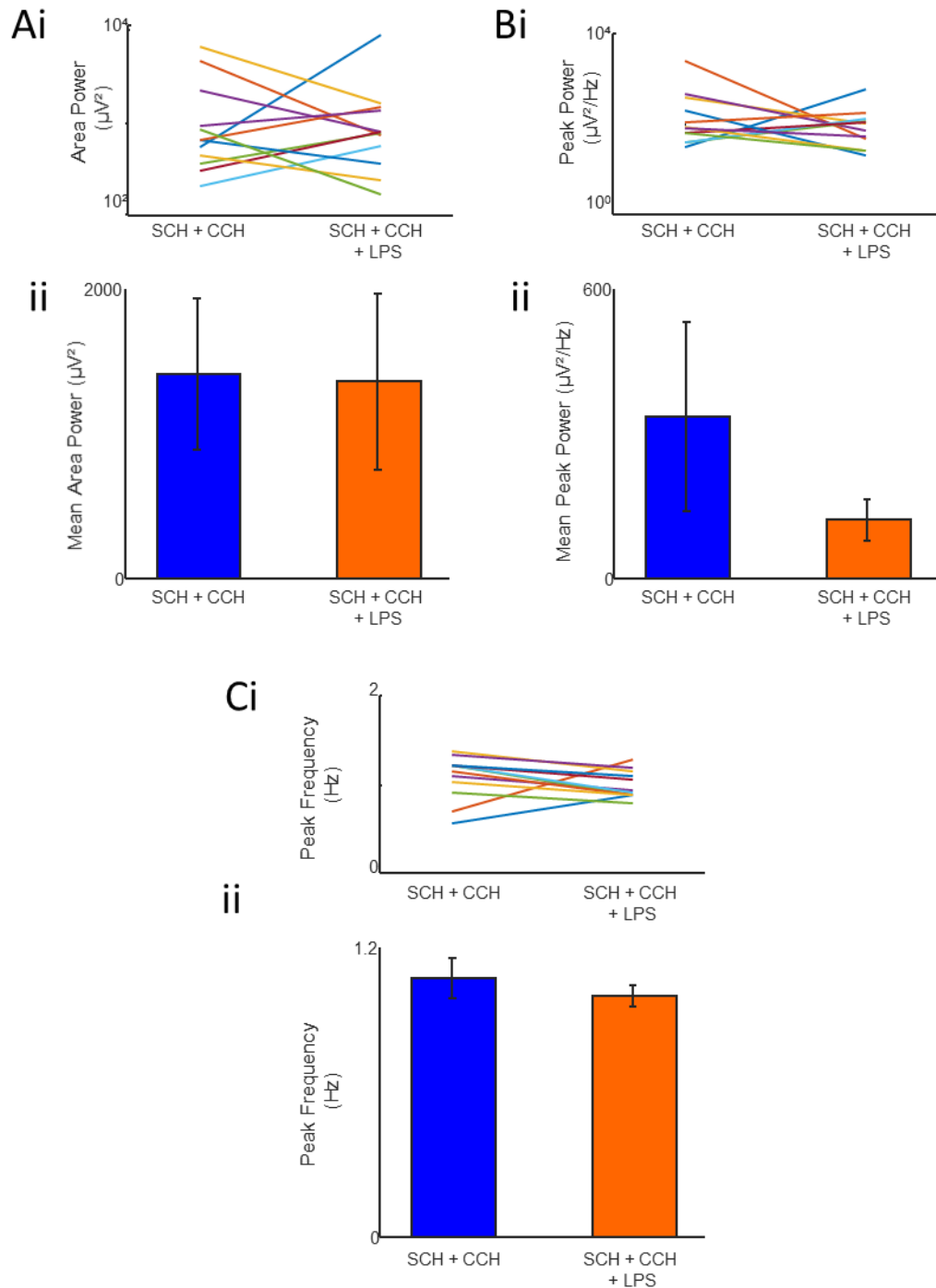
Figure 4.3. Cortical delta oscillations do not change after acute application of LPS. Ai. The area power of the cortical delta oscillation in each slice (n = 11) before and after addition of LPS. N.B. y axis is logarithmic. **Aii.** The mean area power of the cortical delta oscillations before and after addition of LPS (n = 11) . Error bars show SEM. **Bi.** The peak power of the cortical delta oscillation in each slice (n = 11) before and after addition of LPS. N.B. y axis is logarithmic. **Bii.** The mean peak power of the cortical delta oscillations before and after addition of LPS (n = 11) . Error bars show SEM. **Ci.** The modal peak frequency of the cortical delta oscillation in each slice (n = 11) before and after addition of LPS. **Cii.** The mean modal peak frequency of cortical delta oscillations (n = 11) before and after addition of LPS. Error bars show SEM.

4.2.2 Acute and Chronic systemic infection effects on oscillations

We investigated the effects of prior systemic infection of the animal on the ability to generate oscillations in *in* vitro brain slices. Infection was induced with 0.9% saline (which was also the vehicle), 250ug/ml LPS, 6mg/ml Poly I: C. Animals were dosed either once, 24 hr/1 days prior to sacrifice, or every three days for 7, or 28 days. All statistical analysis was carried out using a Two-Way ANOVA with Holm-Sidak multiple comparisons procedure for significant results. However, the low n numbers obtained in the Poly I:C condition prevented the analysis of interactions between time course and inflammation in this case so only the LPS data set was analysed.

In hippocampal slices, stable oscillatory activity was measured in CA3 after the bath application of 50nM KA. The mean area power of CA3 oscillations was lower after LPS treatment at each time point though this was not significant (*Figure 4.4)* (Area Power, Vehicle vs. LPS, 1 day: 9028.1 ± 927.0 vs. 7192.5 ± 1345.5 μV^2, Two Way ANOVA, p = 0.455; 7 days: 10215.7 ± 2315.1 vs 5977.4 ± 975.65 μV^2, Two Way ANOVA, p = 0.062; 28 days: 8604.7 ± 2315.1 vs. 3655.2 ± 2646.95 μV^2, Two Way ANOVA, p = 0.115). The mean area power was also lower in the Poly I:C treated condition, but again not significantly so (Area Power, 7 days: 7612.7 ± 1310.2 μV^2; 28 days: 6172.7μV^2, n=1).

The peak power showed no significant difference between any groups (Peak Power, Vehicle vs. LPS, 1 day: 709.0 ± 102.22 vs. 536.0 ± 168.4 $\mu V^2/Hz$, 7 days 970.0 ± 630.8 vs. 503.7 ± 148.0 $\mu V^2/Hz$, 28 days 386.7 ± 94.2 vs. 357.5 ± 301.43 $\mu V^2/Hz$, Two Way ANOVA, Treatment Time, p = 0.650, Condition, p = 0.825, Interaction = 0.789). Again, the mean peak power after Poly I:C treatment was closer to that of the LPS condition than control (Peak Power, 7 days: 503.7 ± 148.03 $\mu V^2/Hz$; 28 days: 438.5 $\mu V^2/Hz$, n=1). The frequency of the oscillation in CA3 showed a bidirectional change, with an apparent increase after 1 day treatment with LPS which was not significant (Peak Frequency, Vehicle vs. LPS, 1 day: 23.4 ± 0.28 vs. 26.6 ± 1.2 Hz, Two Way ANOVA with Holm-Sidak correction, p = 0.082) but with 7 days dosing, the decrease compared to vehicle was significant (Peak Frequency, Vehicle vs. LPS, 7 days: 28.1 ± 1.5 vs. 24.7 ± 0.6 Hz, Two Way ANOVA with Holm-Sidak correction, p = 0.033). There was no significant difference between treatments after 28 days (Peak Frequency, Vehicle vs. LPS, 28 days: 25.0 ± 1.8 vs. 25.6 ± 0.5 Hz, Two Way ANOVA with Holm-Sidak correction, p = 0.751). The data for Poly I:C seemed to match that of LPS (Peak Frequency, 7 days: 23.7 ± 1.01 Hz; 28 days: 24.7 Hz, n = 1). Interestingly there was also a difference in the comparison for treatment time vehicle data between 1 and 7 days

(Figure 4.4C) (Peak Frequency, Vehicle, 1 day vs. 7 days: 23.4 ± 0.28 vs. 28.1 ± 1.54, Two Way ANOVA with Holm-Sidak correction, p = 0.030).

For cortical gamma rhythms *(Figure 4.5)* the mean area power and peak power was higher after LPS treatment than in control slices after 7 days, but lower after 28 days of treatment. (Area Power, Vehicle vs. LPS, 7 days: 69.4 ± 8.1 vs. 101.9 ± 30.2 μV^2; 28 days: 115.6 ± 17.1 vs. 51.7 μV^2, n =1, Two Way ANOVA, Treatment Time, p = 0.953, Condition, p = 0.644, Interaction = 0.185) (Peak Power, Vehicle vs. LPS, 7 days: 1.1 ± 0.4 vs. 1.6 ± 0.6 μV^2/Hz; 28 days: 1.8 ± 0.8 vs. 1.1 μV^2/Hz, n = 1, Two Way ANOVA, Treatment Time, p = 0.889, Condition, p = 0.925, Interaction = 0.442). The mean frequency was lower after LPS treatment compared to control after 7 days, but is increased after 28 days, but this difference was not significant (Peak Frequency, Vehicle vs. LPS, 7 days: 37.1 ± 2.5 vs. 33.2 ± 2.9 Hz; 28 days: 33.0 ± 6.6 vs. 38.2 Hz, n = 1, Two Way ANOVA, Treatment Time, p = 0.917, Condition, p = 0.897 , Interaction = 0.343). The differences in all oscillatory parameters after Poly I:C treatment compared to control were not significant but followed the same pattern as LPS for area power (7 days: 187.11 ± 111.9 μV^2; 28 days: 65.8 ± 49.1 μV^2) and peak frequency (7 days: 34.7 ± 5.6 Hz; 28 days: 35.8 ± 3.9 Hz). The mean peak power after Poly I:C treatment increased similarly to LPS after 7 days but remained similar to the vehicle after 28 days (7 days: 187.11 ± 111.9 μV^2/Hz; 28 days: 65.8 ± 49.1 μV^2/Hz).

Looking at cortical delta oscillations, the area power and peak power of the oscillations in the LPS treated condition did not change significantly compared to the control *(Figure 4.6)* (Area Power, Vehicle vs. LPS, 1 day: 361.8 ± 255.1 vs. 425.3 ± 113.6μV^2, 7 days: 1384.1 ± 449.9 vs. 2004.6 ± 673.4 μV^2; 28 days: 1854.0 ± 508.7 vs. 1169.9 ± 142.07 μV^2;Two Way ANOVA, Treatment Time, p = 0.113, Condition, p = 0.999, Interaction = 0.535) (Peak Power, Vehicle vs. LPS, 1 day: 32.6 ± 18.4 vs. 74.7 ± 33.1 μV^2/Hz, 7 days: 284.9 ± 127.0 vs. 632.65 ± 274.0 μV^2; 28 days: 1854.0 ± 508.7 vs. 1169.9 ± 142.0 μV^2; Two Way ANOVA, Treatment Time, p = 0.142, Condition, p = 0.911, Interaction = 0.298). The mean peak frequency of the delta oscillations lower with treatment with inflammatory agents. However, extricating reliable statistical results from the peak frequency data was difficult due unequal variances. Therefore, separate ANOVA/Kruskal-Wallis tests were performed for the data in each treatment time separately.

There were no significant differences found in treatment conditions that last 1 or 28 days. (Peak Frequency, Vehicle vs. LPS, 1 day: 1.30 ± 0.28 vs. 1.15 ± 0.06 Hz, Kruskal-Wallis ANOVA on Ranks, Vehicle vs LPS, p = 0.999; Vehicle vs. LPS. Vs. Poly I:C, 28 days: 1.30 ± 0.10 vs. 1.23 ± 0.12 vs. 0.86

± 0.269, Kruskal-Wallis ANOVA on Ranks, Vehicle vs LPS, p = 0.400). There was a significant decrease in the frequency of the delta rhythm after 7 day treatment of LPS, but not Poly I:C (Peak Frequency, Vehicle vs. LPS vs. Poly I:C, 7 days: 1.40 ± 0.08 vs. 1.18 ± 0.02 vs. 1.16 ± 0.05 Hz, One Way ANOVA with Holm Sidak correction, Vehicle vs LPS, p = 0.47, Vehicle vs. Poly I:C = 0.058).
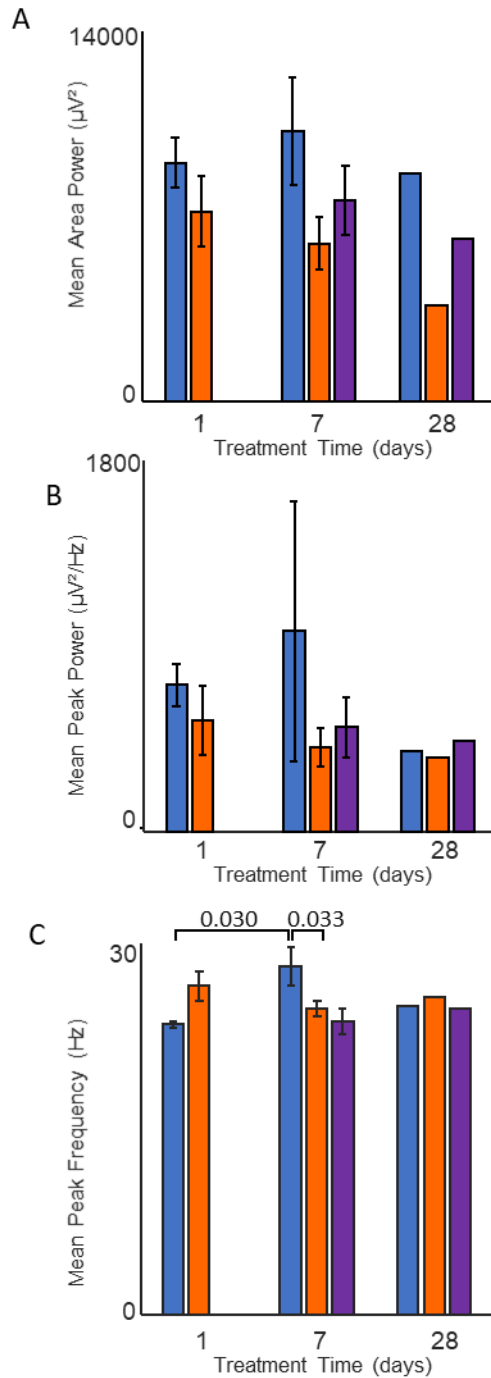
Figure 4.4. Acute and chronic systemic inflammation changes hippocampal KA induced oscillation frequency. A. The mean area power of the oscillation in CA3 after dosing with vehicle (blue), LPS (orange) and Poly I:C (purple). Error bars show SEM. N number of bars left to right (3,3,4,4,3,2,2,1) **B.** The mean peak power of the oscillation in CA3 after dosing with vehicle (blue), LPS (orange) and Poly I:C (purple). Error bars show SEM. N number of bars left to right (3,3,4,4,3,2,2,1 **C.** The mean peak frequency of the oscillation in CA3 after dosing with vehicle (blue), LPS (orange) and Poly I:C (purple). Error bars show SEM. N number of bars left to right (3,3,4,4,3,2,2,1).
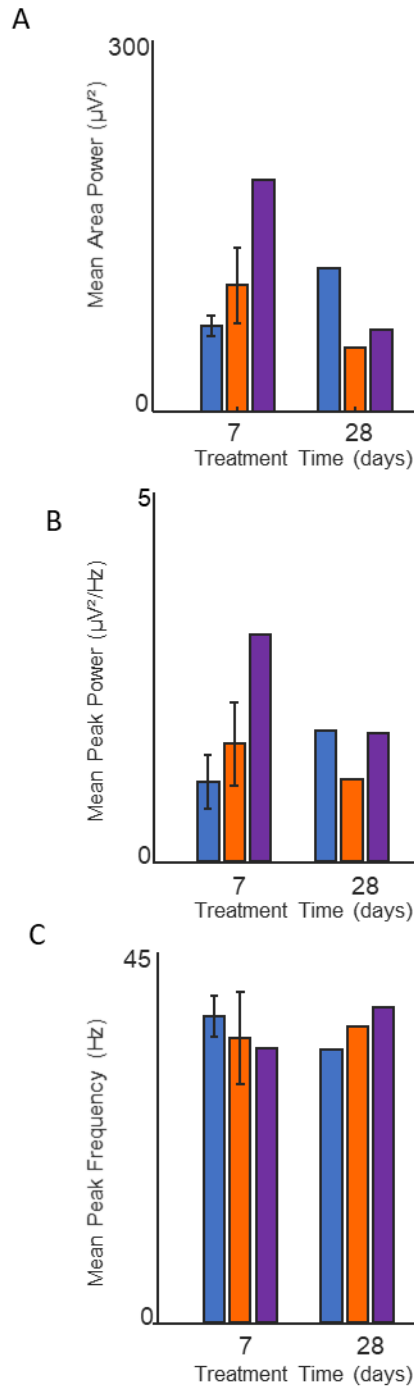
Figure 4.5. Chronically induced systemic inflammation does not alters cortical gamma oscillations. . A. The mean area power of cortical gamma oscillations after dosing with vehicle (blue), LPS (orange) and Poly I:C (purple). Error bars show SEM. N numbers, bars left to right (3,4,2,2,2,1). **B.** The mean peak power of cortical gamma oscillations after dosing with vehicle (blue), LPS (orange) and Poly I:C (purple). Error bars show SEM. N numbers, bars left to right (3,4,2,2,2,1). **C.** The mean peak frequency of cortical gamma oscillations after dosing with vehicle (blue), LPS (orange) and Poly I:C (purple). Error bars show SEM. N numbers, bars left to right (3,4,2,2,2,1).
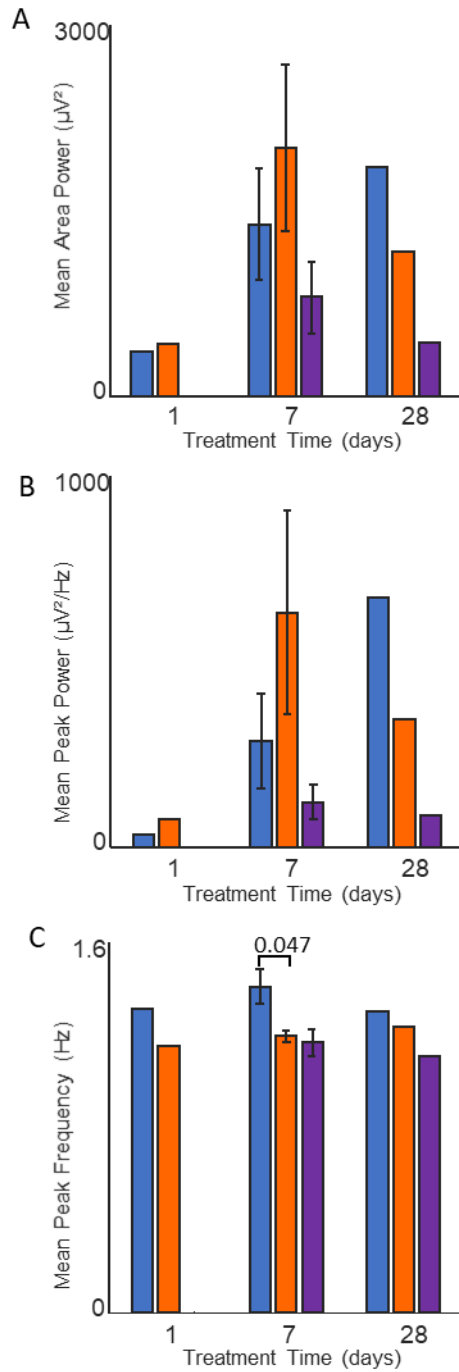
Figure 4.6. Chronically induced systemic inflammation slightly alters cortical delta oscillations. A. The mean area power of cortical delta oscillations after dosing with vehicle (blue), LPS (orange) and Poly I:C (purple). Error bars show SEM. N numbers, bars left to right (2,2,0,4,4,3,2,2,2) **B.** The mean peak power of cortical delta oscillations after dosing with vehicle (blue), LPS (orange) and Poly I:C (purple). Error bars show SEM. N numbers, bars left to right (2,2,0,4,4,3,2,2,2) **C.** The mean peak frequency of cortical delta oscillations after dosing with vehicle (blue), LPS (orange) and Poly I:C (purple). Error bars show SEM. N numbers, bars left to right (2,2,0,4,4,3,2,2,2).

4.2.3 The effect of chronic systemic infection on neuroinflammatory mediators

To analyse the inflammatory environment of the brain after systemic infection, surplus tissue from the preparation of brains slices was taken and analysed for 27 cytokines and chemokines using a multiplex bead-based protein assay. This compared 7 and 28-day dosed animals to vehicle dosed controls for the levels of 27 different cytokine and chemokines in the cerebral homogenate.

Six cytokines/chemokines were significantly increased after 7 days dosing with LPS (*Figure 4.7)*. These were Fractalkine (Vehicle vs. LPS: 842.4 ± 100.7 vs. 1166.0 ± 64.0 pg/ml, One-Way ANOVA with post hoc Holm-Sidak, p-value = 0.027), IL-1β (Vehicle vs. LPS: 57.2 ± 1.7 vs. 70.0 ± 2.7 pg/ml, One-Way ANOVA with post hoc Holm-Sidak, p-value = 0.004), IL-4 (Vehicle vs. LPS: 80.6 ± 1.9 vs. 63.0 ± 4.5 pg/ml, One-Way ANOVA with post hoc Holm-Sidak, p-value = 0.007), IL-13 (Vehicle vs. LPS: 14.1 ± 2.1 vs. 21.3 ± 0.7 pg/ml, One-Way ANOVA with post hoc Holm-Sidak, p-value = 0.014), VEGF (Vehicle vs. LPS: 124.1 ± 11.4 vs. 155.6 ± 6.1 pg/ml, One-Way ANOVA with post hoc Holm-Sidak, p-value = 0.004) and RANTES (Vehicle vs. LPS: 16.3 ± 1.4 vs. 20.7 ± 0.85 pg/ml, One-Way ANOVA with post hoc Holm-Sidak, p-value = 0.043). Only two chemokines were increased after 7 days Poly I:C dosing, these were IP-10 (Vehicle vs. Poly I:C: 189.4 ± 14.2 vs. 696.0 ± 198.4 pg/ml, One-Way ANOVA with post hoc Holm-Sidak, p-value = 0.034) and RANTES (Vehicle vs. Poly I:C: 16.3 ± 1.4 vs. 24.3 ± 3.0 pg/ml, One-Way ANOVA with post hoc Holm-Sidak, p-value = 0.027).

As for the 28-day dosing regime, only 3 cytokines were significantly changed after LPS dosing *(Figure 4.8)*: IFN-γ (Vehicle vs. LPS: 673.2 ± 25.1 vs. 803.8 ± 46.4 pg/ml, One-Way ANOVA with post hoc Holm-Sidak, p-value = 0.048), TNF-α (Vehicle vs. LPS: 7.8 ± 0.5 vs. 11.3 ± 1.2 pg/ml, One-Way ANOVA with post hoc Holm-Sidak, p-value = 0.029) and IL-1α (Vehicle vs. LPS: 104.6 ± 11.6 vs. 154.0 ± 8.4 pg/ml, One-Way ANOVA with post hoc Holm-Sidak, p-value = 0.014). The only cytokine that was increased after 28 days dosing with Poly I:C was IL-5 (Vehicle vs. Poly I:C: 188.4 ± 5.2 vs. 168.0 ± 5.2 pg/ml, One-Way ANOVA with post hoc Holm-Sidak, p-value = 0.033)
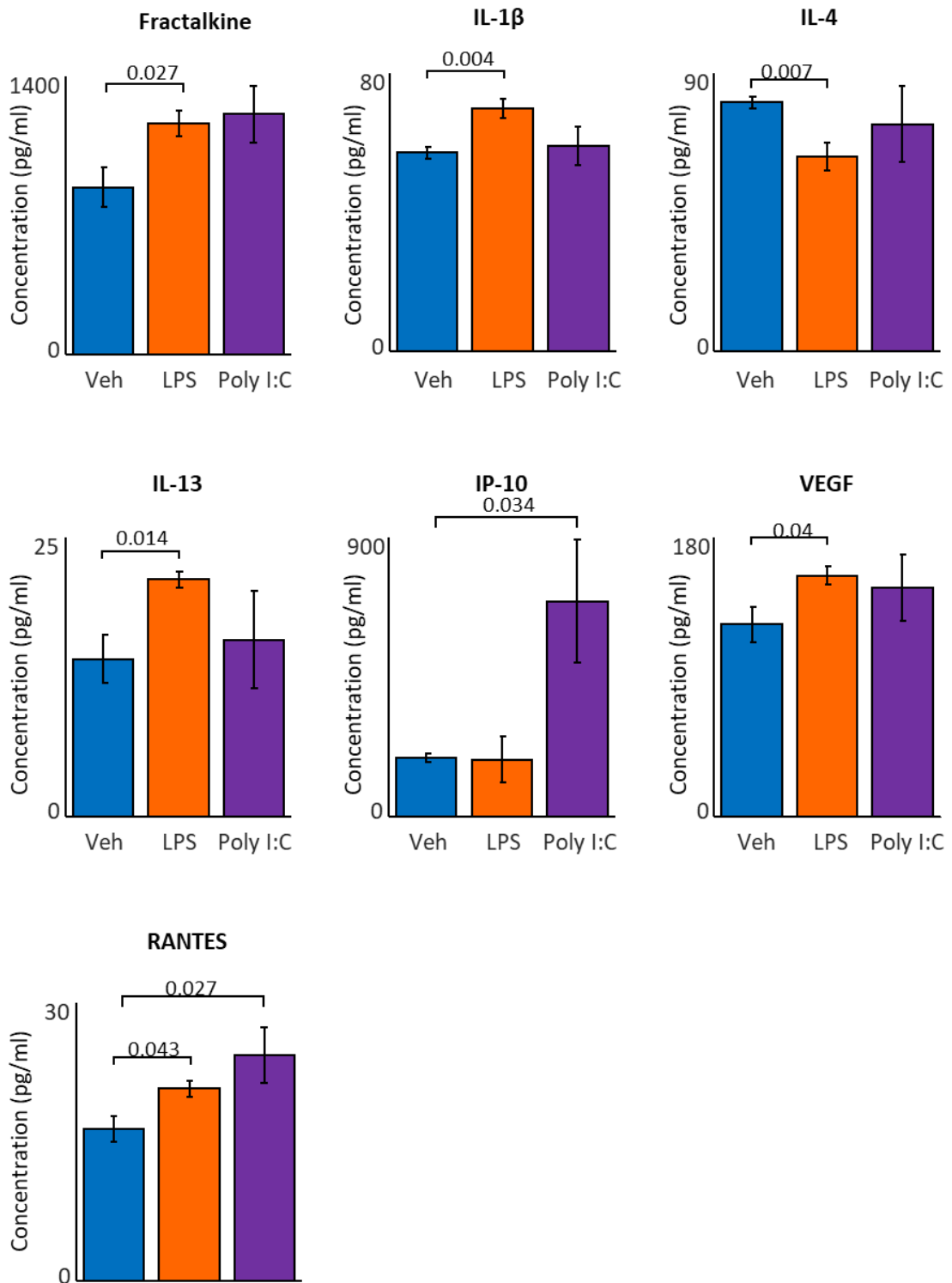
Figure 4.7. Cytokine and chemokine levels are changed in the brain after 7 day systemic inflammatory challenge. Mean concentrations of cytokines and chemokines in cerebral homogenate after 7 day treatment with LPS (orange, n =4), Poly I:C (purple, n=4) and vehicle (Blue, n=4). Error bars show standard error of the mean. Values displayed are significant p-values from One-Way ANOVA. N.B. Veh = Vehicle.
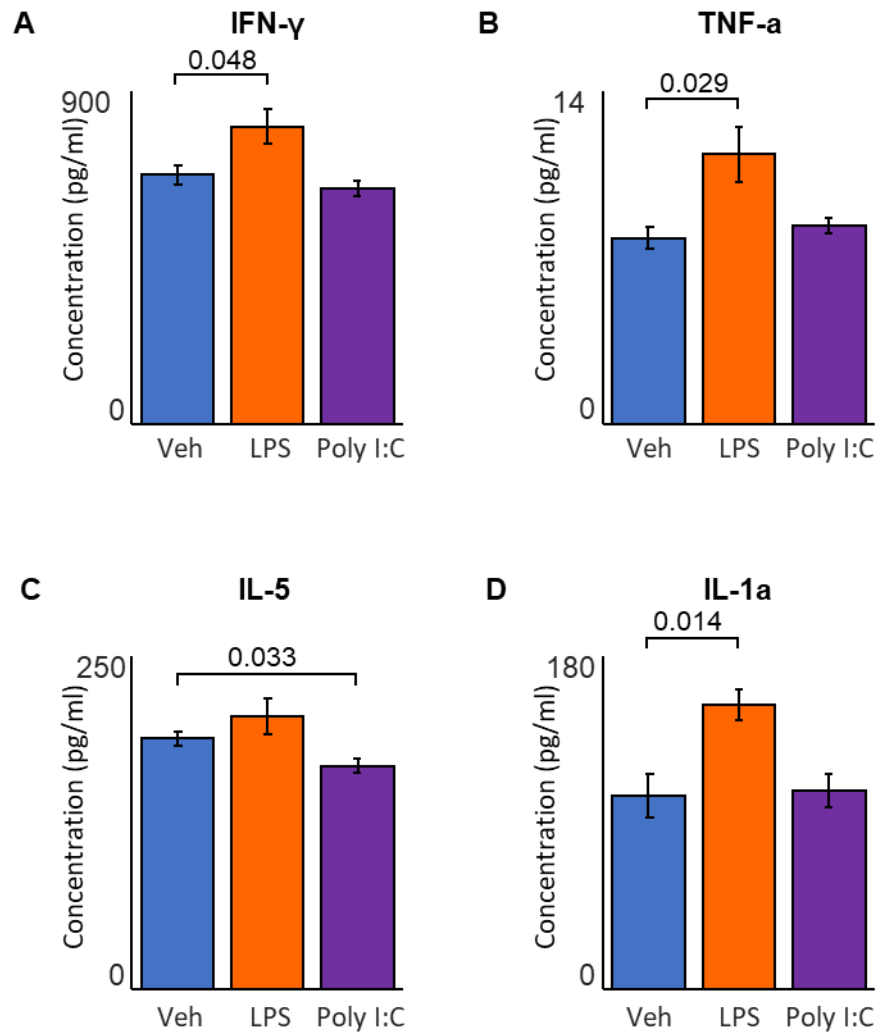
Figure 4.8. Cytokine levels are changed in the brain after 28 day systemic inflammatory challenge. Mean concentrations of cytokines and chemokines in cerebral homogenate after 28 day treatment with LPS (orange, n =4), Poly I:C (purple, n=4) and vehicle (Blue, n=4). Error bars show standard error of the mean. Values displayed are significant p values from One-Way ANOVA. N.B. Veh = Vehicle.

4.2.4 The effect of chronic systemic infection on microglial morphology

To further confirm the presence of inflammation in the brain, microglia were analysed. Under inflammatory conditions, microglia are known to retract their processes and become ramified in structure. The morphology was assessed following a stain for Iba1. This allowed the visual and analytical comparison of microglia. The area of each microglia cell was calculated and found to be significantly lower after 28 days dosing with LPS or Poly I:C *(Figure 4.9)* (Area, Vehicle vs. LPS vs. Poly I:C, 58.9 ± 6.0 vs. 43.8 ± 4.1 vs. 44.5 ± 3.3 μm^2, p values from One-Way ANOVA with post-hoc Tukey's Multiple comparisons procedure: Vehicle vs LPS = 0.089, Vehicle vs Poly I:C = 0.042). Area of a cell does not necessarily show how spread out the projections are, so a bounding box was fitted around each cell (the smallest rectangle that would encompass the whole object), the area of which gives a better indication of the amount of spread of the projections of the cell. This was also significantly lower in the inflammation condition meaning that the spread of the projections was smaller (bounding box area, Vehicle vs. LPS vs. Poly I:C, 282.3.9 ± 43.5 vs. 140.3 ± 18.1 vs. 160.0 ± 15.1 μm^2, p values from One-Way ANOVA with post-hoc Tukey's Multiple comparisons procedure: Vehicle vs LPS, p = 0.002, Vehicle vs Poly I:C, p = 0.003).
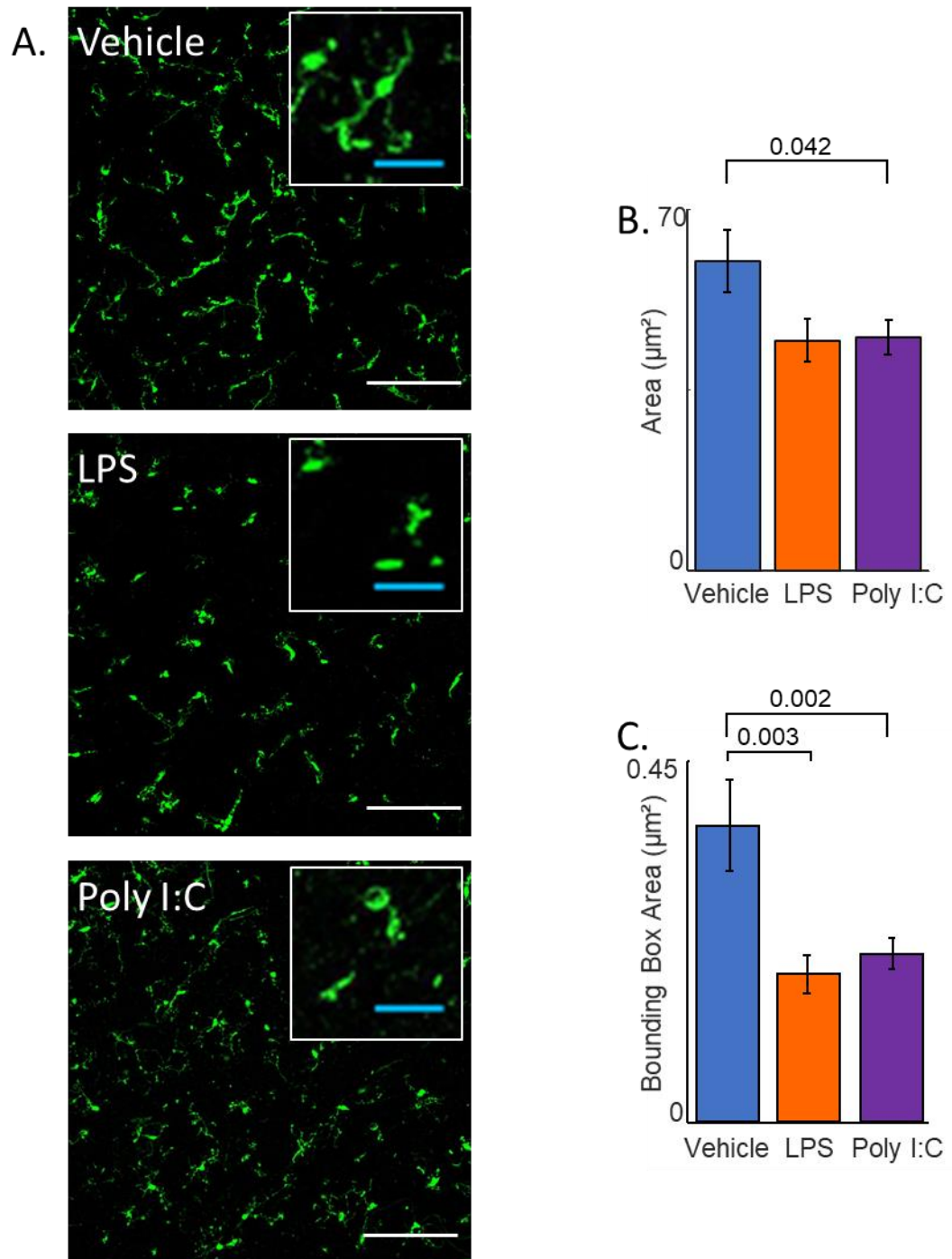
Figure 4.9. Peripheral inflammatory challenge changes the morphology of microglia in the brain. A. Examples of microglia as stained with Iba1 antibody after dosing every 3rd day for 28 days with 0.9% saline, 500ug/kg LPS, 6mg/kg Poly I:C. Scale bars = white: 100μm, blue: 25μm **B.** The mean area of each Iba1+ve cell in each example image from A. Error bar is SEM. Values are from One-Way ANOVA with post-hoc Tukey's multiple comparison procedure. **C.** The mean area of the bounding box (the smallest rectangle containing each object) of each Iba1+ve cell in each example image from A. Error bar is SEM. Values are from One-Way ANOVA with post-hoc Tukey's multiple comparison procedure.

4.3. Discussion

4.3.1 Summary

In this chapter, the effect of inflammation on *in vitro* models of certain brain rhythms was analysed. The effect of the direct application of lipopolysaccharide was monitored along with the changes after the systemic dosing of LPS and Poly I:C for up to 28 days. These changes were also related to changes to cytokine and chemokine expression as well as microglial morphological changes.

The summary of key findings from this investigation are:

- The direct application of LPS had no significant effect on characteristics of *in vitro* models of cortical gamma and delta oscillations, and hippocampal oscillations.
- There was a bidirectional change in hippocampal oscillation frequency only, after systemic immune challenge, which is related to the longevity of the 'infection'.
- The systemic immune challenge did not change the area power, peak power or frequency of cortical gamma oscillations or delta oscillations but did reduce the frequency of delta oscillations after 7 days but not over 28 days.
- The landscape of inflammatory cytokines and chemokines was different between 7 days immune challenge compared to 28-day immune challenge.
- Microglia were activated upon systemic immune challenge with LPS and Poly I:C.

4.3.2 A note about hippocampal gamma oscillations and temperature.

The oscillations recorded from the CA3 region of the hippocampus were found to be between 25 – 30 Hz. This range normally describes beta oscillations; however, it is known that slice preparations often have lower frequencies than *in vivo*. This is due to the reduction of temperature that *in vitro* slices are maintained at (compared to body temperature) so that the correct amount of oxygen may be dissolved. This phenomenon has been recorded in the carbachol-induced oscillation in the CA1 region of the hippocampus, showing a 3.3 Hz decrease with every 1°C decrease in temperature (Dickinson et al., 2003). This temperature relationship is suggested to be driven by elongated GABAergic IPSCs leading to a long latency between IPSPs, which set the tempo of the oscillation. It would appear that both hippocampal gamma and beta rhythms have a similar GABA$_A$ dependent mechanism (Tsintsadze et al., 2015). Previous research has accepted *in vivo* oscillations with a frequency as low as 25Hz as gamma oscillations (Colgin et al., 2009a). This, along with the temperature dependent frequency change would suggest that the oscillations generated may be gamma oscillations despite having a frequency below 30Hz.

4.3.3 The acute application of LPS onto slices

The first studies in this chapter showed that the addition of LPS to the circulating ACSF had no effect on the stable *in vitro* hippocampal/cortical gamma oscillations. The pattern recognition receptor for LPS (TLR4) has been documented in neurons (Leow-Dyke et al., 2012). In cultured neurons, TLR4 activation (by LPS) has been shown to produce TNFα, IL-6, CXCL1 And RANTES (Aurelian et al., 2016). However, these experiments showed that LPS does not directly affect electrical activity. It also has been shown in cultured cells that LPS has no effect on neuronal survival in the absence of microglia. Whereas in neuron/microglia co-culture there is almost a complete destruction of all cells (Lehnardt et al., 2003). This shows not only that neurons do not possess mechanisms to induce their own toxicity after LPS application, but also, in the presence of microglia, toxicity occurs on a time scale of many hours to days (Rupalla et al., 1998; Rangroo Thrane et al., 2012). Other studies also corroborate the idea that microglia are responsible for stimulating neuronal apoptosis (Tseng et al., 2012; Zhang et al., 2013). This is thought to be through the upregulation of pro-inflammatory cytokines released by microglia such as TNFα, IL-1β as well as iNOS. These were shown to be upregulated downstream of IFN-y (Wang et al., 2015a) after at least 2 hours.

Changes to induced hippocampal gamma oscillations in organotypic slices were seen after treatment with LPS, however, the time scale of the LPS treatment was to be 72 hours (Papageorgiou et al., 2016). Using a microelectrode array system, enhanced excitability generated epileptiform discharges after LPS application, though again after >6 hours (Gullo et al., 2014). Only a much more immediate effect has been seen *in vivo,* with the epi-pial application of LPS generating epileptiform activity within an hour of application. Although the concentration of LPS used was 40x that used in this thesis (Rodgers et al., 2009)

4.3.4. Changes to *in vitro* rhythms related to longevity of immune challenge.

The initial experiments in this chapter showed that LPS had no effect upon the oscillatory activity of *in vitro* brain slices after 1 hour. These findings (along with the studies outlined above) suggest that LPS driven changes to neuronal excitability occur at a timescale that is longer than reasonable to observe in acute brain slice preparations. Furthermore, the impact of systemic infection on the oscillatory activity of the brain is of particular importance, especially with growing research into the effects of systemic infection on neurodegenerative disorders (Perry et al., 2003).

After 24 hours, there were no significant changes to the area power, peak power, or peak frequency of any of the oscillations measured. This is in line with *in vivo* data showing that although initial changes to delta and gamma oscillations may occur after intraperitoneal (i.p.) LPS injection, these changes stabilise to control condition after 24 hours (Mamad et al., 2018).

We found two significant aberrations in the oscillatory activity across the dosing regimes. Reductions were in the frequency of both hippocampal gamma oscillations and cortical delta oscillations after 7 days treatment with LPS. Poly I:C broadly followed this trend though 'n' numbers were too low for inclusion in statistical tests. The slowing of the background EEG is related to cerebral dysfunction and often associated with lesions, delirium and dementia (Britton et al., 2016). Further findings included an interesting trend in the electrophysiology data, with the time scale of the apparent change of the power of delta frequency oscillations *(Figure 4.10).* At one day post-infection the delta power is unchanged compared to control. However, after 7 days the mean delta power is increased by ~50%. This increase is reversed after 28 days when there was an insignificant reduction compared to control.
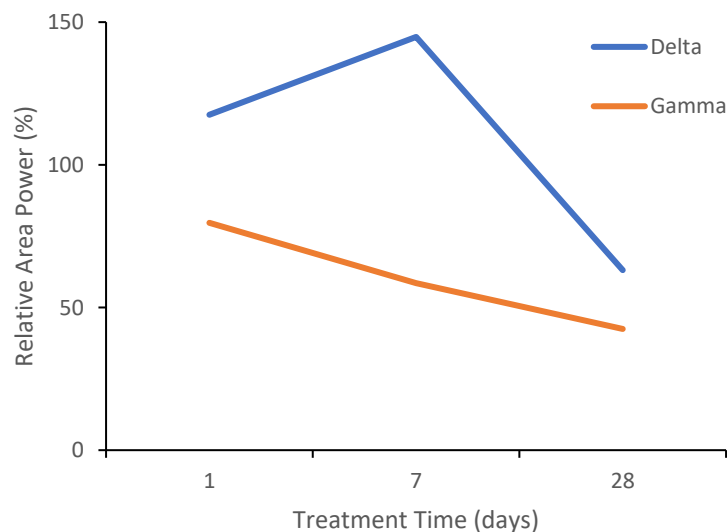
Figure 4.10. The relative area power of generated rhythms compared to control
The mean area power as a percentage of the mean control reading in LPS rats treated with 250ug/kg LPS for 1, 7 and 28 days, red = hippocampal gamma oscillations, Blue = cortical delta oscillations.

These data would suggest a changed propensity for sleep as SWS levels correlate with sleep need (Brunner et al., 1990; Rodriguez et al., 2016). Sleep changes in humans after neuroinflammation (especially following traumatic brain injury) are common, with increases in sleep need and daytime sleepiness (Imbach et al., 2015), as well as increases in the power of delta rhythms during SWS, (Parsons et al., 1997). This is likely a result of the cytokine upregulation as cytokine i.p. IL-1β injection has also been shown to increase delta power during slow wave sleep in rats (Hansen and Krueger, 1997). The same is true for the cortical infusion and i.p. injection of TNFα (Kubota et al., 2001; Yoshida et al., 2004).

In humans, many conditions related to neuroinflammation have shown an increase in delta oscillations, including delirium from a range of causes (Koponen et al., 1989). Increases in delta rhythms during wakefulness has also be seen as a result of sports-related concussion (Gosselin et al., 2009) and mild traumatic brain injury) (Modarres et al., 2017). Intrusions of this sort have also been noted in healthy rats during prolonged wakefulness and termed 'local sleep' (Vyazovskiy et al., 2011). Inflammatory cytokines may be involved in this process, as sleep deprivation is known to increase IL-1β (Frey et al., 2007) and TNFα (Shearer et al., 2001). It could follow that the sickness behaviour seen after i.p. injection of LPS (Biesmans et al., 2013) is a cognitive behavioural response to the sleep debt highlighted by our studies.

There was also a general decrease in the mean area power of hippocampal gamma oscillations upon systemic LPS injection over time, compared to control *(Figure 4.10)*. These oscillations were recorded from the CA3 region of the hippocampus which is known to exhibit "slow" gamma rhythms (~25 – 50 Hz) (Colgin et al., 2009a) and are in the range of the rhythmic activity seen in these experiments. The synchrony of activity in the frequency band between CA3 and CA1 regions for the hippocampus is believed to be important for memory retrieval (Colgin, 2016). Reductions in slow gamma have been shown in the hippocampus in triple mutant (Psen1, APPS and tau) Alzheimer's mouse models (Mably et al., 2017) and a model of tauopathy (Booth et al., 2016) both of which are associated with memory loss (Jahn, 2013) (Van der Jeugd et al., 2011). The decrease in these oscillations after chronic LPS injections suggest that the induction of inflammation in the brain may play a role in aberrations to gamma oscillations.

4.3.5 Cytokine/chemokine levels differ with duration of the immune challenge.

It is likely that the electrophysiological changes seen in slices from animals subjected to a systemic immune challenge (in this chapter) were due to neuroinflammation. This was confirmed with experiments that showed significant changes to pro- and anti-inflammatory cytokines and chemokines in the brain.

After 7 days dosing with LPS (doses occurred on day 0, 3, and 6) (Tchessalova and Tronson, 2019) several pro- and anti-inflammatory cytokines and chemokines were found to be increased. These were IL-1β, IL-13, VEGF and the chemokines Fractalkine and RANTES. Interestingly, three cytokines classically associated with a pro-inflammatory environment were not changed after 7 days (TNFα, IL-1α and IFN-γ).

The increased expression, after the inflammatory challenge, of IL-1β is unsurprising as IL-1 interleukins are considered the archetypal pro-inflammatory cytokines. The upregulation of its expression is likely to be due to its secretion from microglia and astrocytes after inflammatory challenge (Rothwell and Luheshi, 2000). Generally, IL-1β is seen to be the more important IL-1 cytokine and here it is increased and IL-1α is not significantly different. However, this may be due to a possible redundancy mechanism in the cytokine signalling system whereby both IL-1α and β exert their effects through the same receptor (IL-1RI) (Sims et al., 1988).

The increase in fractalkine is also indicative of a proinflammatory response as it is released by neurones undergoing apoptosis as a chemoattractant signal to microglia and astrocytes (Sokolowski et al., 2014) which exclusively house the CX3CR1 receptor – that binds fractalkine (Maciejewski-Lenoir et al., 1999). Through this chemotactic mechanism, fractalkine has been implicated in the uptake of aggregated alpha-synuclein by microglia in a mouse model of PD model (Thome et al., 2015) and knockout of the CX3CR1 receptor causes protracted microglial activation after LPS immune stimulation (Corona et al., 2010). This may be due to the lack of signalling to attract microglia to sites of exogenous material that requires phagocytosis. In our experiments, the presence of fractalkine suggest an induction of neuroinflammatory mechanism requiring microglial migration and phagocytosis.

Another chemokine showing increased expression after 7 days treatment is RANTES (CCL5). RANTES is a pleiotropic chemokine, probably due to its promiscuity in terms of receptor binding (Pease, 2006). RANTES is constitutively active in the healthy brain, having roles in myelination (Kadi et al., 2006), differentiation of astrocytes (Bakhiet et al., 2001) glucose uptake and metabolism (Chou et al., 2016). However during inflammation RANTES is generally considered proinflammatory as it has been shown to be expressed by T-cells, and recruits various immune cells to sites of inflammation (Maghazachi et al., 1996) and also mobilises mononuclear phagocytes and aid their BBB penetration (Sadek et al., 1998). Conversely RANTES has also been shown to be neuroprotective, inducing the expression of neurotrophic factors (Tokami et al., 2013).

The increase in pro- inflammatory cytokines and chemokines (Il-1β, Fractalkine and RANTES) after a 7-day inflammatory challenge occurs in tandem with anti-inflammatory cytokines, suggesting that there is a balance immune response occurring, mediated by VEGF and IL-13. IL-13 is considered an anti-inflammatory inhibiting the expression of other pro-inflammatory cytokines in monocytes such as IL-1β, TNFα and GRO in monocytes and IFN-γ (Minty et al., 1993) In the brain IL-13 is also known to promote an anti-inflammatory phenotype in microglia (Chawla et al., 2011) and contribute to the removal of pro-inflammatory microglia (Mori et al., 2016). These effects are seen in tandem with IL-4, which is often linked to IL-13 due to the overlap of their biological function (Chomarat and Banchereau, 1998) and their ability to act through the dimerization of their receptors. (Rael and Lockey, 2011). Unusually however, we found that whilst IL-13 was significantly increased after 7-day immune challenge, IL-4 was decreased. VEGF is also suggested to be anti-inflammatory and it has been shown that exogenous peripheral injection with VEGF leads to decreased levels of pro-inflammatory cytokines IL-1β and TNF-α (Xu et al., 2017) highlighting its role in the reversal of inflammation.

However, the cytokines present in the brains of rats treated for 28 days with LPS (every 3rd day) reflect tipping of the balance to a more pro-inflammatory environment. The three main pro-inflammatory cytokines IL-1a, TNFα and IFN-y are all increased with respect to the vehicle-treated animals, all of which are known to activate microglia (Gibson et al., 2004; Kuno et al., 2005; Rock et al., 2005).

4.3.6 Microglia are activated upon systemic immune challenge

The neuroinflammatory environment of the brain, induced after 28-day treatment with LPS and Poly I:C was confirmed by assessing the morphology of microglia. Looking at the surface area of the microglia gave a good indication of their ramification and thus their status of activation. This is due to the fact that activated microglia retract their projections to become more amoeboid to facilitate phagocytosis (Dheen et al., 2007). It was not clear whether the activation of microglia occurred due to the infiltration of LPS or Poly I:C molecules into the brain, OR indirectly. However it has been shown that LPS does not readily cross the blood-brain barrier (Singh and Jiang, 2004), suggesting that the activation of microglia in the brain occurs through indirect methods either through the activation of TLR4 receptors, or cytokine receptors in astrocytes and microglia in the circumventricular organs (Nadeau and Rivest, 1999), or peripheral cytokine interacting with endothelial cells to transfer the inflammatory signal across the BBB. This is most likely though TNFα signalling as it is the first proinflammatory cytokine to be upregulated by intraperitoneal LPS treatment, shortly after IL-1β and IL-6 (Fong et al., 1989). All of these cytokines are likely to propagate the peripheral infection to the CNS but targeting receptors on the endothelium of brain capillaries, which then causes the diffusion of prostaglandins and NOS to the brain parenchyma (Elmquist et al., 1997).

4.3.7 Experimental limitations.

A major caveat to the results in this chapter is the low number of repeats used for the electrophysiology experiments. In some cases, visual trends are apparent due to the difference in compared means and separation of the error bars, however, there is no significant difference. It is not possible to know without further repeats whether these trends are legitimate. In other cases (especially where n numbers are particularly low) large error bars make it difficult to discern any trends even visually. Furthermore, it was intended that slices from the electrophysiology experiments would be stained for immediate early gene markers to analyse if changes in cortical dynamics were related to changes in synaptic plasticity. Unfortunately, the tissue was transported from the US to the UK for this purpose and when it was, much of it was not useable for immunohistochemistry, and those slices were structurally compromised. The example in Figure 11 shows the best example of Arc staining in the US tissue compared to tissue collected in the UK. This issue also affected the Iba1 staining of this tissue, which meant therefore that only one animal per condition was compared. This meant that whilst we could confirm that intraperitoneal injection of LPS and Poly I:C at the doses used was capable of activating microglia, it could not be confirmed for all animals tested.

A.

B.
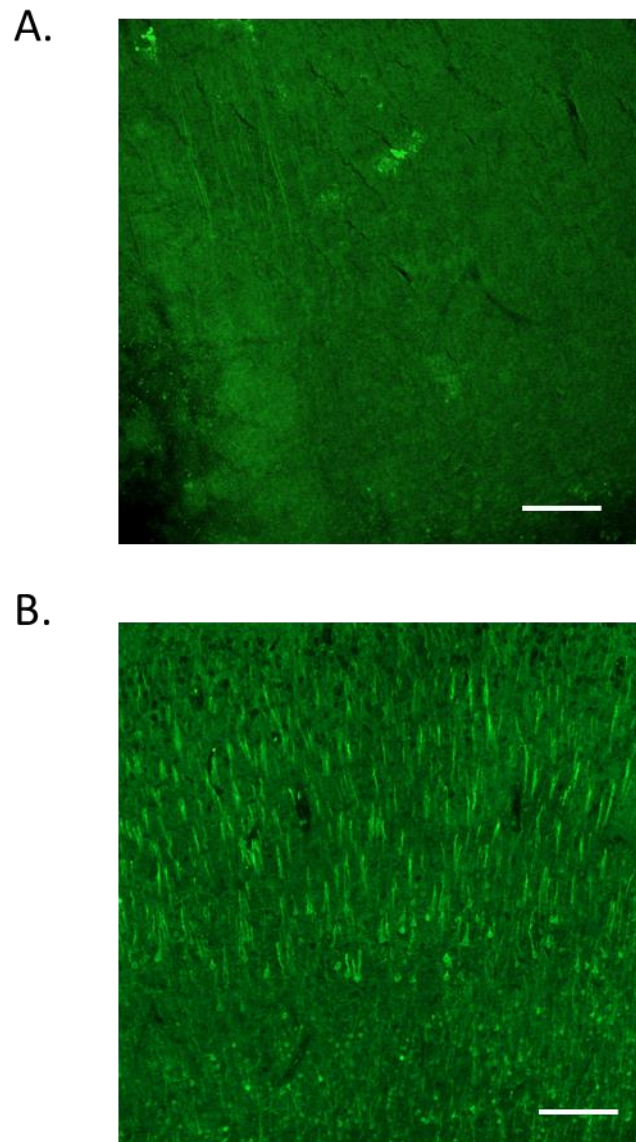
Figure 4.11. Example staining of tissue from dosing experiments compared to fresh tissue. A. Example of Arc staining in neocortical tissue processed after shipping from the USA (28 day treated vehicle). Scale bar is 200µm. B. Example of Arc staining in neocortical tissue collected and processed in the UK (control treated horizontal section). Scale bar is 200µm.

Chapter Five – The effect of *Leishmaniasis donovani* sleep- and wake-related oscillations.

5.1 Introduction

The previous chapter dealt with experimental models of systemic infection and, while revealing trends in oscillatory characteristics, lack of sufficient 'n' numbers and poor quality imported, matched tissue meant only suggestions of effects of neuroinflammation were possible. In this chapter, we switch to using a genuine pathogen to examine these suggestions further.

The parasitic disease, Leishmaniasis is a systemic disease, whereby protozoa of the Leishmania genus are transmitted to a host through the bite of an infected female phlebotomine sandfly (only females blood feed during egg production). The promastigote phase of the parasite has highly motility and travels in the host's bloodstream until engulfed by macrophages. The parasites then enter the amastigote phase and duplicate until they rupture the macrophage and are engulfed by others. In this way, the infection can spread around the body.

Some specific parasites stay close to the initial bite site and thus damage the cutaneous or mucocutaneous tissues causing cutaneous/mucocutaneous leishmaniases. The form of Leishmaniasis of interest in this thesis is the visceral form, which spreads around the body primarily affecting the liver and spleen but also invading other organs. Although visceral leishmaniasis classically presents with parasites infecting the visceral organs and bone marrow, viable Leishmania donovani (Melo et al., 2017) and L. infantum (Cardinot et al., 2016; Oliveira et al., 2017) parasites (responsible for VL infections) have been shown to infiltrate the brain. This is in tandem with increased leukocyte and macrophage presence in the brain tissue (Melo et al., 2017). These cell types could provide the route by which the intracellular parasite infiltrates the CNS, and the disruption of the blood-brain barrier secondary to systemic inflammation may aid the infiltration of these cells (Melo et al., 2015).

Visceral leishmaniasis is known to induce proinflammatory responses in the periphery, with increasing levels of pro-inflammatory cytokines such as IL-2 (Kaye, 1987) and TNF (Pinto et al., 2017), which stimulate T cells to release IFNγ and causes macrophage activation (Kaye et al., 1991) Leishmaniasis infection has also shown to upregulate proinflammatory cytokines in the CNS, such as IL-1β, IL-6, IFN- γ and TNFα (Melo et al., 2017). These proinflammatory changes engage microglia to phagocytose Leishmania parasites, whose presence is increased in tandem with T lymphocytes in ependymal areas of the brain, in correlation with T lymphocyte numbers (Melo and Machado, 2011). It has also been shown that microglia are better at dealing with Leishmania parasites than macrophages, showing higher levels of phagocytosis, and more

cytotoxicity to Leishmania parasites in vitro. This highlights the importance of microglia in the protection of the CNS tissues against Leishmania infection (Ramos et al., 2014)**.**

There is evidence that further to the neurological manifestation of Leishmania parasites neurological symptoms can develop. These include tremor, delirium, thought delusions (Chunge et al., 1985) and depression-like symptoms (Carswell, 1953; Maru, 1979). In mice, Leishmania infection increased anxiety behaviour and decreased locomotion (Portes et al., 2016)**.** Whilst neurological presentations and cognitive symptoms of leishmaniasis are uncommon, neuroinflammation is known to affect the oscillatory activity of the brain (Mamad et al., 2018). This may also occur secondary to leishmaniasis infection and may even have a knock-on effect on the normal plasticity-related mechanisms that occur in a healthy brain (Chapter 3).

5.1.2 Aims and objectives

This chapter aimed to use a mouse model of the Ethiopian form of visceral leishmaniasis (caused by Leishmania *donovani.)* to assess changes to sleep and wake state related oscillations in acute *in vitro* cortical slice preparations. Further to this, the effect of the real-life systemic infection (with potential for CNS infection involvement), on changes to synaptic plasticity across these brain rhythms (shown in Chapter 3) was investigated.

5.2 Results

5.2.1 Confirmation of parasitic infections

To investigate the effects of a real-world infection on the ability of brain slices to generate cortical oscillation *in vitro* we used Leishmaniasis infected mice and uninfected control mice. To ensure these mice were suitably infected, they were weighed prior to sacrifice. This showed that the total body weight of infected mice was significantly lower than that of naïve controls (*Figure 5.1A)* (naïve vs infected, mean total body weight, 31.84 ± 0.66 vs 27.67 ± 1.08 g, T-test, p = 0.009).

Further confirmation of infection came from the weight of the two organs primarily infected in leishmaniasis, the spleen and the liver. The weight of the spleen was significantly increased in infected mice compared to naïve control mice (*Figure 5.1B),* naïve vs infected, mean spleen weight, 0.08 ± 0.01 vs 0.71 ±0.04 g, T-test, p values < 0.001. The liver weight was similarly increased (naïve vs infected, mean liver weight, 2.36 ± 0.09 vs 1.47 ± 0.05 g, T-test, p values < 0.001). These difference were even more profound when the weight of the spleen or liver was taken as a percentage of the entire body weight (BW) *(Figure 5.1C)* (naïve vs infected, % BW, spleen: 2.57 ± 0.18 vs 0.26 ± 0.02 %, T-test, p values < 0.001, liver: 8.57 ± 0.30 vs 4.64 ± 0.20 %, T-test, p values < 0.001,).
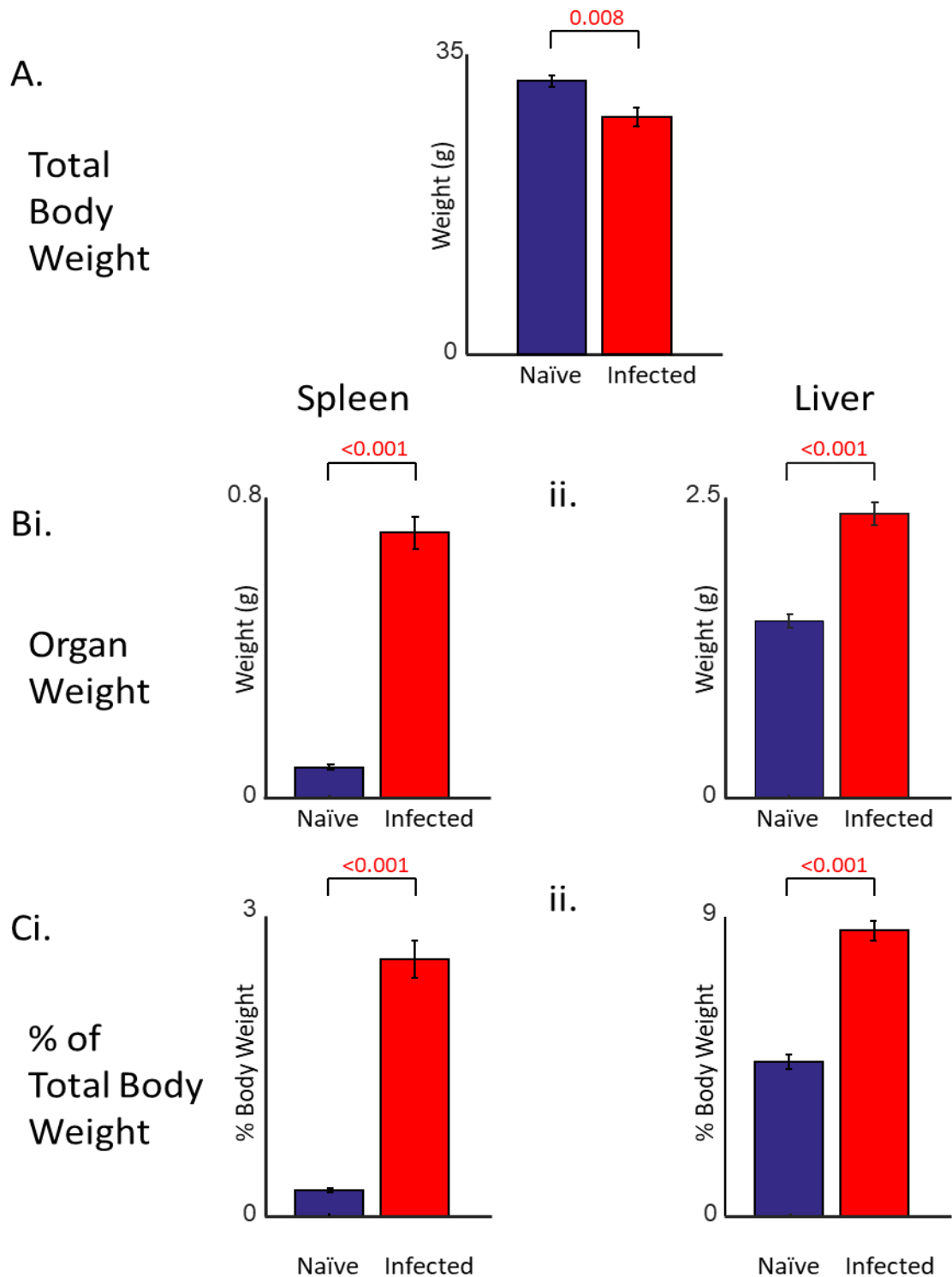
Figure 5.1. There are differences in total and single organ weights between naïve and Leishmaniasis infected animals. A. Mean total body weights in grams of naïve (blue, n = 6) and infected (red, n = 6) mice. Error bars show SEM. Displayed P value is from T-test. **Bi.** Mean weight of the spleens (in grams) of naïve (blue, n = 6) and infected (red, n = 6) mice. Error bars show SEM. Displayed P value is from T-test **ii.** Mean weight of the livers (in grams) of naïve (blue, n = 6) and infected (red, n = 6) mice. Error bars show SEM. Displayed P value is from T-test **Ci.** Mean percentage of the total body weight that is the spleen (in grams) of naïve (blue, n = 6) and infected (red, n = 6) mice. Error bars show SEM. Displayed P value is from T-test **ii.** Mean percentage of the total body weight that is the liver (in grams) of naïve (blue, n = 6) and infected (red, n = 6) mice. Error bars show SEM. Displayed P value is from T-test. Data collected by Najmeeyah Brown.
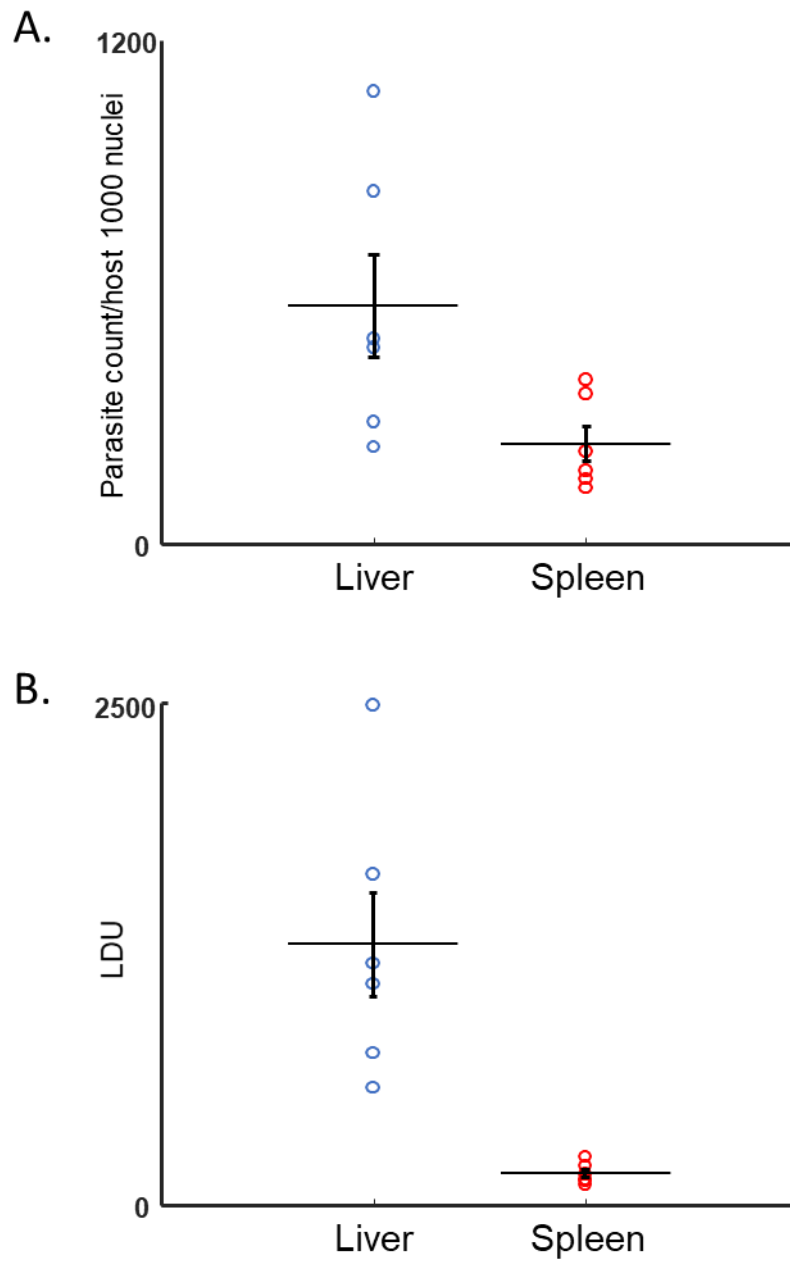
Figure 5.2. The parasite loads is higher in the liver than the spleen in mice infected with Leishmania donovani. A. Parasite counts in the liver (blue) and spleen (red) of leishmaniasis infected animals. Horizontal bars show mean, vertical error bars show SEM **B.** Parasite load of infected in the liver (blue) and spleen (red) in Leishman-Donovan units Horizontal bars show mean, vertical error bars show SEM. Data was collected by Najmeeyah Brown.

To get a better picture of the infection rates in each mouse, parasite counts were undertaken. Again, the liver and spleen were used, and counts of parasites/1000 host nuclei *(Figure 5.2)* (liver vs spleen, parasite count/1000 host nuclei, liver: 568.5 ± 134.5 vs 240 ± 44.9, parasite counts for naïve controls were zero). To normalise these count numbers to the size of the organ, the parasite count was multiplied by the organ's weight (liver vs spleen, LDU, liver: 1298.8 ± 281.6 vs 161.1 ± 21.5, LDUs for naïve controls were zero).

<u>5.2.2 Effect of Leishmaniasis infection on cortical oscillations</u>

Having confirmed that the mice were indeed infected, *in vitro* brain slice preparations were made and the effect of the Leishmaniasis infection on the ability to generate sleep and wake-related rhythms in these slices was investigated.

Bath application of 400nM KA was used to generate cortical gamma oscillations. The mean area power of the gamma oscillation was lower in animals that were infected with leishmaniasis, although this was not significant for Au1 or S2 *(Figure 5.3)* (Naïve vs. Infected, Au1: 218.8 ± 46.9 vs. 97.4 ± 29.0 µV², T-test, p-value = 0.052, S2: 223.9 ± 29.4 vs 123.1 ± 39.1 µV², T-test, p-value = 0.066). Peak power was similarly lower, but to a significant level in S2 (Naïve vs. Infected, Au1: 7.4 ± 2.9 vs. 2.6 ± 0.5 µV²/Hz, T-test, p-value = 0.136, S2: 6.5 ± 1.1 vs 2.9 ± 0.9 µV²Hz, T-test, p-value = 0.026). There was no change to the frequency of the cortical gamma rhythm in infected animals in either Au1 or S2 (Naïve vs. Infected, Au1: 35.2 ± 1.5 vs. 36.4 ± 1.7 Hz, S2: 35.8 ± 1.9 vs 37.1 ± 1.4 Hz).

Delta oscillations generated by the bath application of 4µM CCH 10µM SCH23990 were also investigated. The generation of rhythms of delta frequency 0.5– 4 Hz did not change after leishmaniasis infection in either S1 or S2 *(Figure 5.4)* (Naïve vs. Infected, Area Power, S1: 4599.4 ± 2563.0 vs. 2512.7 ± 820.8 µV², S2: 3608.23 ± 1684.9 vs. 2109.9 ± 472.0 µV², Peak Power, S1: 294.3 ± 157.4 vs. 216.6 ± 86.6 µV²/Hz, S2: 372.0 ± 156.9 vs. 246.8 ± 87.34 µV²/Hz, Peak Frequency, S1: 1.01 ± 0.13 vs. 0.94 ± 0.10 Hz, S2: 0.92 ± 0.06 vs. 1.05 ± 0.08Hz).
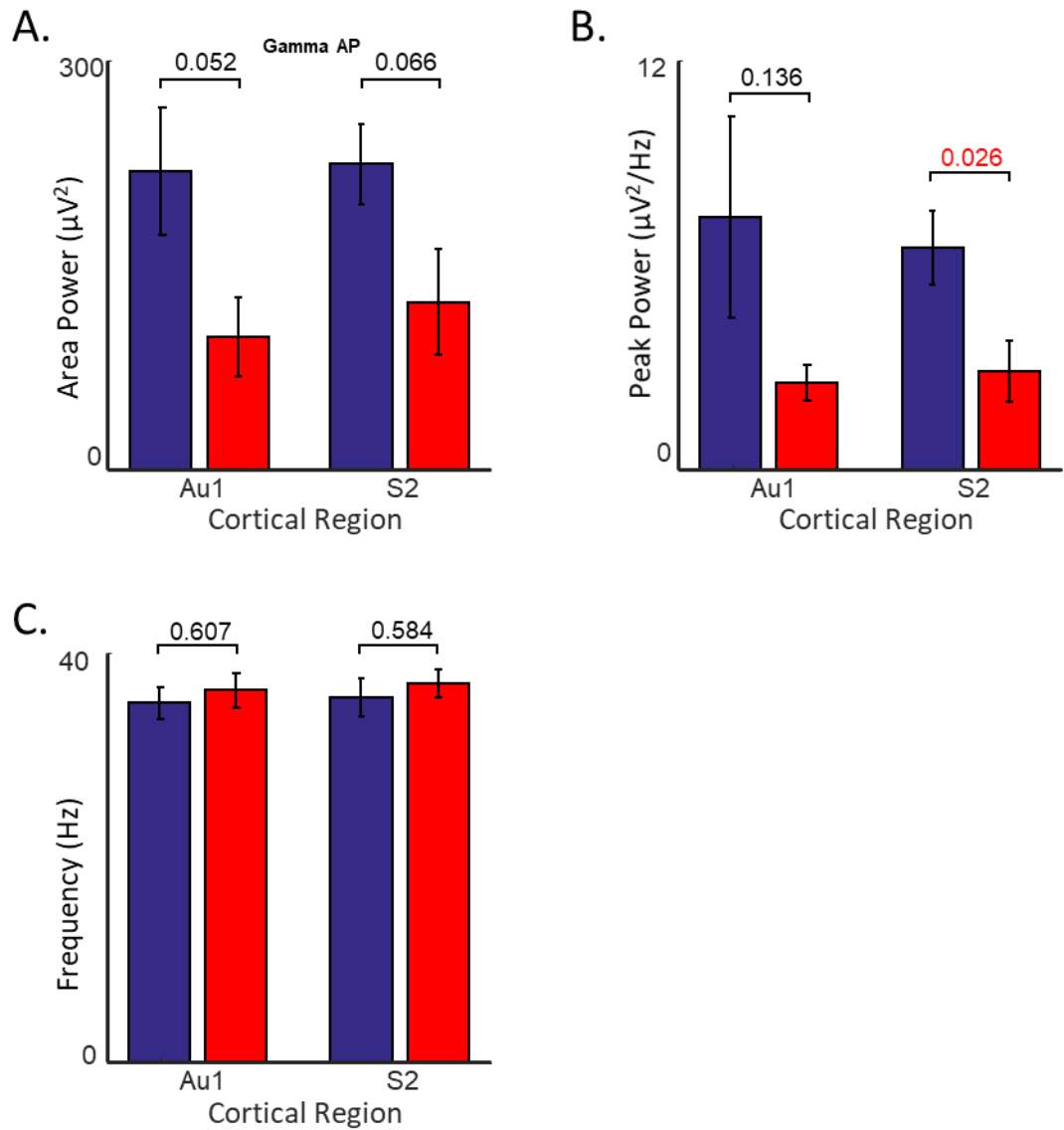
Figure 5.3 Gamma oscillations are decreased in frequency in the neocortical slices from leishmaniasis infected mice. A. Mean area power between 30 and 40Hz in naïve (blue, n=6) and leishmaniasis infected mice (red, n=6). Error bars show SEM. **B.** The mean peak power between 30 and 40Hz in naïve (blue, n=6) and leishmaniasis infected mice (red, n=6). Error bars show SEM. **C.** The mean frequency of the highest powered peak between 30 and 40Hz in naïve (blue, n=6) and leishmaniasis infected mice (red, n=6). Error bars show SEM.
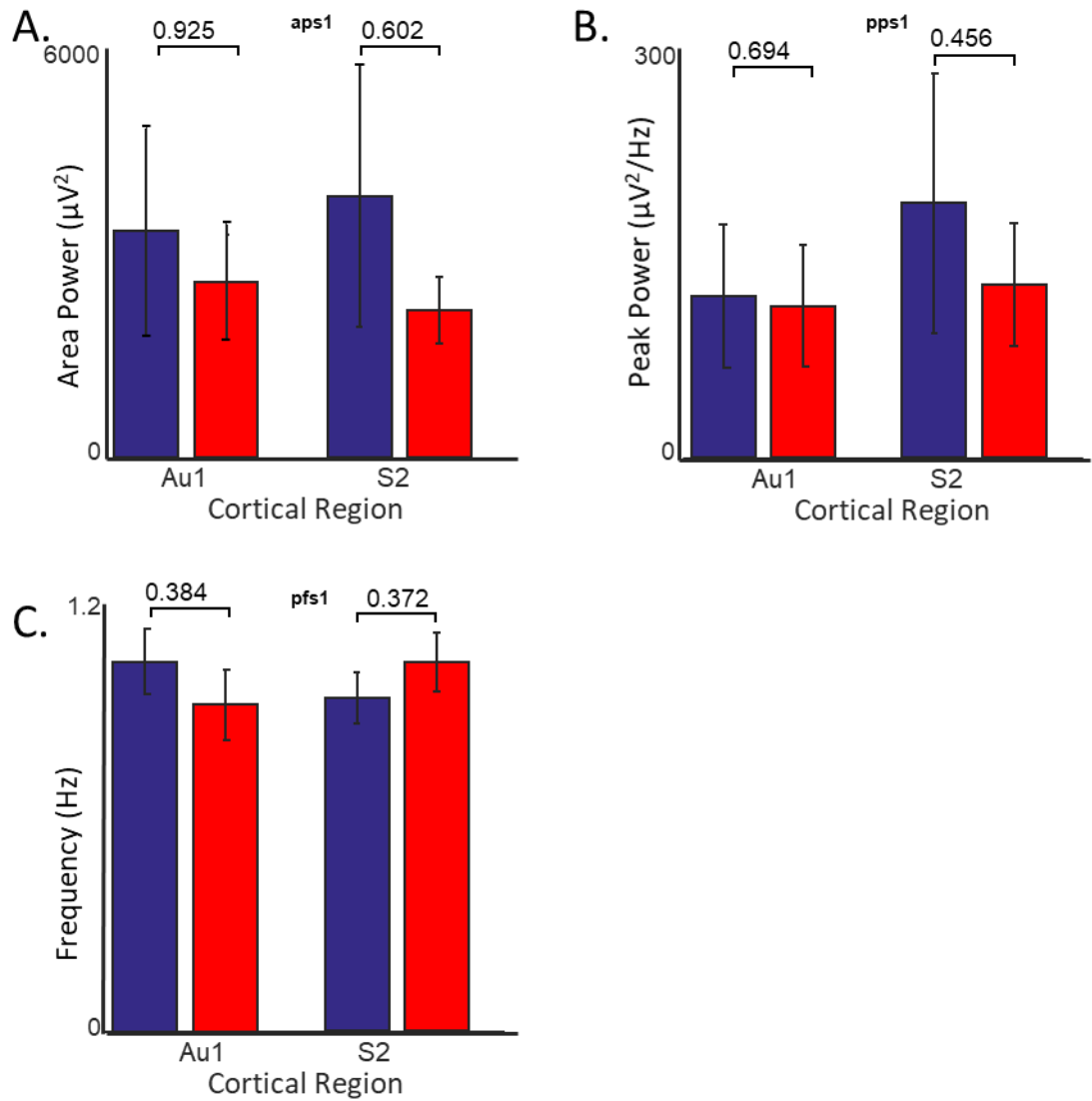
Figure 5.4 Delta oscillations are unchanged in neocortical slices from leishmaniasis infected mice. A. Mean area power between 0.5 and 4Hz in naïve (blue, n=6) and leishmaniasis infected mice (red, n=6). Error bars show SEM. **B.** The mean peak power between 0.5 and 4Hz in naïve (blue, n=6) and leishmaniasis infected mice (red, n=6). Error bars show SEM. **C.** The mean frequency of the highest powered peak between 0.5 and 4Hz in naïve (blue, n=6) and leishmaniasis infected mice (red, n=6). Error bars show SEM.

5.2.3 Effect of Leishmaniasis infection and oscillation on Arc in dendrites

Finally, to assess whether a systemic infection induced by a biological pathogen can cause changes to the environment of plasticity in the brain, slices used in the experiments above were processed and stained for Arc. The dendritic Arc signal was then analysed. We only analysed Arc as this was the one plasticity marker which was shown to significantly change between sleep and wake-related rhythms.

The largest mean changes in laminar expression of Arc in dendrites in naïve mice was during delta rhythms (compared to gamma rhythms) in primary and secondary cortical regions. Despite large differences in the means there was no significant difference *(Figure 5.5)* (1ry, 254.8µm, Naive Delta vs. Gamma: 60.2 ± 12.8 vs. 16.6 ± 4.5, T-test, p = 0.013, with FDR, q = 0.400; 2ry, 55.8 µm, Naive Delta vs. Gamma: 35.0 ± 17.7 vs. 2.2 ± 1.4, T-test, p = 0.101, with FDR q = 0.193). The non-significant increases during delta in superficial layers were conserved in Leishmaniasis infected slices however the effect was still not significant even where the difference was the largest (1ry, 213.9µm, Infected Delta vs. Gamma: 62.9 ± 17.3 vs. 11.3 ± 5.7, T-test, p = 0.022, with FDR, q = 0.358; 2ry, 229.8µm, Naive Delta vs. Gamma: 58.5 ± 14.2 vs. 25.2 ± 8.0, T-test, p = 0.076, with FDR q = 0.502).

When comparing the profile of dendritic Arc during delta rhythms in slices from naïve and infected mice there was no difference *(Figure 5.6)* (S1, 159.3µm, Delta, Naïve vs. Infected: 18.5 ± 7.1 vs. 50.5 ± 16.6, T-test, p = 0.115, with FDR q = 0.872: S2, 82.6, Delta, Naïve vs. Infected: 37.0 ± 11.0 vs. 25.9 ± 10.8, T-test, p = 0.49, with FDR, q = 0.912). The leishmaniasis infection also had no overall effect on dendritic Arc expression during gamma oscillations, though individual significances were found at some cortical depths: Au1, 463.5µm, Gamma, Naïve vs. Infected: 41.4 ± 5.0 vs. 16.9 ± 5.7, T-test, p = 0.012, with FDR, q = 0.999, S2: 528.15µm, Gamma, Naïve vs. Infected: 40.5 ± 5.1 vs. 14.1 ± 4.1, T-test, p = 0.004, with FDR, q = 0.270.
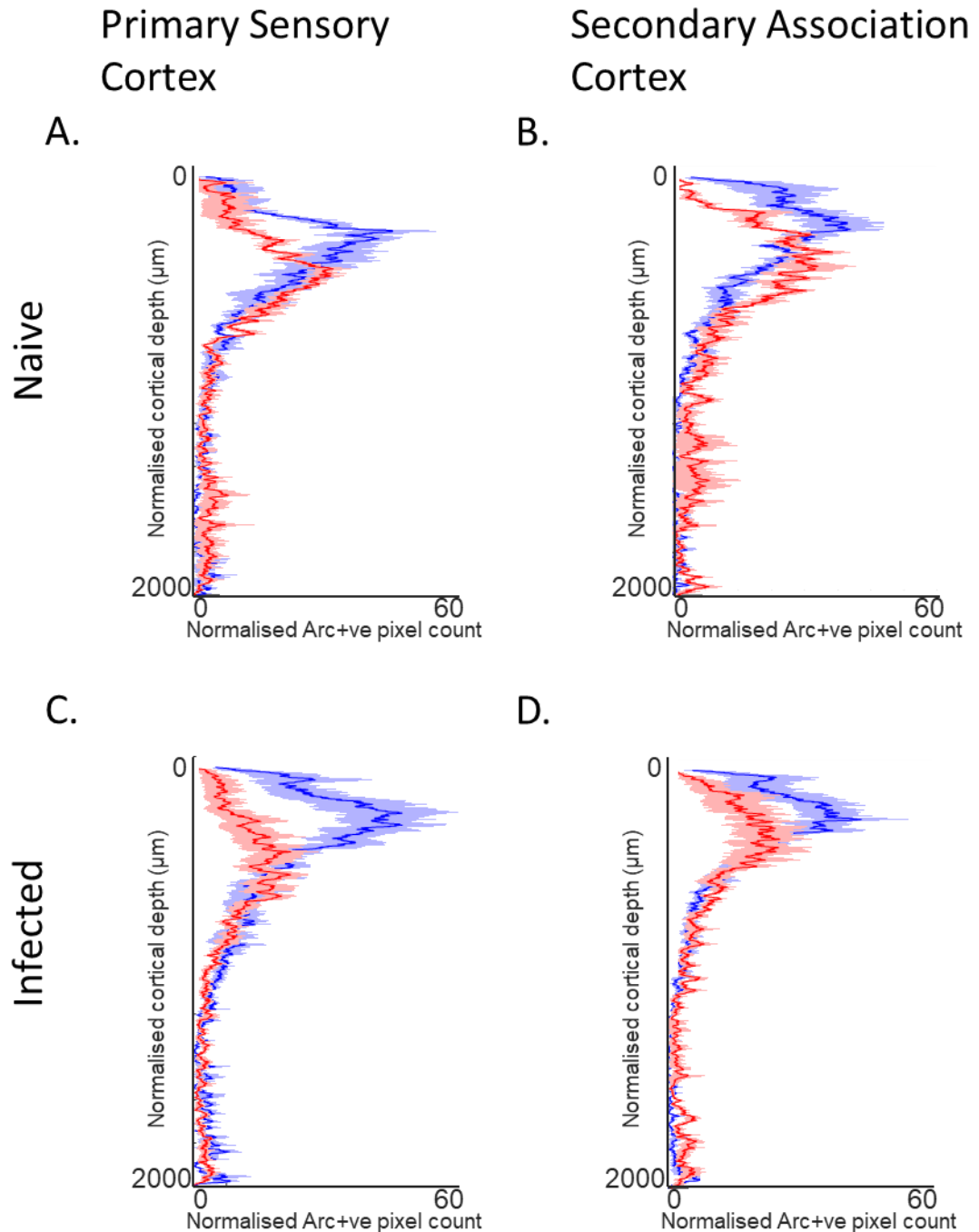
Figure 5.5 The laminar distribution of dendritic Arc expression does not change during different brain rhythms, in control and Leishmaniasis infected mice. A – The distribution of Arc in dendrites from pia (0) to subcortical white matter (1950) in primary sensory cortex of naïve mice during delta oscillations (Blue, n=5) and gamma oscillations (Red, n=5). Error shown is SEM. **B –** The distribution of Arc in dendrites from pia (0) to subcortical white matter (1950) in secondary sensory cortex of naïve mice during delta oscillations (Blue, n=5) and gamma oscillations (Red, n=5). Error shown is SEM. **C –** The distribution of Arc in dendrites from pia (0) to subcortical white matter (1950) in primary sensory cortex of Leishmaniasis infected mice during delta oscillations (Blue, n=5) and gamma oscillations (Red, n=5). Error shown is SEM. **D –** The distribution of Arc in dendrites from pia (0) to subcortical white matter (1950) in secondary sensory cortex of Leishmaniasis infected mice during delta oscillations (Blue, n=5) and gamma oscillations (Red, n=5). Error shown is SEM.

Figure 5.6 The laminar distribution of dendritic Arc expression does not change due to infection, during different brain rhtyhms in control and Leishmaniasis infected mice. A – The distribution of Arc in dendrites from pia (0) to subcortical white matter (1950) in S1 during delta oscillations in naïve mice (Blue, n=5) and Leishmaniasis infected mice (Red, n=5). Error shown is SEM. **B –** The distribution of Arc in dendrites from pia (0) to subcortical white matter (1950) in S2 during delta oscillations in naïve mice (Blue, n=5) and Leishmaniasis infected mice (Red, n=5). Error shown is SEM. **C –** The distribution of Arc in dendrites from pia (0) to subcortical white matter (1950) in Au1 during gamma oscillations in naïve mice (Blue, n=5) and Leishmaniasis infected mice (Red, n=5). Error shown is SEM. **D –** The distribution of Arc in dendrites from pia (0) to subcortical white matter (1950) in S2 during gamma oscillations in naïve mice (Blue, n=5) and Leishmaniasis infected mice (Red, n=5). Error shown is SEM.

5.3 Discussion

5.3.1 Summary

In this chapter, the effect of a biological pathogen on *in vitro* models of certain brain rhythms has been investigated. The pathogen used was the parasite Leishmania *donovani,* which causes visceral leishmaniasis and is known to elicit systemic inflammation. The effect of this infection on synaptic plasticity in the neocortex of mice was also explored.

The summary of key findings from this investigation are:

- The injection of Leishmania *donovani* parasites into the tail vein successfully led to an infection in mice that had the characteristics of visceral leishmaniasis and lasted for at least 28 days.

- There was a decrease in the peak power of cortical gamma oscillations in the secondary somatosensory cortex in mice infected with L. *donovani.*

- There was no significant change to delta oscillation dynamics in L. *donovani* infected mice compared to naïve mice.

- There was no significant difference in dendritic Arc expression between brain slices in naïve mice exhibiting gamma or delta oscillations, or between these oscillations in infected mice.

- The Leishmaniasis infection caused no significant difference in dendritic Arc staining during either gamma or delta oscillations, compared to control.

5.3.2. Leishmania *donovani.* IV injection causes visceral leishmaniasis in mice.

After the intravenous injection of Leishmania *donovani* parasites, mice displayed many signs that were consistent with visceral leishmaniasis presentation in humans. Firstly, the mice exhibited weight loss, a symptom typical of visceral leishmaniasis in humans (Araujo Lima Verde et al., 2011). Unusually in humans, this symptom occurs despite no loss of appetite.

The two organs known to be most affected by experimental are the spleen and the liver (Berman, 1997; Polley et al., 2005; Melo, 2017). The weights of the spleen and liver were tested in infected and naïve mice and both organs were found to be significantly increased in weight compared to control. This is consistent with the human disease, with splenomegaly and hepatomegaly being common pathologies in the disease (Melchionda et al., 2014). In patients with visceral leishmaniasis, parasites are seen in Kupffer cells leading to their hyperplasia, as well as the 'ballooning' degeneration of hepatocytes. There is also an increase in parasite-

infected macrophages (el Hag et al., 1994). The hypertrophy of the spleen is known to be due to the build-up of histiocytes, macrophages and plasma cells. Parasite counts showed that infection in the liver was more pronounced than in the spleen, especially when the weight of the organ was taken into consideration when calculating the LDU index. Although the LDU index is suggested to be less sensitive than qPCR methods in quantifying parasite load (Moreira et al., 2012), the presence of the Leishmania parasites in these organs could be reliably confirmed compared to uninfected naïve mice. As well as increased parasite load, studies have also shown that the inflammatory response to leishmaniasis infection is stronger in the liver than the spleen with the upregulation of IL-1β and TNFα in the liver exceeding and preceding enhanced expression by the spleen (Melo et al., 2013). Although we did not test serum or tissues for inflammatory markers, it is likely that pro-inflammatory cytokines are also upregulated in our models as has been shown by previous studies (Melo et al., 2017; Grano et al., 2018). To confirm this to be the case, an analysis of cerebral cytokines or microglial activation would show the inflammatory environment of the brains of these mice after Leishmaniasis infection.

5.3.3. Leishmaniasis infection impacts only gamma oscillations in the neocortex.

In assessing changes to the oscillatory activity in brain slices from naïve and L. *donovani* infected animals, the mean peak power of somatosensory gamma rhythms was significantly reduced. This change was partially reflected in the primary sensory cortex and decreases in mean area power were also seen in both regions, however these changes did not reach significance. The presence of oscillatory changes in the brain in these mice is indicative of a central neurological element to visceral leishmaniasis. This neurological alteration may have been due to neuroinflammation secondary to the peripheral infection (as shown in Chapter 4). This is corroborated by previous evidence that shows increases in proinflammatory cytokines in the brain (IL-1β, IL-6, IFN- γ, TNFα) in experimental leishmaniasis models (Melo et al., 2017) as well as leukocyte infiltration of the BBB (Melo et al., 2009), both of which are classic signs neuroinflammation. However, there have been reports of small numbers of parasites invading the CNS tissue of naturally and experimentally infected dogs, suggesting that some degree of primary activation of neuroinflammatory pathways may also occur (Nieto et al., 1996; Vinuelas et al., 2001; Tafuri et al., 2004). The number of CNS infiltrates are very small though, so if it is an inflammatory response leading to these oscillatory changes, it is more likely to be due to the propagation of the systemic immune response and this mode of cytokine production is a common feature of the disease (Pinto et al., 2017) (Kaye et al., 1991).

Gamma power decreases have previously been reported in the neocortex under neuroinflammatory conditions. The injection of the inflammatory cytokine IL-1β, into the striatum of rats, led to a decrease in the power of the stimulus-evoked gamma oscillations in the barrel cortex (Bray et al., 2016). Changes to oscillatory activity have also been recognised after systemic cytokine administration (Hansen and Krueger, 1997; Kubota et al., 2001; Yoshida et al., 2004), though the changes shown in these studies were largely associated with alterations in rhythmic activity in the delta frequency range. Unusually, there was no change in delta activity when comparing slices from infected and naïve mice in this thesis. This is surprising as changes to delta frequency rhythms are more often associated with neuroinflammation (Parsons et al., 1997; Opp and Toth, 1998; Mamad et al., 2018), and see *Chapter 4.*

Cytokine-driven changes to the gamma oscillations may occur through the activity of NMDA receptors. NMDA has been implicated in controlling the power of gamma oscillations with the blockage of the NMDA receptor increasing gamma power (Hakami et al., 2009). IL-1β is known to enhance NMDA receptor activity through (Viviani et al., 2003) the action of tyrosine kinases to increase intracellular calcium and through this mechanism may decrease the power of gamma oscillations (Debray et al., 1997). Interleukin 1β is known to be produced by macrophages and monocytes during Leishmaniasis infection (Sani et al., 2014) (Santos et al., 2018). If the systemic upregulation of this pro-inflammatory signal reaches the brain it may cause the changes to gamma oscillations seen through the activity of IL-1β. To test this theory, the expression of IL-1β in the brain could be analysed after infection.

5.3.4. No change occurs in dendritic Arc expression by brain rhythm or infection in mice.

Because only dendritic Arc expression showed any significant difference in rhythm-related expression in Chapter 3 of this thesis, only the expression of Arc in dendrites was analysed in the *L. donovani* infected mice. Firstly, to establish whether the phenomenon discovered in rats previously in this thesis is conserved in mice, the dendritic Arc expression during delta and gamma rhythms was compared to naive mice. Despite a visible increase in dendritic Arc in superficial layers in mice and non-overlapping error bars, there was no significant change in the dendritic Arc expression between rhythms in healthy mice. The trend of an increase would appear to corroborate the results found in Chapter 3 albeit to a non-significant level.

The visible increase in superficial dendritic Arc during delta rhythms is conserved in leishmaniasis infected mice, yet this difference was also not significant, despite appearing larger in infected

animals – especially in the primary sensory cortex. The lack of significance in the laminar expression of Arc is surprising due to the small error bars in the data. Indeed, some significant changes were seen in individual sub-laminae. However, the consideration of multiple comparisons by calculation of the false detection rate led to the rejection of these changes as significant when considering the overall expression profile. The effect of the presence of the systemic leishmaniasis infection on rhythm-related Arc expression was also assessed. No significant difference was seen in Arc signalling between naive and infected mice in either area of the cortex during either rhythm. This suggests that the compromised power of the gamma oscillation has no effect on the overall plasticity mechanism in dendrites of these cells.

The lack of change to dendritic Arc signalling in response to oscillatory state or infection suggests that the changing landscape of synaptic plasticity is of lower magnitude in the neocortex of mice than in rat between wakefulness and SWS. Although there is species difference between these studies (this chapter and Chapter 3) the mechanisms for oscillation generation are largely conserved (Buzsaki and Wang, 2012; Beltramo et al., 2013). However, a decreased propensity for plasticity in layer V neurons has been seen between species, related to a decreased ratio of layer V IB cells to RS cells in mice compared to rats (Jacob et al., 2012). Since our previous findings have been related to the expression of Arc in these diminished number of IB cells this suggests that this disparity between species may account for the non-significance of the changes.

5.3.5. Experimental limitations

Due to regulatory restrictions, availability and precedence in the literature, mice (as opposed to rats) were used to model visceral leishmaniasis. This added an element of complexity as the *in vitro* models of oscillations used had been established in rats rather than mice (Ainsworth et al., 2011; Carracedo et al., 2013). Indeed, the concentrations of oscillating generating drugs - kainate (400nM) for gamma rhythms and carbachol (4μm) and SCH23390 (10μm) for delta rhythms - were optimised in rats only. These concentrations have been optimised for generating the most robust oscillation possible in particular regions of rat brains. Whilst the regions chose from mice experiments were the same, the optimal drug concentrations to generate the most robust oscillations may be different. Whilst these concentrations are indeed successful at generating gamma and delta oscillations respectively in mice, to generate the most robust oscillation possible in mice would require an additional survey of dose response.

This species difference between this chapter and Chapter 3 may account for the lack of change in dendritic Arc signalling both between rhythms and as a result of infection. As mentioned above, the lower percentage of intrinsically bursting cells in layer V in mice may account for the disparity in Arc changes compared to rats.

Chapter Six – General Discussion and Future Directions

6.1 Overview

Sleep has been an area of great mystery to neuroscience for centuries. Through decades of research, immediate early genes have emerged as an interesting target of research concerning their important roles in neuronal activity (c-Fos) and plasticity (Arc). This has led to findings that recognise changes to IEG levels across the sleep-wake cycle. Earlier studies into these immediate early genes took crude samples of brains of awake and sleeping animals and noticed profound changes (Cirelli and Tononi, 1999; Cirelli and Tononi, 2000b). More recently, research has involved more regionally specific surveys and relationships between brain states and memory (Ribeiro et al., 1999; Hanlon et al., 2009).

Still, many of the studies into gene expression changes during the sleep-wake cycle are *in vivo,* and claims relating them specific brain rhythms have mostly been correlative rather than mechanistic. These studies have been informative, though, and it is from them that the synaptic homeostasis hypothesis (SHY) was developed. However, the mechanisms through which the downscaling of synaptic strength occurs during sleep (as the SHY theorises) are still being explored, mainly in attempts to reconcile the seemingly contradictory nature of decreased synaptic strength correlating with increased memory performance (consolidation) – something that currently stands opposed to the long-standing synaptic weight doctrine for learning and recall (Bliss and Collingridge, 1993). One potentially critical factor here may be temporal: understanding how specific network activities, distributed over time in the form of brain rhythms, might pinpoint causative changes in engrams linked to the observed immediate early gene and AMPA receptor number changes.

With this in mind, this thesis attempted to relate changes in c-Fos and Arc to specific sleep- and wake-related brain rhythms using previously characterised, pharmacologically induced *in vitro* models. Cortical gamma and delta oscillation models were compared due to their known importance in the formation and consolidation of memories respectively. Once gross regional changes had been discovered, investigations were carried out to localise the source of the changes on a laminar, cellular, and sub-cellular level. These changes could then reciprocally inform studies into the changes that occur to these cortical rhythms upon the induction of neuroinflammation – an insult known to have profound effects on memory - either by models of immune challenge or with a biological pathological infection.

6.2.1 Plasticity-related gene changes in cortical oscillation models

The initial investigation compared regional changes in immediate early gene expression during *in vitro* delta and gamma rhythms. Whilst the general decrease in Arc levels during sleep-related rhythms was broadly in line with changes seen in previous studies (Cirelli and Tononi, 2000a), the increase in c-Fos opposed previous findings (Pompeiano et al., 1995; Hanlon et al., 2009). This opposition may be due to the mismatch between what is defined as sleep and wake, compared to specific network activities (gamma and delta rhythms). These in vivo studies could not separate SWS from REM sleep whereas the current study looked solely at SWS. In addition, the results may also have been complicated by extracellular and non-neuronal staining – a clear dichotomy was seen, for example, between gross Arc levels (Figure 3.1) and the specific expression in IB neuronal apical dendrites (Figures 3.11, 3.12) (see below).

To hone in further on the cells responsible for these changes, the distribution of c-Fos and Arc stained neuron and interneuron somata was analysed. In principal cell and interneuron somata, whilst expression of c-Fos and Arc was apparent, there were no changes seen in either IEG in response to the two oscillation models. What was observed, however, was an abundance of Arc stained dendrites, or sections of dendrites particularly in layer II/III of the cortex. Examination of this dendritic staining and comparison between rhythms highlighted a phenomenon whereby the generation of delta rhythms in secondary- and particularly primary- sensory cortex increases this dendritic Arc staining above that seen during gamma oscillations. As Arc increases are linked to changes in many types of synaptic plasticity (both in potentiation and depression), it would suggest that the majority of the synaptic alterations in the cortex occur in dendrites, during slow wave sleep. This plasticity is likely to be in the weakening of synaptic connections as LTD is known to be the dominating mechanism change during sleep (Tononi and Cirelli, 2003; Shepherd, 2012). The mechanism through which Arc is known to induce synaptic depression is through AMPA receptor internalisation (Chowdhury et al., 2006), which is upregulated during SWS and implicated in synaptic scaling (Diering et al., 2017).

Intracellular experiments identified the specific cell type in which this dendritic Arc change occurred as the layer V intrinsically bursting cell (IB). The layer II/III localisation of the dendritic signal in these IBs corresponds with calcium spike initiation zones, which are important for mediating Ca^{2+} entry to pyramidal cells (Perez-Garci et al., 2013). This Ca^{2+} influx is increased by the burst firing of pyramidal cells during delta oscillations and aids in AMPA receptor

internalisation through inhibition of the anchorage of the receptor to the postsynaptic membrane (Chowdhury et al., 2018).

Further to localising the major synaptic changes related to synaptic scaling during SWS in the cortex, a spatial arrangement in the contributing IB cells was found. This showed that not only was synaptic plasticity increased in bundles of IB dendrites, but these dendrites also work as a unit with other cells and their arrangement in a hexagonal pattern may facilitate this coordination (Maruoka et al., 2017). Thus slow wave sleep appears to associate with an enhanced state of excitatory synaptic plasticity in modules of neocortical cells known to be vital for both the generation of SWS itself and for linking neocortical activity to multiple subcortical structures (Groh et al., 2010; Kim et al., 2015).

6.3.1 The effect of neuroinflammation on cortical oscillations models.

Following the findings of the relationship between Arc mediated plasticity and cortical oscillation mode, further investigations were carried out to determine if perturbation in oscillatory dynamics occurred after neuroinflammation and whether this was related to changes in impaired or altered plasticity. Studies that investigate biological changes to pathogen-related inflammation (in the brain or otherwise) often use LPS to mimic a bacterial infection through its activation of TLR4 receptors (Lund et al., 2006).

We first saw no immediate effects of LPS on stable cortical oscillations. There are many possibilities for this lack of effect. It is known that whilst peripheral sensory neurons express TLR4 receptors (Leow-Dyke et al., 2012), cortical neurons do not (Lehnardt et al., 2003). This being the case, it is unlikely that triggering signalling pathways in other (TLR4 +ve) cell types would directly affect neuronal excitability at the timescale measured. In fact the timescale for induction of inflammatory cytokines known to cause changes to oscillatory dynamics is longer than the time tested (Wang et al., 2015a).

Following this and with increasing awareness of the implications of systemic infection for neurodegenerative diseases (Perry et al., 2003), a dosing study was set up to assess the effects of systemic infection on the inflammatory environment in the brain and monitor the resulting oscillatory changes. It was also hoped that dosing with either LPS or poly I:C (an agent that mimics viral DNA, and ligand for TLR3 receptors) would allow the comparison of bacterial and viral infection changes. The chosen dosing schedule allowed the comparison of acute and

chronic inflammatory conditions by the recording of oscillations 24 hours after a single dose of LPS or after doses every 3 days for 7 or 28 days. Since the doses used were relatively low, it allowed the build-up of chronic inflammation, which meant that no change was seen after 24 hours. This lack of change may also have been because the conclusion of the first 'wave' of inflammation occurs less than 24 hours after dosing (Mamad et al., 2018).

The longer timescale of infection was sufficient to induce oscillatory changes, significantly in the frequency of hippocampal gamma oscillations and cortical delta rhythms. These changes were thought to be related to deficits in cognitive function (Britton et al., 2016) and specifically sensory/memory processing (Jahn, 2013).

Beyond these frequency changes, other differences in the oscillatory activity were apparent, however due to low n numbers, these were not found to be significant. The bidirectional trend towards changes in delta rhythms suggested changes in sleep-need depending on the nature of neuroinflammation present. Shorter-term dosing increases are likely to be related to changes in the brain after infection or TBI leading to delirium (Parsons et al., 1997) (Koponen et al., 1989), and may also be related to increased sleep need (Vyazovskiy et al., 2011). The trend towards a decrease seen over the longer term (28 days here) may be due to more serious changes in the cortical networks supporting these rhythms and could even be a result of neuronal cell death (Pevzner et al., 2016). This may also underlie the trend in decrease of the hippocampal slow gamma rhythms, which is a dysfunction seen in Alzheimer's disease. These oscillatory changes could also be linked to changes in the neuroinflammatory state with mostly just 'classic' proinflammatory cytokines upregulated after 28-day dosing, whereas after 7 days a balance between pro- and anti-inflammatory cytokines and chemokines was seen. This was reflected in the proven capability of 28 days dosing with inflammatory agents to change microglia morphology to their active, pro-inflammatory state. It was hoped that these changes could also be related to changes in plasticity mechanism, but due to available tissue integrity problems, this analysis was not possible during the time course of this thesis.

6.4 The effect of visceral leishmaniasis on cortical oscillations and plasticity.

Neuroinflammation is prevalent in many biological diseases, and is a growing area of research, particularly in neurodegenerative diseases. A mouse model of visceral leishmaniasis was used to assess the effects of neuroinflammation in biological disease. There is only sparse evidence of an association between this disease and neurological defects, particularly related to the CNS.

However, leishmaniasis is linked with large amounts of systemic inflammation and there is also evidence of upregulation of neuroinflammatory cytokines in the brain. The infection was incubated for 28 days (similar to the last time point described above) before experiments were carried out.

In line with features of the infection in humans and animals, mice showed decreased body weight, despite increases in the size of the spleen and the liver. These visceral changes were related to increased parasite loads in the liver and the spleen, with the former showing a higher parasite load.

Changes in the power of cortical gamma oscillations were observed when the characteristics of sleep and wake-related oscillations were compared in infected mice. These changes are likely to be related to neuroinflammatory effects because inflammatory cytokines have been shown to change cortical oscillation dynamics through interactions the NMDA receptors (Bray et al., 2016). These changes were not matched with any aberration in delta rhythm activity, which is unusual as the delta rhythm is more susceptible to alterations rising from neuroinflammation. However, this lack of change may be due to the lack of refinement of the *in vitro* delta rhythm in mice.

Finally, the dendritic distribution of Arc was compared, firstly in different rhythms in control mice, and then between control and infected mice. The non-significant change in Arc in dendrites in control mice may indicate that the phenomenon evaluated in Chapter 1 can be conserved in mice, albeit to a lesser extent. Additionally, it was found that infection, despite causing changes to cortical gamma oscillatory dynamics had no effect on the levels of plasticity in cortical dendrites. The importance of the delta rhythm in plasticity was highlighted, so the fact that the change to oscillatory dynamics in infected mice was to gamma rhythms may show that these have a lesser impact on affecting synaptic changes in cortical neurons.

6.5 Overview

In conclusion, this thesis shows that delta rhythms that occur during SWS induce more plasticity compared to wake-related gamma rhythms, through the induction of the IEG Arc. This occurred predominantly in layer V intrinsically bursts cells and may lead to the scaling of their synaptic connections in order to maintain synaptic homeostasis, consolidate network representations of memory and/or simply provide a feedback signal to set the duration of SWS. These changes occur in hexagonally organised bundles of dendrites, which are multicellular units that process

information together and broadcast it principally to subcortical structures. Inducing systemic infection, either by agents mimicking bacterial or viral infection or by infection with a biological pathogen, caused subtle changes to the dynamics of the observed cortical oscillations. These oscillatory changes are likely to be due to an inflammatory response in the brain, propagated from the systemic immune response. Changes to these rhythms, however, do not seem to have any overt effect on plasticity-related Arc expression in the neocortex.

6.6 Future directions

6.6.1 Further investigation of synaptic changes during in vitro slice oscillations

The main finding in the first chapter of this thesis is with regards to the immunofluorescent staining of Arc. It is important to note that Arc staining is only representative of changing synaptic strength and does not necessarily imply a direction. Indeed Arc has been shown to be increased during both synaptic potentiation and depression. Although it is likely that the increase in Arc found in the basal dendrites of layer V IB cells synaptic scaling further experiments would be necessary to confirm this. Synaptic scaling involves long term depression and therefore intracellular electrophysiological experiments would be require to confirm decreased synaptic strength. The underlying mechanism could also be further explored using immunohistochemistry.

Intracellular recordings of layer V intrinsically bursting cells before and during the induction of delta and gamma oscillations would allow for the comparison of EPSPs and EPSCs in terms of amplitude or time course. These recordings could be taken naturally during the oscillations, or as part of a stimulus response curves after oscillatory activity. This would be done by recording from IB cells and stimulating presynaptic neurons with increasing voltages. Currently changes to these parameters have already been shown in layer V cells after evoked bursting activity (Czarnecki et al., 2007). These experiments may require recordings to be made from the apical dendrite at layer II/III which adds a level of complexity due to the small size compared to the cell soma.

Structural investigations of IB cell synapses may also be useful in providing evidence of LTD. Since LTD is associated with the internalisation of AMPA receptors, immunohistochemical analysis of the relative presence of full AMPA receptors or their subunits (GluA 1-4) could provide evidence of this. This would need to be done in conjunction with intracellular

experiments to electrophysiologically characterise IB cells, and highlight them with biocytin. It may be possible however to use dual immunohistochemical staining to show up layer V cell bodies (such as CTIP2) (Brunjes and Osterberg, 2015) as well as dendrites (βIII tubulin). It would then be required to distinguish IB cells based on their cell body location and morphology, which would add a level of subjectivity avoided by electrophysiological characterisation. However if this technique were to successfully highlight IB cells then it would be easier to analyse more cells for the presence of AMPA subunits at the layer II/III level of the apical dendrites. This could be compared between gamma and delta conditions to see if endocytosis does occur during delta rhythms. Much more coarsely, the general AMPA level could be compared across the layer II/III level between conditions.

To compare this to the human condition (and perhaps even uncover something more profound regarding the function of sleep) *in vivo* measurements of AMPA receptors in humans would be vital. There is current research regarding the development of positron emission tomography (PET) tracers that recognise AMPA receptors to enable this to occur (Takahata et al., 2017; Chen et al., 2018; Fu et al., 2018). Once valid tracers are available, it would be possible to compare the levels of AMPA receptors before and after sleep, however this may not be successful for subtle changes.

Monitoring the number and possibly the size of dendritic spines in layer V IB cells, would also give an indication of changes in plasticity in these neurones. Several immunohistochemical markers, such as PSD95 and drebrin, could be used to monitor changes in dendritic spines. These highlight synapses and would allow the number of dendritic spines and possibly also the size of those spines to be analysed (though this would require imaging at very high magnification and resolution). An alternative way to measure the surface area and contact of dendritic spines would be through scanning electron microscopy to reconstruct axon-spine interface (de Vivo et al., 2017).

Although it is clear that ARC is upregulated during delta rhythms in this thesis, the mechanism by which this occurs is uncertain. ARC mRNA can be translated distally from the cell soma in the dendrites (Steward et al., 1998). It is therefore unclear whether the ARC induced by *in vitro* delta rhythms is representative of upregulated translation of the protein, or downstream in the *de novo* synthesis at the level of the mRNA. This could be tested by inducing cortical rhythms, but in the presence of a transcriptions blocker (actinomycin D) or a protein synthesis inhibitor

(cycloheximide). However this may mean that it is not possible to induce oscillations, or even be sure that any effects that are see are related specifically to ARC as opposed to 'dirty' off targets effects of blocking overall transcription or translation. Another way to answer the question however would be to look at the relative expression of RNA and protein during delta and gamma conditions. A process similar to immunohistochemistry that allows localisation of specific RNA sequence is in situ hybridisation. This could be employed to see if there are also alterations in ARC RNA levels in neurons and also indicate their location in the cell.

One feature to note is that in the Arc immuno-stained tissue, there was rarely continuity between the dendrite and the soma in terms of the presence of Arc. This meant that it was not always possible to match up dendrites to specific soma. Carrying out the immunohistochemistry with the presence of a marker to highlight the whole neuronal cell (MAP2) would help show whether there is tandem staining in the soma and the dendrites. Dual staining of RNA and protein is possible with certain *in situ* hybridisation techniques (Turkekul et al., 2017) which would also allow full observation of the relative abundance of Arc at different stages in its synthesis within one neuron.

6.3.2 Further investigation into the effect of neuroinflammation on cortical oscillations

LPS does not cause changes to neuronal network activity changes when applied to acute slices of rat brain. To investigate further whether there are any direct effects of neuroinflammation on neuronal activity, similar experiments could be carried out using cytokines. This would involve the bath application of pro-inflammatory cytokines after the generation of an oscillation. Of particular importance are Il-1α and β, IL-6 (Dinarello, 2011) and TNFα (Probert, 2015) which are known to have neuronal receptor expression.

To have a better understanding of the effect of *in vivo* induction of inflammation it would be important to repeat the dosing experiments and subsequent recordings in this thesis to increase the sample size. This would avoid Type I or Type II errors and increase the statistical power of tests employed to analyse the results of the dosing study. Further analyses of these experiments could also be carried out to assess the state of neuroinflammation at different time points. Since the dose used was subchronic, it may also be interesting to see what effect a higher dose of the infections agents had. Monitoring the rats for sickness behaviour may also be useful to better relate the level of illness caused by the dosing of LPS and Poly I:C to levels of infection likely to

cause neurological changes in humans. Often measures of food and water intake, body temperature and activity (Barrientos et al., 2009b) as well as body weight (Kon Kim et al., 2013), and anxious and depressive behaviours as shown by maze and open field tests (Sulakhiya et al., 2016).

Further effects of peripheral infections on neuroinflammatory state of the brain could be done by analysis of different populations of cells in the brains. Simple analyses of microglia were carried out in this thesis which showed evidence of microglial activation, however these only compared LPS and control. Furthermore these only looked at crude measures of microglia morphology, where a more involved measurements such as a Scholl analysis to quantify the ramification index size would be more sensitive. Also no measurement was taken as to the number of microglial cells which is an indication of neuroinflammation. Astrocyte proliferation is also a sing of neuroinflammation and can be investigated by the simple immunostaining for GFAP.

Another simple immunohistochemistry experiment that could start to link neuroinflammation and changes to the electrical activity of the brains would be to stain for NeuN. This is a marker of neuronal cells and its use would allow for a comparison of cell numbers in the cortex and hippocampus at different dosing time scales, to see if there is significant cell death. Interneurons are more sensitive to changes in their local environment and are more susceptible to excitotoxicity, so monitoring GABA or GAD+ve cell numbers would show if neuroinflammation is more likely to lead to interneuron cell death. The presence or lack of cell death would highlight whether changes to electrical activity are driven by reduced populations of cells or failure of synaptic communication. The latter could be further investigated in a manner similar to that outlined in Chapter 6.6.1.

Indeed, the initial intention of this thesis was to analyse the state of synaptic plasticity in the brain after peripheral infection, similarly to the analysis carried out in Chapter 3. However due to problems of tissue integrity this was not possible. This would still be very interesting to investigate, not least to shed more light on the link between memory deficits and neuroinflammation. In fact there have already been some studies linking neuroinflammatory factors like TNFα and synaptic plasticity markers like AMPA (He et al., 2012).

6.3.3 Further investigation into the effect of visceral leishmaniasis on cortical oscillations

Many of the further experiments suggested in the previous section (6.3.2) would also be applicable to the work on Leishmaniasis. Especially including the measurement of: sickness behaviour, microglial/astrocyte number and morphology, and neuronal cell death. However since these two chapters were carried out of different animal models it would also be interesting to compare inflammation induced in the same way between mice and rats. This is particularly important as previous studies have shown differences in neuroinflammation between species *in vitro* (Lam et al., 2017) and *in vitro* (Potter-Baker et al., 2014).

In Chapter 5 no measurement of neuroinflammation (or even peripheral inflammation signals) were taken. Despite precedence in the literature (Melo et al., 2017), it is necessary to confirm I this is the case in our mouse model. To do this (further to microglia and astrocyte analysis) a cytokine panel could be employed (as in Chapter 4), to monitor pro- and anti-inflammatory cytokines and chemokines in the brain following the parasitic infection.

In Chapter 5 only experiments monitoring peripheral populations of parasites were carried out. Since there is previous evidence of migration of parasites into CNS tissue, it would be important to confirm whether parasites make it into the brain. If this were the case it could bring into question whether any neuroinflammation caused was a propagation of the peripheral inflammation signalling or due to parasitic presence in the brain.

References

Abraham, W.C., et al. (1991). The role of immediate early genes in the stabilization of long-term potentiation. *Molecular Neurobiology* **5**(2): 297.

Adrian, E.D. (1942). Olfactory reactions in the brain of the hedgehog. *J Physiol* **100**(4): 459-473.

Ahn, J.Y., et al. (2015). Activation of immediate-early response gene c-Fos protein in the rat paralimbic cortices after myocardial infarction. *Neural Regen Res* **10**(8): 1251-1257.

Ainsworth, M., et al. (2011). Dual gamma rhythm generators control interlaminar synchrony in auditory cortex. *J Neurosci* **31**(47): 17040-17051.

Ainsworth, M., et al. (2016). GABAB receptor-mediated, layer-specific synaptic plasticity reorganizes gamma-frequency neocortical response to stimulation. *Proc Natl Acad Sci U S A* **113**(19): E2721-2729.

Ajami, B., et al. (2007). Local self-renewal can sustain CNS microglia maintenance and function throughout adult life. *Nat Neurosci* **10**(12): 1538-1543.

Alper, K.R., et al. (2006). Correlation of PET and qEEG in normal subjects. *Psychiatry Res* **146**(3): 271-282.

Alvar, J., et al. (2012). Leishmaniasis worldwide and global estimates of its incidence. *PLoS One* **7**(5): e35671.

Amzica, F. and Steriade, M. (1998). Electrophysiological correlates of sleep delta waves. *Electroencephalogr Clin Neurophysiol* **107**(2): 69-83.

Andreone, B.J., et al. (2017). Blood-Brain Barrier Permeability Is Regulated by Lipid Transport-Dependent Suppression of Caveolae-Mediated Transcytosis. *Neuron* **94**(3): 581-594.e585.

Anokhin, K.V., et al. (1991). Effects of early experience on c-fos gene expression in the chick forebrain. *Brain Res* **544**(1): 101-107.

Araujo Lima Verde, F., et al. (2011). Hormonal Disturbances in Visceral Leishmaniasis (Kala-Azar). *Am J Trop Med Hyg* **84**(5): 668-673.

Attarian, S., et al. (2003). [Guillain-Barre syndrome revealing visceral leishmaniasis in an immunocompetent woman]. *Rev Neurol (Paris)* **159**(11): 1046-1048.

Aurelian, L., et al. (2016). TLR4 signaling in VTA dopaminergic neurons regulates impulsivity through tyrosine hydroxylase modulation. *Translational Psychiatry* **6**: e815.

Axmacher, N., et al. (2006). Memory formation by neuronal synchronization. *Brain Res Rev* **52**(1): 170-182.

Baillet, S. (2017). Magnetoencephalography for brain electrophysiology and imaging. *Nat Neurosci* **20**(3): 327-339.

Bakhiet, M., et al. (2001). RANTES promotes growth and survival of human first-trimester forebrain astrocytes. *Nat Cell Biol* **3**(2): 150-157.

Banks, W.A., et al. (1995). Passage of cytokines across the blood-brain barrier. *Neuroimmunomodulation* **2**(4): 241-248.

Barcia, C., et al. (2011). IFN-γ signaling, with the synergistic contribution of TNF-α, mediates cell specific microglial and astroglial activation in experimental models of Parkinson's disease. *Cell Death &Amp; Disease* **2**: e142.

Barrientos, R.M., et al. (2009a). Time course of hippocampal IL-1 beta and memory consolidation impairments in aging rats following peripheral infection. *Brain Behav Immun* **23**(1): 46-54.

Barrientos, R.M., et al. (2009b). Characterization of the sickness response in young and aging rats following E. coli infection. *Brain Behav Immun* **23**(4): 450-454.

Beauchamp, M.S. and Ro, T. (2008). Neural substrates of sound-touch synesthesia after a thalamic lesion. *J Neurosci* **28**(50): 13696-13702.

Béïque, J.-C., et al. (2011). Arc-dependent synapse-specific homeostatic plasticity. *Proceedings of the National Academy of Sciences* **108**(2): 816-821.

Beltramo, R., et al. (2013). Layer-specific excitatory circuits differentially control recurrent network dynamics in the neocortex. *Nat Neurosci* **16**(2): 227-234.

Berger, H. (1929). Über das Elektroenkephalogramm des Menschen. *Arch. Psychiatr.* **87**: 527-570.

Berman, J.D. (1997). Human leishmaniasis: clinical, diagnostic, and chemotherapeutic developments in the last 10 years. *Clin Infect Dis* **24**(4): 684-703.

Bi, G.Q. and Poo, M.M. (1998). Synaptic modifications in cultured hippocampal neurons: dependence on spike timing, synaptic strength, and postsynaptic cell type. *J Neurosci* **18**(24): 10464-10472.

Biesmans, S., et al. (2013). Systemic Immune Activation Leads to Neuroinflammation and Sickness Behavior in Mice. *Mediators of Inflammation* **2013**: 14.

Bjelobaba, I., et al. (2017). Multiple Sclerosis and Neuroinflammation: The Overview of Current and Prospective Therapies. *Curr Pharm Des* **23**(5): 693-730.

Bjorness, T.E. and Greene, R.W. (2009). Adenosine and sleep. *Curr Neuropharmacol* **7**(3): 238-245.

Bliss, T.V. and Collingridge, G.L. (1993). A synaptic model of memory: long-term potentiation in the hippocampus. *Nature* **361**(6407): 31-39.

Boado, R.J., et al. (1999). Selective expression of the large neutral amino acid transporter at the blood-brain barrier. *Proc Natl Acad Sci U S A* **96**(21): 12079-12084.

Boado, R.J., et al. (1994). Enhanced expression of the blood-brain barrier GLUT1 glucose transporter gene by brain-derived factors. *Brain Res Mol Brain Res* **22**(1-4): 259-267.

Bode-Greuel, K.M., et al. (1987). A current source density analysis of field potentials evoked in slices of visual cortex. *Experimental Brain Research* **69**(1): 213-219.

Bojovic, O., et al. (2015). Time course of immediate early gene protein expression in the spinal cord following conditioning stimulation of the sciatic nerve in rats. *PLoS One* **10**(4): e0123604.

Bonjean, M., et al. (2012). Interactions between core and matrix thalamocortical projections in human sleep spindle synchronization. *J Neurosci* **32**(15): 5250-5263.

Booth, C.A., et al. (2016). Altered Intrinsic Pyramidal Neuron Properties and Pathway-Specific Synaptic Dysfunction Underlie Aberrant Hippocampal Network Function in a Mouse Model of Tauopathy. *J Neurosci* **36**(2): 350-363.

Brambilla, D., et al. (2005). Adenosine mediation of presynaptic feedback inhibition of glutamate release. *Neuron* **46**(2): 275-283.

Bramham, C.R., et al. (2010). The Arc of synaptic memory. *Exp Brain Res* **200**(2): 125-140.

Bramham, C.R. and Srebro, B. (1989). Synaptic plasticity in the hippocampus is modulated by behavioral state. *Brain Res* **493**(1): 74-86.

Bray, N., et al. (2016). Decreased haemodynamic response and decoupling of cortical gamma-band activity and tissue oxygen perfusion after striatal interleukin-1 injection. *Journal of Neuroinflammation* **13**(1): 195.

Breton, J.D. and Stuart, G.J. (2012). Somatic and dendritic GABA(B) receptors regulate neuronal excitability via different mechanisms. *J Neurophysiol* **108**(10): 2810-2818.

Brett-Green, B., et al. (2004). Two distinct regions of secondary somatosensory cortex in the rat: topographical organization and multisensory responses. *J Neurophysiol* **91**(3): 1327-1336.

Brightman, M.W. and Reese, T.S. (1969). Junctions between intimately apposed cell membranes in the vertebrate brain. *J Cell Biol* **40**(3): 648-677.

Britton, J.W., et al. (2016). Electroencephalography (EEG): An introductory text and atlas of normal and abnormal findings in adults, children, and infants, American Epilepsy Society, Chicago.

Brodie, C., et al. (1998). Functional IL-4 receptors on mouse astrocytes: IL-4 inhibits astrocyte activation and induces NGF secretion. *J Neuroimmunol* **81**(1-2): 20-30.

Bronzuoli, M.R., et al. (2016). Targeting neuroinflammation in Alzheimer's disease. *J Inflamm Res* **9**: 199-208.

Brown, A.M. and Ransom, B.R. (2002). Neuroprotective effects of increased extracellular Ca(2+) during aglycemia in white matter. *J Neurophysiol* **88**(3): 1302-1307.

Brown, R.E., et al. (2012). Control of sleep and wakefulness. *Physiol Rev* **92**(3): 1087-1187.

Brumberg, J.C., et al. (1999). Cortical columnar processing in the rat whisker-to-barrel system. *J Neurophysiol* **82**(4): 1808-1817.

Brunjes, P.C. and Osterberg, S.K. (2015). Developmental Markers Expressed in Neocortical Layers Are Differentially Exhibited in Olfactory Cortex. *PLoS One* **10**(9): e0138541.

Brunner, D.P., et al. (1990). Effect of partial sleep deprivation on sleep stages and EEG power spectra: evidence for non-REM and REM sleep homeostasis. *Electroencephalogr Clin Neurophysiol* **75**(6): 492-499.

Bsibsi, M., et al. (2002). Broad Expression of Toll-Like Receptors in the Human Central Nervous System. *Journal of Neuropathology & Experimental Neurology* **61**(11): 1013-1021.

Buchanan, J.B., et al. (2008). Cognitive and neuroinflammatory consequences of mild repeated stress are exacerbated in aged mice. *Psychoneuroendocrinology* **33**(6): 755-765.

Bunn, P.T., et al. (2014). Tissue requirements for establishing long-term CD4+ T cell-mediated immunity following Leishmania donovani infection. *J Immunol* **192**(8): 3709-3718.

Burchell, T.R., et al. (1998). Gamma frequency oscillations gate temporally coded afferent inputs in the rat hippocampal slice. *Neurosci Lett* **255**(3): 151-154.

Burguillos, M.A., et al. (2011). Caspase signalling controls microglia activation and neurotoxicity. *Nature* **472**(7343): 319-324.

Bushey, D., et al. (2011). Sleep and synaptic homeostasis: structural evidence in Drosophila. *Science* **332**(6037): 1576-1581.

Butovsky, O., et al. (2005). Activation of microglia by aggregated beta-amyloid or lipopolysaccharide impairs MHC-II expression and renders them cytotoxic whereas IFN-gamma and IL-4 render them protective. *Mol Cell Neurosci* **29**(3): 381-393.

Buzsaki, G. (1998). Memory consolidation during sleep: a neurophysiological perspective. *J Sleep Res* **7 Suppl 1**: 17-23.

Buzsaki, G. and Wang, X.J. (2012). Mechanisms of gamma oscillations. *Annu Rev Neurosci* **35**: 203-225.

Cardinot, C.B., et al. (2016). Detection of Ehrlichia canis, Babesia vogeli, and Toxoplasma gondii DNA in the Brain of Dogs Naturally Infected with Leishmania infantum. *J Parasitol* **102**(2): 275-279.

Carlo, C.N. and Stevens, C.F. (2013). Structural uniformity of neocortex, revisited. *Proceedings of the National Academy of Sciences* **110**(4): 1488-1493.

Carracedo, L.M., et al. (2013). A neocortical delta rhythm facilitates reciprocal interlaminar interactions via nested theta rhythms. *J Neurosci* **33**(26): 10750-10761.

Carswell, J. (1953). Kala-azar at Kitui. *East Afr Med J* **30**(7): 287-293.

Carter, D.A. and Murphy, D. (1990). Regulation of c-fos and c-jun expression in the rat supraoptic nucleus. *Cell Mol Neurobiol* **10**(3): 435-445.

Cash, S.S., et al. (2009). The human K-complex represents an isolated cortical down-state. *Science* **324**(5930): 1084-1087.

Caton, R. (1875). Electrical Currents of the Brain. *The Journal of Nervous and Mental Disease* **2**(4): 610.

Cavinato, M., et al. (2012). Preservation of auditory P300-like potentials in cortical deafness. *PLoS One* **7**(1): e29909.

Chapin, J.K. (1986). Laminar differences in sizes, shapes, and response profiles of cutaneous receptive fields in the rat SI cortex. *Exp Brain Res* **62**(3): 549-559.

Chapman, C.A. and Lacaille, J.C. (1999). Cholinergic induction of theta-frequency oscillations in hippocampal inhibitory interneurons and pacing of pyramidal cell firing. *J Neurosci* **19**(19): 8637-8645.

Chappuis, F., et al. (2007). Visceral leishmaniasis: what are the needs for diagnosis, treatment and control? *Nat Rev Microbiol* **5**(11): 873-882.

Chawla, A., et al. (2011). Macrophage-mediated inflammation in metabolic disease. *Nat Rev Immunol* **11**(11): 738-749.

Chechik, G. and Nelken, I. (2012). Auditory abstraction from spectro-temporal features to coding auditory entities. *Proc Natl Acad Sci U S A* **109**(46): 18968-18973.

Chen, Z., et al. (2012). Lipopolysaccharide-Induced Microglial Activation and Neuroprotection against Experimental Brain Injury Is Independent of Hematogenous TLR4. *J Neurosci* **32**(34): 11706-11715.

Chen, Z., et al. (2018). Synthesis, pharmacology and preclinical evaluation of (11)C-labeled 1,3-dihydro-2H-benzo[d]imidazole-2-ones for imaging gamma8-dependent transmembrane AMPA receptor regulatory protein. *Eur J Med Chem* **157**: 898-908.

Chen, Z., et al. (2016). Adenosine A1 Receptor-Mediated Endocytosis of AMPA Receptors Contributes to Impairments in Long-Term Potentiation (LTP) in the Middle-Aged Rat Hippocampus. *Neurochem Res* **41**(5): 1085-1097.

Chomarat, P. and Banchereau, J. (1998). Interleukin-4 and lnterleukin-13: Their Similarities and Discrepancies. *International Reviews of Immunology* **17**(1-4): 1-52.

Chou, S.Y., et al. (2016). CCL5/RANTES contributes to hypothalamic insulin signaling for systemic insulin responsiveness through CCR5. *Sci Rep* **6**: 37659.

Chowdhury, D., et al. (2018). Ca(2+)/calmodulin binding to PSD-95 mediates homeostatic synaptic scaling down. *Embo j* **37**(1): 122-138.

Chowdhury, G.M., et al. (2000). Induction and adaptation of Fos expression in the rat brain by two types of acute restraint stress. *Brain Res Bull* **52**(3): 171-182.

Chowdhury, S., et al. (2006). Arc/Arg3.1 interacts with the endocytic machinery to regulate AMPA receptor trafficking. *Neuron* **52**(3): 445-459.

Chunge, C.N., et al. (1985). Is neurological involvement possible in visceral leishmaniasis in Kenya. *Trans R Soc Trop Med Hyg* **79**(6): 872.

Cirelli and Tononi (1999). Differences in brain gene expression between sleep and waking as revealed by mRNA differential display and cDNA microarray technology. *J Sleep Res* **8**(S1): 44-52.

Cirelli, C., et al. (2004). Extensive and divergent effects of sleep and wakefulness on brain gene expression. *Neuron* **41**(1): 35-43.

Cirelli, C., et al. (1995). Sleep deprivation and c-fos expression in the rat brain. *J Sleep Res* **4**(2): 92-106.

Cirelli, C. and Tononi, G. (2000a). Differential expression of plasticity-related genes in waking and sleep and their regulation by the noradrenergic system. *J Neurosci* **20**(24): 9187-9194.

Cirelli, C. and Tononi, G. (2000b). Gene expression in the brain across the sleep-waking cycle. *Brain Res* **885**(2): 303-321.

Cirelli, C. and Tononi, G. (2000c). On the functional significance of c-fos induction during the sleep-waking cycle. *Sleep* **23**(4): 453-469.

Coggeshall, R.E. (2005). Fos, nociception and the dorsal horn. *Prog Neurobiol* **77**(5): 299-352.

Colgin, L.L. (2016). Rhythms of the hippocampal network. *Nat Rev Neurosci* **17**(4): 239-249.

Colgin, L.L., et al. (2009a). Frequency of gamma oscillations routes flow of information in the hippocampus. *Nature* **462**: 353.

Colgin, L.L., et al. (2009b). Frequency of gamma oscillations routes flow of information in the hippocampus. *Nature* **462**(7271): 353-357.

Combrinck, M.I., et al. (2002). Peripheral infection evokes exaggerated sickness behaviour in pre-clinical murine prion disease. *Neuroscience* **112**(1): 7-11.

Combs, C.K., et al. (2001). β-Amyloid Stimulation of Microglia and Monocytes Results in TNFα-Dependent Expression of Inducible Nitric Oxide Synthase and Neuronal Apoptosis. *The Journal of Neuroscience* **21**(4): 1179-1188.

Coomber, B.L. and Stewart, P.A. (1985). Morphometric analysis of CNS microvascular endothelium. *Microvasc Res* **30**(1): 99-115.

Corona, A.W., et al. (2010). Fractalkine receptor (CX3CR1) deficiency sensitizes mice to the behavioral changes induced by lipopolysaccharide. *J Neuroinflammation* **7**: 93.

Cortese, G.P. and Burger, C. (2017). Neuroinflammatory challenges compromise neuronal function in the aging brain: Postoperative cognitive delirium and Alzheimer's disease. *Behav Brain Res* **322**(Pt B): 269-279.

Costa, M.R. and Muller, U. (2014). Specification of excitatory neurons in the developing cerebral cortex: progenitor diversity and environmental influences. *Front Cell Neurosci* **8**: 449.

Creutzfeldt, O.D., et al. (1977). The distribution of degenerating axons after small lesions in the intact and isolated visual cortex of the cat. *Experimental Brain Research* **27**(3): 419-440.

Cunningham, M.O., et al. (2003). Gamma oscillations induced by kainate receptor activation in the entorhinal cortex in vitro. *J Neurosci* **23**(30): 9761-9769.

Cunningham, M.O., et al. (2004). A role for fast rhythmic bursting neurons in cortical gamma oscillations in vitro. *Proc Natl Acad Sci U S A* **101**(18): 7152-7157.

Czarnecki, A., et al. (2007). Cellular mechanisms of burst firing-mediated long-term depression in rat neocortical pyramidal cells. *J Physiol* **578**(Pt 2): 471-479.

d'Avila, J.C., et al. (2018). Age-related cognitive impairment is associated with long-term neuroinflammation and oxidative stress in a mouse model of episodic systemic inflammation. *Journal of Neuroinflammation* **15**(1): 28.

Daneman, R. and Prat, A. (2015). The blood-brain barrier. *Cold Spring Harb Perspect Biol* **7**(1): a020412.

Dang-Vu, T.T., et al. (2010). Spontaneous brain rhythms predict sleep stability in the face of noise. *Curr Biol* **20**(15): R626-627.

Das, S., et al. (2018). A transgenic mouse for imaging activity-dependent dynamics of endogenous Arc mRNA in live neurons. *Science Advances* **4**(6).

Davis, D.H., et al. (2012). Delirium is a strong risk factor for dementia in the oldest-old: a population-based cohort study. *Brain* **135**(Pt 9): 2809-2816.

de Vivo, L., et al. (2017). Ultrastructural evidence for synaptic scaling across the wake/sleep cycle. *Science* **355**(6324): 507-510.

Debray, C., et al. (1997). Contributions of AMPA and GABA(A) receptors to the induction of NMDAR-dependent LTP in CA1. *Neurosci Lett* **238**(3): 119-122.

Desjeux, P. (2001). The increase in risk factors for leishmaniasis worldwide. *Trans R Soc Trop Med Hyg* **95**(3): 239-243.

Dheen, S.T., et al. (2007). Microglial activation and its implications in the brain diseases. *Curr Med Chem* **14**(11): 1189-1197.

Dickinson, R., et al. (2003). The effects of general anaesthetics on carbachol-evoked gamma oscillations in the rat hippocampus in vitro. *Neuropharmacology* **44**(7): 864-872.

Dickson, C.T. and Alonso, A. (1997). Muscarinic induction of synchronous population activity in the entorhinal cortex. *Journal of Neuroscience* **17**(17): 6729-6744.

Diekelmann, S. and Born, J. (2010). The memory function of sleep. *Nat Rev Neurosci* **11**(2): 114-126.

Diering, G.H., et al. (2017). Homer1a drives homeostatic scaling-down of excitatory synapses during sleep. *Science* **355**(6324): 511-515.

Dik, M.G., et al. (2005). Serum inflammatory proteins and cognitive decline in older persons. *Neurology* **64**(8): 1371-1377.

Dinarello, C.A. (2011). Interleukin-1 in the pathogenesis and treatment of inflammatory diseases. *Blood* **117**(14): 3720-3732.

Diniz, L.M., et al. (2010). Neurological involvement in visceral leishmaniasis: case report. *Rev Soc Bras Med Trop* **43**(6): 743-745.

Donovan, C. (1994). On the possibility of the occurrence of trypanosomiasis in India. 1903. *Natl Med J India* **7**(4): 196, 201-192.

Dragunow, M., et al. (1989). Long-term potentiation and the induction of c-fos mRNA and proteins in the dentate gyrus of unanesthetized rats. *Neurosci Lett* **101**(3): 274-280.

Dragunow, M., et al. (1990). Induction of c-fos mRNA and protein in neurons and glia after traumatic brain injury: Pharmacological characterization. *Experimental Neurology* **107**(3): 236-248.

Dudai, Y. and Eisenberg, M. (2004). Rites of passage of the engram: reconsolidation and the lingering consolidation hypothesis. *Neuron* **44**(1): 93-100.

Dudai, Y., et al. (2015). The Consolidation and Transformation of Memory. *Neuron* **88**(1): 20-32.

Dupret, D., et al. (2008). Inhibitory interneurons and network oscillations. *Proc Natl Acad Sci U S A* **105**(47): 18079-18080.

Duyckaerts, C., et al. (2009). Classification and basic pathology of Alzheimer disease. *Acta Neuropathol* **118**(1): 5-36.

Dzirasa, K., et al. (2006). Dopaminergic control of sleep-wake states. *J Neurosci* **26**(41): 10577-10589.

Eagle, A.L., et al. (2016). Role of hippocampal activity-induced transcription in memory consolidation. *Rev Neurosci* **27**(6): 559-573.

Edling, Y., et al. (2007). Glutamate activates c-fos in glial cells via a novel mechanism involving the glutamate receptor subtype mGlu5 and the transcriptional repressor DREAM. *Glia* **55**(3): 328-340.

el Hag, I.A., et al. (1994). Liver morphology and function in visceral leishmaniasis (Kala-azar). *J Clin Pathol* **47**(6): 547-551.

Elmquist, J.K., et al. (1997). Mechanisms of CNS response to systemic immune challenge: the febrile response. *Trends Neurosci* **20**(12): 565-570.

Emri, Z., et al. (2000). Backpropagation of the delta oscillation and the retinal excitatory postsynaptic potential in a multi-compartment model of thalamocortical neurons. *Neuroscience* **98**(1): 111-127.

Engel, A.K., et al. (2001). Dynamic predictions: oscillations and synchrony in top-down processing. *Nat Rev Neurosci* **2**(10): 704-716.

Engel, A.K. and Singer, W. (2001). Temporal binding and the neural correlates of sensory awareness. *Trends Cogn Sci* **5**(1): 16-25.

Engwerda, C.R. and Kaye, P.M. (2000). Organ-specific immune responses associated with infectious disease. *Immunol Today* **21**(2): 73-78.

Eugene, A.R. and Masiak, J. (2015). The Neuroprotective Aspects of Sleep. *MEDtube Sci* **3**(1): 35-40.

Eyo, U.B., et al. (2016). Regulation of Physical Microglia–Neuron Interactions by Fractalkine Signaling after Status Epilepticus. *eNeuro* **3**(6).

Fasanaro, A.M., et al. (1991). Guillain-Barre syndrome as presenting manifestation of visceral leishmaniasis. *Lancet* **338**(8775): 1142.

Fell, J., et al. (2002). Human scalp recorded sigma activity is modulated by slow EEG oscillations during deep sleep. *Int J Neurosci* **112**(7): 893-900.

Fell, J., et al. (2001). Human memory formation is accompanied by rhinal-hippocampal coupling and decoupling. *Nat Neurosci* **4**(12): 1259-1264.

Finkel, M.P., et al. (1966). Virus induction of osteosarcomas in mice. *Science* **151**(3711): 698-701.

Fisahn, A., et al. (1998). Cholinergic induction of network oscillations at 40 Hz in the hippocampus in vitro. *Nature* **394**(6689): 186-189.

Fleischmann, A., et al. (2003). Impaired long-term memory and NR2A-type NMDA receptor-dependent synaptic plasticity in mice lacking c-Fos in the CNS. *J Neurosci* **23**(27): 9116-9122.

Fong, T.G., et al. (2009). Delirium accelerates cognitive decline in Alzheimer disease. *Neurology* **72**(18): 1570-1575.

Fong, Y., et al. (1989). Antibodies to cachectin/tumor necrosis factor reduce interleukin 1 beta and interleukin 6 appearance during lethal bacteremia. *J Exp Med* **170**(5): 1627-1633.

Foxe, J.J., et al. (2002). Auditory-somatosensory multisensory processing in auditory association cortex: an fMRI study. *J Neurophysiol* **88**(1): 540-543.

Frankenhaeuser, B. (1957). The effect of calcium on the myelinated nerve fibre. *J Physiol* **137**(2): 245-260.

Frankenhaeuser, B. and Hodgkin, A.L. (1957). The action of calcium on the electrical properties of squid axons. *J Physiol* **137**(2): 218-244.

Frei, K., et al. (1989). On the cellular source and function of interleukin 6 produced in the central nervous system in viral diseases. *Eur J Immunol* **19**(4): 689-694.

Frey, D.J., et al. (2007). The effects of 40 hours of total sleep deprivation on inflammatory markers in healthy young adults. *Brain Behav Immun* **21**(8): 1050-1057.

Fu, H., et al. (2018). Positron Emission Tomography (PET) Ligand Development for Ionotropic Glutamate Receptors: Challenges and Opportunities for Radiotracer Targeting N-Methyl-d-aspartate (NMDA), alpha-Amino-3-hydroxy-5-methyl-4-isoxazolepropionic Acid (AMPA), and Kainate Receptors. *J Med Chem*.

Gahring, L.C., et al. (1996). Neuronal expression of tumor necrosis factor alpha in the murine brain. *Neuroimmunomodulation* **3**(5): 289-303.

Gais, S. and Born, J. (2004). Low acetylcholine during slow-wave sleep is critical for declarative memory consolidation. *Proc Natl Acad Sci U S A* **101**(7): 2140-2144.

Gao, M., et al. (2010). A specific requirement of Arc/Arg3.1 for visual experience-induced homeostatic synaptic plasticity in mouse primary visual cortex. *J Neurosci* **30**(21): 7168-7178.

Gao, W.J. and Zheng, Z.H. (2004). Target-specific differences in somatodendritic morphology of layer V pyramidal neurons in rat motor cortex. *J Comp Neurol* **476**(2): 174-185.

Gautron, L., et al. (2002). Spatiotemporal analysis of signal transducer and activator of transcription 3 activation in rat brain astrocytes and pituitary following peripheral immune challenge. *Neuroscience* **112**(3): 717-729.

Gehrmann, J., et al. (1995). Microglia: Intrinsic immuneffector cell of the brain. *Brain Res Rev* **20**(3): 269-287.

Gentz, R., et al. (1989). Parallel association of Fos and Jun leucine zippers juxtaposes DNA binding domains. *Science* **243**(4899): 1695-1699.

Georgiadou, S.P., et al. (2015). Leishmaniasis revisited: Current aspects on epidemiology, diagnosis and treatment. *J Transl Int Med* **3**(2): 43-50.

Gibson, M.E. (1983). The identification of kala-azar and the discovery of Leishmania donovani. *Med Hist* **27**(2): 203-213.

Gibson, R.M., et al. (2004). CNS injury: the role of the cytokine IL-1. *Vet J* **168**(3): 230-237.

Gilbert, C.D. and Wiesel, T.N. (1979). Morphology and intracortical projections of functionally characterised neurones in the cat visual cortex. *Nature* **280**(5718): 120-125.

Gilbert, C.D. and Wiesel, T.N. (1983). Clustered intrinsic connections in cat visual cortex. *J Neurosci* **3**(5): 1116-1133.

Gillies, M.J., et al. (2002). A model of atropine-resistant theta oscillations in rat hippocampal area CA1. *J Physiol* **543**(Pt 3): 779-793.

Ginhoux, F., et al. (2010). Fate Mapping Analysis Reveals That Adult Microglia Derive from Primitive Macrophages. *Science*.

Gloveli, T., et al. (1999). Carbachol-induced changes in excitability and [Ca2+] i signalling in projection cells of medial entorhinal cortex layers II and III. *European Journal of Neuroscience* **11**(10): 3626-3636.

Godbout, J.P., et al. (2005). Exaggerated neuroinflammation and sickness behavior in aged mice following activation of the peripheral innate immune system. *Faseb j* **19**(10): 1329-1331.

Gómez-Nicola, D., et al. (2013). Regulation of Microglial Proliferation during Chronic Neurodegeneration. *The Journal of Neuroscience* **33**(6): 2481-2493.

Gordon, G.R., et al. (2011). Bidirectional control of arteriole diameter by astrocytes. *Exp Physiol* **96**(4): 393-399.

Gosselin, N., et al. (2009). Sleep following sport-related concussions. *Sleep Med* **10**(1): 35-46.

Gouty-Colomer, L.A., et al. (2016). Arc expression identifies the lateral amygdala fear memory trace. *Mol Psychiatry* **21**(3): 364-375.

Grano, F.G., et al. (2018). Toll-like receptors and cytokines in the brain and in spleen of dogs with visceral leishmaniosis. *Vet Parasitol* **253**: 30-38.

Gray, C.M., et al. (1989). Oscillatory responses in cat visual cortex exhibit inter-columnar synchronization which reflects global stimulus properties. *Nature* **338**(6213): 334-337.

Gray, C.M. and Singer, W. (1989). Stimulus-specific neuronal oscillations in orientation columns of cat visual cortex. *Proc Natl Acad Sci U S A* **86**(5): 1698-1702.

Gregersen, R., et al. (2000). Microglia and macrophages are the major source of tumor necrosis factor in permanent middle cerebral artery occlusion in mice. *J Cereb Blood Flow Metab* **20**(1): 53-65.

Groh, A., et al. (2010). Cell-Type Specific Properties of Pyramidal Neurons in Neocortex Underlying a Layout that Is Modifiable Depending on the Cortical Area. *Cerebral Cortex* **20**(4): 826-836.

Gross, J. (2007). Gamma Oscillations in Human Primary Somatosensory Cortex Reflect Pain Perception. **5**(5).

Gullo, F., et al. (2014). Atypical "seizure-like" activity in cortical reverberating networks in vitro can be caused by LPS-induced inflammation: a multi-electrode array study from a hundred neurons. *Front Cell Neurosci* **8**: 361.

Gulyas, A.I., et al. (1999). Total number and ratio of excitatory and inhibitory synapses converging onto single interneurons of different types in the CA1 area of the rat hippocampus. *J Neurosci* **19**(22): 10082-10097.

Gusel'nikova, V.V. and Korzhevskiy, D.E. (2015). NeuN As a Neuronal Nuclear Antigen and Neuron Differentiation Marker. *Acta Naturae* **7**(2): 42-47.

Guzowski, J.F., et al. (2000). Inhibition of activity-dependent arc protein expression in the rat hippocampus impairs the maintenance of long-term potentiation and the consolidation of long-term memory. *J Neurosci* **20**(11): 3993-4001.

Guzowski, J.F., et al. (2001). Experience-dependent gene expression in the rat hippocampus after spatial learning: a comparison of the immediate-early genes Arc, c-fos, and zif268. *J Neurosci* **21**(14): 5089-5098.

Haack, M., et al. (2001). Effects of sleep on endotoxin-induced host responses in healthy men. *Psychosom Med* **63**(4): 568-578.

Haenschel, C., et al. (2000). Gamma and beta frequency oscillations in response to novel auditory stimuli: A comparison of human electroencephalogram (EEG) data with in vitro models. *Proceedings of the National Academy of Sciences* **97**(13): 7645-7650.

Hakami, T., et al. (2009). NMDA receptor hypofunction leads to generalized and persistent aberrant gamma oscillations independent of hyperlocomotion and the state of consciousness. *PLoS One* **4**(8): e6755.

Halasy, K., et al. (1996). Synaptic target selectivity and input of GABAergic basket and bistratified interneurons in the CA1 area of the rat hippocampus. *Hippocampus* **6**(3): 306-329.

Halazonetis, T.D., et al. (1988). c-Jun dimerizes with itself and with c-Fos, forming complexes of different DNA binding affinities. *Cell* **55**(5): 917-924.

Hämäläinen, H., et al. (2002). Activation of somatosensory cortical areas varies with attentional state: an fMRI study. *Behavioural Brain Research* **135**(1): 159-165.

Hanisch, U.K. (2002). Microglia as a source and target of cytokines. *Glia* **40**(2): 140-155.

Hanlon, E.C., et al. (2009). Effects of skilled training on sleep slow wave activity and cortical gene expression in the rat. *Sleep* **32**(6): 719-729.

Hansen, M.K. and Krueger, J.M. (1997). Subdiaphragmatic vagotomy blocks the sleep- and fever-promoting effects of interleukin-1beta. *Am J Physiol* **273**(4 Pt 2): R1246-1253.

Harmony, T., et al. (1996). EEG delta activity: an indicator of attention to internal processing during performance of mental tasks. *Int J Psychophysiol* **24**(1-2): 161-171.

Harms, A.S., et al. (2012). Regulation of microglia effector functions by tumor necrosis factor signaling. *Glia* **60**(2): 189-202.

Harrison, J.K., et al. (1998). Role for neuronally derived fractalkine in mediating interactions between neurons and CX3CR1-expressing microglia. *Proc Natl Acad Sci U S A* **95**(18): 10896-10901.

Hashim, F.A., et al. (1995). Neurologic changes in visceral leishmaniasis. *Am J Trop Med Hyg* **52**(2): 149-154.

Hashimoto, D., et al. (2013). Tissue-resident macrophages self-maintain locally throughout adult life with minimal contribution from circulating monocytes. *Immunity* **38**(4): 792-804.

Hasselmo, M.E. (1999). Neuromodulation: acetylcholine and memory consolidation. *Trends Cogn Sci* **3**(9): 351-359.

He, P., et al. (2012). Genetic deletion of TNF receptor suppresses excitatory synaptic transmission via reducing AMPA receptor synaptic localization in cortical neurons. *Faseb j* **26**(1): 334-345.

Headley, D.B. and Weinberger, N.M. (2011). Gamma-band activation predicts both associative memory and cortical plasticity. *J Neurosci* **31**(36): 12748-12758.

Heneka, M.T., et al. (2015). Neuroinflammation in Alzheimer's disease. *Lancet Neurol* **14**(4): 388-405.

Henrie, J.A. and Shapley, R. (2005). LFP power spectra in V1 cortex: the graded effect of stimulus contrast. *J Neurophysiol* **94**(1): 479-490.

Herreras, O., et al. (1988). Sensory modulation of hippocampal transmission. II. Evidence for a cholinergic locus of inhibition in the Schaffer-CA1 synapse. *Brain Res* **461**(2): 303-313.

Hirshler, Y.K., et al. (2010). Intracranial electrode implantation produces regional neuroinflammation and memory deficits in rats. *Exp Neurol* **222**(1): 42-50.

Hodgson, N., et al. (2011). Undiagnosed Illness and Neuropsychiatric Behaviors In Community-residing Older Adults with Dementia. *Alzheimer Dis Assoc Disord* **25**(2): 109-115.

Hoffman, G.E., et al. (1993). c-Fos and related immediate early gene products as markers of activity in neuroendocrine systems. *Front Neuroendocrinol* **14**(3): 173-213.

Holden, J.M., et al. (2008). Lipopolysaccharide-induced immune activation impairs attention but has little effect on short-term working memory. *Behav Brain Res* **194**(2): 138-145.

Holmes, C., et al. (2009). Systemic inflammation and disease progression in Alzheimer disease. *Neurology* **73**(10): 768-774.

Holmes, C., et al. (2003). Systemic infection, interleukin 1beta, and cognitive decline in Alzheimer's disease. *J Neurol Neurosurg Psychiatry* **74**(6): 788-789.

Holz, J., et al. (2012). EEG sigma and slow-wave activity during NREM sleep correlate with overnight declarative and procedural memory consolidation. *J Sleep Res* **21**(6): 612-619.

Hsiao, S.S., et al. (1993). Effects of selective attention on spatial form processing in monkey primary and secondary somatosensory cortex. *J Neurophysiol* **70**(1): 444-447.

Hu, E., et al. (1994). Targeted disruption of the c-fos gene demonstrates c-fos-dependent and -independent pathways for gene expression stimulated by growth factors or oncogenes. *Embo j* **13**(13): 3094-3103.

Huang, Y.Y. and Kandel, E.R. (2005). Theta frequency stimulation induces a local form of late phase LTP in the CA1 region of the hippocampus. *Learn Mem* **12**(6): 587-593.

Hubel, D.H. and Wiesel, T.N. (1962). Receptive fields, binocular interaction and functional architecture in the cat's visual cortex. *J Physiol* **160**: 106-154.

Huber, R., et al. (2004). Local sleep and learning. *Nature* **430**(6995): 78-81.

Hughes, S.W., et al. (1998). Dynamic clamp study of Ih modulation of burst firing and delta oscillations in thalamocortical neurons in vitro. *Neuroscience* **87**(3): 541-550.

Humphries, C., et al. (2010). Tonotopic organization of human auditory cortex. *Neuroimage* **50**(3): 1202-1211.

Hunt, S.P., et al. (1987). Induction of c-fos-like protein in spinal cord neurons following sensory stimulation. *Nature* **328**(6131): 632-634.

Imbach, L.L., et al. (2015). Increased sleep need and daytime sleepiness 6 months after traumatic brain injury: a prospective controlled clinical trial. *Brain* **138**(Pt 3): 726-735.

Ioannides, A.A., et al. (2009). MEG identifies dorsal medial brain activations during sleep. *Neuroimage* **44**(2): 455-468.

Irwin, M.R., et al. (2008). Sleep loss activates cellular inflammatory signaling. *Biol Psychiatry* **64**(6): 538-540.

Isaac, S.O. and Berridge, C.W. (2003). Wake-promoting actions of dopamine D1 and D2 receptor stimulation. *J Pharmacol Exp Ther* **307**(1): 386-394.

Jacob, V., et al. (2012). Regular Spiking and Intrinsic Bursting Pyramidal Cells Show Orthogonal Forms of Experience-Dependent Plasticity in Layer V of Barrel Cortex. *Neuron* **73**(2): 391-404.

Jahn, H. (2013). Memory loss in Alzheimer's disease. *Dialogues Clin Neurosci* **15**(4): 445-454.

Jones, E.G. (2002). Thalamic organization and function after Cajal. *Prog Brain Res* **136**: 333-357.

Joo, J.Y., et al. (2016). Stimulus-specific combinatorial functionality of neuronal c-fos enhancers. *Nat Neurosci* **19**(1): 75-83.

Jutras, M.J. and Buffalo, E.A. (2014). Oscillatory correlates of memory in non-human primates. *Neuroimage* **85**: 694-701.

Kaas, J.H. (1993). The functional organization of somatosensory cortex in primates. *Annals of Anatomy - Anatomischer Anzeiger* **175**(6): 509-518.

Kaas, J.H., et al. (1983). The reorganization of somatosensory cortex following peripheral nerve damage in adult and developing mammals. *Annu Rev Neurosci* **6**: 325-356.

Kadi, L., et al. (2006). Differential effects of chemokines on oligodendrocyte precursor proliferation and myelin formation in vitro. *J Neuroimmunol* **174**(1-2): 133-146.

Kahana, M.J. (2006). The cognitive correlates of human brain oscillations. *J Neurosci* **26**(6): 1669-1672.

Kaiser, J. and Lutzenberger, W. (2005). Human gamma-band activity: a window to cognitive processing. *Neuroreport* **16**(3): 207-211.

Kalisman, N., et al. (2005). The neocortical microcircuit as a tabula rasa. *Proc Natl Acad Sci U S A* **102**(3): 880-885.

Kampa, B.M., et al. (2006). Cortical feed-forward networks for binding different streams of sensory information. *Nat Neurosci* **9**(12): 1472-1473.

Katche, C., et al. (2010). Delayed wave of c-Fos expression in the dorsal hippocampus involved specifically in persistence of long-term memory storage. *Proc Natl Acad Sci U S A* **107**(1): 349-354.

Kattler, H., et al. (1994). Effect of unilateral somatosensory stimulation prior to sleep on the sleep EEG in humans. *J Sleep Res* **3**(3): 159-164.

Kaye, P.M. (1987). Acquisition of cell-mediated immunity to Leishmania. I. Primary T-cell activation detected by IL-2 receptor expression. *Immunology* **61**(3): 345-349.

Kaye, P.M., et al. (1991). Differential production of Th1- and Th2-derived cytokines does not determine the genetically controlled or vaccine-induced rate of cure in murine visceral leishmaniasis. *The Journal of Immunology* **146**(8): 2763-2770.

Kellaway, P., et al. (1966). Electrical activity of the isolated cerebral hemisphere and isolated thalamus. *Experimental Neurology* **14**(3): 281-304.

Kelly, M.P. and Deadwyler, S.A. (2003). Experience-dependent regulation of the immediate-early gene arc differs across brain regions. *J Neurosci* **23**(16): 6443-6451.

Khodagholy, D., et al. (2016). Organic electronics for high-resolution electrocorticography of the human brain. *Sci Adv* **2**(11): e1601027.

Kim, Euiseok J., et al. (2015). Three Types of Cortical Layer 5 Neurons That Differ in Brain-wide Connectivity and Function. *Neuron* **88**(6): 1253-1267.

Kim, Y.K., et al. (2016). The role of pro-inflammatory cytokines in neuroinflammation, neurogenesis and the neuroendocrine system in major depression. *Prog Neuropsychopharmacol Biol Psychiatry* **64**: 277-284.

Kleim, J.A., et al. (1996). Synaptogenesis and Fos expression in the motor cortex of the adult rat after motor skill learning. *J Neurosci* **16**(14): 4529-4535.

Komine, O. (2015). Neuroinflammation in motor neuron disease. **77**(4): 537-549.

Kon Kim, K., et al. (2013). Herpes Virus Entry Mediator Signaling in the Brain Is Imperative in Acute Inflammation-Induced Anorexia and Body Weight Loss.

Koponen, H., et al. (1989). EEG spectral analysis in delirium. *J Neurol Neurosurg Psychiatry* **52**(8): 980-985.

Kovacs, K.J. (2008). Measurement of immediate-early gene activation- c-fos and beyond. *J Neuroendocrinol* **20**(6): 665-672.

Krueger, J.M., et al. (1986). Enhancement of slow-wave sleep by endotoxin and lipid A. *American Journal of Physiology-Regulatory, Integrative and Comparative Physiology* **251**(3): R591-R597.

Krueger, J.M., et al. (1984). Sleep-promoting effects of endogenous pyrogen (interleukin-1). *Am J Physiol* **246**(6 Pt 2): R994-999.

Kubba, R., et al. (1987). Peripheral nerve involvement in cutaneous leishmaniasis (Old World). *Int J Dermatol* **26**(8): 527-531.

Kubota, T., et al. (2001). Vagotomy attenuates tumor necrosis factor-alpha-induced sleep and EEG delta-activity in rats. *Am J Physiol Regul Integr Comp Physiol* **280**(4): R1213-1220.

Kuno, R., et al. (2005). Autocrine activation of microglia by tumor necrosis factor-alpha. *J Neuroimmunol* **162**(1-2): 89-96.

Labiner, D.M., et al. (1993). Induction of c-fos mRNA by kindled seizures: complex relationship with neuronal burst firing. *J Neurosci* **13**(2): 744-751.

Lam, D., et al. (2017). Responses of rat and mouse primary microglia to pro- and anti-inflammatory stimuli: molecular profiles, K+ channels and migration. *Journal of Neuroinflammation* **14**(1): 166.

Lante, F., et al. (2011). Removal of synaptic Ca(2)+-permeable AMPA receptors during sleep. *J Neurosci* **31**(11): 3953-3961.

Lata, S. and Raghava, G.P.S. (2009). Prediction and classification of chemokines and their receptors. *Protein Engineering, Design and Selection* **22**(7): 441-444.

Lauter, J.L., et al. (1985). Tonotopic organization in human auditory cortex revealed by positron emission tomography. *Hear Res* **20**(3): 199-205.

Le Bé, J.-V. and Markram, H. (2006). Spontaneous and evoked synaptic rewiring in the neonatal neocortex. *Proceedings of the National Academy of Sciences* **103**(35): 13214-13219.

LeBeau, F.E., et al. (2002). Fast network oscillations induced by potassium transients in the rat hippocampus in vitro. *J Physiol* **542**(Pt 1): 167-179.

Lee, J., et al. (2002). Adverse effect of a presenilin-1 mutation in microglia results in enhanced nitric oxide and inflammatory cytokine responses to immune challenge in the brain. *Neuromolecular Med* **2**(1): 29-45.

Lee, J.L., et al. (2004). Independent cellular processes for hippocampal memory consolidation and reconsolidation. *Science* **304**(5672): 839-843.

Lefort, S., et al. (2009). The excitatory neuronal network of the C2 barrel column in mouse primary somatosensory cortex. *Neuron* **61**(2): 301-316.

Lehnardt, S., et al. (2003). Activation of innate immunity in the CNS triggers neurodegeneration through a Toll-like receptor 4-dependent pathway. *Proceedings of the National Academy of Sciences* **100**(14): 8514-8519.

Leishman, W.B. (2006). On the possibility of the occurrence of trypanosomiasis in India. 1903. *Indian J Med Res* **123**(3): 1252-1254; discussion 1279.

Lemstra, A.W., et al. (2007). Microglia activation in sepsis: a case-control study. *J Neuroinflammation* **4**: 4.

Leow-Dyke, S., et al. (2012). Neuronal Toll-like receptor 4 signaling induces brain endothelial activation and neutrophil transmigration in vitro. *J Neuroinflammation* **9**: 230.

Li, S., et al. (2003). Dopamine-dependent facilitation of LTP induction in hippocampal CA1 by exposure to spatial novelty. *Nat Neurosci* **6**(5): 526-531.

Lin, Y., et al. (2015). EEG gamma-band activity during audiovisual speech comprehension in different noise environments. *Cogn Neurodyn* **9**(4): 389-398.

Link, W., et al. (1995). Somatodendritic expression of an immediate early gene is regulated by synaptic activity. *Proc Natl Acad Sci U S A* **92**(12): 5734-5738.

Liu, Z.W., et al. (2010). Direct evidence for wake-related increases and sleep-related decreases in synaptic strength in rodent cortex. *J Neurosci* **30**(25): 8671-8675.

Luckman, S.M., et al. (1994). Induction of c-fos expression in hypothalamic magnocellular neurons requires synaptic activation and not simply increased spike activity. *J Neurosci* **14**(8): 4825-4830.

Luheshi, N.M., et al. (2011). Interleukin-1α expression precedes IL-1β after ischemic brain injury and is localised to areas of focal neuronal loss and penumbral tissues. *Journal of Neuroinflammation* **8**(1): 186.

Lund, S., et al. (2006). The dynamics of the LPS triggered inflammatory response of murine microglia under different culture and in vivo conditions. *J Neuroimmunol* **180**(1-2): 71-87.

Lundqvist, M., et al. (2016). Gamma and beta bursts underlie working memory. *Neuron* **90**(1): 152-164.

Lüscher, C. and Huber, K.M. (2010). Group 1 mGluR-dependent synaptic long-term depression: mechanisms and implications for circuitry and disease. *Neuron* **65**(4): 445-459.

Luscher, C., et al. (1999). Role of AMPA receptor cycling in synaptic transmission and plasticity. *Neuron* **24**(3): 649-658.

Luz, C., et al. (2003). Impact of psychological and endocrine factors on cytokine production of healthy elderly people. *Mech Ageing Dev* **124**(8-9): 887-895.

Lyford, G.L., et al. (1995). Arc, a growth factor and activity-regulated gene, encodes a novel cytoskeleton-associated protein that is enriched in neuronal dendrites. *Neuron* **14**(2): 433-445.

Mably, A.J., et al. (2017). Impairments in spatial representations and rhythmic coordination of place cells in the 3xTg mouse model of Alzheimer's disease. *Hippocampus* **27**(4): 378-392.

Maciejewski-Lenoir, D., et al. (1999). Characterization of fractalkine in rat brain cells: migratory and activation signals for CX3CR-1-expressing microglia. *J Immunol* **163**(3): 1628-1635.

Madsen, P.L. and Vorstrup, S. (1991). Cerebral blood flow and metabolism during sleep. *Cerebrovasc Brain Metab Rev* **3**(4): 281-296.

Magaki, S., et al. (2007). Increased production of inflammatory cytokines in mild cognitive impairment. *Exp Gerontol* **42**(3): 233-240.

Magazzini, L. and Singh, K.D. (2018). Spatial attention modulates visual gamma oscillations across the human ventral stream. *Neuroimage* **166**: 219-229.

Maghazachi, A.A., et al. (1996). CC chemokines induce the generation of killer cells from CD56+ cells. *Eur J Immunol* **26**(2): 315-319.

Mamad, O., et al. (2018). Differential response of hippocampal and prefrontal oscillations to systemic LPS application. *Brain Res* **1681**: 64-74.

Managò, F., et al. (2016). Genetic disruption of Arc/Arg3.1 in mice causes alterations in dopamine and neurobehavioral phenotypes related to schizophrenia. *Cell Rep* **16**(8): 2116-2128.

Maquet, P. (1997). Positron emission tomography studies of sleep and sleep disorders. *J Neurol* **244**(4 Suppl 1): S23-28.

Maret, S., et al. (2011). Sleep and waking modulate spine turnover in the adolescent mouse cortex. *Nat Neurosci* **14**(11): 1418-1420.

Markram, H., et al. (2012). Spike-Timing-Dependent Plasticity: A Comprehensive Overview. *Front Synaptic Neurosci* **4**.

Markram, H., et al. (1997). Regulation of Synaptic Efficacy by Coincidence of Postsynaptic APs and EPSPs. *Science* **275**(5297): 213-215.

Marrosu, F., et al. (1995). Microdialysis measurement of cortical and hippocampal acetylcholine release during sleep-wake cycle in freely moving cats. *Brain Res* **671**(2): 329-332.

Maru, M. (1979). Clinical and laboratory features and treatment of visceral leishmaniasis in hospitalized patients in Northwestern Ethiopia. *Am J Trop Med Hyg* **28**(1): 15-18.

Maruoka, H., et al. (2011). Periodic organization of a major subtype of pyramidal neurons in neocortical layer V. *J Neurosci* **31**(50): 18522-18542.

Maruoka, H., et al. (2017). Lattice system of functionally distinct cell types in the neocortex. *Science* **358**(6363): 610-615.

McCormick, D.A. (1992). Neurotransmitter actions in the thalamus and cerebral cortex and their role in neuromodulation of thalamocortical activity. *Prog Neurobiol* **39**(4): 337-388.

McManus, R.M. and Heneka, M.T. (2017). Role of neuroinflammation in neurodegeneration: new insights. *Alzheimers Res Ther* **9**.

Melchionda, F., et al. (2014). Spleen nodules: a potential hallmark of Visceral Leishmaniasis in young children. *BMC Infect Dis* **14**.

Melo, G.D. (2017). New insights into experimental visceral leishmaniasis: Real-time in vivo imaging of Leishmania donovani virulence. **11**(9).

Melo, G.D., et al. (2017). Unveiling Cerebral Leishmaniasis: parasites and brain inflammation in Leishmania donovani infected mice. *Sci Rep* **7**(1): 8454.

Melo, G.D. and Machado, G.F. (2011). Glial reactivity in dogs with visceral leishmaniasis: correlation with T lymphocyte infiltration and with cerebrospinal fluid anti-Leishmania antibody titres. *Cell Tissue Res* **346**(3): 293-304.

Melo, G.D., et al. (2009). Leukocyte entry into the CNS of Leishmania chagasi naturally infected dogs. *Vet Parasitol* **162**(3-4): 248-256.

Melo, G.D., et al. (2013). Pro-inflammatory cytokines predominate in the brains of dogs with visceral leishmaniasis: a natural model of neuroinflammation during systemic parasitic infection. *Vet Parasitol* **192**(1-3): 57-66.

Melo, G.D., et al. (2015). Leishmania infection and neuroinflammation: Specific chemokine profile and absence of parasites in the brain of naturally-infected dogs. *J Neuroimmunol* **289**: 21-29.

Menzel, R.R. and Barth, D.S. (2005). Multisensory and Secondary Somatosensory Cortex in the Rat. *Cerebral Cortex* **15**(11): 1690-1696.

Messaoudi, E., et al. (2007). Sustained Arc/Arg3.1 synthesis controls long-term potentiation consolidation through regulation of local actin polymerization in the dentate gyrus in vivo. *J Neurosci* **27**(39): 10445-10455.

Middleton, S., et al. (2008). NMDA receptor-dependent switching between different gamma rhythm-generating microcircuits in entorhinal cortex. *Proc Natl Acad Sci U S A* **105**(47): 18572-18577.

Miles, R. and Poncer, J.C. (1993). Metabotropic glutamate receptors mediate a post-tetanic excitation of guinea-pig hippocampal inhibitory neurones. *J Physiol* **463**: 461-473.

Minty, A., et al. (1993). Interleukin-13 is a new human lymphokine regulating inflammatory and immune responses. *Nature* **362**: 248.

Mishkin, M. (1979). Analogous neural models for tactual and visual learning. *Neuropsychologia* **17**(2): 139-151.

Miyamoto, D. and Murayama, M. (2016). The fiber-optic imaging and manipulation of neural activity during animal behavior. *Neurosci Res* **103**: 1-9.

Miyawaki, H. and Diba, K. (2016). Regulation of Hippocampal Firing by Network Oscillations during Sleep. *Curr Biol* **26**(7): 893-902.

Modarres, M.H., et al. (2017). EEG slow waves in traumatic brain injury: Convergent findings in mouse and man. *Neurobiology of Sleep and Circadian Rhythms* **2**: 59-70.

Monif, M., et al. (2016). Interleukin-1β has trophic effects in microglia and its release is mediated by P2X7R pore. *Journal of Neuroinflammation* **13**(1): 173.

Monti, J.M., et al. (1990). Sleep during acute dopamine D1 agonist SKF 38393 or D1 antagonist SCH 23390 administration in rats. *Neuropsychopharmacology* **3**(3): 153-162.

Monti, J.M. and Jantos, H. (2008). The roles of dopamine and serotonin, and of their receptors, in regulating sleep and waking. *Prog Brain Res* **172**: 625-646.

Moreira, N., et al. (2012). Parasite burden in hamsters infected with two different strains of leishmania (Leishmania) infantum: "Leishman Donovan units" versus real-time PCR. *PLoS One* **7**(10): e47907.

Morgan, J.I., et al. (1987). Mapping patterns of c-fos expression in the central nervous system after seizure. *Science* **237**(4811): 192-197.

Morgan, J.I. and Curran, T. (1989). Stimulus-transcription coupling in neurons: role of cellular immediate-early genes. *Trends Neurosci* **12**(11): 459-462.

Mori, S., et al. (2016). Neuroimmunology of the Interleukins 13 and 4. *Brain Sci* **6**(2).

Mormann, F., et al. (2008). Independent delta/theta rhythms in the human hippocampus and entorhinal cortex. *Front Hum Neurosci* **2**: 3.

Mountcastle, V.B. (1957). Modality and topographic properties of single neurons of cat's somatic sensory cortex. *J Neurophysiol* **20**(4): 408-434.

Mountcastle, V.B., et al. (1957). Response properties of neurons of cat's somatic sensory cortex to peripheral stimuli. *J Neurophysiol* **20**(4): 374-407.

Mullington, J.M., et al. (2010). Sleep Loss and Inflammation. *Best Pract Res Clin Endocrinol Metab* **24**(5): 775-784.

Murdoch, C. and Finn, A. (2000). Chemokine receptors and their role in inflammation and infectious diseases. *Blood* **95**(10): 3032-3043.

Murphy, P.M. (1994). The molecular biology of leukocyte chemoattractant receptors. *Annu Rev Immunol* **12**: 593-633.

Mustafa, D. (1965). Neurological disturbances in visceral leishmaniasis. *J Trop Med Hyg* **68**(10): 248-250.

Nadeau, S. and Rivest, S. (1999). Effects of circulating tumor necrosis factor on the neuronal activity and expression of the genes encoding the tumor necrosis factor receptors (p55 and p75) in the rat brain: a view from the blood-brain barrier. *Neuroscience* **93**(4): 1449-1464.

Nadeau, S. and Rivest, S. (2000). Role of microglial-derived tumor necrosis factor in mediating CD14 transcription and nuclear factor kappa B activity in the brain during endotoxemia. *J Neurosci* **20**(9): 3456-3468.

Nakanishi, H., et al. (1997). Positive correlations between cerebral protein synthesis rates and deep sleep in Macaca mulatta. *Eur J Neurosci* **9**(2): 271-279.

Nakao, S., et al. (2002). Ketamine-induced c-Fos expression in the mouse posterior cingulate and retrosplenial cortices is mediated not only via NMDA receptors but also via sigma receptors. *Brain Res* **926**(1-2): 191-196.

Natalwala, A., et al. (2008). Reasons for hospital admissions in dementia patients in Birmingham, UK, during 2002-2007. *Dement Geriatr Cogn Disord* **26**(6): 499-505.

Neniskyte, U., et al. (2014). Tumour necrosis factor alpha-induced neuronal loss is mediated by microglial phagocytosis. *FEBS Lett* **588**(17): 2952-2956.

Nieto, C.G., et al. (1996). Detection of Leishmania infantum amastigotes in canine choroid plexus. *Vet Rec* **139**(14): 346-347.

Nimmerjahn, A., et al. (2005). Resting Microglial Cells Are Highly Dynamic Surveillants of Brain Parenchyma in Vivo. *Science* **308**(5726): 1314-1318.

Nishida, M., et al. (2008). Cortical glucose metabolism positively correlates with gamma-oscillations in nonlesional focal epilepsy. *Neuroimage* **42**(4): 1275-1284.

Nishioku, T., et al. (2009). Detachment of brain pericytes from the basal lamina is involved in disruption of the blood-brain barrier caused by lipopolysaccharide-induced sepsis in mice. *Cell Mol Neurobiol* **29**(3): 309-316.

O'Keeffe, S.T. and Ni Chonchubhair, A. (1994). Postoperative delirium in the elderly. *Br J Anaesth* **73**(5): 673-687.

Ohmori, Y. and Hamilton, T.A. (1998). STAT6 is required for the anti-inflammatory activity of interleukin-4 in mouse peritoneal macrophages. *J Biol Chem* **273**(44): 29202-29209.

Oliveira, V.D.C., et al. (2017). Occurrence of Leishmania infantum in the central nervous system of naturally infected dogs: Parasite load, viability, co-infections and histological alterations. *PLoS One* **12**(4): e0175588.

Opal, S.M. and DePalo, V.A. (2000). Anti-inflammatory cytokines. *Chest* **117**(4): 1162-1172.

Opp, M.R. and Toth, L.A. (1998). Somnogenic and pyrogenic effects of interleukin-1beta and lipopolysaccharide in intact and vagotomized rats. *Life Sci* **62**(10): 923-936.

Oppenheim, J.J., et al. (1989). Relationship between interleukin 1 (IL1), tumor necrosis factor (TNF) and a neutrophil attracting peptide (NAP-1). *Agents Actions* **26**(1-2): 134-140.

Pace-Schott, E.F. and Hobson, J.A. (2002). The neurobiology of sleep: genetics, cellular physiology and subcortical networks. *Nat Rev Neurosci* **3**(8): 591-605.

Paolicelli, R.C., et al. (2014). Fractalkine regulation of microglial physiology and consequences on the brain and behavior. *Front Cell Neurosci* **8**.

Paolicelli, R.C., et al. (2011). Synaptic pruning by microglia is necessary for normal brain development. *Science* **333**(6048): 1456-1458.

Papageorgiou, I.E., et al. (2016). TLR4-activated microglia require IFN-γ to induce severe neuronal dysfunction and death in situ. *Proceedings of the National Academy of Sciences* **113**(1): 212-217.

Pape, H.C. (1992). Adenosine promotes burst activity in guinea-pig geniculocortical neurones through two different ionic mechanisms. *J Physiol* **447**: 729-753.

Park, S., et al. (2008). Elongation factor 2 and fragile X mental retardation protein control the dynamic translation of Arc/Arg3.1 essential for mGluR-LTD. *Neuron* **59**(1): 70-83.

Parsons, L.C., et al. (1997). Longitudinal sleep EEG power spectral analysis studies in adolescents with minor head injury. *J Neurotrauma* **14**(8): 549-559.

Paxinos, G. and Watson, C. (1998). The Rat Brain: In Stereotaxic Coordinates, Academic Press.

Pease, J.E. (2006). Tails of the unexpected - an atypical receptor for the chemokine RANTES/CCL5 expressed in brain. *Br J Pharmacol* **149**(5): 460-462.

Perez-Garci, E., et al. (2006). The GABAB1b isoform mediates long-lasting inhibition of dendritic Ca2+ spikes in layer 5 somatosensory pyramidal neurons. *Neuron* **50**(4): 603-616.

Perez-Garci, E., et al. (2013). Inhibition of dendritic Ca2+ spikes by GABAB receptors in cortical pyramidal neurons is mediated by a direct Gi/o-beta-subunit interaction with Cav1 channels. *J Physiol* **591**(7): 1599-1612.

Perin, R., et al. (2011). A synaptic organizing principle for cortical neuronal groups. *Proceedings of the National Academy of Sciences* **108**(13): 5419-5424.

Perry, V.H., et al. (2003). The impact of systemic infection on the progression of neurodegenerative disease. *Nature Reviews Neuroscience* **4**: 103.

Pevzner, A., et al. (2016). Making Waves in the Brain: What Are Oscillations, and Why Modulating Them Makes Sense for Brain Injury. *Front Syst Neurosci* **10**.

Pinto, et al. (2017). TNF signalling drives expansion of bone marrow CD4+ T cells responsible for HSC exhaustion in experimental visceral leishmaniasis. *PLoS Pathog* **13**(7): e1006465.

Plath, N., et al. (2006). Arc/Arg3.1 is essential for the consolidation of synaptic plasticity and memories. *Neuron* **52**(3): 437-444.

Ploner, M., et al. (1999). Parallel activation of primary and secondary somatosensory cortices in human pain processing. *J Neurophysiol* **81**(6): 3100-3104.

Polley, R., et al. (2005). Chronic Leishmania donovani Infection Promotes Bystander CD8⁺-T-Cell Expansion and Heterologous Immunity. *Infection and Immunity* **73**(12): 7996-8001.

Pollmacher, T., et al. (1993). Influence of endotoxin on nocturnal sleep in humans. *Am J Physiol* **264**(6 Pt 2): R1077-1083.

Pompeiano, M., et al. (1995). c-Fos expression during wakefulness and sleep. *Neurophysiologie Clinique/Clinical Neurophysiology* **25**(6): 329-341.

Porkka-Heiskanen, T., et al. (1997). Adenosine: a mediator of the sleep-inducing effects of prolonged wakefulness. *Science* **276**(5316): 1265-1268.

Portes, A., et al. (2016). Leishmania amazonensis infection induces behavioral alterations and modulates cytokine and neurotrophin production in the murine cerebral cortex. *J Neuroimmunol* **301**: 65-73.

Potter-Baker, K.A., et al. (2014). A comparison of neuroinflammation to implanted microelectrodes in rat and mouse models. *Biomaterials* **35**(22): 5637-5646.

Prasad, L.S. and Sen, S. (1996). Migration of Leishmania donovani amastigotes in the cerebrospinal fluid. *Am J Trop Med Hyg* **55**(6): 652-654.

Prat, A., et al. (2001). Glial cell influence on the human blood-brain barrier. *Glia* **36**(2): 145-155.

Probert, L. (2015). TNF and its receptors in the CNS: The essential, the desirable and the deleterious effects. *Neuroscience* **302**: 2-22.

Purves, D., et al. (2008). Neuroscience. 4th. *Sunderland, Mass.: Sinauer. xvii* **857**: 944.

Rael, E.L. and Lockey, R.F. (2011). Interleukin-13 Signaling and Its Role in Asthma. *World Allergy Organ J* **4**(3): 54-64.

Ramesh, G., et al. (2013). Cytokines and Chemokines at the Crossroads of Neuroinflammation, Neurodegeneration, and Neuropathic Pain. *Mediators of Inflammation* **2013**: 20.

Ramm, P. and Smith, C.T. (1990). Rates of cerebral protein synthesis are linked to slow wave sleep in the rat. *Physiol Behav* **48**(5): 749-753.

Ramón y Cajal, S. (1991). Histologie du Systeme Nerveux de l'Homme et des Vertébrés, Maloine, Paris.

Ramos, P.K., et al. (2014). In vitro cytokines profile and ultrastructural changes of microglia and macrophages following interaction with Leishmania. *Parasitology* **141**(8): 1052-1063.

Rangroo Thrane, V., et al. (2012). Real-time analysis of microglial activation and motility in hepatic and hyperammonemic encephalopathy. *Neuroscience* **220**: 247-255.

Ransohoff, R.M. (2009). Chemokines and chemokine receptors: Standing at the crossroads of immunobiology and neurobiology. *Immunity* **31**(5): 711-721.

Ransohoff, R.M., et al. (2007). Chemokines and Chemokine Receptors: Multipurpose Players in Neuroinflammation. International Review of Neurobiology, Academic Press. **82:** 187-204.

Rao, V.R., et al. (2006). AMPA receptors regulate transcription of the plasticity-related immediate-early gene Arc. *Nat Neurosci* **9**(7): 887-895.

Ray, S., et al. (2008). Effect of stimulus intensity on the spike-local field potential relationship in the secondary somatosensory cortex. *J Neurosci* **28**(29): 7334-7343.

Rechtschaffen, A. (1998). Current perspectives on the function of sleep. *Perspect Biol Med* **41**(3): 359-390.

Rector, D.M., et al. (2005). Local functional state differences between rat cortical columns. *Brain Res* **1047**(1): 45-55.

Reed-Geaghan, E.G., et al. (2009). CD14 and toll-like receptors 2 and 4 are required for fibrillar A{beta}-stimulated microglial activation. *J Neurosci* **29**(38): 11982-11992.

Reichenberg, A., et al. (2001). Cytokine-associated emotional and cognitive disturbances in humans. *Arch Gen Psychiatry* **58**(5): 445-452.

Rial Verde, E.M., et al. (2006). Increased expression of the immediate-early gene arc/arg3.1 reduces AMPA receptor-mediated synaptic transmission. *Neuron* **52**(3): 461-474.

Ribeiro, S., et al. (1999). Brain gene expression during REM sleep depends on prior waking experience. *Learn Mem* **6**(5): 500-508.

Ribeiro, S., et al. (2007). Novel experience induces persistent sleep-dependent plasticity in the cortex but not in the hippocampus. *Front Neurosci* **1**(1): 43-55.

Riedner, B.A., et al. (2007). Sleep Homeostasis and Cortical Synchronization: III. A High-Density EEG Study of Sleep Slow Waves in Humans. *Sleep* **30**(12): 1643-1657.

Ringheim, G.E., et al. (1995). Interleukin-6 mRNA expression by cortical neurons in culture: evidence for neuronal sources of interleukin-6 production in the brain. *J Neuroimmunol* **63**(2): 113-123.

Ro, T., et al. (2013). A neural link between feeling and hearing. *Cereb Cortex* **23**(7): 1724-1730.

Ro, T., et al. (2009). Sound enhances touch perception. *Exp Brain Res* **195**(1): 135-143.

Rock, R.B., et al. (2005). Transcriptional response of human microglial cells to interferon-gamma. *Genes Immun* **6**(8): 712-719.

Rockel, A.J., et al. (1980). The basic uniformity in structure of the neocortex. *Brain* **103**(2): 221-244.

Rockland, K.S. and Drash, G.W. (1996). Collateralized divergent feedback connections that target multiple cortical areas. *J Comp Neurol* **373**(4): 529-548.

Rodgers, K.M., et al. (2009). The cortical innate immune response increases local neuronal excitability leading to seizures. *Brain* **132**(Pt 9): 2478-2486.

Rodriguez, A.V., et al. (2016). Why Does Sleep Slow-Wave Activity Increase After Extended Wake? Assessing the Effects of Increased Cortical Firing During Wake and Sleep. *J Neurosci* **36**(49): 12436-12447.

Roopun, A.K., et al. (2008). Period concatenation underlies interactions between gamma and beta rhythms in neocortex. *Front Cell Neurosci* **2**: 1.

Roopun, A.K., et al. (2006). A beta2-frequency (20-30 Hz) oscillation in nonsynaptic networks of somatosensory cortex. *Proc Natl Acad Sci U S A* **103**(42): 15646-15650.

Rosen, K.M., et al. (1992). Brief visual experience induces immediate early gene expression in the cat visual cortex. *Proceedings of the National Academy of Sciences* **89**(12): 5437-5441.

Ross, R. (1903a). Further notes on Leishman's bodies. *Br Med J* **2**(2239): 1401.

Ross, R. (1903b). Note on the bodies recently described by Leishman and Donovan. *Br Med J* **2**(2237): 1261-1262.

Rossato, J.I., et al. (2009). Dopamine controls persistence of long-term memory storage. *Science* **325**(5943): 1017-1020.

Rossiter, H.E., et al. (2013). Gamma oscillatory amplitude encodes stimulus intensity in primary somatosensory cortex. *Front Hum Neurosci* **7**: 362.

Rothenburg, L.S., et al. (2010). The relationship between inflammatory markers and post stroke cognitive impairment. *J Geriatr Psychiatry Neurol* **23**(3): 199-205.

Rothwell, N.J. and Luheshi, G.N. (2000). Interleukin 1 in the brain: biology, pathology and therapeutic target. *Trends Neurosci* **23**(12): 618-625.

Rovira, C., et al. (1983). Pharmacology of the dendritic action of acetylcholine and further observations on the somatic disinhibition in the rat hippocampus in situ. *Neuroscience* **8**(1): 97-106.

Rubio-Garrido, P., et al. (2009). Thalamic input to distal apical dendrites in neocortical layer 1 is massive and highly convergent. *Cereb Cortex* **19**(10): 2380-2395.

Rumah, K.R., et al. (2013). Isolation of Clostridium perfringens type B in an individual at first clinical presentation of multiple sclerosis provides clues for environmental triggers of the disease. *PLoS One* **8**(10): e76359.

Rupalla, K., et al. (1998). Time course of microglia activation and apoptosis in various brain regions after permanent focal cerebral ischemia in mice. *Acta Neuropathol* **96**(2): 172-178.

Sadek, M.I., et al. (1998). Chemokines induced by infection of mononuclear phagocytes with mycobacteria and present in lung alveoli during active pulmonary tuberculosis. *Am J Respir Cell Mol Biol* **19**(3): 513-521.

Sahara, S., et al. (2012). The fraction of cortical GABAergic neurons is constant from near the start of cortical neurogenesis to adulthood. *J Neurosci* **32**(14): 4755-4761.

Sallmann, S., et al. (2000). Induction of interleukin-6 by depolarization of neurons. *J Neurosci* **20**(23): 8637-8642.

Sampson, T.R., et al. (2016). Gut Microbiota Regulate Motor Deficits and Neuroinflammation in a Model of Parkinson's Disease. *Cell* **167**(6): 1469-1480.e1412.

Sani, M.R.M., et al. (2014). Investigation of caspase-1 activity and interleukin-1β production in murine macrophage cell lines infected with Leishmania major. *Asian Pacific Journal of Tropical Medicine* **7**: S70-S73.

Santos, D., et al. (2018). IL-1β Production by Intermediate Monocytes Is Associated with Immunopathology in Cutaneous Leishmaniasis. *Journal of Investigative Dermatology* **138**(5): 1107-1115.

Sanyal, S., et al. (2002). AP-1 functions upstream of CREB to control synaptic plasticity in Drosophila. *Nature* **416**(6883): 870-874.

Schall, T.J. and Proudfoot, A.E.I. (2011). Overcoming hurdles in developing successful drugs targeting chemokine receptors. *Nature Reviews Immunology* **11**: 355.

Schoenenberger, P., et al. (2009). Temporal control of immediate early gene induction by light. *PLoS One* **4**(12): e8185.

Sederberg, P.B., et al. (2007). Hippocampal and neocortical gamma oscillations predict memory formation in humans. *Cereb Cortex* **17**(5): 1190-1196.

Seibt, J., et al. (2012). Protein synthesis during sleep consolidates cortical plasticity in vivo. *Curr Biol* **22**(8): 676-682.

Semmler, A., et al. (2005). Systemic inflammation induces apoptosis with variable vulnerability of different brain regions. *J Chem Neuroanat* **30**(2-3): 144-157.

Servant, G., et al. (2000). Polarization of Chemoattractant Receptor Signaling During Neutrophil Chemotaxis. *Science* **287**(5455): 1037-1040.

Servant, G., et al. (1999). Dynamics of a chemoattractant receptor in living neutrophils during chemotaxis. *Mol Biol Cell* **10**(4): 1163-1178.

Shearer, W.T., et al. (2001). Soluble TNF-alpha receptor 1 and IL-6 plasma levels in humans subjected to the sleep deprivation model of spaceflight. *J Allergy Clin Immunol* **107**(1): 165-170.

Shepherd, J.D. (2012). Memory, plasticity and sleep - A role for calcium permeable AMPA receptors? *Front Mol Neurosci* **5**.

Shepherd, J.D., et al. (2006). Arc/Arg3.1 mediates homeostatic synaptic scaling of AMPA receptors. *Neuron* **52**(3): 475-484.

Shin, Y.W., et al. (2011). Gamma oscillation in schizophrenia. *Psychiatry Investig* **8**(4): 288-296.

Siami, S., et al. (2008). The encephalopathy in sepsis. *Crit Care Clin* **24**(1): 67-82, viii.

Simen, A.A., et al. (2011). Cognitive Dysfunction with Aging and the Role of Inflammation. *Ther Adv Chronic Dis* **2**(3): 175-195.

Simons, D.J. (1978). Response properties of vibrissa units in rat SI somatosensory neocortex. *J Neurophysiol* **41**(3): 798-820.

Sims, J.E., et al. (1988). cDNA expression cloning of the IL-1 receptor, a member of the immunoglobulin superfamily. *Science* **241**(4865): 585-589.

Singer, W. (1993). Synchronization of cortical activity and its putative role in information processing and learning. *Annu Rev Physiol* **55**: 349-374.

Singh, A.K. and Jiang, Y. (2004). How does peripheral lipopolysaccharide induce gene expression in the brain of rats? *Toxicology* **201**(1-3): 197-207.

Sly, L.M., et al. (2001). Endogenous brain cytokine mRNA and inflammatory responses to lipopolysaccharide are elevated in the Tg2576 transgenic mouse model of Alzheimer's disease. *Brain Res Bull* **56**(6): 581-588.

Smeyne, R.J., et al. (1992). fos-lacZ transgenic mice: mapping sites of gene induction in the central nervous system. *Neuron* **8**(1): 13-23.

Sokolowski, J.D., et al. (2014). Fractalkine is a "find-me" signal released by neurons undergoing ethanol-induced apoptosis. *Front Cell Neurosci* **8**.

Soltesz, I., et al. (1991). Two inward currents and the transformation of low-frequency oscillations of rat and cat thalamocortical cells. *J Physiol* **441**: 175-197.

Sriram, K., et al. (2006). Deficiency of TNF receptors suppresses microglial activation and alters the susceptibility of brain regions to MPTP-induced neurotoxicity: role of TNF-α. *The FASEB Journal* **20**(6): 670-682.

Stamatovic, S.M., et al. (2008). Brain endothelial cell-cell junctions: how to "open" the blood brain barrier. *Curr Neuropharmacol* **6**(3): 179-192.

Steinmetz, P.N., et al. (2000). Attention modulates synchronized neuronal firing in primate somatosensory cortex. *Nature* **404**(6774): 187-190.

Steriade, M. (2003). The corticothalamic system in sleep. *Front Biosci* **8**: d878-899.

Steriade, M., et al. (1991). Network modulation of a slow intrinsic oscillation of cat thalamocortical neurons implicated in sleep delta waves: cortically induced synchronization and brainstem cholinergic suppression. *J Neurosci* **11**(10): 3200-3217.

Stevenson, R., et al. (2014). The interaction between stimulus factors and cognitive factors during multisensory integration of audiovisual speech.

Steverding, D. (2017). The history of leishmaniasis. *Parasit Vectors* **10**(1): 82.

Steward, O., et al. (1998). Synaptic activation causes the mRNA for the IEG Arc to localize selectively near activated postsynaptic sites on dendrites. *Neuron* **21**(4): 741-751.

Steward, O. and Worley, P.F. (2001). Selective targeting of newly synthesized Arc mRNA to active synapses requires NMDA receptor activation. *Neuron* **30**(1): 227-240.

Storey, J.D. and Tibshirani, R. (2003). Statistical significance for genomewide studies. *Proc Natl Acad Sci U S A* **100**(16): 9440-9445.

Strandberg, T.E., et al. (2004). Cognitive impairment and infectious burden in the elderly. *Arch Gerontol Geriatr Suppl*(9): 419-423.

Sulakhiya, K., et al. (2016). Lipopolysaccharide induced anxiety- and depressive-like behaviour in mice are prevented by chronic pre-treatment of esculetin. *Neurosci Lett* **611**: 106-111.

Svarnik, O.E., et al. (2005). Fos expression and task-related neuronal activity in rat cerebral cortex after instrumental learning. *Neuroscience* **136**(1): 33-42.

Svarnik, O.E., et al. (2013). Expression of c-Fos in the rat retrosplenial cortex during instrumental re-learning of appetitive bar-pressing depends on the number of stages of previous training. *Front Behav Neurosci* **7**: 78.

Tafuri, W.L., et al. (2004). An alternative immunohistochemical method for detecting Leishmania amastigotes in paraffin-embedded canine tissues. *J Immunol Methods* **292**(1-2): 17-23.

Takahata, K., et al. (2017). A human PET study of [(11)C]HMS011, a potential radioligand for AMPA receptors. *EJNMMI Res* **7**(1): 63.

Tallon-Baudry, C. and Bertrand, O. (1999). Oscillatory gamma activity in humans and its role in object representation. *Trends Cogn Sci* **3**(4): 151-162.

Taylor, D.L., et al. (2003). Activation of microglial group III metabotropic glutamate receptors protects neurons against microglial neurotoxicity. *J Neurosci* **23**(6): 2150-2160.

Taylor, D.L., et al. (2005). Stimulation of microglial metabotropic glutamate receptor mGlu2 triggers tumor necrosis factor alpha-induced neurotoxicity in concert with microglial-derived Fas ligand. *J Neurosci* **25**(11): 2952-2964.

Tchessalova, D. and Tronson, N.C. (2019). Memory deficits in males and females long after subchronic immune challenge. *Neurobiol Learn Mem*.

Thome, A.D., et al. (2015). Fractalkine Signaling Regulates the Inflammatory Response in an alpha-Synuclein Model of Parkinson Disease. *PLoS One* **10**(10): e0140566.

Thompson, C.L., et al. (2010). Molecular and anatomical signatures of sleep deprivation in the mouse brain. *Front Neurosci* **4**: 165.

Thompson, W.L., et al. (2008). MCP-1-deficient mice show reduced neuroinflammatory responses and increased peripheral inflammatory responses to peripheral endotoxin insult. *Journal of Neuroinflammation* **5**(1): 35.

Thomson, A.M. and Bannister, A.P. (2003). Interlaminar connections in the neocortex. *Cereb Cortex* **13**(1): 5-14.

Thomson, A.M., et al. (2002). Synaptic connections and small circuits involving excitatory and inhibitory neurons in layers 2-5 of adult rat and cat neocortex: triple intracellular recordings and biocytin labelling in vitro. *Cereb Cortex* **12**(9): 936-953.

Thuc, O., et al. (2015). The complex contribution of chemokines to neuroinflammation: switching from beneficial to detrimental effects. *Annals of the New York Academy of Sciences* **1351**(1): 127-140.

Timofeev, I., et al. (2000). Origin of slow cortical oscillations in deafferented cortical slabs. *Cereb Cortex* **10**(12): 1185-1199.

Ting, J.T., et al. (2014). Acute brain slice methods for adult and aging animals: application of targeted patch clamp analysis and optogenetics. *Methods Mol Biol* **1183**: 221-242.

Tokami, H., et al. (2013). RANTES has a potential to play a neuroprotective role in an autocrine/paracrine manner after ischemic stroke. *Brain Res* **1517**: 122-132.

Tononi, G. and Cirelli, C. (2001). Some considerations on sleep and neural plasticity. *Arch Ital Biol* **139**(3): 221-241.

Tononi, G. and Cirelli, C. (2003). Sleep and synaptic homeostasis: a hypothesis. *Brain Res Bull* **62**(2): 143-150.

Tononi, G. and Cirelli, C. (2006). Sleep function and synaptic homeostasis. *Sleep Med Rev* **10**(1): 49-62.

Tononi, G. and Cirelli, C. (2014). Sleep and the price of plasticity: from synaptic and cellular homeostasis to memory consolidation and integration. *Neuron* **81**(1): 12-34.

Toth, L.A. and Krueger, J.M. (1989). Effects of microbial challenge on sleep in rabbits. *Faseb j* **3**(9): 2062-2066.

Traub, R.D., et al. (1997). Simulation of gamma rhythms in networks of interneurons and pyramidal cells. *J Comput Neurosci* **4**(2): 141-150.

Traub, R.D., et al. (1996). Analysis of gamma rhythms in the rat hippocampus in vitro and in vivo. *J Physiol* **493 (Pt 2)**: 471-484.

Traub, R.D., et al. (2017). Does Epileptiform Activity Represent a Failure of Neuromodulation to Control Central Pattern Generator-Like Neocortical Behavior? *Front Neural Circuits* **11**: 78.

Tseng, Y.T., et al. (2012). Paeonol attenuates microglia-mediated inflammation and oxidative stress-induced neurotoxicity in rat primary microglia and cortical neurons. *Shock* **37**(3): 312-318.

Tsintsadze, V., et al. (2015). Ontogeny of kainate-induced gamma oscillations in the rat CA3 hippocampus in vitro. *Front Cell Neurosci* **9**: 195.

Tsunoda, K., et al. (2001). Complex objects are represented in macaque inferotemporal cortex by the combination of feature columns. *Nat Neurosci* **4**(8): 832-838.

Turkekul, M., et al. (2017). Automated Double In Situ Detection of Mouse Lgr5 mRNA and Lysozyme Protein in Examining the Neighboring Cell Types of the Mouse Intestinal Crypt. Signal Transduction Immunohistochemistry: Methods and Protocols. A. E. Kalyuzhny. New York, NY, Springer New York**:** 263-272.

Turner, R. and Tjian, R. (1989). Leucine repeats and an adjacent DNA binding domain mediate the formation of functional cFos-cJun heterodimers. *Science* **243**(4899): 1689-1694.

Turrigiano, G.G. and Nelson, S.B. (2000). Hebb and homeostasis in neuronal plasticity. *Curr Opin Neurobiol* **10**(3): 358-364.

Tuvikene, J., et al. (2016). AP-1 Transcription Factors Mediate BDNF-Positive Feedback Loop in Cortical Neurons. *J Neurosci* **36**(4): 1290-1305.

Ubeda-Contreras, J., et al. (2018). Brain c-fos expression patterns induced by emotional stressors differing in nature and intensity. *Brain Struct Funct* **223**(5): 2213-2227.

Udan, M.L., et al. (2008). Toll-like receptors 2 and 4 mediate Abeta(1-42) activation of the innate immune response in a human monocytic cell line. *J Neurochem* **104**(2): 524-533.

Van der Jeugd, A., et al. (2011). Hippocampal tauopathy in tau transgenic mice coincides with impaired hippocampus-dependent learning and memory, and attenuated late-phase long-term depression of synaptic transmission. *Neurobiol Learn Mem* **95**(3): 296-304.

van Munster, B.C., et al. (2011). Neuroinflammation in Delirium: A Postmortem Case-Control Study. *Rejuvenation Res* **14**(6): 615-622.

van Munster, B.C., et al. (2008). Time-course of cytokines during delirium in elderly patients with hip fractures. *J Am Geriatr Soc* **56**(9): 1704-1709.

van Vugt, M.K., et al. (2010). Hippocampal gamma oscillations increase with memory load. *J Neurosci* **30**(7): 2694-2699.

VanElzakker, M., et al. (2008). Environmental novelty is associated with a selective increase in Fos expression in the output elements of the hippocampal formation and the perirhinal cortex. *Learn Mem* **15**(12): 899-908.

Varatharaj, A. and Galea, I. (2017). The blood-brain barrier in systemic inflammation. *Brain Behav Immun* **60**: 1-12.

Varela, C. and Sherman, S.M. (2009). Differences in response to serotonergic activation between first and higher order thalamic nuclei. *Cereb Cortex* **19**(8): 1776-1786.

Vassalli, A. and Dijk, D.J. (2009). Sleep function: current questions and new approaches. *Eur J Neurosci* **29**(9): 1830-1841.

Vgontzas, A.N., et al. (2004). Marked decrease in sleepiness in patients with sleep apnea by etanercept, a tumor necrosis factor-alpha antagonist. *J Clin Endocrinol Metab* **89**(9): 4409-4413.

Viaene, A.N., et al. (2011). Synaptic Properties of Thalamic Input to Layers 2/3 and 4 of Primary Somatosensory and Auditory Cortices. *J Neurophysiol* **105**(1): 279-292.

Vinet, J., et al. (2012). Neuroprotective function for ramified microglia in hippocampal excitotoxicity. *Journal of Neuroinflammation* **9**(1): 27.

Vinuelas, J., et al. (2001). Meningeal leishmaniosis induced by Leishmania infantum in naturally infected dogs. *Vet Parasitol* **101**(1): 23-27.

Viviani, B., et al. (2003). Interleukin-1beta enhances NMDA receptor-mediated intracellular calcium increase through activation of the Src family of kinases. *J Neurosci* **23**(25): 8692-8700.

Vyazovskiy, V.V., et al. (2008). Molecular and electrophysiological evidence for net synaptic potentiation in wake and depression in sleep. *Nat Neurosci* **11**: 200.

Vyazovskiy, V.V. and Harris, K.D. (2013). Sleep and the single neuron: the role of global slow oscillations in individual cell rest. *Nat Rev Neurosci* **14**(6): 443-451.

Vyazovskiy, V.V., et al. (2011). Local sleep in awake rats. *Nature* **472**(7344): 443-447.

Vyazovskiy, V.V., et al. (2009). Cortical firing and sleep homeostasis. *Neuron* **63**(6): 865-878.

Walker, M.P. (2009). The role of slow wave sleep in memory processing. *J Clin Sleep Med* **5**(2 Suppl): S20-26.

Wall, M.J. and Correa, S.A.L. (2018). The mechanistic link between Arc/Arg3.1 expression and AMPA receptor endocytosis. *Semin Cell Dev Biol* **77**: 17-24.

Wallace, C.S., et al. (1998). Differential intracellular sorting of immediate early gene mRNAs depends on signals in the mRNA sequence. *J Neurosci* **18**(1): 26-35.

Wallace, M.T., et al. (2004). A revised view of sensory cortical parcellation. *Proceedings of the National Academy of Sciences* **101**(7): 2167-2172.

Wang, F., et al. (2015a). Resveratrol Rescues the Impairments of Hippocampal Neurons Stimulated by Microglial Over-Activation In Vitro. *Cell Mol Neurobiol* **35**(7): 1003-1015.

Wang, Q., et al. (2015b). Neuroinflammation in Parkinson's disease and its potential as therapeutic target. *Transl Neurodegener* **4**.

Wang, X.J. (2010). Neurophysiological and Computational Principles of Cortical Rhythms in Cognition. *Physiol Rev* **90**(3): 1195-1268.

Watson, B.O., et al. (2016). Network Homeostasis and State Dynamics of Neocortical Sleep. *Neuron* **90**(4): 839-852.

Watson, C.J., et al. (2010). Neuropharmacology of Sleep and Wakefulness. *Sleep Med Clin* **5**(4): 513-528.

Watts, J. and Thomson, A.M. (2005). Excitatory and inhibitory connections show selectivity in the neocortex. *J Physiol* **562**(Pt 1): 89-97.

Waung, M.W., et al. (2008). Rapid translation of Arc/Arg3.1 selectively mediates mGluR-dependent LTD through persistent increases in AMPAR endocytosis rate. *Neuron* **59**(1): 84-97.

Weber, A., et al. (2010). Interleukin-1 (IL-1) Pathway. *Science Signaling* **3**(105): cm1-cm1.

Weiner, O.D., et al. (1999). Spatial control of actin polymerization during neutrophil chemotaxis. *Nat Cell Biol* **1**(2): 75-81.

Weitzman, E.D. and Kremen, H. (1965). Auditory evoked responses during different stages of sleep in man. *Electroencephalography and Clinical Neurophysiology* **18**(1): 65-70.

Wespatat, V., et al. (2004). Phase sensitivity of synaptic modifications in oscillating cells of rat visual cortex. *J Neurosci* **24**(41): 9067-9075.

West, A.E. and Greenberg, M.E. (2011). Neuronal activity-regulated gene transcription in synapse development and cognitive function. *Cold Spring Harb Perspect Biol* **3**(6).

Whittington, M.A., et al. (2011). Multiple origins of the cortical gamma rhythm. *Dev Neurobiol* **71**(1): 92-106.

Whittington, M.A., et al. (1997). Spatiotemporal patterns of gamma frequency oscillations tetanically induced in the rat hippocampal slice. *J Physiol* **502 (Pt 3)**: 591-607.

Whittington, M.A. and Traub, R.D. (2003). Interneuron diversity series: inhibitory interneurons and network oscillations in vitro. *Trends Neurosci* **26**(12): 676-682.

Whittington, M.A., et al. (1998). Morphine disrupts long-range synchrony of gamma oscillations in hippocampal slices. *Proceedings of the National Academy of Sciences* **95**(10): 5807-5811.

Whittington, M.A., et al. (1995). Synchronized oscillations in interneuron networks driven by metabotropic glutamate receptor activation. *Nature* **373**(6515): 612-615.

Whittington, M.A., et al. (2000). Inhibition-based rhythms: experimental and mathematical observations on network dynamics. *Int J Psychophysiol* **38**(3): 315-336.

Widmann, C.N. and Heneka, M.T. (2014). Long-term cerebral consequences of sepsis. *Lancet Neurol* **13**(6): 630-636.

Williams, S.R. and Stuart, G.J. (1999). Mechanisms and consequences of action potential burst firing in rat neocortical pyramidal neurons. *J Physiol* **521**(Pt 2): 467-482.

Wisor, J.P., et al. (2001). Dopaminergic role in stimulant-induced wakefulness. *J Neurosci* **21**(5): 1787-1794.

Xu, T.X. and Yao, W.D. (2010). D1 and D2 dopamine receptors in separate circuits cooperate to drive associative long-term potentiation in the prefrontal cortex. *Proc Natl Acad Sci U S A* **107**(37): 16366-16371.

Xu, Z., et al. (2017). Vascular endothelial growth factor is neuroprotective against ischemic brain injury by inhibiting scavenger receptor A expression on microglia. *J Neurochem* **142**(5): 700-709.

Yi, G., et al. (2017). Action potential initiation in a two-compartment model of pyramidal neuron mediated by dendritic Ca2+ spike. *Scientific Reports* **7**: 45684.

Yoshida, H., et al. (2004). State-specific asymmetries in EEG slow wave activity induced by local application of TNFalpha. *Brain Res* **1009**(1-2): 129-136.

Zhang, F., et al. (2013). Resveratrol protects cortical neurons against microglia-mediated neuroinflammation. *Phytother Res* **27**(3): 344-349.

Zhang, J.M. and An, J. (2007). Cytokines, inflammation, and pain. *Int Anesthesiol Clin* **45**(2): 27-37.

Zhu, J.J. and Connors, B.W. (1999). Intrinsic firing patterns and whisker-evoked synaptic responses of neurons in the rat barrel cortex. *J Neurophysiol* **81**(3): 1171-1183.

Zhu, X., et al. (2016). A distinct brain pathway links viral RNA exposure to sickness behavior. *Scientific Reports* **6**: 29885.

Zlotnik, A. and Yoshie, O. (2012). The chemokine superfamily revisited. *Immunity* **36**(5): 705-716.